Photovoltaics

Konstanty Marszałek
Katarzyna Dyndał
Gabriela Lewińska
Jerzy Sanetra

2022

AGH open E-PODRĘCZNIKI

AGH

The publication is available under the Creative Commons Attribution-ShareAlike 4.0 (CC BY-SA 4.0). Some rights reserved for the authors and the AGH University of Science and Technology. This license allows reusers to distribute, remix, adapt, and build upon the material in any medium or format, so long as attribution is given to the authors and the AGH University of Science and Technology. The full text of the license is available at https://creativecommons.org/licenses/by-sa/4.0/deed.en

1. Introduction
    1.1 Introduction
2. Environmental-climatic aspects
    2.1 Solar energy reaching the Earth's surface
    2.2 Solar spectrum
    2.3 The geographical aspects of the solar radiation
    2.4 Daily variations in solar energy
3. The background of photovoltaics
    3.1 The beginning of photovoltaics
    3.2 Photovoltaics at the turn of the 20th and 21st century
    3.3 Physical properties of materials used in photovoltaics
    3.4 The p-n junction
    3.5 Physical fundamentals of solar energy conversion to electricity
    3.6 Photovoltaic cell parameters
    3.7 Cell's model
4. Components of a cell structure
    4.1 Photovoltaic cell structure components
    4.2 Metallic electrodes
    4.3 Transparent and conductive electrodes
    4.4 Antireflective layers
    4.5 Passivation layers
5. Photovoltaic cells generations
    5.1 Classification of photovoltaic cells
    5.2 Changes in conversion efficiency
    5.3 Silicon cells
    5.3.1 Monocrystalline silicon production
    5.3.2 Production of polycrystalline silicon
    5.4 Thin-film cells
    5.5 Multi-junction cells
    5.6 Organic cells
    5.7 Dye cells
    5.8 Perovskite cells
    5.9 Hybrid cells
    5.10 Concentrator photovoltaics
6. Cell technologies
    6.1 Busbar cells
    6.2 PERL cells
    6.3 Interdigitated Back Contact cells
    6.4 Smartwires cells
    6.5 HIT technology cells
    6.6 Thin-film photovoltaic cells
    6.7 PERC and PERT type PV cells
7. Photovoltaic modules
    7.1 Photovoltaic modules
    7.2 Photovoltaic modules technologies
    7.3 Photovoltaic modules made of PERC technology
    7.4 Half-cut modules
    7.5 Bifacial modules
    7.6 PVT systems
8. Cell and modules parameters
    8.1 Measurement of cell parameters
    8.2 Simulation of cell parameters changes using PC1D software
    8.3 Temperature dependence of cell parameters
    8.4 Module parameters measurements
9. Photovoltaic systems
    9.1 Off-grid photovoltaic systems
    9.2 On-grid photovoltaic systems
    9.3 Ground mount installations
    9.4 Floating installations
    9.5 Tracking systems
    9.6 Portable installations - everyday objects
    9.7 Portable installations - vehicles
10. Inverters
    10.1 Inverters functions
    10.2 Inverters classification

10.3 Inverters selection methods
11. Electricity storage
11.1 Energy storage methods
11.2 Accumulators
11.3 Compressed air tanks
11.4 Liquid gas tanks
12. Computer-aided design of PV installations
12.1 PV simulation programs
12.2 PV*SOL software for system planning
12.2.1 3D objects design
12.2.2 PV plant design
12.2.3 PV plant efficiency
12.3 Polysun designing of PV installation
13. Connection of a power plant to the grid
13.1 Legal rules concerning the connection of power plants
13.2 Connection of a power plant to the grid
13.3 Lightning protection systems
14. Assembly of a photovoltaic system
14.1 Assembly requirements
14.2 Ground mount and flat roof installation assembly
14.2.1 Ground mount and flat roof installation assembly without ballast
14.2.2 Ground mount and flat roof installation assembly with ballast
14.2.3 Self-supporting PV systems
14.3 Assembly of a PV on a pitched roof
14.4 Assembly of PV tracking system
15. Panels and PV installation tests
15.1 Photovoltaic installation control
15.2 Testing a new installation
15.3 Selection and verification of modules for testing
15.4 Module strings functioning accuracy tests
15.5 Hail test
15.6 Mechanical static load on module test
15.7 Electroluminescence tests
16. Photovoltaic systems damage
16.1 Types of damage in PV installations
16.2 Hot spots
16.3 Delamination
16.4 Cracks and micro-cracks in PV cells
16.5 Connector and junction box defects
16.6 Glass cracks
16.7 Corrosion of TCO layer in amorphous silicon cells
16.8 Potential Induced Degradation (PID)
16.9 Technology markers on cell edges
17. Economic aspects of photovoltaics
17.1 Photovoltaic installation costs
17.2 Module prices
17.3 Installations development in Poland
17.4 Installations development in Europe
17.5 Installations development in the World

1. Introduction

1.1 Introduction

Renewable energy sources have been with humanity since time immemorial. The burning of biomass has been a source of heat. Wind energy has been used to power boats and sailing rafts, to transport water to elevated or more distant agricultural areas, and lastly to produce flour in windmills with initially vertical and, as technology developed, horizontal axes. When analysing the physical basis of photovoltaics, it is important to consider that this type of energy production has a source outside the Earth. Fortunately, from the point of view of humanity, the Sun is an inexhaustible supply of energy. However, it has one disadvantage that must be taken into account, i.e., it provides energy only to the side of the Earth that happens to be facing the Sun. This means that electricity can be produced only during the daytime and with varying intensity depending on the time of day. There is also a dependence on the geographical location of the power plant due to differences in insolation. The photovoltaic phenomenon was discovered in the 19th century by Alexander Edmond Becquerel (1839). However, it found real application only after World War II with the rapid development of electronics and semiconductor materials (in the initial phase of space and military applications). In particular, it was the competition and the space race that pushed the development of photovoltaics significantly forward, as solar cells provided a lightweight (cost of transport to orbit) and inexhaustible (constant access to solar energy) source of electricity to power satellite equipment. The first post-war energy crisis of the mid-1970s and the Club of Rome's Report on the Depletion of Earth's Fossil Resources focused public attention on renewable energy issues. Sources such as hydroelectric power plants, wind power plants, and finally photovoltaic power plants have become the subject of analysis by engineers, designers, and economists all over the world.

Hydroelectric power is an investment that takes decades (just filling the reservoir took more than 18 years in Colorado, for example). High-capacity wind turbines (individual windmills range from 2 to 10 MW) face protests from environmentalists due to their environmental impact and bird migration. Photovoltaics, however, is an attractive alternative to conventional energy sources as mentioned above, because electricity is obtained directly from solar energy without noise, pollution and other factors causing adverse environmental changes. The almost unlimited demand for monocrystalline silicon of the electronics industry limited the development of photovoltaics in the second half of the 20th century. Only the transfer of many technologies to China, especially the vacuum Czochralski technology for the production of monocrystalline silicon, became the beginning of the exponential development of photovoltaics in the first two decades of the 21st century. Every dynamic development attracts the attention of researchers and engineers. This was also the case with photovoltaics. A number of modifications have significantly increased the energy conversion efficiency of monocrystalline photovoltaic cells. A method of relatively inexpensive production of polycrystalline silicon for making photovoltaic cells has been developed. Semiconductor research has led to the application of a number of new semiconductor materials for photovoltaic cell manufacturing. Thin-film technology, in which material consumption is a hundred times less than in silicon cells, has proven particularly promising. And the last 10 years have seen the introduction of low-cost materials like perovskites and polymers into the photovoltaic field.

The dynamic development of photovoltaic installations and research has, in many cases, preceded long-term educational cycles. Hence the need for publications that provide a source of knowledge and information for an ever-widening circle of people involved in the development of the photovoltaic industry: materials engineers, power engineers all the way to the end consumers of electricity. At this point, we should pay tribute to Prof. Jan Stopczyk who created the concept and philosophy of the prosumer, i.e., the producer and consumer of micro-scale electricity at the same time. However, this individual contribution multiplied by millions of prosumers becomes a serious contribution to the national energy system. No one has the slightest doubt that after the depletion of fossil fuels humanity will have no cheaper alternative to renewable energy sources, especially photovoltaics. The rapid growth of photovoltaic production and installation has led to a drastic drop in energy prices per kWp from photovoltaic sources, which had previously been a major barrier to the development of installations.

This book is intended primarily for students studying renewable energy sources, including photovoltaics, but also for anyone interested in learning about photovoltaics, its development and prospects. It does not constitute instructional material for photovoltaic installers, since such materials are already available in bookstores. The electronic form of the textbook was chosen because of the change in the way the material can reach the student and the reader as well as the possibility of making modifications to the content resulting from the dynamic changes occurring in this developing field of technology.

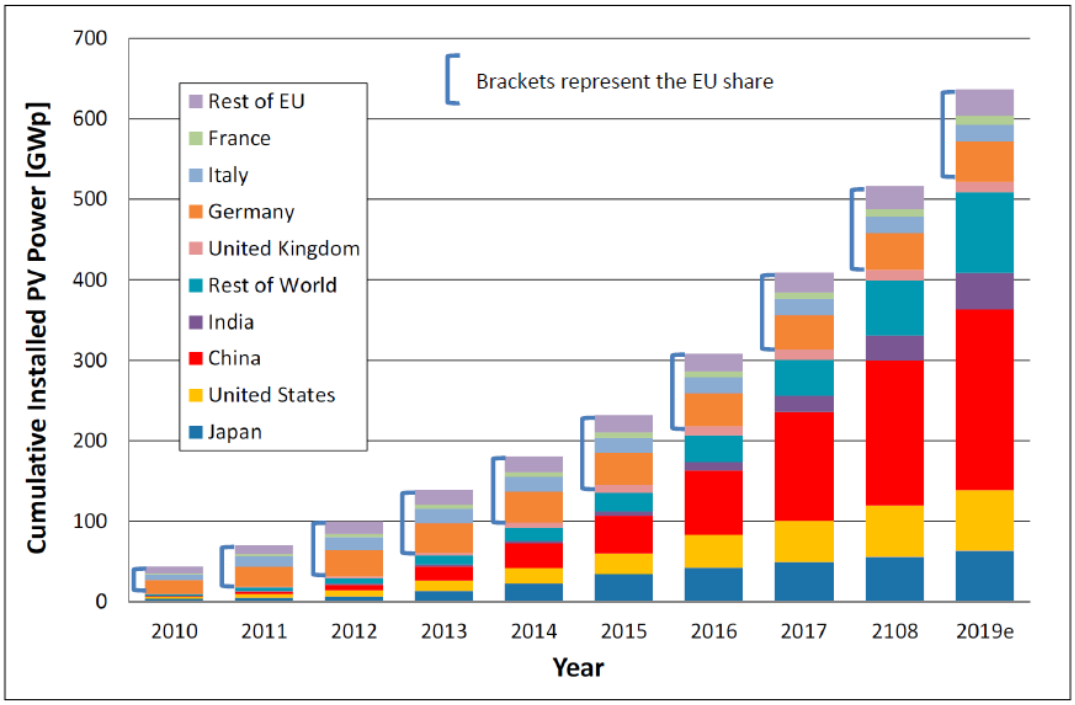

Figure 1: PV capacities installed in different countries from 2010 to 2019. Fig. Arnulf Jäger-Waldau, CC-BY 4.0 license, source: MDPI .

How dynamic changes are taking place in the world in the field of renewable energy sources, including photovoltaics, can be seen by observing the changes taking place in the continuously increasing share of these sources in energy production. A comparison of countries which in the last decade have seen a very strong increase in installed photovoltaic capacity does not correspond to the location of the sunniest areas of the globe. Presently, it is the political decisions about the methods of subsidizing PV installations or energy storage that are the basis of the installation dynamics. The second factor is major investments in the expansion of the PV industry such as China's dominance in silicon substrate production. When comparing 2010, when almost the entire installed capacity bar was occupied by Europe, to the latest data from 2019, one can see how colossal the changes have been (Fig. 1) [1]. The installed capacity in countries such as China, the USA, Japan and the rest of the world has overtaken that of Europe many times over. The installed capacity is still far from being sufficient to cover the entire energy needs of the world. However, the dynamics of change indicates that many countries understand the dangers of CO_2 and the role that renewable energy sources play because of climate conditions and in the global energy mix.

2. Environmental-climatic aspects

2.1 Solar energy reaching the Earth's surface

The tilt of the Earth's axis with respect to the Earth's orbit around the Sun generates a change in the seasons, which affects the amount of solar energy that reaches different areas of the Earth during the year. The northern hemisphere receives the most energy in summer and the least in winter. This is due to the change in the angle of the Earth's plane to the direction of the sun's rays and the time of insolation (length of day), in which solar radiation reaches the Earth. The insolation depends not only on your location on the parallel, but also on the cloud cover in your region.

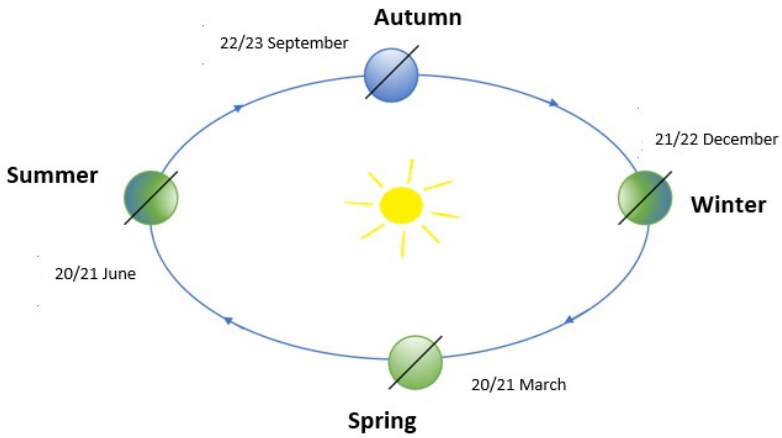

Figure 2: Seasons in the Northern Hemisphere. Own elaboration.

The power of solar radiation thus depends on the time of day, the season, and the geographic location where it will be measured (Fig. 2).

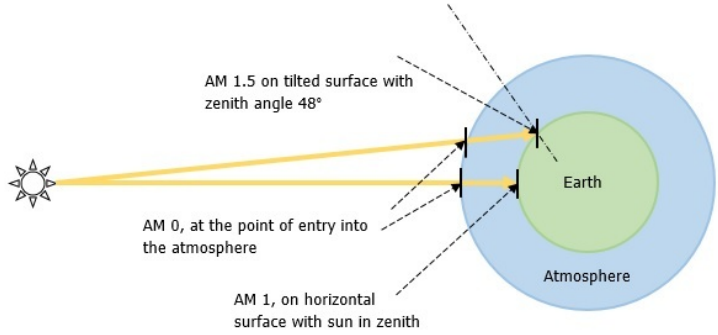

Figure 3: Standardizing the Sun, Committee Internationale d'Eclaraige (CIE) and the American Society for Testing and Materials (ASTM). Own elaboration.

The distance traveled by solar radiation (Fig. 3) in the atmosphere varies with the position of the sun above the horizon. The seasonal dependence is related to the tilt of the Earth's axis of rotation with respect to the plane in which the Earth moves (Fig. 2).
The photovoltaic phenomenon is inextricably linked to the energy source, which is the Sun. The average power delivered by the Sun to the boundary of the Earth's atmosphere is $1362\frac{W}{m^2}$ (solar constant) [2], that is, about 175* $10^{15}\ W$ of solar irradiance power (energy per second) falls on the entire surface of the Earth. This energy, after passing through the atmosphere, is converted in photovoltaic cells into electricity. The amount of energy reaching the Earth's surface obviously varies in different geographical areas. It is usually determined by the amount of insolation, which is the amount of energy of solar radiation falling per unit time on a unit area. The unit of insolation is $\frac{W}{m^2}$ or $\frac{kWh}{m^2 year}$. The distribution of insolation over the globe is shown in Fig. 4.

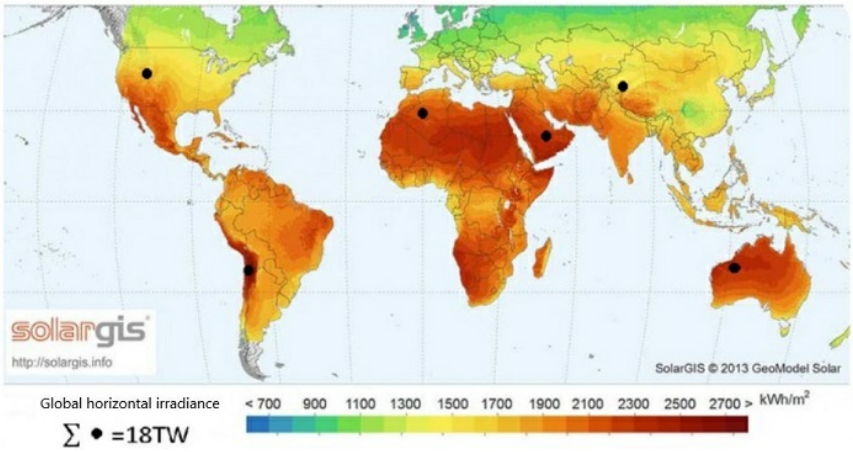

Figure 4: Annual average solar irradiance distribution over the surface of the Earth. The impact of the Earth's atmosphere is taken into account. Fig. OpenStreetMap, CC BY-SA 2.0 license, source: OpenStreetMap .

Black dots depicted in Fig. 4 cover an area that, when covered with photovoltaic cells with a conversion efficiency of 8%, can generate 568 EJ of energy (EJ= 10^{18} J), which covers the entire world electricity demand [3], [4].
Photovoltaic installations are usually mounted in a south-facing tilt. The tilt angle is chosen such that the amount of solar energy reaching the cell surface is maximized. Ideally, the cell surface should follow the movement of the sun, tracking the apparent movement of the Sun across the sky (aligning the plane perpendicular to the incident solar radiation). However, the tracking system generates additional costs associated with the fixation, with the drive of the entire cell system, and with its maintenance. Therefore, this solution is used less frequently than permanent mounting of photovoltaic panels.

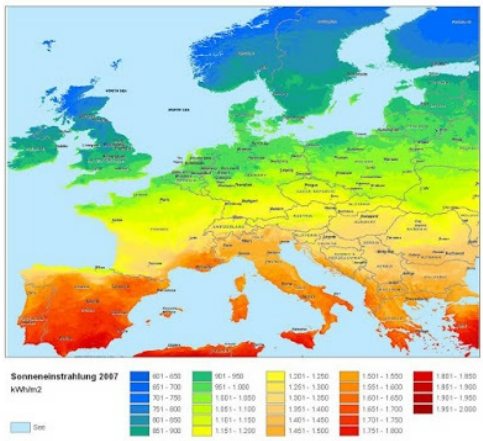

Figure 5: Solar energy reaching Europe at an area of 1 square metre in one year. Solar insolation of the surface of Europe taking into account the influence of the Earth's atmosphere (different overcover in different areas). Fig. OpenStreetMap, CC BY-SA 2.0 license, source: OpenStreetMap .

Fig. 5 [3], [4] presents the contour map of Europe, while Fig. 6 shows contours of Poland; they present the average insolation (solar radiation power per unit horizontal area) for Europe (in 1994-2010) and for Poland (in 1994-2013) [3], [4]. The intensity of the color illustrates the amount of insolation, which depends not only on the latitude (it does not coincide exactly with the system of parallels), but also on the cloud cover that is present in a given area.

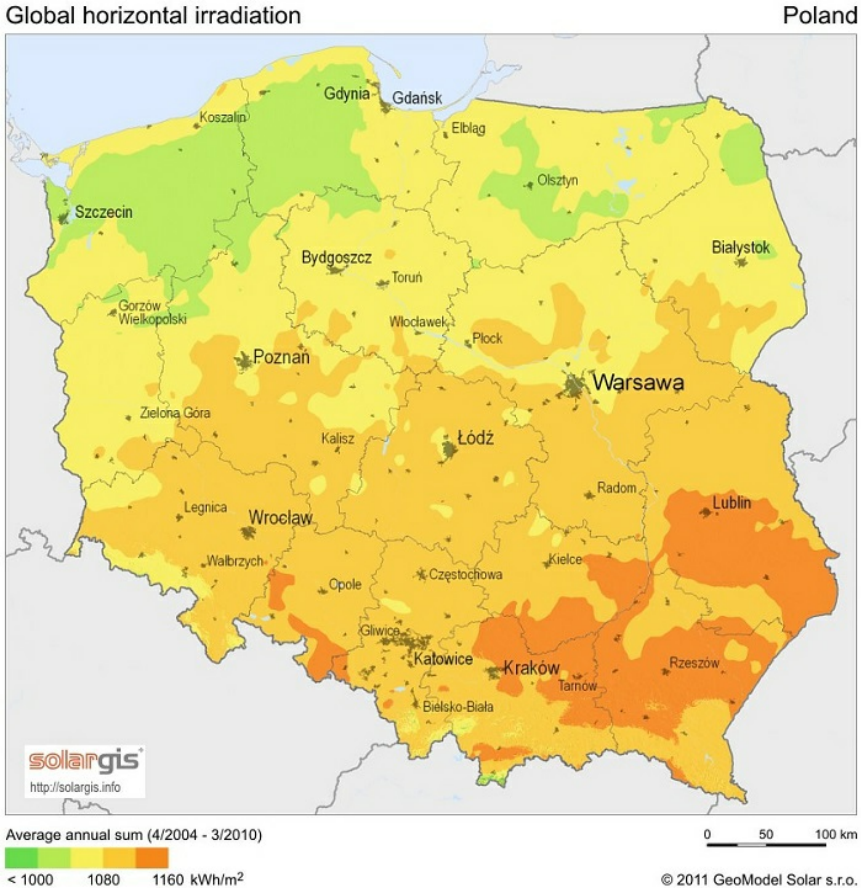

Figure 6: Solar energy reaching the Polish the surface of a square meter in one year. Fig. OpenStreetMap, CC BY-SA 2.0 license, source: OpenStreetMap .

Fig. 6 presents a map of Poland with the insolation (incident energy per 1 m^2 during the year in kWh/ m^2) marked. The map shows that the insolation during the year is the highest in south-eastern Poland. The differences in the amount of energy in different areas reach 30%, which must be taken into account in the economic calculation, especially for large photovoltaic installations.

The diagrams of the course of the solar disk along the sky are determined individually for each location and can be presented using the PVSol program (e.g., for Krakow in Fig. 7) (own work). Thus, in summer the altitude at zenith is about 70^o, and in winter about 25^o, whereby in summer, the azimuth varies from about 60^o to about 300^o. In contrast, the winter Sun rises when the azimuth is about 120^o, and occurs when the azimuth is approximately 240^o.

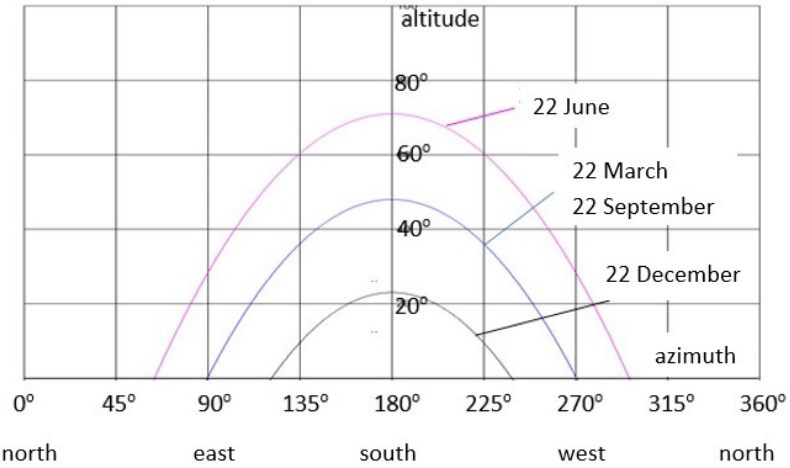

Figure 7: Location of the solar shield in the sky at different times of the year for the location of Krakow (according to the PVSol program). Own elaboration.

In summary, light of H=1.362 $\frac{kW}{m^2}$ (the solar constant) reaches the boundary of the Earth's atmosphere, while about 73% of this magnitude reaches the Earth's surface.

Vosti Lublin, Wojewódzki Program Rozwoju Alternatywnych Źródeł Energii dla Województwa Lubelskiego – see Nasłonecznienie w Polsce a panele fotowoltaiczne .

2.2 Solar spectrum

After analyzing where, when, and how much solar energy reaches us, the frequency analysis of electromagnetic radiation was addressed. The spectra of solar radiation as a function of wavelength are shown in Fig. 8. The solar radiation spectra shown are those reaching the boundaries of the atmosphere (AM 0) and the solar radiation spectrum reaching the Earth's surface after the solar ray has passed through the Earth's atmosphere entering at an angle of 42^o above the horizon denoted by AM 1.5. The letter d next to the spectrum designation indicates that it is incident radiation directly from the Sun, while the letter g indicates that it is the sum of direct radiation from the Sun plus Rayleigh scattering and radiation reflected from clouds.
The energy percentages of the different areas of the spectrum are as follows:

- 49% – visible range and near infrared,
- 44% – wavelengths greater than 800 nm,
- 7% – near ultraviolet (120-300 nm),
- 0.001% – x-ray and far ultraviolet.

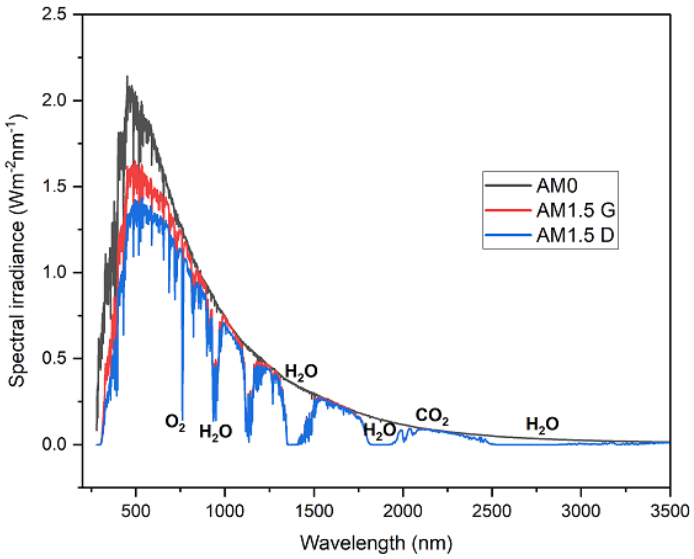

Figure 8: The intensity of solar radiation reaching the boundary of the Earth's atmosphere (AM0) and on the Earth's surface (AM1) depending on the wavelength. Selected elements absorbing the appropriate lengths of light. Own elaboration.

The energy radiated by the Sun in the form of electromagnetic waves before it reaches the Earth's surface is reflected (about 30%) and absorbed by the Earth's atmosphere (about 20%).

Approximately $175 \cdot 10^{15}\ W$ reaches the surface of the Earth's atmosphere, and approximately $89 \cdot 10^{15}\ W$ reaches the surface of the Earth. Absorption in the Earth's atmosphere occurs due to the presence of oxygen molecules, ozone, carbon dioxide, water vapor, etc. In addition, Rayleigh scattering on dust particles occurs in the troposphere.
The intensity of solar radiation at the distance of the Earth from the Sun is at 1362 $\frac{W}{m^2}$. This quantity was called the solar constant and it is the energy of solar radiation that falls on the surface of one square meter per second at a distance of the Earth from the Sun (the average distance is 150 million km). Based on this, the energy emitted per second by the Sun was calculated and it amounts to $9.65 \cdot 10^{25}\ W$. The total energy that reaches the Earth's surface throughout the year ranges from 600 $kWh/m^2/year$ in Scandinavian countries, and up to over 2200 $kWh/m^2/year$ in central Africa. In Poland it is about 990 $kWh/m^2/year$ [5].
Solar radiation originates from the photosphere, the outer surface of the gaseous layer of the Sun, which temperature is about 5770 K. The maximum of the blackbody continuous spectrum electromagnetic radiation, as for solar radiation, is in the visible spectral region with a wavelength of about 500 nm (Fig. 8).

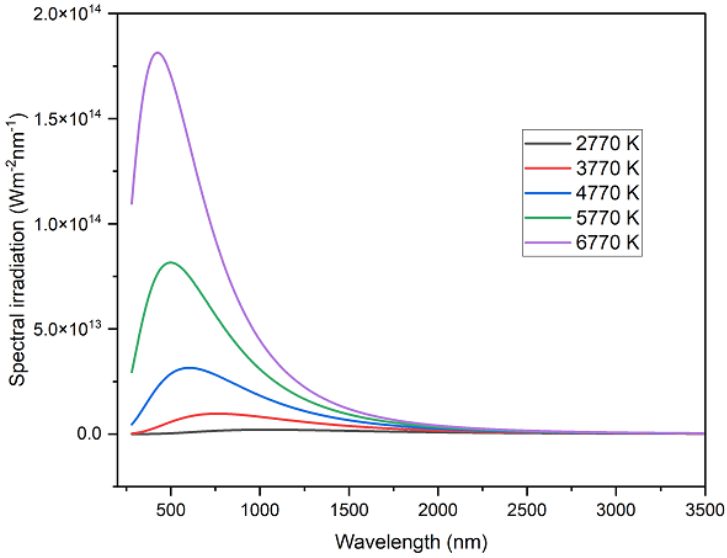

Figure 9: Spectrum of perfectly black body emissions at different temperatures. Own elaboration.

The visible region of the spectrum is from $4 \cdot 10^{-7}\ m$ to $7.8 \cdot 10^{-7}\ m$. Comparing the blackbody spectrum (Fig. 9) with that of the Sun, it can be assumed to a first approximation that they are similar (Fig. 8).
The operating range of the solar panels (green) against the solar radiation spectrum is shown in Fig. 10.
The radiation from the Sun above the Earth's atmosphere corresponds approximately to the radiation from a blackbody with a temperature of 5762 K (~6000 K). The solar radiation that reaches the Earth's surface is even more distinctly different from the blackbody spectrum. This is due to the absorption, scattering and reflection of radiation into space, which causes a significant modification in the distribution of its spectrum [6].

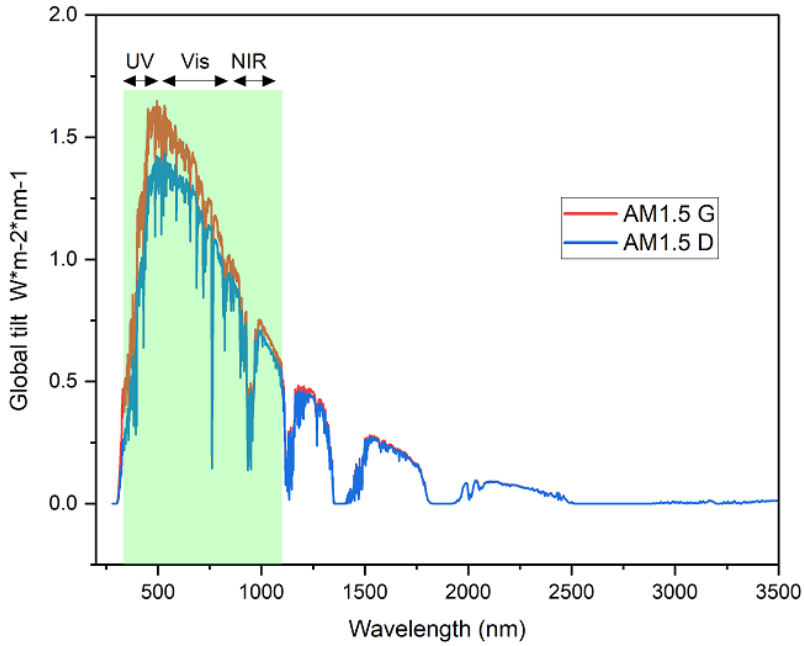

Figure 10: Comparison of sunlight spectrum AM 1.5d (direct) and AM 1.5g (global). The range of operation of solar panels (green color) against the background of the spectrum of solar

radiation (UV- ultraviolet light, Vis - visible light, NIR - close infrared). Own elaboration.

Fig. 10 shows the spectrum of solar radiation at the Earth's surface (AM1) after passing through the atmosphere [7].

As solar radiation passes through the atmosphere, there are losses associated with:

- Rayleigh scattering (proportional to λ^{-4}),
- absorption by the electron shell of gases O_2, N_2, O_3,
- molecular absorption (rotations and oscillations) of molecules H_2O and CO_2,
- dispersion on dust and aerosol particles,
- change in refractive index due to temperature, pressure, turbulence,
- change in the humidity of the atmosphere.

In Poland, about 1000 $\frac{W}{m^2}$ of solar radiation reaches the Earth's surface. The use of a portion of solar radiation for conversion to electricity is related to the physical properties of semiconductors.
The energy region that is used to convert solar energy in photovoltaic devices is highlighted in Fig. 10. This region is almost 50% solar energy, the rest of the spectrum is not used.
Research is being conducted on phenomena and technologies to extend the range of frequencies used, such as the thermoelectric effect [8]; nevertheless, in practice, of the solar installations available only the photovoltaic effect is widely used commercially.

2.3 The geographical aspects of the solar radiation

Solar radiation must pass through Earth's atmosphere before it reaches Earth's surface. Earth's atmosphere is composed primarily of nitrogen (78.084% by volume), oxygen (20.946%), argon (0.934%), carbon dioxide (0.0408%), and water vapor, the content of which fluctuates. In addition to these components, methane, hydrogen, nitrogen oxides, sulfur compounds, ozone, radon, iodine, ammonia, and atmospheric aerosols (0.05-0.35 μm in diameter) are present in trace amounts. The atmosphere causes radiation to be absorbed and scattered on its way to the Earth's surface.

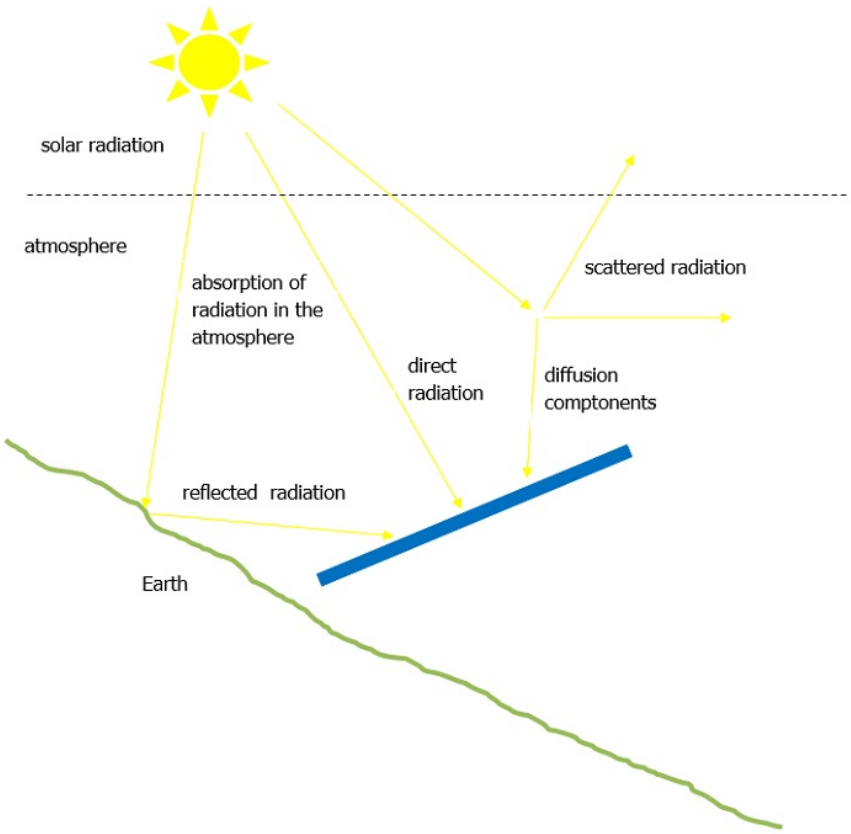

Figure 11: Losses of solar radiation on the way to the Earth's surface (photovoltaic panel). Own elaboration.

Solar radiation undergoes absorption and diffusion (Fig. 11). In addition to the direct radiation from the Sun, there is also reflected light and a scattering component that reach the surface of the PV panel [9].

Solar radiation incident on the Earth's surface is composed of direct I_b (beam radiation) and scattered I_d (diffuse radiation), sometimes called diffuse or sky radiation (Fig. 12). Diffuse radiation is radiation from the Sun that has scattered in the Earth's atmosphere (1).

$$I = I_b + I_d \tag{1}$$

If solar radiation falls on a plane deflected from Earth level, the radiation consists of direct radiation I_b scattered I_d and reflected radiation I_{od} from the surface of the surrounding ground (2).

$$I_\alpha = I_{\alpha b} + I_{\alpha d} + I_{\alpha o} \tag{2}$$

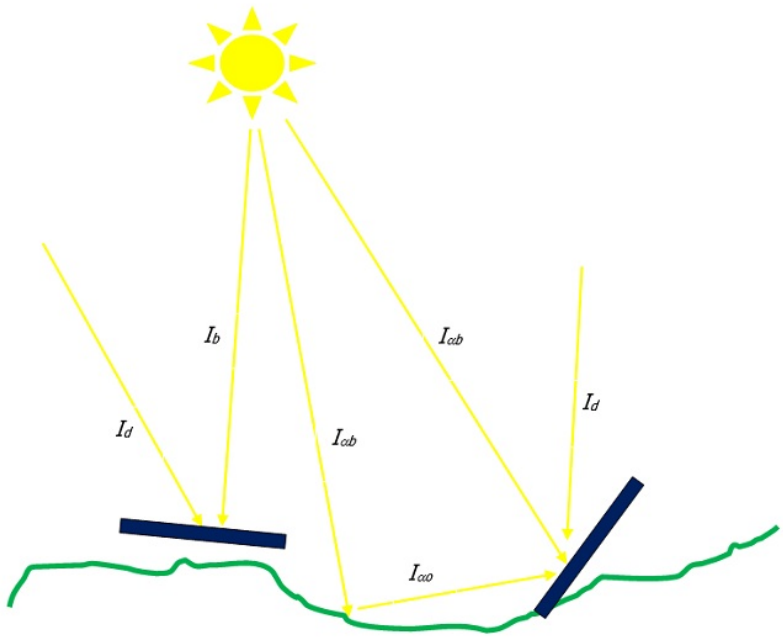

Figure 12: The path that solar radiation will take through the atmosphere to the earth's surface. Own elaboration.

On Fig. 12 marks I_b - direct radiation, I_d - diffuse radiation, $I_{\alpha b}$ - direct incident radiation at an angle α, $I_{\alpha o}$ - radiation reflected from the surface of the surrounding ground.

The radiation reaches the Earth's surface through different thicknesses of air layers depending on the location on the globe, so different intensities of solar radiation are observed (Fig. 13).

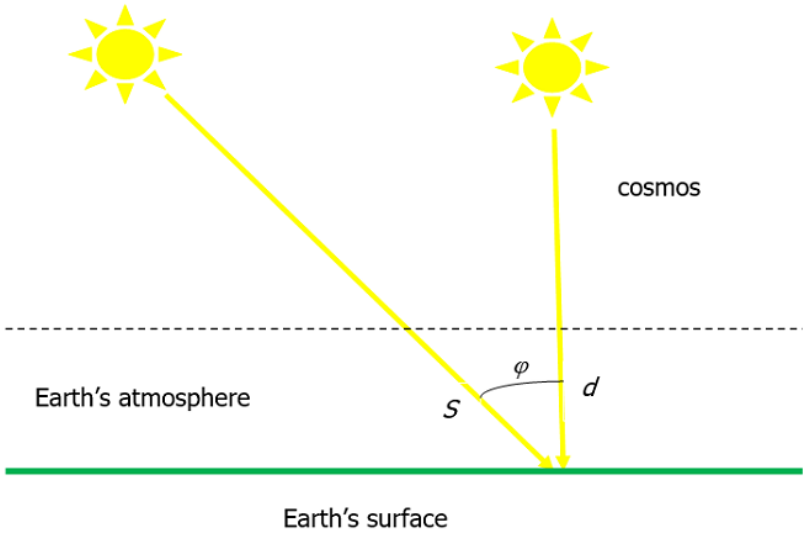

Figure 13: Components of solar radiation falling on a horizontal plane and deviating from Earth level. Own elaboration.

The change in the path length of a solar ray S through the Earth's atmosphere when the incidence angle ϕ changes is shown in Fig. 13.

$$S = \frac{d}{cos\phi} \tag{3}$$

where the angle ϕ is between the direction the Sun is facing and the direction of the zenith.

This causes a change in the power of solar radiation reaching the Earth's surface. This illustrates the fact that different locations on Earth have significantly different amounts of solar energy for use in conversion to electricity.

The ratio of the path length traveled by the Sun's rays when incident radiation is at a certain angle to the path length traveled at a right angle is called the air mass number AMm (Air Mass m). If the air mass number is m=1, then the Sun's rays reach the earth at right angles. A simplified scheme for determining the air mass number of the atmosphere is shown in Fig. 14. Radiation above the Earth's atmosphere is m=0 and is denoted AM0; radiation at sea level when the Sun is at zenith is m=1 and is denoted AM1. The air mass number is approximated by the formula:

$$m = \frac{1}{cos\varphi} \tag{4}$$

where the angle ϕ is between the direction in which the Sun is located and the direction of the zenith (Fig. 14).

If there is a need to determine the air mass number with greater accuracy, one should know the atmospheric pressure and then use the following formula (5) (own elaboration) [10].

$$m = \frac{p}{p_0}\left(cos\varphi + \frac{0{,}15}{(93{,}885-\varphi)^{1{,}258}}\right)^{-1} \tag{5}$$

where p_0=1013 hPa, p – current atmospheric pressure, hPa=100 Pa.

For Poland, an air mass number of AM1.5 was assumed (latitude of approximately 48^o, see Fig. 15).

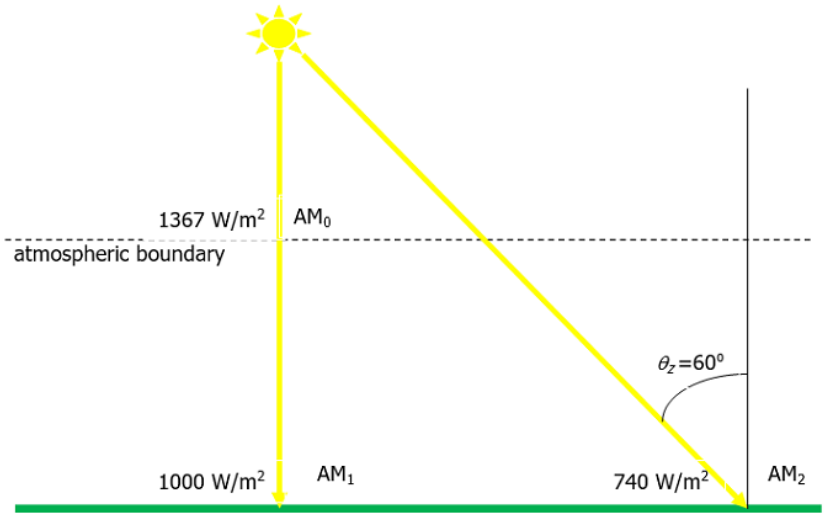

Figure 14: Simplified way of determining the number of air masses of the AM atmosphere. Own elaboration.

Spectrum designation	Geographical area of use on the globe	Power mW/cm²
AM0	The AM0 corresponds to conditions that prevail at a distance of 1 astronomical unit from the Sun when there is no suppression of solar radiation by the atmosphere	136.2
AM1	AM1 corresponds to irradiation intensity when sunlight at the zenith penetrates the atmosphere and is equal to approximately 0.7 AM0 values	94.7
AM1.5	AM1.5 is normally assumed as the mean intensity to which the angle θ = 48.19°	84.4
AM2	AM2 means that the radius has travelled 2x the thickness of the Earth's atmosphere	70-75

Figure 15: Types of solar radiation spectrum as a function of the position in the Earth's atmosphere. Own elaboration.

Differences in lighting conditions at different locations on the Earth's surface have forced the standardization of conducting tests on all photovoltaic panels in exactly [10] the same environmental conditions. Standard Test Conditions (STC) have been introduced. They define the radiation spectrum (AM1.5), illuminance - the amount of incident energy per 1 m^2 within 1S (1000 $\frac{W}{m^2}$) and the temperature at which the (25^oC) tests are conducted.

2.4 Daily variations in solar energy

The Sun above the horizon changes its position depending on the time of day. The horizon of the observer at the center and the position of the Sun relative to it as a function of time of day is shown in Fig. 16.

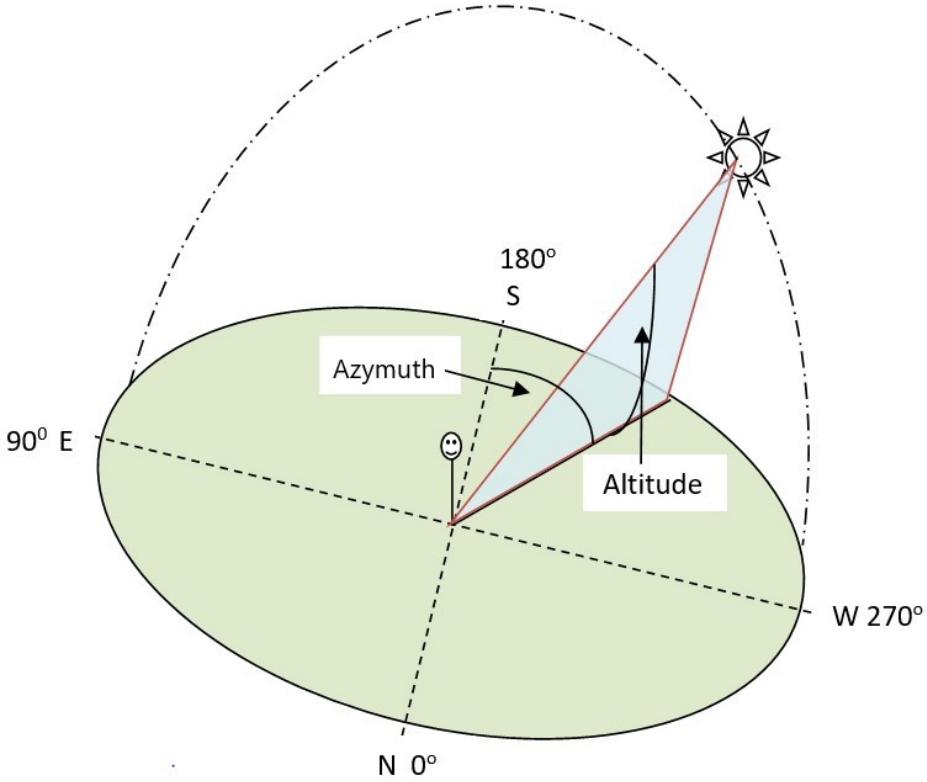

Figure 16: The solar azimuth angle is the position of the Sun east or west of the geographical south, and the altitude angle is the position of the Sun above the horizon. Own elaboration.

The sun changes its position in the sky from east to west, as well as rising above the horizon, throughout the day. It reaches its highest point at solar noon and then decreases until sunset. The horizontal position of the Sun is called the solar azimuth (Fig. 16), which for the Northern Hemisphere is measured in degrees east and west of geographic south (not magnetic south). The Sun's azimuth angle is 180^o for geographic south. The vertical position of the Sun, or the angular height of the Sun (altitude), is measured in degrees above the horizon. At sunrise, it is 0^o. As the Sun rises, the angle increases to a maximum value at noon and reaches up to 90^o (depending on latitude). The position of the Sun according to season and day is shown in Fig. 17 (based on data from Sunrise and Sunset in Kraków - see Wschód i zachód Słońca w Krakowie [11]). The observer's horizon is in the center, and the position of the Sun relative to it depends on the time of day and year. In the northern hemisphere, the highest angular height of the Sun is reached in the summer season and the lowest in the winter. The dashed line shows the impression of the projected motion of the Sun on the plane of the horizon as seen by the observer.

In order to make effective use of solar insolation, photovoltaic panels should be positioned in such a way that the energy of solar radiation falling on the panel is maximized. If the orientation of the panel is stationary, that is, it does not follow the sun, then the panel should be oriented toward the south. The angle of the photovoltaic panel is set according to its location on the Earth's surface (that is, according to the latitude of the PV panel's mounting) so that it can receive maximum sunlight. On Fig. 18 (data taken from [12]) an example of insolation differences for southern and northern Poland is shown. The optimal tilt angle of the photovoltaic panel for northern Poland is larger than for southern Poland.

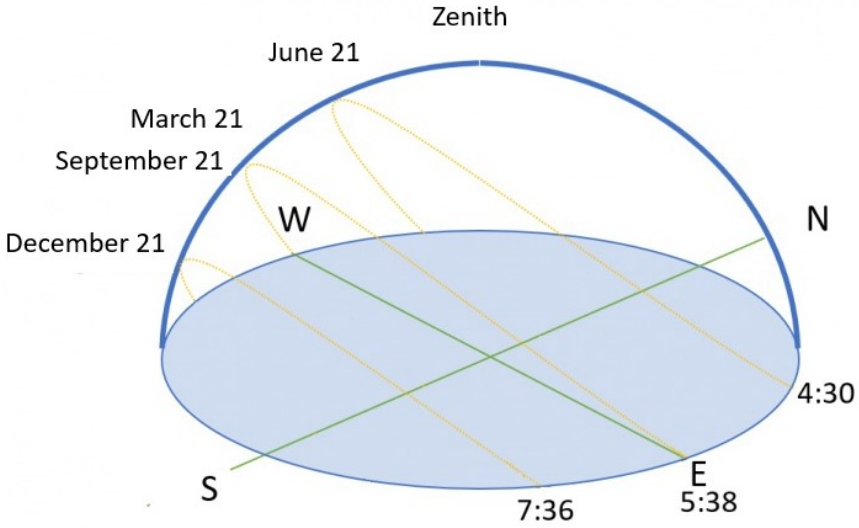

Figure 17: The position of the Sun above the horizon at different times of the year. Own elaboration.

From the above graph, it can be concluded, that setting the photovoltaic panel at an angle within 20^o- 50^o changes solar energy consumption from $1175\frac{kWh}{m^2}$ to $1204\frac{kWh}{m^2}$, that is in a range of less than 3%.
Photovoltaic panels are usually placed on the roof of a building, and this roof does not always face exactly south. Therefore, you should also analyze the situation where the photovoltaic panels have a different orientation with respect to the south.

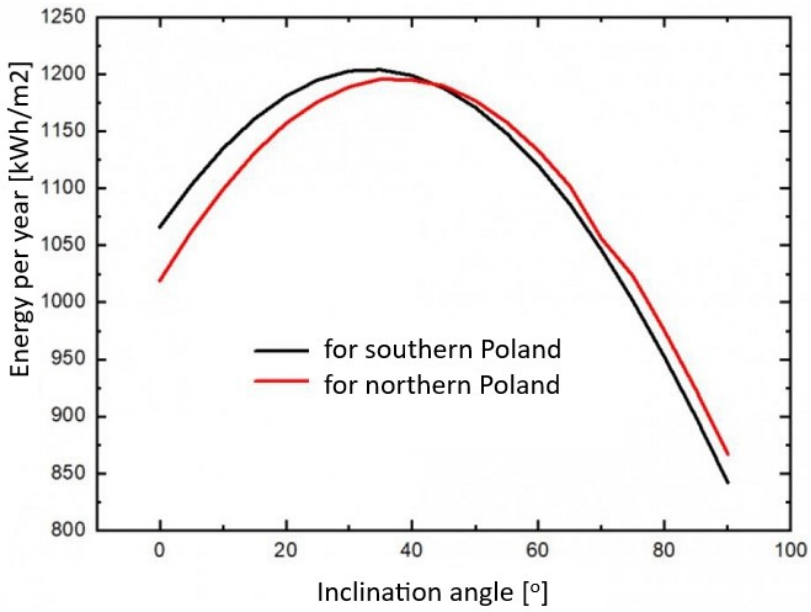

Figure 18: Change of the energy of solar radiation falling on a square meter during the year depending on the angle of inclination of the photovoltaic panel, oriented to the south for southern and northern Poland. Own elaboration.

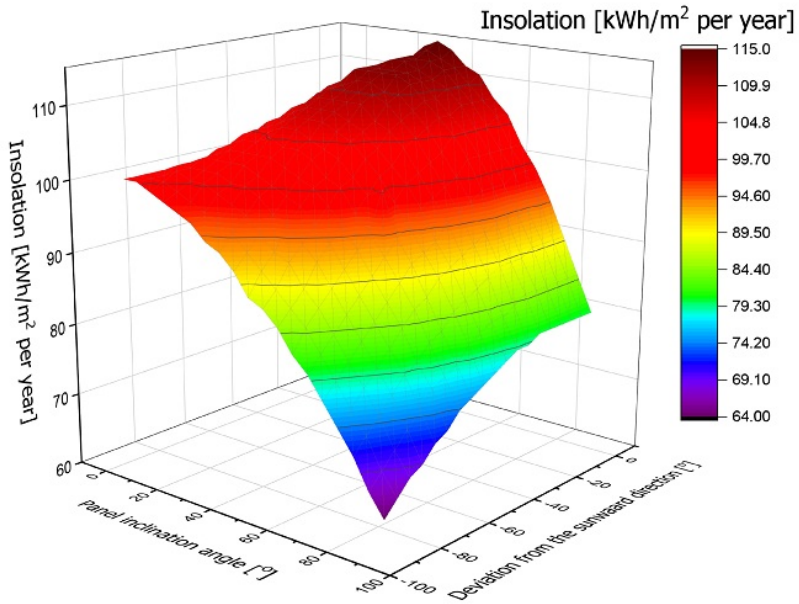

Figure 19: Change in incident solar radiation energy per square meter during the year depending on the angle of inclination of the photovoltaic panel towards the south photovoltaic panel. Own elaboration.

Based on the experimental data presented (Fig. 19) (data taken from [12]) it can be concluded that the more the photovoltaic panel is tilted away from the southern direction, the less solar energy it reaches. If the tilt away from the south direction does not exceed 30^o, the solar insolation reduction of the panel will not exceed 5%. To summarize, deviation of the panel alignment from the south direction to 30^o and a possible change in the tilt angle within 20^o to 50^o do not result in larger losses than 8%. However, larger values of the aforementioned angles will result in a greater reduction in solar insolation for a given panel.
If there is a need for a so-called special photovoltaic installation, e.g., on a summer house, you need to take advantage of the largest insolation during the period when the house is used, i.e., in summer. Then the angle of deviation from the southern direction should not exceed 30^o, while the angle of inclination of the panel should be adjusted to the summer season when the cottage will be used.

3. The background of photovoltaics

3.1 The beginning of photovoltaics

The photovoltaic effect is a phenomenon involving the creation of an electromotive force in a solid under the influence of solar radiation. The photovoltaic effect is used in photovoltaic cells, devices that produce electricity directly from solar radiation. Photovoltaic cells are the basic building blocks of solar cells (also called photovoltaic modules or panels). Based on solar cells, photovoltaic installations are built. The table in Fig. 20 shows some dates related to the discovery of the phenomenon and the modifications made until the beginning of the 21st century (figures in the table are own elaboration, photographs are from: [13], [14], [15], [16], photo of satellite on a base [17]; free license photographs).

Year	Discovery	
1839	Alexander Edmund Becquerel, a French physicist discovers the photoelectric effect. During experiments with electrodes and electrolyte, he noticed that the conductivity increases due to the illumination of the system. The French scientist was 19 years old at the time. During the experiment he used different types of light, he got the best effect with blue light/ultraviolet radiation.	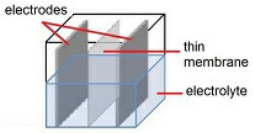 Schematic of the experiment conducted by Becquerel
1873	First observation of the photoelectric effect in a solid by Willoughby Smith.	Willoughby Smith
	W. G. Adams and R. E. Day observe the photovoltaic phenomenon in selenium. They placed a rod of selenium in a glass tube, at the ends of	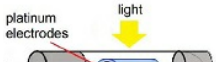

1877	which they mounted platinum electrodes. The purpose of the experiment was to see if a current would be produced in selenium when exposed to light. A positive result of the experiment meant that a simplified model of a photovoltaic cell was created.	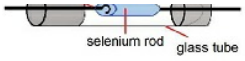 Schematic of Adams and Day's 1877 experiment.
1883	Charles Fritts creates the first selenium cell. It consists of a thin layer of selenium coated with gold. This cell had a very low efficiency of close to 1%.	
1902	Philipp von Lenard discovered a relation between the energy of emitted electrons and the intensity of incident light. Lenard found that the intensity of the photocurrent depended on the intensity of the incident light, while the energy of the electrons was independent of the intensity, a result that contradicted classical electrodynamics theory.	Philipp von Lenard
1904	Wilhelm Hallwachs reveals that the copper junction and copper oxides are photosensitive.	Wilhelm Hallwachs
1918	Jan Czochralski developed a method to produce single crystals of metals and their alloys. This is one of the most common methods for producing e.g. single crystals of silicon.	Jan Czochralski
1932	Audobert and Stora discover the photovoltaic effect in cadmium selenide. Cadmium selenide is sensitive to electromagnetic radiation with a maximum at a wavelength of 730 nm (infrared light). This property makes it possible to use it in the production of photoresistors, phototransistors, optoelectronic elements, infrared radiation detectors, optical sensors or photovoltaic cells.	
1953	Bell Lab, Chapin, Fuller, Pearson - first Li-doped C-Si (4%) cell, stability issues. Dr. Dan Trivich made first theoretical calculation of conversion efficiency for materials with different energy gap widths based on solar spectrum.	
1954	American scientists at Bell Labs - Pearson, Chapin and Fuller - have developed a solar cell with an efficiency of 4%. In a short time they were able to increase the efficiency of the device to 6%. Daryl Chapin was working on selenium solar cells. While experimenting with selenium, he could not exceed 1% efficiency of the cell. Calvin Fuller and Gerald Pearson were working on silicon transistor projects. During one of their experiments, they noticed that the transistor produced an electric current when exposed to light. In 1954, the three of them demonstrated a solar cell that powered a toy windmill and a radio. The cell reached a maximum efficiency of 6%, which made its mass production unprofitable.	
1958	Hoffman Electronics built a solar cell with 9% efficiency. In the same year, solar panels were used on the Vanguard 1 satellite. Subsequent space projects Explorer and Sputnik 3 used solar cells to power some of the on-board equipment (e.g., radios). Photovoltaic power became the standard for space applications and remains so today.	
1959	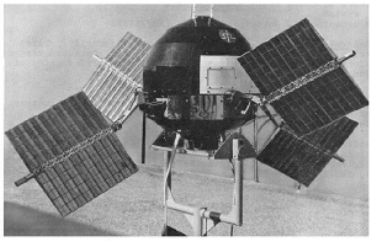 The Explorer 6 satellite is powered by a battery made up of 9600 cells that are 1x2cm in size.	
1959-1960	Hoffman Electronics builds photovoltaic cells with 10% efficiency, then 14% efficiency Silicon Sensors Inc. has begun manufacturing selenium and silicon solar cells.	

Figure 20: History of achievements in photovoltaic effect research (from 1839 to 1960). Own elaboration.

3.2 Photovoltaics at the turn of the 20th and 21st century

The chapter presented here shows the further development of discoveries and achievements in the field of photovoltaics from 1960 to the present (photographs in the Fig. 21 are from [18], [19]; used for educational purposes).

Year	Discovery
1960	A cell research program related to satellites has been developed where high efficiencies, lifetime, and resistance to cosmic radiation are required, while price plays a lesser role. The Vanguard 1 satellite with the 10.4% (AMO) cell operated for 8 years.
1962	Bell Telephone Laboratories has launched the first TELSTAR telecommunications satellite.
1963	Sharp Corporation has begun producing useful silicon modules. The world's largest 242W photovoltaic array was used in Japan.
1964	NASA has launched the first NIMBUS satellite powered by a 470W photovoltaic array.
1966	NASA has launched a satellite observatory powered by a 1kW photovoltaic array to study UVi X-rays.
1970	Dr. Eliot Berman in cooperation with Exxon Corporation developed significantly cheaper photovoltaic cells (price drop from $100 to $20 per Wp). Photovoltaics began to be used in a variety of locations away from conventional power lines.
1972	The French have installed a photovoltaic power system (CdS) to power educational television at a school in Gondel, Nigeria.
1972	The University of Delaware has launched the first Institute of Energy Conversion dedicated to the development of thin film photovoltaics 1 solar thermal systems.
1972	J. H. Mandelkorn and J. Lamneck introduce BSF (Back Surface Field).
1973	Lindmayer and Ellison presented a violet cell with reduced radiation loss in the non-beam/violet region due to the reduction of the n-layer.
1975	Brandt et al. published work on a CNR (Comsat Non Reflecting) cell with a textured top surface with an efficiency of 16%.
1976	NASA John H. Glenn Research Center at Lewis Field - The institute began installing 83 photovoltaic power plants on every continent except Australia. The project was carried out in two periods 1976-1985 and 1992-1995, ending in 1995.
1976	David Carlson and Christofer Wronski of RCA Laboratories have produced the first photovoltaic cell from amorphous silicon.
1977	The U.S. Department of Energy established the Solar Energy Research Institute dedicated to solar energy conversion research, transformed by President George Bush in 1991 into the National Renewable Energy Laboratory.
1977	The production level of solar cells has reached 500kW.
1980	ARCO Solar was the first manufacturer in the world to reach a production level of 1MWp per year.
1980	The first thin-film photovoltaic battery with 10% CuS/CdS efficiency has been fabricated at the University of Delaware.
1981	Paul MacCready built the first solar-powered aircraft, the Solar Challenger, which flew over the English Channel. The plane was powered by 16,000 3kW solar cells.
1982	ARCO Solar has launched California's first 1MW photovoltaic power plant built with 108 dual-axis trackers.
1982	Australian Hans Tholstrup built the first solar-powered car, the Quiet Achiever, which he drove 2,800 miles from Sydney to Perth.
1982	Global photovoltaic battery production reached 9.3 MW.
1983	ARCO Solar launched the production of a 6MW photovoltaic power plant to supply electricity to 2000-2500 households.
1983	Global solar cell production reached 21.3 MW with sales value of $250 million.
1985	The University of South Wales has broken the 20% conversion efficiency barrier for a silicon photovoltaic cell.
1985	Hezel presented a cell with an inversion layer and good passivation of both surfaces with silicon nitride.
1986	ARCO Solar has produced the first photovoltaic commercial thin film panel.
1992	The University of South Florida has produced the first thin-film cell to break the 15% barrier with CdTe at 15.6% efficiency.
1992	Swanson et al. developed a cell with point contacts (22.7%). Contacts-point contacts were located on the back surface, alternating between p and n, high quality n-type silicon.
1992	Green and others at the University of New South Wales, developed a PERL (Passivated Emitter and Rear Locally Diffused) cell - inverted pyramids to minimize reflection, front and back side passivated with oxides - reduce surface recombination, small area metal contacts on top and local p' contacts of the back layer.
1999	National Research Energy Laboratory has developed a photovoltaic thin-film cell with a conversion efficiency of 18.8%.
1999	The global installed level of photovoltaic cells has reached 1GW.
1999	Spectrolab Inc. and the National Renewable Energy Laboratory have built a photovoltaic solar cell with a conversion efficiency of 32.3%. This high efficiency was achieved by building the battery with three layers of semiconductors in a single cell.
1999	The 4 Times Square building in New York is being completed. Between the 37th and 43rd floors on the south and west walls, the façade is clad with photovoltaic cells that supply the building with electricity.
2001	Japan's National Space Development Agency announced a plan for a satellite system with a power plant in orbit. Energy was to be transmitted by laser to an aircraft at an altitude of 12 miles and then to the ground.
2001	NASA has built a solar-powered Helios aircraft that has soared more than 18 miles.
2001	A modified PERL structure with a conversion efficiency of 24.5% is presented.
2002	NASA conducted a test of two solar-powered, remote-controlled flight units (Pathfinder Plus).
2008-2018	Subsequent years have seen the introduction of two types of materials that are growing in competition with silicon. These are perovskite and polymer materials. Both classes of materials are being studied extremely intensively due to the extremely low cost of cell manufacturing and the rapidly increasing conversion efficiencies being achieved in the emerging photovoltaic materials and architectures on the market.

Figure 21: History of achievements in photovoltaic effect research from 1960 to the present. Own elaboration.

3.3 Physical properties of materials used in photovoltaics

Two types of materials are currently used to build solar cells: namely inorganic and organic materials. To understand the performance of solar cells, it is necessary to become familiar with the properties of these materials. In the case of inorganic materials, the crystal structure in which atoms or groups of atoms form a crystal lattice is largely responsible for their properties. The atoms in a crystal lattice are so close together that interactions between them create electron energy bands in place of the quantized energy levels in the isolated atoms.

A simplified model of the energy bands is shown in Fig. 22. It consists of a valence band, an excited band and a conduction band. The valence band (VB) is completely filled with electrons that are not allowed to move in it (the Pauli exclusion principle). The bandgap (so-called energy gap E_g) is an area where electrons cannot reside because there are no energy levels in it. There are no electrons in the conduction band (CB) in the ground state of the atom. When an electron is transferred from the valence band to the conduction band, the possibility of electron transport arises.

Using this model, materials can be divided according to the size of their energy gap E_g. Materials for which the energy gap E_g =

0 are called conductors. Materials with a gap E_g < 3.5 eV are called semiconductors, and insulators are materials with a very large energy gap E_g > 3.5 eV.

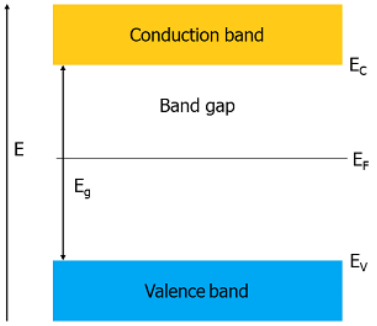

Figure 22: Schematic of the energy band model: E_g - width of the excited band, E_C - bottom of the conduction band, E_F - Fermi level, E_V - top of the valence band energy level. Own elaboration.

In the energy band model, it is useful to use the concept of the Fermi level. The Fermi level E_F is the theoretical value of the energy of an electron in a semiconductor such that the probability of occupying the VB and CB bands is 50%. In a dopant-free (self-consistent) semiconductor, the Fermi level lies halfway between VB and CB.
This simplified model is presented for easier understanding of the behavior of electrons in the crystal lattice of a semiconductor. The detailed model describing the electron behavior is more complex.
Current conduction in semiconductors in the bandgap model can be represented as follows. Electrons are strongly bonded in the lattice and it takes considerable energy to release them from the valence band. This is equal to the bandwidth of the excited band E_g. An electron released from the valence band can move under the influence of an applied electric field. A positively charged ion remains after the released electron. The positive charge thus formed can move in the crystal lattice from atom to atom as the missing electron can be replenished from the adjacent bond and so on. Such movement of positive charges is called hole motion. Electron transport takes place in the conduction band where electrons can move freely. The transport of holes takes place in the valence band. Without an external electric field, the motion of charges is chaotic and disorderly. Application of an external electric field brings order to the movement of holes and electrons, causing current to flow.
Semiconductor materials are, for example, crystals of atoms in group 4 of the periodic table and the compounds shown in Fig. 23. The table in the figure also presents the properties of these compounds, namely the magnitudes of the energy gap, their electron mobility and hole mobility, which are the basic parameters that characterize semiconductors (the data for the table are taken from [20]). Properties of diamond are also given for comparison. The mobility of charge carriers is expressed by the relationship between the drift velocity of the charges and the intensity of the external electric field.

Crystal	Energy gap E_g [eV]	Electrons mobility [cm²/(V*s)]	Holes mobility [cm²/(V*s)]
Diamond	5.33	1800	1200
Si	1.12	1600	400
Ge	0.67	3800	1800
InSb	0.23	77 000	1250
InAs	0.33	23 000	100
InP	1.25	3 400	650
GaSb	0.78	2 500 - 4 000	650
PbS	0.34-0.37	600	200
PbSe	0.27	900	700
PbTe	0.30	17 000	-
AgCl	3.2	50	-
KBr (100°K)	-	100	-

Figure 23: Energy gap values and carrier mobility values at 20°C. Own elaboration.

The mobility of holes in semiconductors is much smaller than that of electrons. This is due to the electrons being bonded to atoms, making it difficult for them to jump to another atom (the hole therefore has a larger so-called effective mass and moves slower - a simplified explanation). The magnitude of the energy band gap of the absorbed E_g indicates the minimum energy of a quantum of radiation that can be absorbed by a semiconductor.
Example:
The maximum wavelength that can be absorbed by a semiconductor can be calculated from :

$$E_g = \frac{1240}{\lambda}$$

where E_g– energy break $[eV]$, λ– wavelength $[nm]$, 1240 $[eV \cdot nm]$.

Using this formula and the Si energy gap, one can easily calculate up to what wavelength solar radiation will be absorbed in a silicon semiconductor. For example, for E_g=1.12 eV the maximum wavelength absorbed by a Si semiconductor is λ_{max} =1100 nm.
The physical properties of semiconductors strongly depend on temperature, e.g., resistivity decreases with increasing temperature.
If the semiconductor crystal is perfect, we say that we are dealing with an intrinsic semiconductor. In an intrinsic semiconductor, the number of electrons in the conduction band is equal to the number of holes in the valence band. The replacement of an atom in the crystal lattice of a semiconductor by another atom is called doping.

The physical properties of semiconductors strongly depend on temperature e.g., the resistance decreases with increasing temperature. If a semiconductor crystal is perfect, we say that we are dealing with an intrinsic semiconductor. In an intrinsic semiconductor, the number of electrons in the conduction band is equal to the number of holes in the valence band. The replacement of an atom in the crystal lattice of a semiconductor by another atom is called doping. The properties of semiconductors depend very strongly on the degree of doping, that is, the number of atoms introduced into the crystal lattice of the semiconductor. The atomic dopants from group 3 of the periodic table introduced into the semiconductor crystal cause electron deficiency and electron capture from the neighboring atom in which the positive charge remains (so-called hole). Such a semiconductor is called a p-type. It conducts via holes, which are majority charges (holes in p-type semiconductors, electrons in n-type semiconductors).
The introduction of p-type dopants creates an energy level in semiconductors, called the acceptor level, in which electrons from the valence band are bound. These electrons leave behind a gap in the valence band that can move and thus is considered a positive charge carrier (Fig. 24). This results in lowering the position of the Fermi level.

The doping with atoms from group 5 of the periodic table into the crystal of an intrinsic semiconductor results in an n-type semiconductor (Fig. 24). Excess electrons are released and form an additional band in the excited region near the conduction band. Such a semiconductor conducts current with electrons that are majority charges. The Fermi level is displaced towards the conduction bands compared to an intrinsic semiconductor.

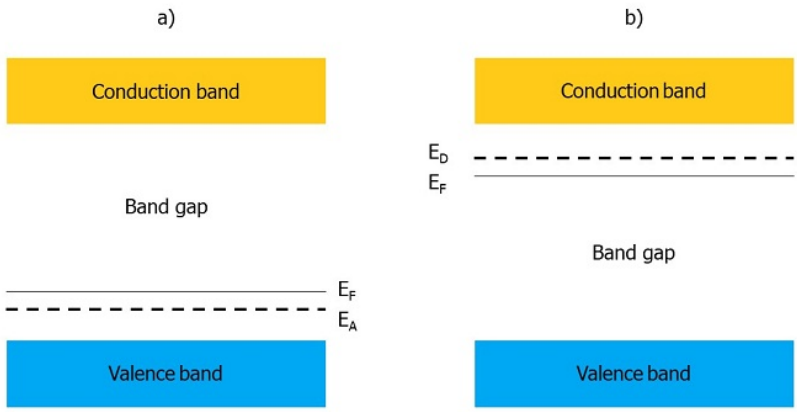

Figure 24: Energy structure of semiconductors: a) p-type acceptor and b) n-type donor. E_F - Fermi levels, E_A - acceptor levels, E_D - donor levels. Own elaboration.

Fig. 24 shows the changes in energy levels produced by the introduction of doped atoms into the intrinsic semiconductor. The introduction of atoms from group 3 of the periodic table creates a p-type semiconductor with an additional energy level E_A – acceptor level (a), and the addition of group 5 atoms creates an n-type semiconductor with an additional energy level E_D – donor level (b). This causes a shift of the Fermi level E_F towards the valence band for doping with atoms from group 3 of the periodic table and towards the conduction band for n-type semiconductors. For a p-type semiconductor, the resulting dopant energy level is called acceptor, and for an n-type semiconductor, the dopant energy level is called donor.

3.4 The p-n junction

N-type semiconductors are characterized by electron conduction, while p-type semiconductors conduct mostly through holes. In conductors, electrons are free charge carriers forming an "electron gas" (the Drudy-Lorentz theory) [21]. The consequence of the possibility of free movement of electrons is high conductivity in metals. In semiconductors, on the other hand, valence electrons are bonded to atoms and only some of them, after being pulled out of valence orbitals, take part in current flow.
The introduction of dopants into semiconductors generates an increase in the concentration of majority charges. For donor dopants these are electrons, and for acceptor dopants these are holes.
The transport of electrons from the valence level to the conduction band is accomplished by absorption of electromagnetic radiation energy or thermal energy. The absorbed energy should be greater than the energy gap E_g. Thanks to their properties,

semiconductors have been used in many technology domains. The quantities influencing the electro-optical properties of semiconductors are: mobility of charge carriers, expressing the relationship between the charge drift velocity and the external electric field, quantum properties such as the lifetime of electrons in individual states, and the absorption coefficient, which depends on the wavelength. These properties determine the possible use of semiconductor materials for the production of solar cells.
Connecting n-type and p-type conductors creates at their boundary a so-called p-n type junction (Fig. 25). The formation of the junction results in the flow of electrons from the n-type region to the p-type region and the formation of holes in the n-type region. The separation of electrons (-) and holes (+) leads to an electric field that produces a potential barrier.

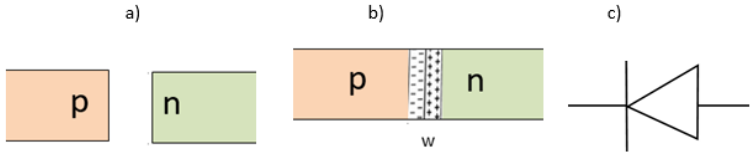

Figure 25: Semiconductors p and n before bonding with no charge (a) and (b) after the bonding of semiconductors p and n, a depleted region w is formed, an electric field appears, (c) symbol of a semiconductor diode. Own elaboration.

When p-type and n-type semiconductors are combined, the Fermi levels are aligned, as visualized in Fig. 26. This causes a curvature of the valence and conduction levels in the region (width of the p-n junction). A layer is formed at the junction where charges exist that cause the disruption of the levels. This is a layer that is depleted of positive charges on one side and negative charges on the other.

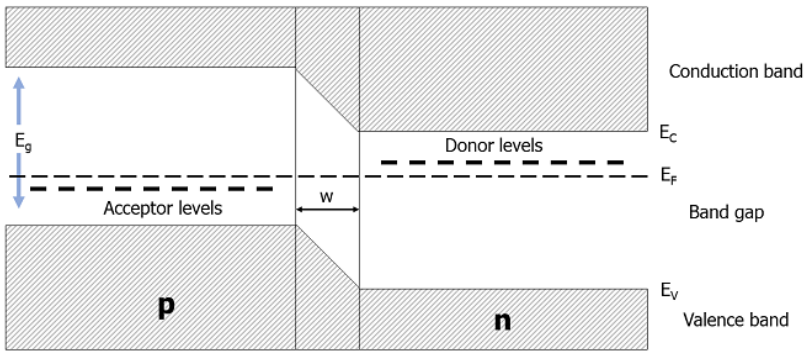

Figure 26: Energy levels at the junction of p- and n-type semiconductors. E_f - Fermi energy, w - width of the p-n junction region, E_g - energy gap in a semiconductor, E_c - energy level of conduction band, E_v - energy level of valence band. Own elaboration.

Such an array of semiconductors is called a semiconductor diode.

Connecting a p-type semiconductor to a positive potential and an n-type semiconductor to a negative potential - that is, applying an external electric field - causes the potential barrier to decrease and the width of the p-n junction region to decrease. There is a flow of electrons from the p area to the electrode and an injection of electrons from the other electrode to the n area of the semiconductor, current flows through the system (Fig. 27 on the positive side of the voltage). Reverse polarization increases the height of the potential barrier and the width of the depleted region, and no current flows through such a circuit (Fig. 27 on the negative voltage side). The junction of a semiconductor p and n is called a diode.

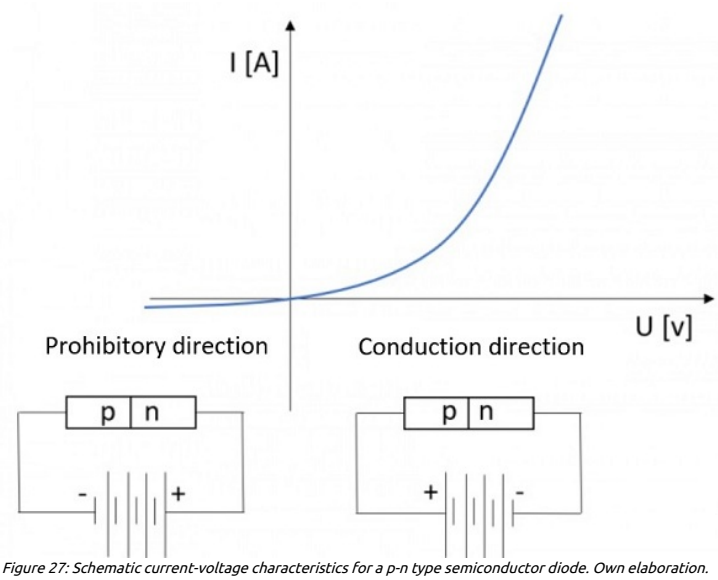

Figure 27: Schematic current-voltage characteristics for a p-n type semiconductor diode. Own elaboration.

The properties of semiconductor diodes are used in a number of different ways. Depending on their structure and purpose, they include rectifier diodes, capacitive diodes, light emitting diodes, laser diodes, pulse diodes, tunnel diodes, Zener diodes, and photovoltaic diodes. A diode used to convert solar energy into electricity is called a photovoltaic cell shown in Fig. 28.
Absorption of incident photons on a photovoltaic diode results in the transfer of an electron from the valence band to the conduction band and the formation of a hole-electron pair. This pair can move in a semiconductor. The binding energy of the hole-electron pair is at an energy level of 16 meV (the thermal energy at room temperature is 25 meV). The hole-electron pair called an exciton decays into a free electron and a free hole [22]. Free electrons are attracted by the positive space charge at the p-n junction. The holes are transferred to the p-type region. The separation of positive and negative charges produces a potential difference.

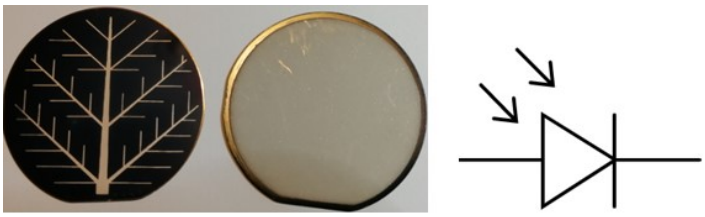

Figure 28: Photovoltaic cell (photovoltaic diode) and its symbol. Own elaboration.

A cross section through the structure of a simple monocrystalline photovoltaic cell is shown in Fig. 29, [23]. The following elements are present:

- the front electrode - on the side of the incident sunlight,
- n-type layer – up to 2 µm thick,
- n-p junction layer,
- p-type layer – 100-300 µm thick layer,
- back electrode (from the side opposite to incident sunlight).

A photovoltaic cell is a diode in which hole-electron pairs are additionally produced under the influence of electromagnetic radiation. The cell structure - as shown in Fig. 29 - is used for all inorganic materials that photovoltaic cells are made of.

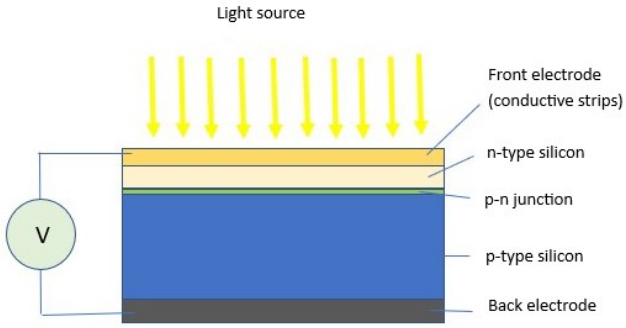

Figure 29: Structure of a monocrystalline solar cell. Own elaboration.

The case is different for organic compounds. For organic semiconductors, single molecules are considered. Each molecule is characterized by energy levels. In the ground state, all levels are occupied up to the Highest Occupied Molecular Orbital called HOMO (Fig. 30a). Above these there are unoccupied levels. The Lowest Unoccupied Molecular Orbital is called LUMO. The difference between the positions of the HOMO and LUMO levels is treated in organic materials as an energy gap E_g.
These levels in organic semiconductors are treated as equivalents of the valence and conduction bands in inorganic semiconductors. The energy structure of the molecules is shown in (Fig. 30a). These apply only to the one molecule.
An incident radiation quantum, when absorbed, will transfer an electron from the HOMO level to the LUMO level in the molecule. The hole-electron pair thus formed (called an exciton) can move through the material. In organic compounds, the binding energy of the exciton is at the level of 0.4 eV. To break the resulting exciton in organic materials, energies much higher than in inorganic semiconductors are required.

The arrangement of two molecules with different HOMO-LUMO levels results in a potential difference (Fig. 30b). The exciton, upon encountering such an arrangement, can be separated into charges. The resulting positive and negative charges in this system are in the same region, which unfortunately allows them to recombine. To force a proper flow of charges, electrodes with different exit works (W_w) are used. The work of exit is the least amount of energy required for an electron to leave a material and become a free electron. A metal electrode with a smaller exit work accumulates electrons, while an electrode with a larger one accumulates holes.

Thus, for photovoltaic cells made of organic semiconductors, contact electrodes play an important role.

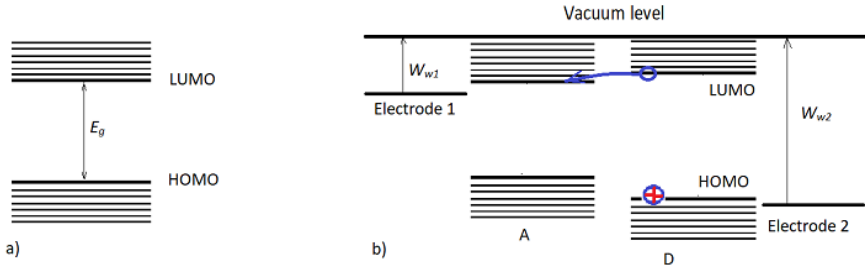

Figure 30: (a) Energy levels in an organic molecule, (b) Energy levels of an organic photovoltaic cell. Own elaboration.

3.5 Physical fundamentals of solar energy conversion to electricity

When two types of semiconductors are joined together, a p-n junction (Fig. 31) with specific energy characteristics is produced. This is due to the excess of free electrons in the n-type semiconductor and holes in the p-type semiconductor. When they are combined, the electrons move to the p-type semiconductor and the holes move to the n-type semiconductor, causing a charge imbalance and creating a potential difference.

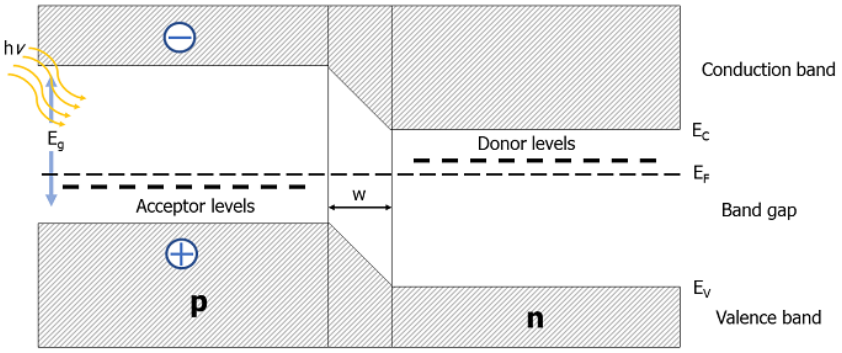

Figure 31: Structure of a semiconductor p-n junction and mechanism of charge generation by electromagnetic waves. Own elaboration.

The delivery of energy in the form of radiation quanta to the atoms of the crystal lattice (depending on the energy gap) can move electrons into the conduction band [24]. For this process to occur, radiation quantum $h\nu$ has to have an energy level greater than the energy gap E_g ($h\nu > E_g$) (h – Planck's constant, ν – frequency).
An exciton can dissociate into charges when exposed to temperature or an electric field. The exciton can travel through the semiconductor until it hits a region where an electric field is present. The electric field present at a p-n junction allows charges to separate. Positive charges accumulate in the p-type semiconductor and negative charges accumulate in the n-type semiconductor.

Light absorption can occur in the n-type region and the p-type region. The charges created by the break-up of the exciton move toward the electrodes. When a receiver is connected to the electrodes, an electric current will flow through it. The current-voltage characteristics of such a semiconductor junction are shown in Fig. 32. If such a junction is not illuminated, the characteristic I(U) will be obtained, the so-called dark characteristic, without illumination (one can say an ordinary diode characteristic). If the p-n junction is illuminated, the I(U) characteristic of the illuminated solar cell is bright.

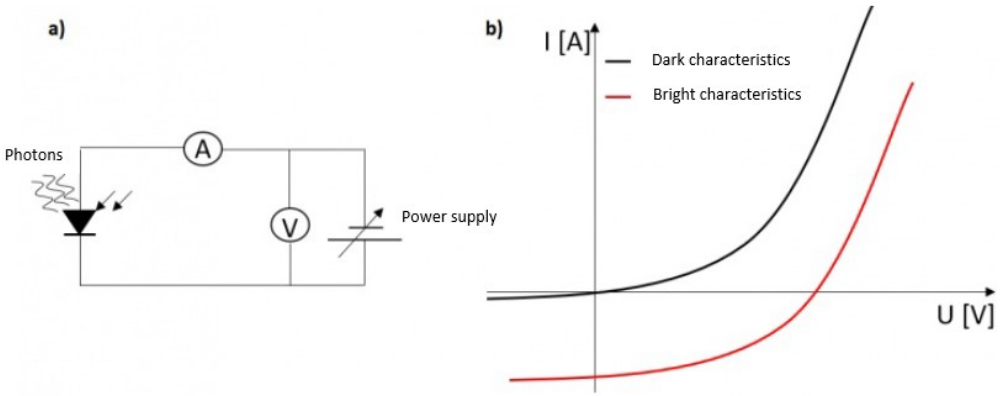

Figure 32: a) Scheme of the circuit for measuring I(V) characteristics of a photovoltaic diode and b) Current-voltage characteristics of a semiconductor junction for a cell unlit (dark characteristics) and lit (bright characteristics). Own elaboration.

The amount of light energy absorbed depends, among other things, on the size of the energy gap (Fig. 33). The quantities shown in the table are the maximum amount of solar energy (in $\%$), that can be absorbed at a given energy gap. If the gap is greater than 4 eV, no part of the solar radiation reaching the Earth will be absorbed because the solar radiation quantum has an energy lower than 4 eV (see solar spectrum figure).

E_g [eV]	4.1	3.5	2.8	2.3	1.9	1.7	1.5	1.3	1.03	0.95	0.69	0.62	0.50
Amount of solar energy [%]	0	0.7	7.6	21	35	48	59	67	81	86	96	97	100

Figure 33: Value of absorbed solar radiation in percentage, depending on the size of E_g energy gap expressed in eV. Own elaboration.

The assumption here is that solar radiation in the region from 300 nm to 2500 nm represents 100% of the radiation. For example, a semiconductor with an energy gap of 1.03 eV can maximally absorb 81% of the solar energy reaching the cell.

Conversion of sunlight energy to electricity is accomplished by several physical processes shown in Fig. 34. After light is absorbed, an exciton is created, which then breaks into charges. The charges move toward the electrodes where they accumulate.
Each of these processes is subject to losses due to imperfections in the device [25].
The incoming light radiation quanta are partially absorbed by the semiconductor material, some of the radiation is reflected from the diode surface, and the remaining unabsorbed radiation undergoes transmission.
The absorbed radiation quantum results in the formation of an exciton (Fig. 34), which can travel through the semiconductor material but can also annihilate, turning into heat. The exciton breaks to form free positive and negative charges. The charges travel to the electrodes. During this process, there are losses associated with charge recombination, mobility limitation, and resistance at the semiconductor-electrode interface.

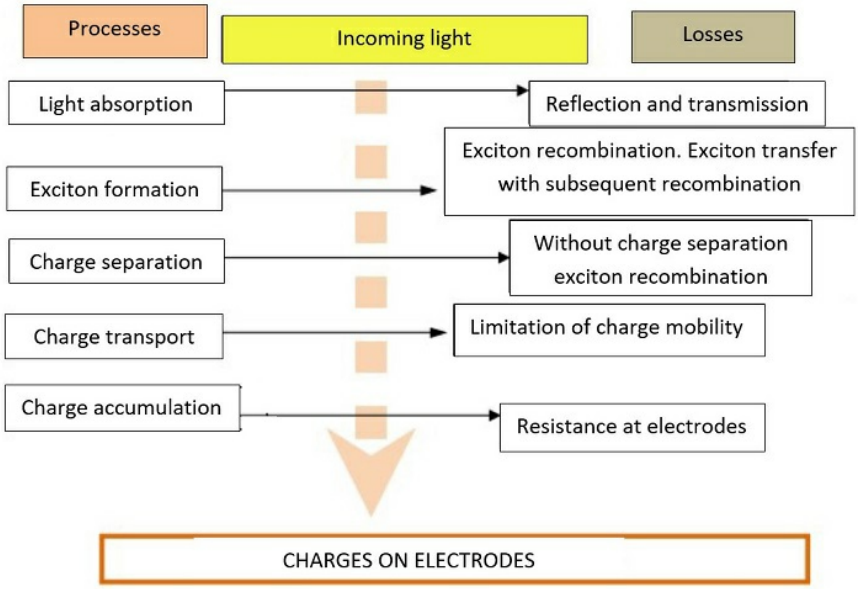

Figure 34: Processes occurring during energy conversion in a photovoltaic diode. Own elaboration.

Some of the losses can be eliminated during the construction of a photovoltaic cell, therefore work is still underway to increase the efficiency of solar radiation energy conversion. Materials for photovoltaic cells should have a number of properties such as:

- the widest possible spectral region (table in Fig. 34),
- creation of the highest possible number of excitons,
- high mobility of electric charges,
- easy transport of charges to electrodes.

Data on the efficiency gains of photovoltaic panels produced with new or modified materials are published annually by the NREL (see chapter: 5.2 Changes in conversion efficiency).

3.6 Photovoltaic cell parameters

Many scientific and industrial laboratories around the world are involved in testing the performance of photovoltaic (PV) cells. From this fact, the need for unified standards for performing these measurements arises. Standard Test Conditions (STC) have been developed for PV cells and panels [26]. These conditions define the parameters for conducting the tests:

- illumination with light of solar spectrum AM 1.5 SPECTRUM,
- illumination intensity per unit area P_{light} = 1000 $\frac{W}{m^2}$ (so 100 $\frac{mW}{cm^2}$),
- temperature measurement 25 ^{o}C.

Conducting tests under standard conditions allows direct comparison of results from different laboratories.

The purpose of the study is to determine the parameters of cells and panels [27]. The basic measurement of a photovoltaic cell is to examine its current-voltage characteristics $I(U)$.
An important parameter of the cell is to determine the efficiency, which is determined from the characteristic $I(U)$. The efficiency of a photovoltaic cell is the amount of maximum electrical power obtained from the PV cell, that is P_{max} to the power provided by solar radiation P_{light}.
The efficiency of a photovoltaic cell is expressed by the following formula:

$$\eta = \frac{P_{max}}{P_{light}} \tag{6}$$

The current-voltage characteristic for the photovoltaic cell is shown in Fig. 35.

From the current-voltage characteristic waveform for a PV cell, the maximum power that can be obtained from the cell under a given illumination is determined. The power maximum P_{mm} is the maximum area of the rectangle $U * I$. For the maximum power point P_{mm} the voltage value V_m, at which the power is maximum and the current value I_m, at which the power maximum are determined.

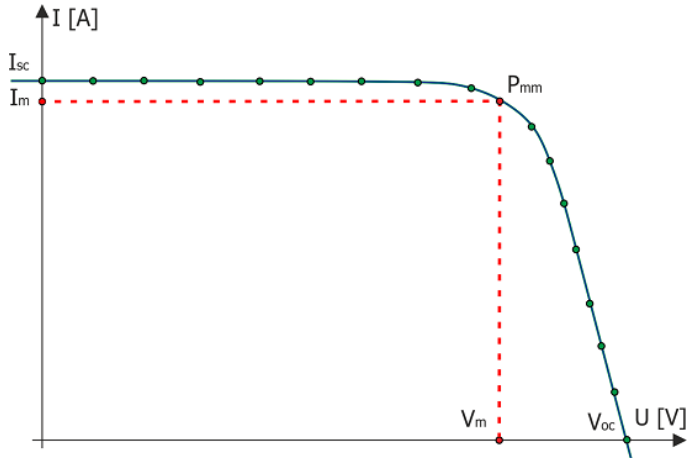

Figure 35: Current-voltage characteristics of the illuminated photovoltaic cell, V_{oc} - open circuit voltage, I_{sc} - short circuit current, P_{mm} - maximum power point, I_m - current at the point of maximum power, V_m - voltage at the point of maximum power. Own elaboration.

The term fill factor FF is also used. The fill factor is the ratio of the maximum power received from a photovoltaic cell P_{max} to the product of the open circuit voltage V_{oc} and the short circuit current I_{sc}. The value of the fill factor is determined from:

$$FF = \frac{P_{max}}{I_{sc} * V_{oc}} \tag{7}$$

The efficiency of photovoltaic cells made of monocrystalline silicon in 2019 is about 26%, and for multicrystalline cells the efficiency is about 23%. As the temperature increases, the efficiency of PV cells decreases on average by 0.2% for each degree of temperature increase above STC conditions. If the temperature rises by 20 ^{o}C then the efficiency decreases by about 4% of the nominal value - that is, the panel with an efficiency of 25% will have an efficiency of 24% after a temperature increase of 20 ^{o}C.
By entering a fill factor into the equation for the efficiency of the photovoltaic cell, the equation for the efficiency η takes the following form:

$$\eta = \frac{FF * I_{sc} * V_{oc}}{P_{light}} \tag{8}$$

The efficiency of the cell depends on the wavelength and absorption coefficient. Considering these parameters, the above equation takes the form:

$$\eta(\lambda) = \frac{FF(\lambda))*I_{sc}(\lambda)*V_{oc}(\lambda)}{P_{light}(\lambda)} \tag{9}$$

Because of the above relationship, it is important to measure the absorption spectra of the materials that make up the PV cell.

The magnitudes of changes in these parameters are given in the data sheets of photovoltaic panels. An example of such a data sheet is the JASOLAR JAM60S09 data sheet $I(U)$ [28] in which data can be found indicating that the voltage V_{oc} decreases as the temperature increases.

In summary, the characteristic quantities of a PV cell are:

- η – the power conversion efficiency factor of a PV cell under STC conditions,
- V_{oc} – open circuit voltage,
- I_{sc} – short circuit current,
- V_m – voltage at which maximum power is transferred to the load,
- I_m – current at which maximum power is transferred to the receiver,
- FF – fill factor,
- P_{max} – the maximum power that can be obtained from the PV cell,
- $\alpha_{I_{sc}}$ – temperature coefficient I_{sc} in units of $\%$ / ^{o}C,
- $\beta_{V_{oc}}$ – temperature coefficient V_{oc} in units of $\%$ / ^{o}C,
- γ_{Pmp} – temperature coefficient of power P_{max} in units of $\%$ / ^{o}C.

In addition to these parameters, the coefficients of change of PV cell properties with time are very often given. Furthermore, the operating time of the cell with an efficiency not less than 90% is given.

3.7 Cell's model

The equivalent circuit diagram of a diode is used to analyze its electrical characteristics. The equivalent circuit diagrams for a rectifying diode and a photovoltaic diode are shown in Fig. 36. The equivalent circuits [7] differ for a photovoltaic diode that there are additionally sources that generate current I_L under the influence of solar radiation (Fig. 36b).

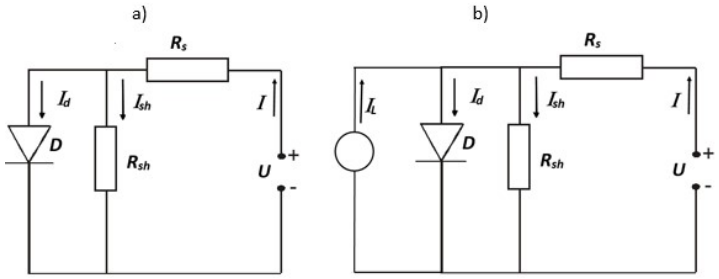

Figure 36: Equivalent circuit diagram (a) for rectifier diode, (b) for photovoltaic diode. Own elaboration.

The circuit contains the following components: D - diode, R_{sh} – shunt resistor representing the resistance resulting from surface recombination of charge carriers, R_s – a shunt resistor representing the sum of series resistances in an external circuit. An equivalent circuit diagram of the PV cell, including the semiconductor diode elements and the current source I_L is shown in Fig. 36b.
Using the equivalent circuit of the solar cell (Fig. 36b) and Kirchhoff's laws (the juncktion law and the mesh law), the following relation can be formulated:

$$(I_L - I_d - I)R_{sh} = U + IR_S \tag{10}$$

where $I_{sh} = I_L - I_d - I$
which can be converted to the form:

$$I\left(\frac{R_s}{R_{sh}} + 1\right) = I_L - I_d - \frac{U}{R_{sh}} \tag{11}$$

The Shockley diode equation [29] describes the current dependence of the voltage of an ideal diode I_d :

$$I_d = I_o\left(e^{\frac{U-IR_s}{nkT/q}} - 1\right) \tag{12}$$

and inserting I_d from equation (12) into equation (11) yielded the relationship for current I:

$$I = \left(I_L - \frac{U}{R_{sh}}\right)\frac{R_{sh}}{R_{sh}+R_s} - I_0\frac{R_{sh}}{R_{sh}+R_s}\left(e^{\frac{U-IR_s}{nkT/q}} - 1\right) \tag{13}$$

Due to the complexity of the equation, DERIVE software was used to determine the current-voltage characteristics and the

power versus voltage relationship. The characteristics are shown in Fig. 37.

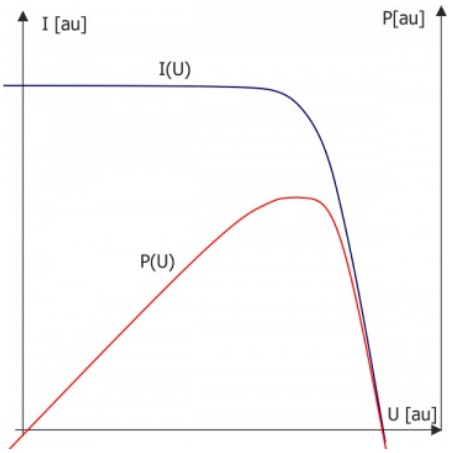

Figure 37: Typical current-voltage characteristic I(U) of PV cell, characteristic of PV cell power change as a function of voltage P(U). Own elaboration.

The obtained relation $I(U)$ is a typical characteristic obtained for photovoltaic cells and has a good agreement with the waveform obtained experimentally. The presented power-voltage dependence $P(U)$ is characterized by the maximum power that can be received from the photovoltaic cell. The maximum power drawn from a system with the characteristics as shown in the figure is at 0.55 V.
The equation (13) describes the operation of the PV cell, and specifically shows the effect on the behavior of current-voltage characteristics caused by series resistance R_s, parallel resistance R_{sh}, the current I_l dependent on illumination intensity, and changes in temperature T. The changes of current-voltage characteristics under the influence of changes in series resistance are shown in Fig. 38. The direction of increase in series resistance is shown by an arrow.

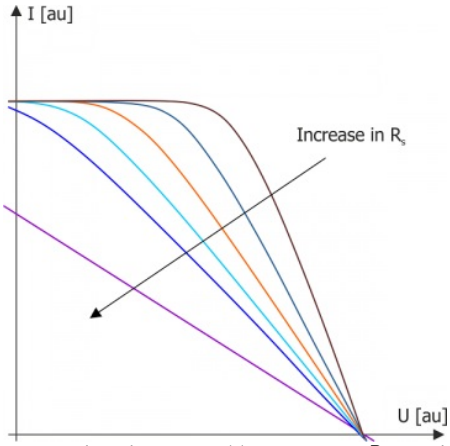

Figure 38: Current-voltage characteristics I(U) versus increase in R_s. Own elaboration.

Increasing series resistance reduces the open circuit voltage U_{oc}, which reflects negatively on the power that can be generated from the PV cell.

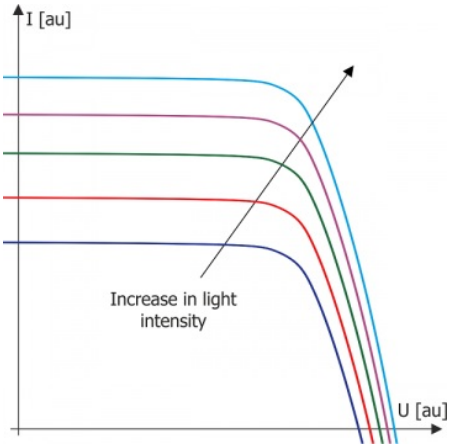

Figure 39: Current-voltage characteristics of I(U) versus irradiance. Own elaboration.

The increase in irradiance is indicated by an arrow in Fig. 39. The increase in irradiance raises the current I_{sc}, while the open circuit voltage U_{oc} increases slightly. The obtained result is consistent with the experimental data.

Current-voltage characteristics for different radiation intensities are shown in Fig. 39.

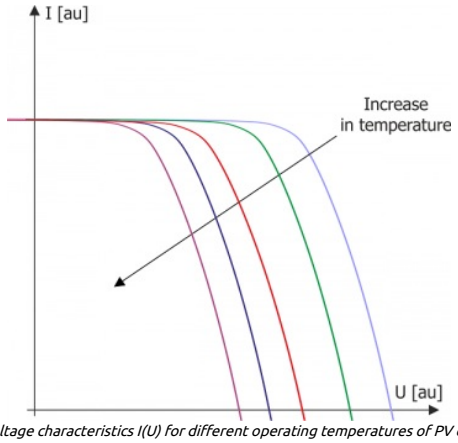

Figure 40: Current-voltage characteristics I(U) for different operating temperatures of PV cell. Own elaboration.

Increasing the operating temperature of the cell reduces the voltage U_{oc} generated by the sunlight. It also reduces the power that can be received from the cell for higher temperatures. The current-voltage characteristics for different operating temperatures of the cell are shown in Fig. 40.

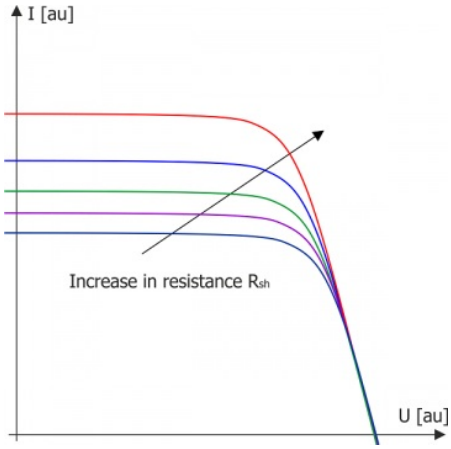

Figure 41: Current-voltage characteristics I(U) for different values of parallel resistance R_{sh} at constant resistance R_s. Own elaboration.

For larger resistance values R_{sh} increases the current and thus the efficiency of converting light energy to electricity. The open circuit voltage changes slightly. If the ratio of R_s/R_{sh} is of the order 10^{-3} or less, then changing the resistance of R_{sh} does not change the I(U) characteristic. The current-voltage characteristics for different values of parallel resistance R_{sh} at constant resistance R_s are shown in Fig. 41.
The obtained current-voltage characteristics determined from the adopted model show good agreement with the experimental results. In order to take into account all processes occurring in the cell, the cell equivalent diagram was modified by additional diode D2 [30], responsible for processes not included in diode D1.

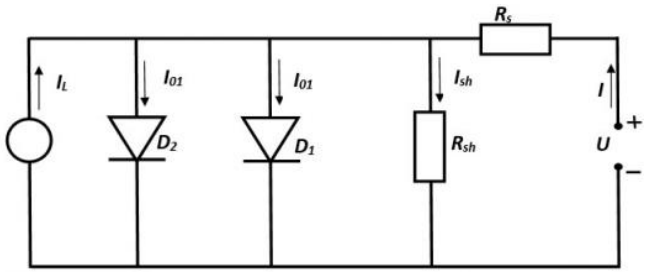

Figure 42: Equivalent circuit diagram of a photovoltaic cell. Own elaboration.

The equivalent circuit model of the photovoltaic cell with the additional diode shown in Fig. 42 [31]. Considering the above system, we obtain a more elaborate formula describing the model used [32]:

$$I = \left(I_L - \frac{U}{R_{sh}}\right)\frac{R_{sh}}{R_{sh}+R_s} - I_{01}\frac{R_{sh}}{R_{sh}+R_s}\left(e^{\frac{U-IR_s}{n_1 kT/q}} - 1\right) - I_{02}\frac{R_{sh}}{R_{sh}+R_s}\left(e^{\frac{U-IR_s}{n_2 kT/q}} - 1\right) \tag{14}$$

where:
I – current in the external circuit,
I_L – current generated by the photovoltaic cell,

I_{01} – the saturation current of the dark current diffusion component,
I_{02} – saturation current of the dark current generation-recombination component,
U – voltage supplied to the system (measurement),
R_s – series resistance of the photovoltaic cell,
R_{sh} – the parallel resistance of the photovoltaic cell,
n_1 – diode quality factor (value close to 1),
n_2 – diode quality factor (value close to 2).

Extending the photovoltaic cell model with further processes occurring during current generation results in more complex algebraic equations describing these phenomena.
To simulate the current-voltage characteristics of a photovoltaic cell various mathematical programs are used, e.g., MATHEMATICA or DERIVE.

4. Components of a cell structure

4.1 Photovoltaic cell structure components

Photovoltaic cells and panels are multilayer structures (Fig. 43, Fig. 44).

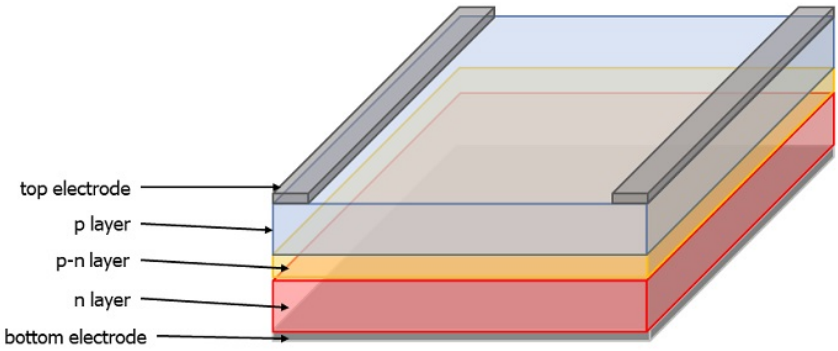

Figure 43: Schematic of the cell construction. Own elaboration.

Some cell components come in a few generations. In addition to the conceptually different active layers in which the photovoltaic phenomenon occurs, each cell includes contact electrodes. The cell electrode located on the side of the Sun may have the form of a thin-film transparent electrode, strips of silver and aluminum paste (busbar electrode), or thin conductive wires (smart wire). The counter-electrode is usually shaped like a metallic aluminium layer. There are also constructions in which both electrodes are placed at the back (so-called HIT, Heterojunction with Intrinsic Thin Layer). By the top electrode we still mean the layer on the Sun side (on which the Sun's radiation falls), while by the bottom electrode we mean the electrode not directly illuminated by the Sun. An encapsulant is used to provide insulation, encapsulation and protection against mechanical and chemical damage to the cell. Polymer films are used for this purpose. The most common material is EVA (ethylene vinyl acetate). The top surfaces in cells are covered with anti-reflective layers [33].
The functions of these layers are detailed in the sections: 4.4 Antireflective layers, 4.5 Passivation layers.

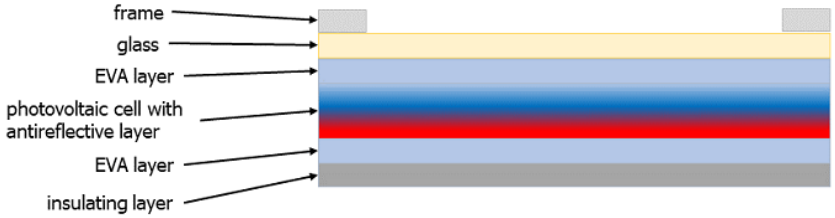

Figure 44: Schematic of cell panel construction. Own elaboration.

4.2 Metallic electrodes

Metallic electrodes, as well as transparent electrodes, are responsible for the current flow from the photovoltaic cell into the circuit and therefore have a significant influence on its electrical parameters. Depending on geometry and architecture, we distinguish between electrodes in the form of thin horizontal tracks (**busbar**[1]), as thin conductive wires (**smart wire**[2]) and the electrodes on the back of the cell (**HIT**[3]).
To ensure that the charge generated by the cell is transferred to the external circuit, it is important to have the lowest possible resistance between the semiconductor material that makes up the active layer of the cell and the metallic electrode. This resistance between the semiconductor and the metal can be linear or non-linear. The occurrence of linear (ohmic) or non-linear

(Schottky) conductivity is determined by the parameters of the materials used. The contact should not influence the current-voltage characteristics of the cell [34]. In practice, the resistance of a cell is influenced by the length of distance an electrical charge has to travel in a plate, an important parameter of electrode materials is the work function of an electron from a metal (Fig. 45 based on [20]). The second parameter affecting the type of conductivity is the Fermi level of the semiconductor.

metal	work function for atoms in polycrystalline form [eV]
silver	4.3
calcium	2.8
indium	4.1
gold	5.1
aluminium	4.3

Figure 45: Work function for polycrystalline materials form. Own elaboration.

The most commonly used electrode material is silver, but other materials such as aluminium and copper are also being implemented. In CIGS cells, molybdenum and aluminium are used [35], [36].

The method most commonly used to apply contacts is screen printing. In order to maintain a large open area of the screen and to produce precise patterns, meshes with increasingly thin stainless-steel wires are used. The advantages of screen printing are the high throughput of the process and the wide availability of materials. Thin film technologies are also being developed (e.g., aerosol jetting).

Przypis

1. Busbar cells are described in chapter: 6.1 Busbar cells.
2. Smartwires are described in chapter: 6.4 Smartwires cells.
3. See chapter: 6.5 HIT technology cells.

4.3 Transparent and conductive electrodes

To ensure the highest possible efficiency in energy conversion, it is necessary to create a design in such a way that as much of the sunlight's energy as possible reaches the absorber. For this purpose, conductive metal oxides are used in solar cells as transparent electrodes.

Most materials that transmit visible light well are insulators. The materials to be used as electrodes become semiconductors after doping and should have a resistivity higher or equal to $10^{-3}\Omega \cdot cm$. A charge carrier concentration of the order of $10^{20} cm^{-3}$. Oxides meeting the above conditions are called transparent conductive oxides (TCO) [37].

The most common material used as a transparent electrode is indium tin oxide (ITO). When used as a transparent electrode, ITO is a mixture of 74% In, 18% O_2 i 8% Sn, by weight. Its energy gap is 3.5- 3.7 eV [38]. The gap width determines the optical properties of ITO. Due to the high concentration of carriers ($10^{20} - 10^{21} cm^{-3}$) ITO conductivity is approaching the level of metallic conductivity. The average thickness of an ITO electrode layer in a photovoltaic system is about 100 nm.

A second common semiconductor material is fluorine-doped tin oxide (FTO) [39]. In the visible range, it achieves a transmission of up to 80% and has a lower surface resistivity (resistance of the material calculated per unit area) than ITO (7~13 $\Omega \cdot m$) [40]. It is a promising material due to its time stability of performance under atmospheric conditions, chemical inertness, strength and abrasion resistance. The FTO energy gap is about 3.80 eV [41].
The transmission of both ITO and FTO is over 80%, and the differences in properties (e.g., absorption spectrum, conductivity) are strongly dependent on the degree of doping, method of application, thickness and other parameters [42], [43].

Zinc oxide ZnO:Al (AZO) doped (usually aluminium) is also used as a transparent electrode [44].
Depending on the amount and type of doping, it shows a change in electrical conductivity in a wide range: from metal conductivity to insulators. For electrode applications, a wide energy gap (3.3 - 3.6 eV) and high transparency are also important [45], [46], [47].

Other transparent metal oxides include $ZnSnO_4$, Cd_2SnO_2, and also CdO (because od their toxicity) Cd oxides have not come into use.
Attempts are being made to use electrode layers made of polymeric materials, e.g., PEDOT, i.e. poly(3,4-ethyl-1,4-dioxytiophene) or its mixture with the polymer PSS (polystyrene sulphonate). PEDOT:PSS is a mixture of polymers with an exit work of - 5.2 eV. PEDOT alone is insoluble, only its combination with the water-soluble PSS polymer allows wet application on flexible surfaces [48].
Graphene electrodes are also proposed as part of research into new materials [49], [50], however, despite promising results from

both transparency and resistance studies, they are not yet widely used.

Despite the development of new materials, ITO and FTO remain the most common transparent electrodes. The price of indium, however, is regularly increasing, which translates into rising costs of electrodes made of this material (FTO is cheaper than ITO). Due to the lower price, the popularity of FTO is increasing [51].

4.4 Antireflective layers

The reflection of light from the surface of the layers making up the cell reduces the amount of light reaching its active layers. In order to reduce the negative effect of this on cell performance, anti-reflective layers (AR or ARC) are applied to the top layer of the cell. These layers are not involved in the photovoltaic conversion. They are usually applied to the top layer of the cell.

Reducing the reflection, while keeping the absorption of the material constant, increases the transmission, allowing more solar radiation to reach the active layer.
The anti-reflective system can be a single layer or a multi-layer system.
A single anti-reflective layer is made of a material with a refractive index value intermediate to that of the layers directly below and above it (e.g., passivation layer and transparent electrode).

In the second case, the operation of anti-reflective systems is based on the phenomenon of electromagnetic wave interference. The choice of thickness and refractive index of the layers making up the system leads to an increase in transmission. Multi-layer anti-reflective systems are based on the LH (low, high) filter theory. This is a set of layers with alternating layers of high and low refractive index. This makes it possible to shape the reflection characteristics in such a way that in the electromagnetic wavelength range of the photovoltaic system operation, the transmission is the highest (highest reflection). An example of an anti-reflective system consists of four bilayers $TiO_2/\ SiO_2$.

The thickness of the anti-reflective layer d is related to the refractive index in the layer n and the wavelength λ of the light from the area of maximum photosensitivity of the cell [52] – equation (15):

$$n \cdot d = \frac{\lambda}{4} \tag{15}$$

Reflection can be reduced by adjusting the refractive index of the coating [53], n_{AR} for materials on both sides marked as follows $n_{surrounding1}$ and $n_{surrounding2}$ based on the relation (16):

$$n_{AR} = \sqrt{n_{surrounding1} \cdot n_{surrounding2}} \tag{16}$$

The reflectance characteristics of the anti-reflection system are shown in Fig. 46. The red colour indicates the system surrounded by air, the blue the system between the two glass panes.
The characteristics were generated using a simulation program Anti-Reflection Coatings [52].

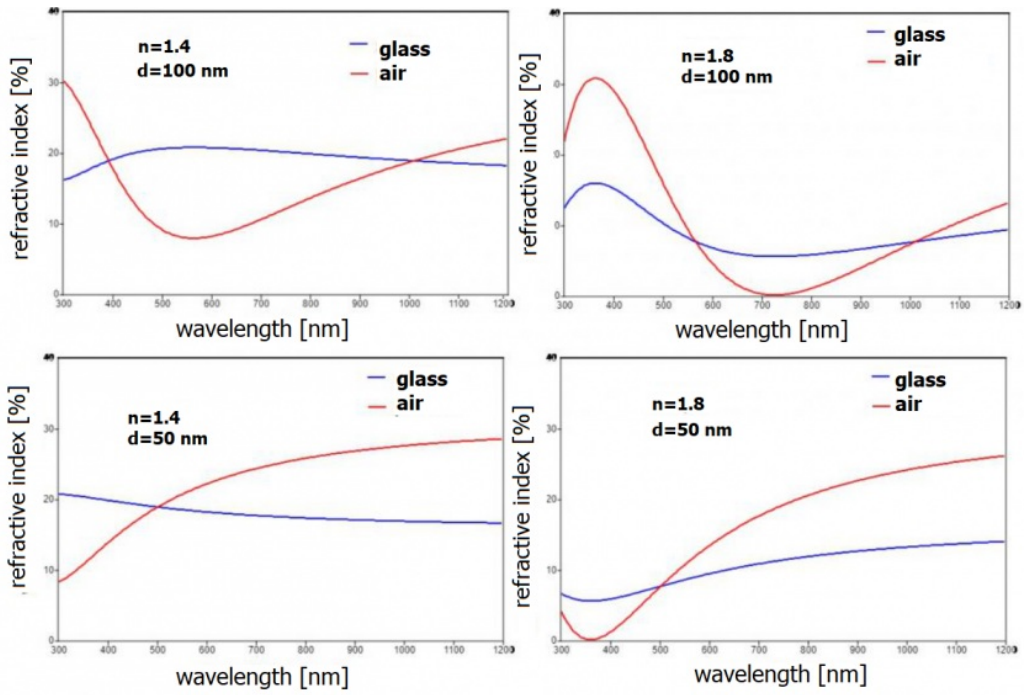

Figure 46: Refractive indices for antireflective layer for specified thickness and refractive index a) n =1.4 d=100 nm, b) n =1.8 d=100 nm, c) n =1.4 d=50 nm, d) n =1.8 d=50 nm. Own elaboration.

As mentioned above, depending on the absorption spectral maximum of the absorber in the solar cell, the reflectance

characteristics of the anti-reflective layer can be controlled. Anti-reflective films Fig. 47 with maximum transmission/minimum reflection (a) at 500 nm, (b) at 400 nm are shown below.

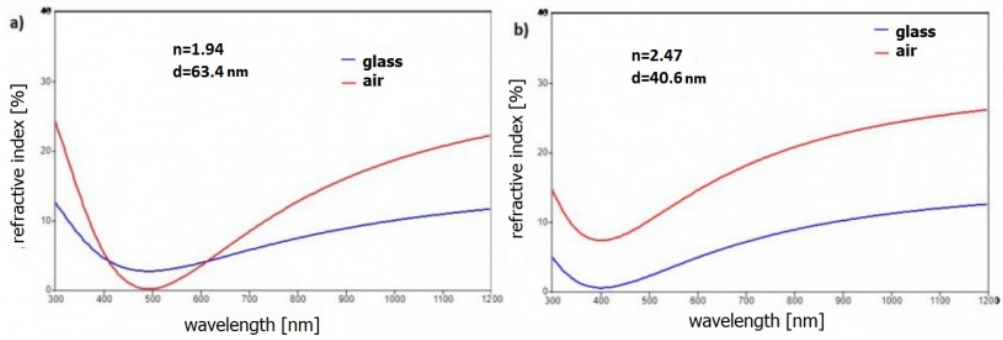

Figure 47: Refractive indices for anti-reflective layer for specified thickness and refractive index (a) n =1.94 d=63.4 nm, (b) n =2.47 d=40.6 nm. Own elaboration.

Thin-film anti-reflective systems are produced by vacuum methods by sputtering or evaporation.

4.5 Passivation layers

Passivation coatings aim to prevent processes that reduce the conversion efficiency of a photovoltaic cell.
The first process is charge recombination on the electrodes. Recombination processes occur in all parts of the cell, including the electrodes, although they are most intense in the active layer. Charges should be transferred from the electrodes to the external circuit, recombination reduces the amount of charge transferred and therefore the conversion efficiency. This is prevented by producing a tight, thin and corrosion resistant passivation layer through a chemical reaction. The second process prevented by passivation is electrode oxidation. Oxidation causes a change (deterioration) in the performance of the photovoltaic cells.
In the case of photovoltaic cells, passivation layers are placed on the front or back surface of the cell. However, the most common systems are those with a passivation layer between the silicon layer and the metal electrode. Simplified schemes of cells with a passivation layer are shown on Fig. 48.

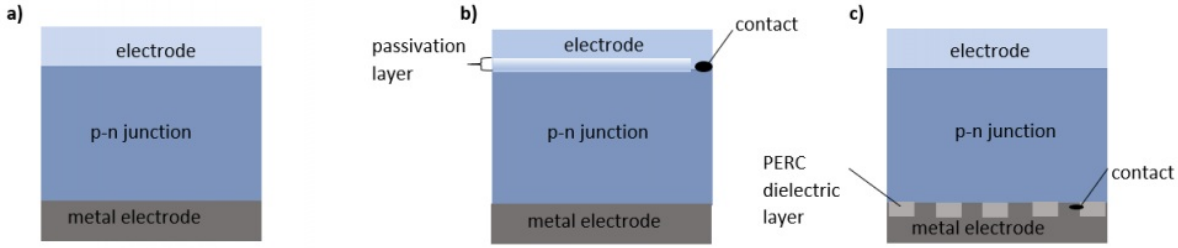

Figure 48: Cell's architecture: a) cell without passivation layer, b) cell with passivation layer, c) cell with bottom passivation layer. Own elaboration.

An example of the passivation process developed by SoLayTec, InPassion is shown in the video "SoLayTec InPassion ALD for Al2O3". It shows the deposition of aluminium oxide films Al_2O_3 using the atomic layer deposition (ALD) technique.

https://pre-epodreczniki.open.agh.edu.pl/openagh-video.php?id=175
SoLayTec passivation process
Roger Görtzen, SoLayTec InPassion ALD for Al2O3 (SoLayTec passivation process), 11.06.2015 (accessed 10.10.2020). Available on YouTube: https://youtu.be/0CFltB-9qbg.

An example of silicon passivation is silicon oxidation. On the silicon dioxide obtained as a result of oxidation (SiO_2) aluminium is then applied. The layers are further processed in 400 ^oC. Unfortunately, the high-temperature processing itself has a negative effect on the electrical properties of silicon [54]. Alternative passivation layers can be silicon nitride layers.

Cells with a bottom passivation layer have been manufactured and mass marketed. The most common cell types are [4]:

- PERC (passivated emitter and rear cell),
- PERL (passivated emitter, rear locally diffused),
- PERT (passivated emitter, rear totally diffused) [55].

The term "passivated emitter" used in the name is understood in this case to mean the top layer of the cell. In all cases, the emitter layer is subjected to a passivation process. Additionally, the surface between semiconductor and metal electrode is passivated. PERC cells have a passivation layer which performs the reflection function. Photons reflected from the passivation layer reach the absorber, increasing the number of generated charge carriers. The principle of the operation of PERL cells is similar, except that the lower passivation layer is dispersed (composed of separated elements). In a PERT cell, the front and back surfaces of the monocrystalline cell are passivated. The back electrode is locally dispersed at the metal contacts only, to minimise recombination while keeping good electrical contact [56]. Cells with passivation layers as standard are becoming increasingly popular. Based on forecasts from ITRPV (International Technology Roadmap for Photovoltaic), PERC technologies will obtain 55% panel market share by 2027 [57].

Przypis

1. Busbar cells are described in chapter: 6.1 Busbar cells.
2. Smartwires are described in chapter: 6.4 Smartwires cells.
3. See chapter: 6.5 HIT technology cells.
4. The cells are described in the chapters: 6.2 PERL cells i 6.7 PERC and PERT type PV cells.

5. Photovoltaic cells generations

5.1 Classification of photovoltaic cells

New cell types, new materials and new technologies have emerged with the development of photovoltaics. Traditional photovoltaics is divided into generations (Fig. 49).

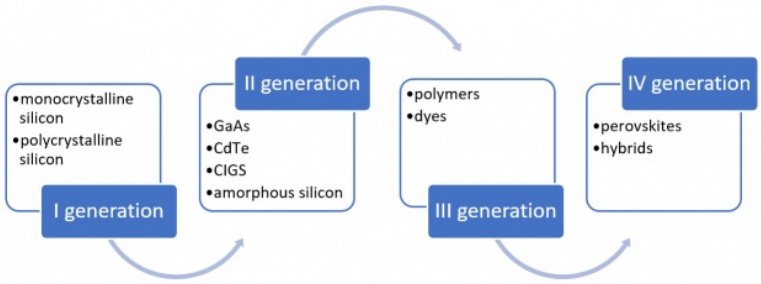

Figure 49: Generation of solar cell's types. Own elaboration.

The first generation are silicon cells: monocrystalline and polycrystalline. The appearance of cells based on amorphous silicon initiated the so-called second generation of cells. This includes thin-film cells made of cadmium telluride (CdTe), a mixture of copper, indium, gallium, selenium (CIGS) or the amorphous silicon, and multi-junction cells. Thin film cells are characterised by a very thin (1-3 micrometre) semiconductor layer.
The third generation includes dye-sensitised and polymer cells. The perovskite cells are also included in the third generation occasionally. However, some sources classify them with hybrid cells in the fourth generation [58]. This classification is therefore chronological. The classification according to the materials used in the manufacture of the cells is shown in Fig. 50 (based on [59]).

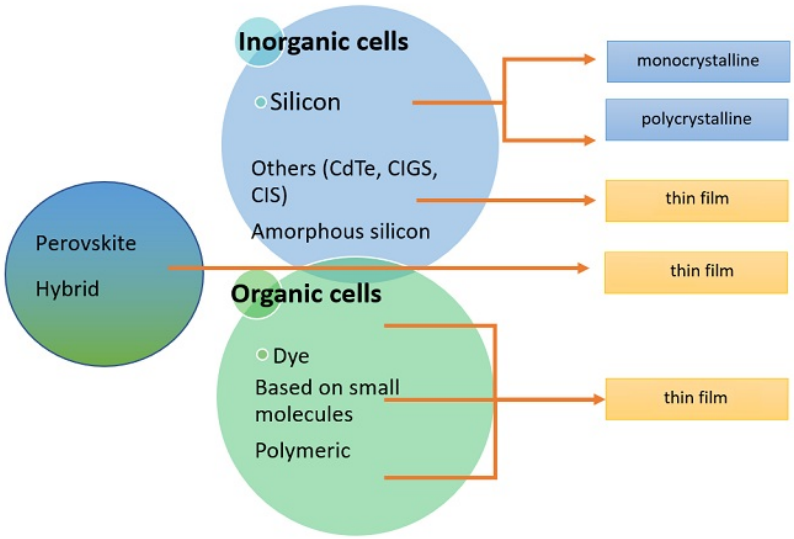

Figure 50: Classification of cells according to the materials used. Own elaboration.

Perovskite cells and hybrids are included in a separate category. Perovskites are inorganic materials, but organic materials (e.g., solvents) are used in the manufacture of the cells. Hybrid cells (e.g., silicon-organic) are also made from both organic and inorganic materials.
Each generation has its advantages and disadvantages (e.g., when it comes to performance, silicon photovoltaics is the most efficient). However, each generation is still being developed and has enormous potential.

5.2 Changes in conversion efficiency

The efficiency of solar energy conversion to electricity is one of the basic parameters of photovoltaic cells. The first values for silicon cells were recorded in the early 1950s in connection with the installation of batteries in satellites. Regular performance publications for all types of photovoltaic cells have been presented annually by the NREL laboratory of the U.S. Department of Energy since 1976 [60]. These data presented in Fig. 51, Fig. 52 illustrate the dynamics of changes in energy conversion efficiency for the different types of photovoltaic sources produced. These data are based on laboratory work. Nevertheless, they show where individual technologies stand and how far they are from the physical limits of conversion efficiency. The first data from 1976 were small. For amorphous silicon 1%, for monocrystalline silicon 14%, for CIGS thin film cells 6%, and CdTe 9%. Only the GaAs cells showed a higher conversion of 21%. Efficiency gains occurred as a result of continually ongoing research efforts in both corporations and research units. Some innovations have led to jumps in cell efficiency. It should also be noted that some research has led to the introduction of completely new designs, such as multi-junction cells, or new materials or even entire classes of materials, such as polymers or perovskites, into photovoltaics. Three classes of materials deserve special attention either because of the performance values that cells constructed with these materials achieve or because of the significantly higher dynamics of change compared to other materials. The first category is that of multi-junction cells especially those built on gallium arsenide GaAs. The introduction of two-, three-, and later four-junction cells started in the second half of the 1980s, the second half of the 1990s, and the last ones already in this century after 2005, respectively. These cells already in the early stages of research had high efficiencies above 28. Intensive work on their development has led to 2019 performance ranges lying in the previously unattainable range from 30% to 47.1%.

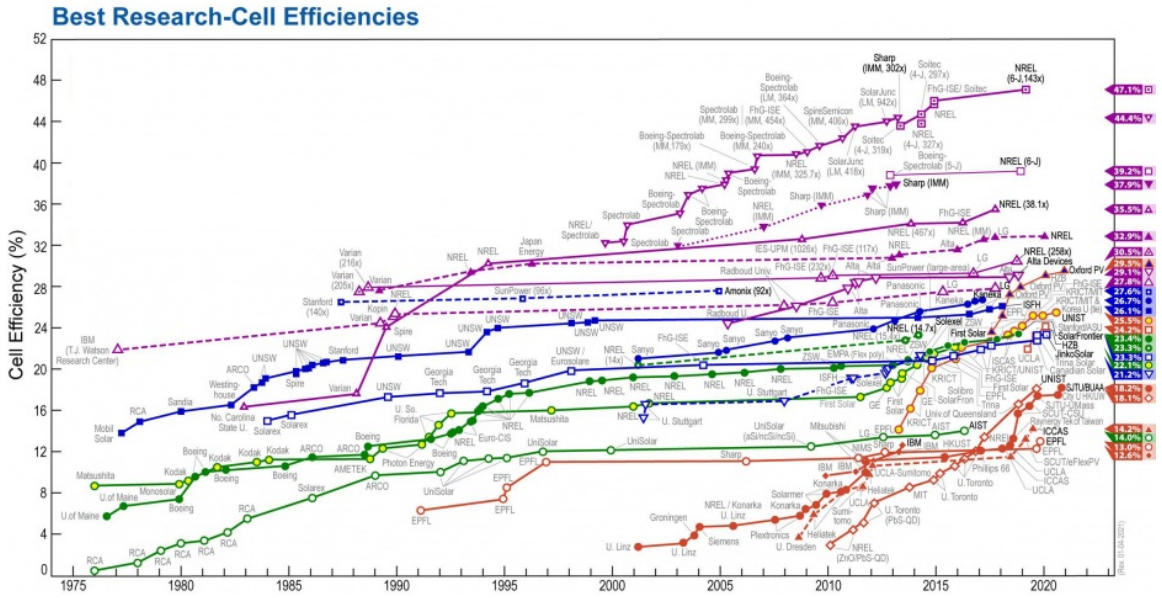

Figure 51: Cell efficiency growth for all cell types from 1976-2019. compiled. National Renewable Energy Laboratory (NREL) graph, CC0 license, source: Wikipedia .

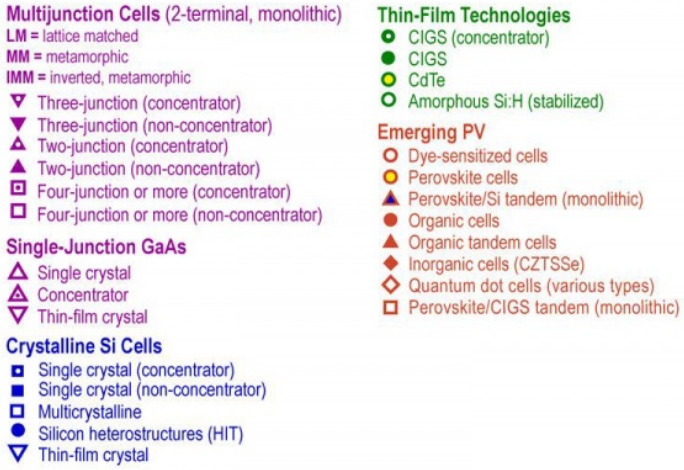

Figure 52: Description of the symbols used in the performance graph. Elaborated from a National Renewable Energy Laboratory (NREL) chart, CC0 license, source: Wikipedia .

The second group of materials are polymers. Their main advantage is undoubtedly their low price. The history of polymers in photovoltaics began only at the beginning of our century, but despite such a short period of time they have already managed to achieve efficiencies of 17%. A second class of materials with an even higher rate of change is perovskites. Produced on mineral-based materials, recent designs have reached 21.5% in less than a decade, bringing them close to the theoretical conversion limit for these materials of about 31%. Unfortunately, both classes of materials lack a feature very important for photovoltaic materials, i.e., long-term stability. Photovoltaic power plants operate for 25 years and more, so work on improving this parameter seems crucial for the widespread use of these cheap and already efficient photovoltaic sources. Constructions using achievements of modern physics, i.e., photovoltaic cells made of quantum dots, are developing equally dynamically. These cells require advanced technology, but in less than 10 years since their discovery they have already achieved 16.6% efficiency. CIGS and CdTe thin-film cells are developing without such spectacular results, however, they have already reached efficiencies of 23.4% and 22.1% respectively, which not long ago was the limit for silicon cells. An unquestionable advantage of these cells is minimal material consumption and possibility of their application on flexible substrates, which significantly extends their installation possibilities. And finally, silicon cells. Started in the 1950s with an efficiency of a few percent in niche applications such as powering satellites, they are now the main material in most of the photovoltaic power plants being built worldwide with efficiencies achieved in laboratory conditions of 27.6%. We currently have two areas of activity related to photovoltaic cell materials. One is the search for materials, especially for multi-component semiconductors with high yields. The second is the area related to the development of methods of production of materials with obtained high efficiencies on an industrial scale. The increasing efficiency of cells and the nearly million-fold increase in production has resulted in a roughly thousand-fold decrease in the price per 1 Wp from 1975 to today. These changes are shown in Fig. 53 (based on data from [61], [62]). Such significant reductions in selling prices have resulted in increased research efforts into low-cost photovoltaic materials such as perovskites and polymers. As a result, in recent years we have seen a dramatic increase in the conversion efficiency (Fig. 53) achieved for cells made from these materials.

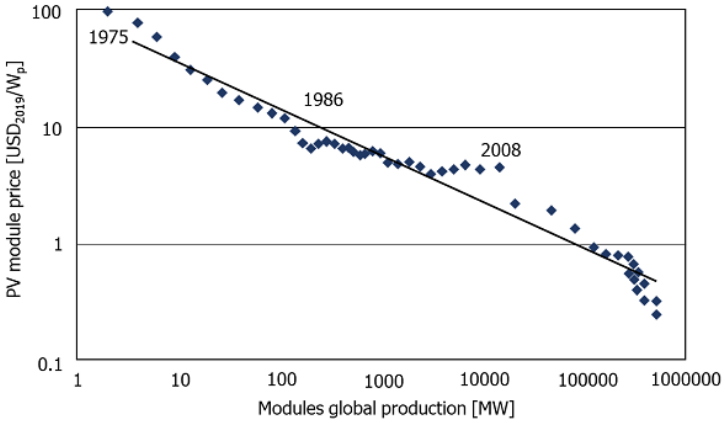

Figure 53: Solar cells prices decrease from 1975 to 2019. Own elaboration.

5.3 Silicon cells

Photovoltaic cells can be divided based on the materials they are made of and the structure of those materials (Fig. 54).

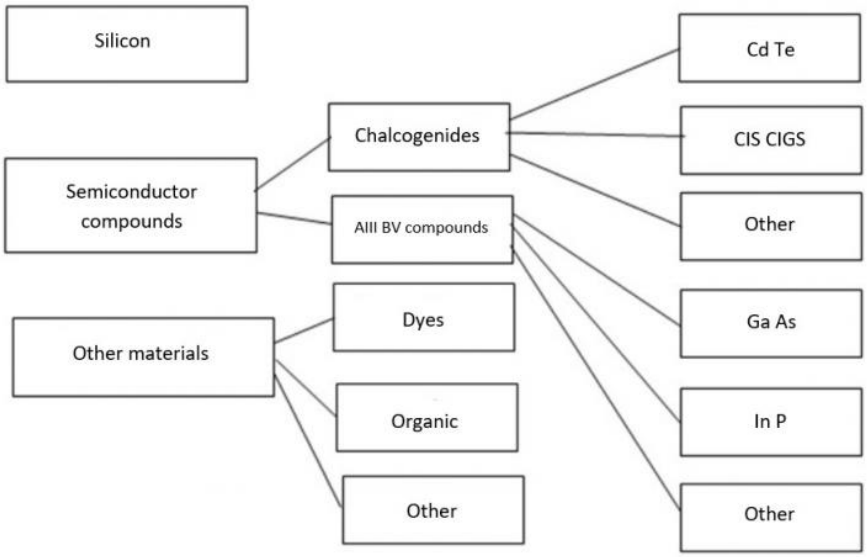

Figure 54: Division of cells by base materials. Own elaboration.

Among silicon cells, the types shown in Fig. 55.

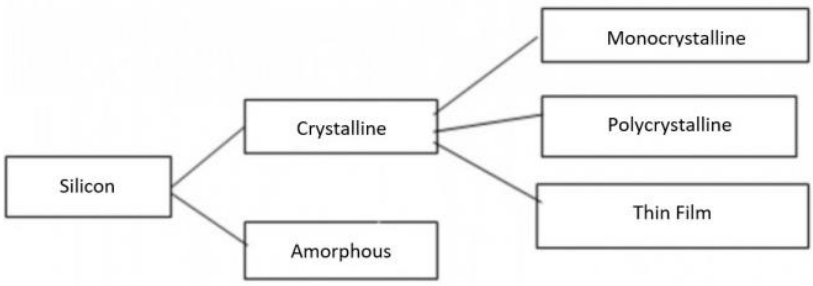

Figure 55: Division of silicon cells. Own elaboration.

Commercially, silicon-based cells are the most common. Four types of cells used to build photovoltaic panels are produced: monocrystalline, polycrystalline, thin-film, and amorphous cells. A cross section through the structure of a monocrystalline solar cell is shown in Fig. 56. The cell structure consists of a front electrode (the one on which the light falls), an n-type layer about 2 μm thick, n-p junctions, a p-type layer, and a back electrode. The p-type layer is characterized by a thickness of 300 μm, but the work reducing its thickness is ongoing and it will soon reach 160 μm. The exciton produced by the absorption of the radiation quantum appears in the vicinity of the n-p junction and breaks into charges. The electric field at the p-n junction shifts the charges in different directions, electrons to the n-type semiconductor and holes to the p-type semiconductor. The charges separated at the junction result in a potential difference.

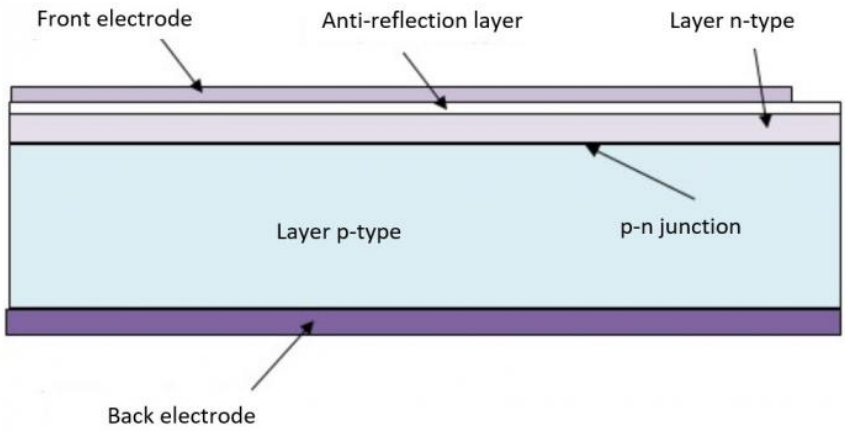

Figure 56: Structure of a monocrystalline cell. The p-type semiconductor is a relatively thick layer and the n-type semiconductor is no more than 2 μm thick. The front and back electrodes receive charges separated at the p-n junction. Own elaboration.

Photovoltaic cells built on monocrystals are carved from a single crystal of silicon, created by pulling a single crystal, usually by the Czochralski method. By adjusting the pulling speed and rotation of the single crystal, monocrystalline rods of a specific diameter can be obtained. The cell is made up of the following layers:

- the front electrode, on the side of the incident sunlight - it can be made of silver or ITO strips, or aluminium strips,
- an anti-reflective layer - it increases the amount of solar radiation reaching the cell,
- a passivation layer - it protects the semiconductor from changing properties over time,
- an n-type layer - up to 2 μm thick, it is usually etched to form a surface consisting of pyramids, which increases the optical path length of radiation quanta in the semiconductor, increasing the probability of radiation absorption,
- a p-n junction layer - intended to separate charges,
- a p-type layer - 180-300 μm thick,
- a back electrode (from the side opposite to incident sunlight) - made as a solid layer of aluminium (or silver), or in the form of strips, it may also be made of ITO, in the case of double-sided electrodes.

Silicon cell manufacturing technology is based on making suitable silicon wafers from a monocrystalline cylinder. An acceptor dopant is introduced into the material base during crystal growth, thus obtaining a p-type semiconductor. The grown cylindrical crystal is then cut with a laser into wafers 0.3 mm thick, in the shape of a square, hexagon or circle. Such wafers are p-type semiconductors, and the resulting wafers are polished to perfect purity and smoothness [63]. In single wafers, an n-type region is produced in a thin surface layer by diffusion, such as phosphor. At the junction of two types of semiconductors linked in this way, a p-n junction is formed. The surface is then textured. Cell wafers are typically 100-200 mm squares with a thickness of 200-300 μm (160 μm thickness is expected to be the future standard) [64]. In electronics, wafers with a diameter of 100-300 mm are used, and soon even those of 450 mm [65]. Silicon wafers thick up to 180 μm are currently used. The surface of crystalline silicon reflects incident sunlight (up to 40%). To prevent this, a thin anti-reflection layer is applied to the wafer surface. Further fabrication involves applying current paths from thin strips of aluminium foil and protecting the entire cell from weathering with a special layer of EVA (Ethylene Vinyl Acid) organic film. Thanks to such hermetic structure, cells can work in year-round installations for over 25 years.

Polycrystalline silicon rods, on the other hand, are produced by the Siemens process (from 1953) with a purity of > 99.99999%. The disadvantage of this technology is the use of high temperatures. The basic material is silicon, ground and cast in a cuboidal form. Through controlled heating and cooling, the block crystallizes in one direction to produce inhomogeneous crystals several millimetres to several centimetres in size. The boundaries between the crystals represent defects that can degrade the efficiency of the photovoltaic cell. The polycrystal fabrication process forces a ribbon polycrystalline structure. A photovoltaic cell fabricated on polycrystalline silicon wafers can be compared to more monocrystalline cells connected in parallel.

Amorphous silicon a-Si is used in the production of photovoltaic cells, LCDs, or OLEDs. In a vacuum chamber, gases (SiH_4 with dopants) are decomposed in a glow discharge and an amorphous silicon layer is deposited on the substrate. With this technology, the production of a-Si is simpler, as well as energy and material efficient. Moreover, it allows obtaining cells with a large surface area (they are very cheap). The disadvantage is the low efficiency, up to 12%. The mechanism of photovoltaic cells is the same, regardless of the materials used to make them.
Fig. 57 shows cells made of (a) monocrystalline, (b) polycrystalline, and (c) amorphous silicon. The monocrystalline cell has truncated corners and a black color, on the polycrystalline one can clearly see the crystal areas, and for the amorphous the color is dark maroon to black.

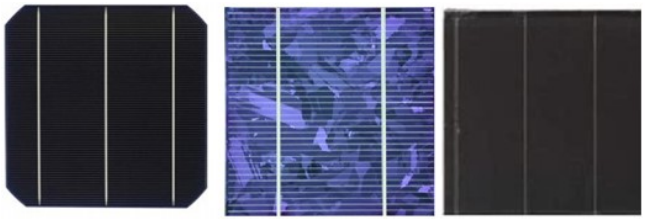

Figure 57: Appearance of a monocrystalline, polycrystalline and amorphous silicon cell. Own elaboration.

Fig. 58 shows the main steps of the screen-printed solar cell manufacturing process. With more or less minor modifications, this process is now used by most photovoltaic cell manufacturers [66]. The main advantages of this 35-year-old photovoltaic technology are easy automation, reliability, good material utilization and high efficiency.

Here is a typical photovoltaic cell fabrication scheme using 180-210 μm thick silicon wafers, provided as an example. The Si wafer is doped with boron to obtain a p-type semiconductor with resistivity in the range of 0.5-6 Ω cm. First, the wafer is cleaned of cutting impurities. The wafer thus prepared is etched in KOH to obtain a surface texture in the form of microscopic pyramids (Fig. 58). Their size has to be optimized, too small leads to light reflection and too large makes it difficult to attach the electrodes, i.e. to receive the charges. Texturing can be done in several ways: alkaline etching, acid etching, plasma etching and mechanical etching. The next step is doping (Fig. 58) usually with phosphorus. This is a process that requires high temperature. This creates an area of n-type semiconductor around the entire wafer, i.e. at the edges it needs to be removed or separated.

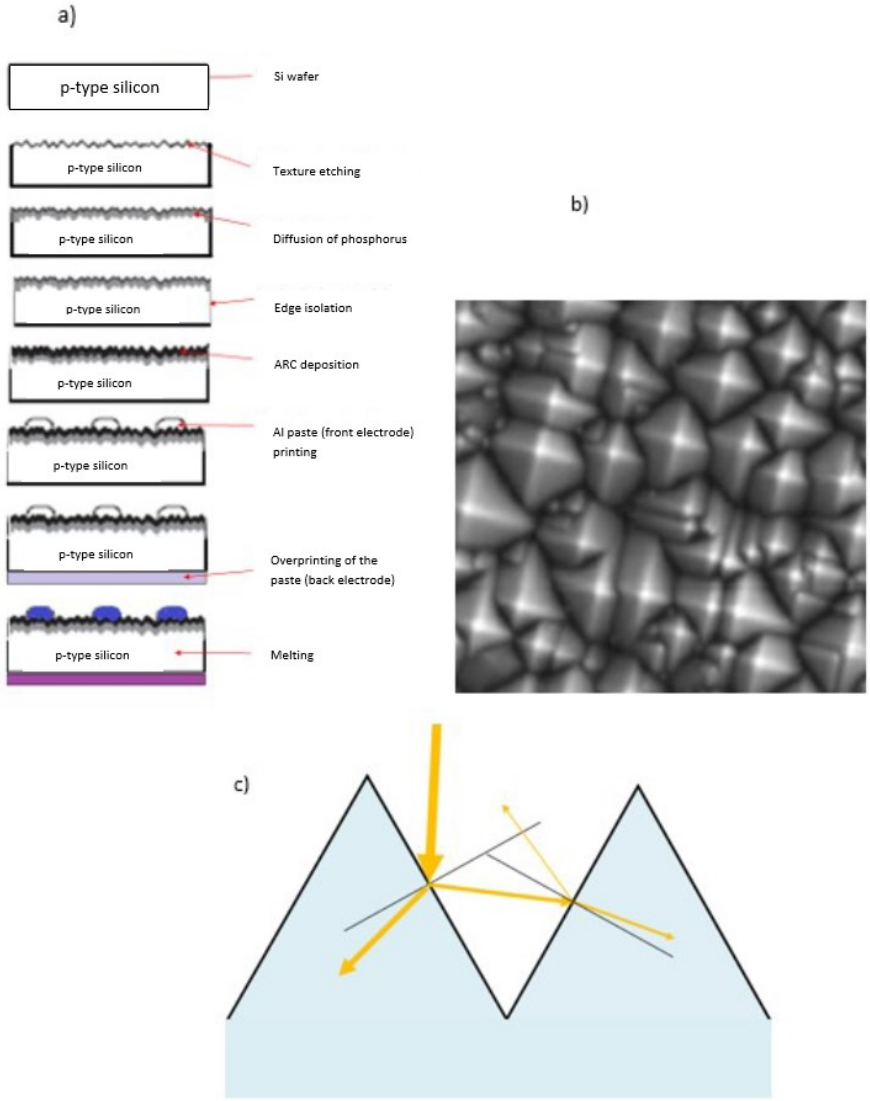

Figure 58: a) Typical photovoltaic cell manufacturing process, b) surface structure after texturing, c) explanation of the reason for surface texturing. Own elaboration.

Titanium dioxide (TiO_2) is applied to the surface on which light falls, and is used to form an antireflective coating because of its good antireflective properties, especially for encapsulated cells [67]. This process can be easily automated in a conveyor belt reactor. Other possibilities include, for example, screen printing of suitable pastes. Front electrode metallization is applied to such a prepared surface and is characterized by good adhesion at the silicon interface, low line width, good mechanical adhesion, solderability, and compatibility with encapsulating materials. Resistivity, price and availability make silver an ideal choice for a contact metal. A screen-printing method is used to make the back electrode using aluminium paste, forming a layer on the back

surface of the cell [68]. The low eutectic temperature of the Al-Si system (577 ^oC) means that some silicon dissolves in Al and recrystallizes upon cooling after the firing step, forming a p-type layer. The characteristics of this layer (thickness, uniformity, reflectivity) depend on the amount of paste.
The finished cells are measured under STC conditions, i.e., a light spectrum consistent with that of Sun AM1.5 and power of 1000 $\frac{W}{m^2}$ at a temperature of 25 ^oC. Defective links are eliminated and the rest are passed on for further production.

5.3.1 Monocrystalline silicon production

Crystal growing is a lengthy and energy-intensive process. The first step is to produce pure silicon from silicon dioxide by chemical methods. Then the material must first be melted and crystallized by cooling. The monocrystal should not contain foreign atoms, so the process must take place under special conditions. The best results are achieved in a vacuum furnace, where crystallization takes place without access of gases and especially oxygen. The method was developed by the Polish scientist Jan Czochralski [69]. A schematic of the silicon monocrystal culture process is shown in Fig. 59.

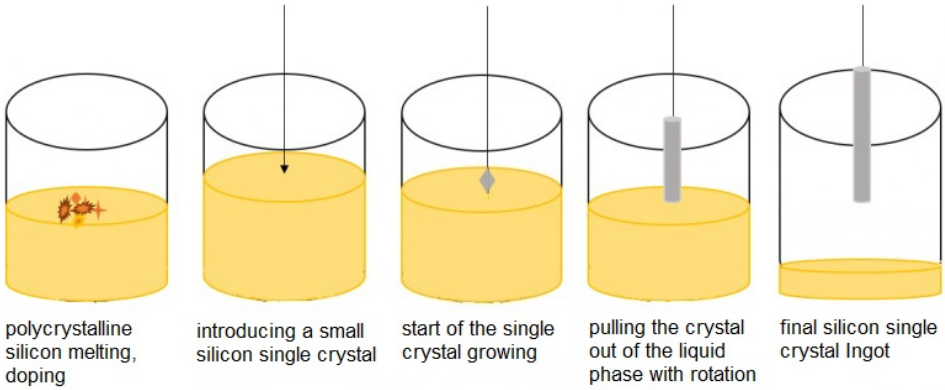

Figure 59: The stages of silicon monocrystal growth. Own elaboration.

The first stage of production is the chemical process of obtaining pure silicon SiO_2. The resulting pieces of pure silicon are placed in a vacuum chamber in a quartz crucible.

After the silicon is loaded into the vacuum chamber, the silicon is melted in a quartz crucible, and then a small silicon crystal is lowered from the top vacuum chamber of the device, which becomes a crystallization nucleus. The embryo with a specific crystallographic orientation touches the surface of the molten silicon. The molten silicon (liquid) adheres to the surface of the embryo, which rises minimally. Moving away from the surface, it enters a region of reduced temperature which starts the crystallization process. In order to homogenize the crystallization process, the embryo rotates around its axis. By adjusting the speed of rotation of the embryo and the speed of ejection upwards, we obtain cylindrical crystals, initially of varying diameter. Once stable process parameters are achieved, the diameter of the grown monocrystal maintains its value until the molten material is exhausted. The orientation of the growing monocrystal is identical to that of the embryo initiating crystallization. The result of the process is the large cylindrical monocrystal shown in Fig. 60 [70].

Figure 60: Silicon monocrystal (ingot) grown by Czochralski method. Photo by Massimiliano Lincetto, licensed under CC BY-SA 4.0, source: Wikimedia Commons .

The steps of this process, the principle of the Czochralski method and the wafer processing steps are presented in the film "Silicon Wafer Production by MicroChemicals".

https://pre-epodreczniki.open.agh.edu.pl/openagh-video.php?id=180
Technological stages of silicon wafer production
Mimotec SA, Silicon Wafer Production by MicroChemicals (Technological stages of silicon wafer production), 09.10.2015 (accessed 12.12.2020). Available on YouTube: https://youtu.be/2qLI-NYdLy8.

Due to the purity requirements of the monocrystals produced, the manufacturing processes take place in high purity class halls. The crystal shown in Fig. 60 is about 1 meter long. With the current demand for monocrystalline silicon for both electronic and photovoltaic production, dozens of Czochralski furnaces are installed in Chinese factories in the halls, and the lengths of monocrystals reach 4.5 m.
The next step in the production of a silicon wafer, because silicon wafers are the material for electronic and photovoltaic production, is the mechanical processing of the ingot (this is what the monocrystal is called after being removed from the furnace). The first step of mechanical processing is to cut off ends of variable diameter and roll the surface of the ingot into a cylinder with fixed geometric parameters. The cylinder is cut into pieces corresponding to the dimensions of a wire saw, which will cut it into wafers 180 micrometres thick. It used to be 300 micrometres, then 200 micrometres, and now it is also cut to a dimension of 160 micrometres. The problem after reducing the wafer thickness is the mechanical resistance of the monocrystalline to cracking, during further processing up to and including panel assembly. Cut wafers have edges as sharp as broken glass, also they need to be blunted before further processing. Each wafer is numbered by laser, which allows further identification of the production process and its parameters. The next process is polishing to the required level. In many cases, this is the atomic level. The next steps are chemical etching, polishing and cleaning the surface from residues of previous processes. Depending on the customer, wafers are covered with a layer of silicon oxide of a specified thickness and then an electronic inspection of the correctness of the state of the wafer and its surface is carried out. The final stage is packing of the wafers into transport trays.

Silicon wafer production has always been catered to the needs of electronic factories and wafers were initially produced in small sizes of 1 inch, then 2 inches, etc. The increase in wafer diameter was driven by the rapidly increasing industrial demand for monocrystalline silicon and the wafer diameter varied from 2 inches in 1970 to 18 inches in 2014. An example of wafers with different diameters is shown in Fig. 61 [71].

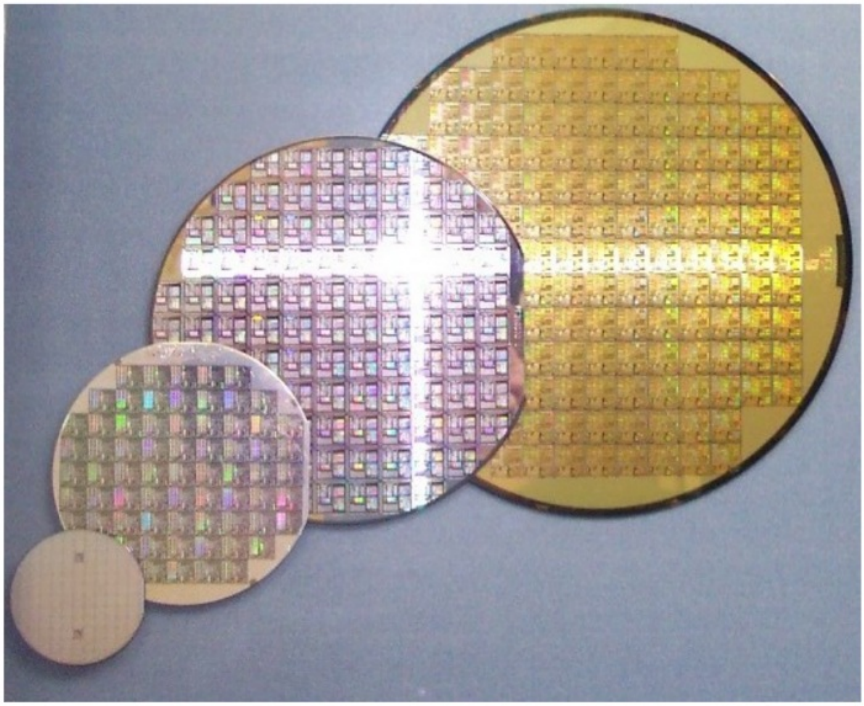

Figure 61: Successive generations of silicon wafers with increasing size. Photo license CC BY-SA 3.0, source: Wikimedia Commons .

Each change in dimension meant new generations of tooling in processor and memory factories. In photovoltaics, where wafer parameters and properties are not as stringent, the standard size for a photovoltaic cell has become 15.6 x 15.6 cm and a wafer from which such a square can be cut with minimal chipping. As a result, monocrystalline silicon photovoltaic panels show an empty space at the junction of the four cells, resulting from the cylindrical symmetry of the starting material. Extremely sterile silicon production conditions also allow the production of silicon with strictly defined dopants. This is particularly important in photovoltaic production. By obtaining a wafer with a specific doping we have a ready component for the production of a diode, which is every photovoltaic cell.

5.3.2 Production of polycrystalline silicon

The production of polycrystalline silicon and wafers from this material is analogous to the production of monocrystalline wafers. There are two fundamental differences. The first is that there is no furnace for growing the monocrystal. Chemically produced silicon pieces are sintered using the process shown in the "Solar Module Manufacturing" video.

https://pre-epodreczniki.open.agh.edu.pl/openagh-video.php?id=181

Processing of polycrystalline silicon

ER, Solar Module Manufacturing (Processing of polycrystalline silicon), 05.04.2013 (accessed 10.12.2020). Available on YouTube: https://youtu.be/5Sgmp1aUjnA .

This part of the process is significantly cheaper and shorter. The second difference is the shape of the silicon block produced. For practical reasons, it is a rectangular block with cross-sectional dimensions close to the standard 15.6 cm x 15.6 cm. After mechanical processing, a square wafer of these dimensions is obtained. The remaining steps of the process are analogous, as described in 5.3.1 Monocrystalline silicon production. Replacing the lengthy and energy-consuming process of growing the monocrystalline with a shorter and much cheaper sintering process reduces the production cost of a single wafer significantly.

5.4 Thin-film cells

Due to technological limitations and the cost of producing cells based on crystalline silicon, alternative materials and methods have been sought to produce photovoltaic cells. About 50% of the production cost of crystalline silicon solar cells comes from the preparation of the silicon, while the processing of the cells and panels is respectively the remaining 20% and 30%. The search was therefore carried out to find materials other than mono- and polycrystalline silicon for cell construction. In the 1970s, the first thin-film cells based on amorphous silicon were successfully produced, followed by other materials.
The most common types of thin film cells (Fig. 62 [72]) are cells made of amorphous silicon, CIGS cells and CIS cells (based on copper, indium, gallium, selenium). Their efficiency ranges from $14-23\%$. Cadmium sulphide and cadmium telluride (CdS and CdTe) are also popular materials. Silicon cells dominate the PV market (92%), followed by cells based on CdTe, 5% CIS/CIGS/CIGSS- 2% and amorphous silicon (1%) [73].

Figure 62: Thin film cell. Aut. photo by Fieldsken Ken Fields, licensed under CC BY-SA 3.0, source: Wikimedia Commons .

Thin film cells are cheaper to produce due to lower material consumption, automated production and less labour-intensive processes. The problem in the future may be a shortage of key materials - the prices of indium and tellurium are constantly rising. Another advantage of cells, and thus thin-film panels, is their weight - they are lighter than silicon cells [74]. They achieve slightly lower efficiencies than crystalline silicon cells and also have a lower lifetime. However, they have the undoubted advantage of being able to be applied to flexible surfaces (foils).

The first thin film cells built were amorphous silicon cells. An important element in the development of this technology was the properties of amorphous silicon - it has a higher light absorption coefficient than crystalline silicon. A cross-section through the cell structure is shown on Fig. 63. A layer of intrinsic conductor with a thickness of about 0.5-1 μm is sandwiched between additional layers of p-type (layer thickness is about 8 nm) and n-type materials (layer thickness is about 20 nm) [75].

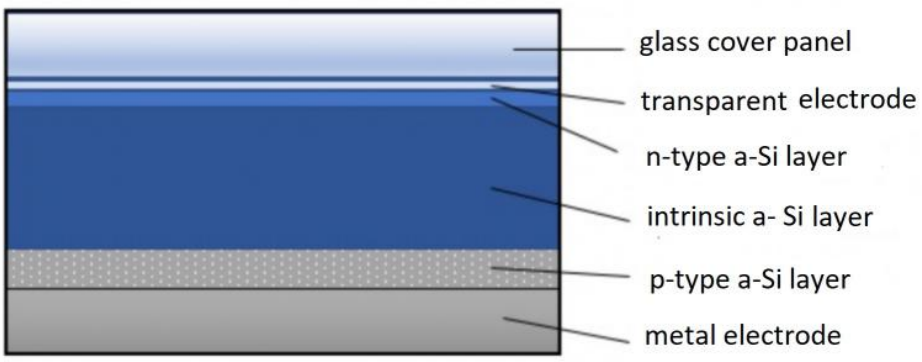

Figure 63: Scheme of amorphous silicon cell structure. Own elaboration.

CIS/CIGS/CIGSS cells are cells in which the structural material is indium copper diselenide $CuInSe_2$ (CIS). This material has a high absorption coefficient (its energy gap is about 1 eV). By adding gallium, a semiconductor compound is formed having the chemical formula $CuIn_{(1-x)}Ga_xSe_2$.

By controlling the gallium content (x in the formula), the energy gap can be modified in the range 1.02 eV-1.64 eV. The energy gap can be increased by adding sulphur. The compound CIGSS is then formed. CIS/CIGS/CIGSS cells are produced by depositing the active layer on sodium glass covered with a molybdenum layer (base contact). The second contact is often a layer of zinc oxide ZnO doped with aluminium [7]. CIGS cells have a characteristic black color.

Another material for photovoltaic cells is cadmium telluride (CdTe). The energy gap of CdTe is 1.45 eV [76], which results in high absorption of the solar spectrum. The material is temperature stable compared to other semiconductor materials. The elements Cd and Te and their oxides are highly toxic, which was a concern before the application of this technology. CdTe has been shown to be minimally harmful to living organisms. The cells were therefore approved for production. CdTe-based cells produce the smallest carbon footprint, the lowest water consumption and the shortest energy payback time. Due to the good combination of thermal properties, CdTe is combined with cadmium selenide (CdS). The structure of a CdTe-based cell is shown in Fig. 64 (based on [77]).

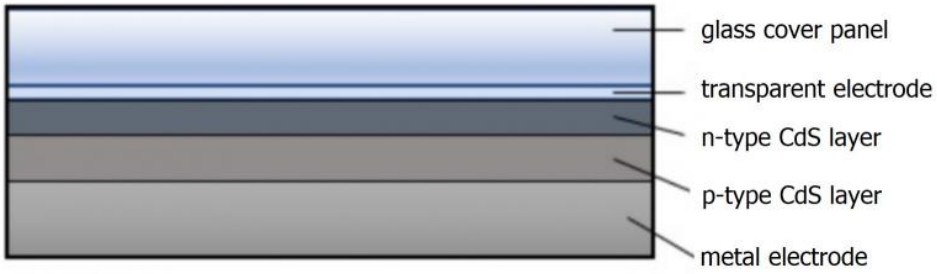

Figure 64: CdTe-based solar cell structure. Own elaboration.

5.5 Multi-junction cells

Multi-junction solar cells (MJSC) consist of multiple layers of semiconductors with different E_g gap values.
To maximize the efficiency of a multi-junction cell, the cell thickness should be chosen so that the greatest portion of the radiation is absorbed. Multi-junction cells are optically an array of layers, each of which absorbs a different part of the solar spectrum. Therefore, it is reasonable to design successive layers of semiconductors so that, counting from the transparent layer, successive layers have a smaller energy gap than the previous layer. For example, the GaInP / GaAs/Ge system, where the energy gaps are GaInP (1.9 eV), GaAs (1.4 eV) and Ge (0.7 eV) with an efficiency of approx. 33% [78], whether AlGaInP/AlGaAs/GaInP/GaInAs/GaInNAs, with energy gaps of AlGaInP (2.2 eV), AlGaAs (1.6 eV), GaInP (1.7 eV), GaInAs (1.2 eV), GaInNAs (1.0-1.1 eV). Depending on the percentage composition, the above systems achieve $30 - 40\%$ [79], [80].

To optimize charge transfer in a multi-junction cell, two consecutive junctions are connected to each other using tunnel junctions (junctions where a particle can penetrate a potential barrier higher than its kinetic energy). It consists of heavily doped layers with low absorption and voltage drop and high peak current. Its thickness should be about 10 mm. In the absence of tunnel junctions, photovoltage from consecutive junctions having opposite sign would partially compensate [81]. In the picture Fig. 65, the cell layout is shown along with the corresponding connectors. The p-n junctions are symbolized by the colored diodes facing up. Tunnel connectors (black and gray) are facing down.

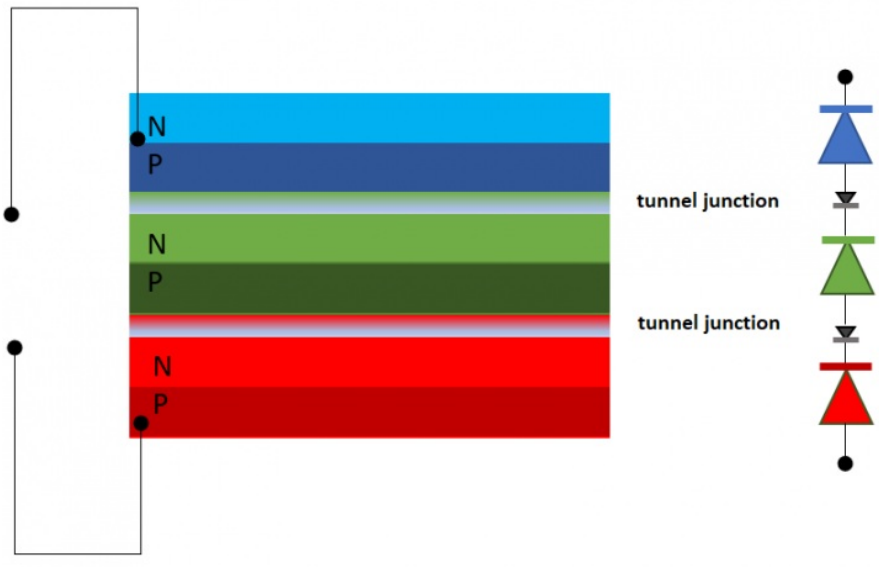

Figure 65: Schematic of a multi-junction cell with corresponding connectors marked with diode symbols. Own elaboration.

High performance exceeding the Shockley-Queisser limitation (SQ limit) can be achieved with multiple connections [82].
The efficiency of multi-junction cells can still increase. Depending on the number of semiconductors, simulations indicate more

than 60% efficiency (Fig. 66 based on [83]). The maximum efficiency with an infinite number of layers would be 86.8% [83] – this is the so-called thermodynamic limit [84].

Number of energy gaps	1	2	3	4	5	6	7	8	9
Theoretical performance of a multi-junction cell	33.3	45.7	51.5	55.6	58.0	59.6	61.0	62.0	63.2

Figure 66: Efficiency value of the multi-junction system as a function of the number of energy gaps. Own elaboration.

Multilayer systems are more expensive. They are usually based on gallium arsenide, whose toxicity and possibility of safe disposal is the subject of intensive research [85]. According to NREL data, multi-junction solar cells have reached an efficiency of 47%. Initially, they were only used in space because of their price. Currently, attempts are being made to put them on the market.

5.6 Organic cells

Organic compounds are chemical compounds based on carbon, with the exception of carbon oxides, carbonic acid, carbonates and bicarbonates. They can also contain virtually all other chemical elements (the most common are hydrogen, oxygen and nitrogen, sulphur, phosphorus and halogens).
The first organic cells were based on anthracene [86] and politiofen [87]. Among conductive organic materials, there are two subtypes: polymeric materials and organic small-molecule materials.
The most groundbreaking feature in organic photovoltaics is the different form of p-n junction. An organic cell is made up of layers - between the electrodes (one of which is transparent) there is usually an active layer - a mixture of two organic materials: a donor and an acceptor. The donor material is the material that supplies electrons during the process. The acceptor material is the material receiving electrons.
We refer to this structure as a bulk heterojunction. Sometimes additional layers are added between the active layer and the electrodes to support hole and electron transport.

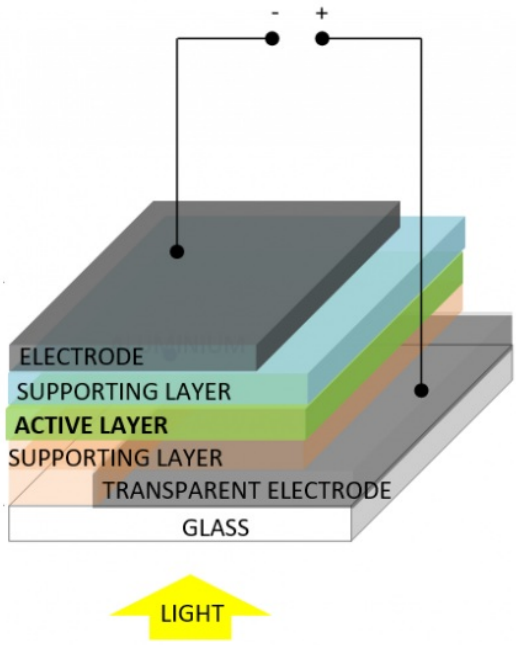

Figure 67: Organic cell scheme. Own elaboration.

Other architectures (e.g. with independent donor and acceptor layers) have also been explored over the years. However, the volume heterojunction proved to be the most efficient. In the sandwich system shown in Fig. 67. The p-n junction occurs only at the donor-acceptor interface. In a mixture of donor and acceptor, the p-n junction occurs basically at the entire molecule interface. This is a very big advantage of organic photovoltaics - the efficiency of converting absorbed light into excitons is higher than in other cells. The other parts of the energy conversion process are not as efficient as in inorganic semiconductors, so the final efficiency of organic cells is lower than traditional silicon or thin-film cells.

The operation of a cell consists of several steps. The first and most important is the absorption of light. As a result of absorption, an electron is excited from the highest occupied molecular orbital (HOMO) of the donor material to the lowest unoccupied molecular orbital (LUMO). The excited electron and the remaining hole form an exciton - a quasiparticle bound by the coulombic interaction. The exciton diffuses (average exciton diffusion path is 10 nm) until the charge separation takes place. Charge

separation usually takes place at the donor-acceptor interface (the point of contact between donor and acceptor molecules), but it also happens at impurities (oxygen traps, all non-intentional dopants). The last steps of the photovoltaic process are the charge transport and its collection on the electrodes. The energy diagram of the cell is shown in Fig. 68, and subsequent action steps on Fig. 69.

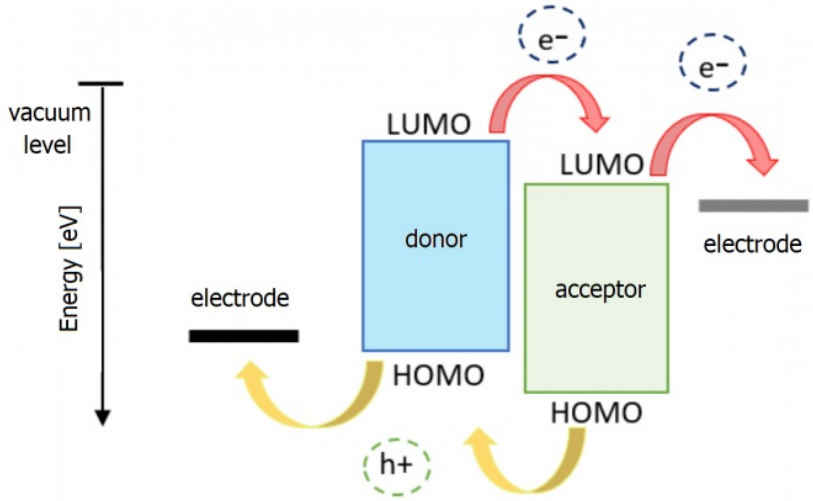

Figure 68: Energy diagram of organic cell operation. Own elaboration.

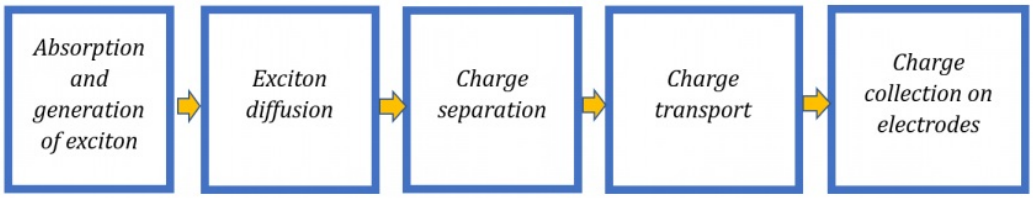

Figure 69: Block diagram of organic cell performance. Own elaboration.

Loss mechanisms are associated with each step of the process: light may be reflected; an exciton may not be formed or an already formed exciton may recombine; hole and electron transport limitations may occur. In the case of transport between the active layer and the electrode, a potential barrier may occur at the electrode preventing charge transfer to the electrode (the barrier occurs when the work of the electrode output is mismatched with the level from which the charge is transported).

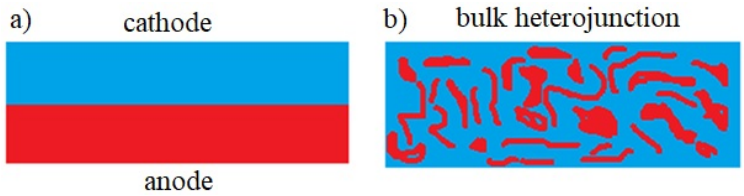

Figure 70: Junction diagram of (a) silicon p-n cell, (b) cell based on bulk-heterojunction. Own elaboration.

In the picture Fig. 70, the blue colour is the n-type area and the red colour is the p-type area. The boundary between them is the junction.
When comparing organic cells to silicon cells, it should be recalled that in semiconductors we are dealing with a crystal lattice and an energy gap. In organic cells, there is no crystalline structure, nor do we have the typical transport of holes and electrons in layers. The junction regions are scattered throughout the volume of the active layer. Instead, we consider a diffusing exciton and then charges transported along the HOMO and LUMO levels.

A comparison of energies as a function of density of states in silicon and organic cells is shown in Fig. 71 (based on [58]).

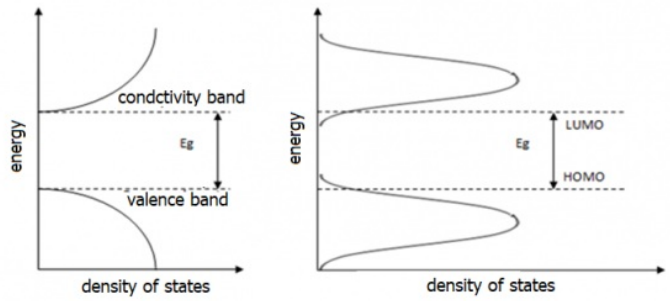

Figure 71: Energy as a function of density of states (a) in silicon cells, (b) in organic cells. Own elaboration.

The materials making up the active layer are divided into donor and acceptor materials. To simplify, we can consider an acceptor to be equivalent to an n-type semiconductor - and a donor to be equivalent to a p-type semiconductor. However, whether a material is a donor or an acceptor in an organic cell, specifically the active layer, depends on the material that co-creates the active layer. The donor is the material that supplies the electrons.
Some of the most commonly used materials are poly(3-hexylthiophene), abbreviated as P3HT, and 6,6-phenyl-C_{61}-butyric acid methyl ester (PCBM). New compounds are constantly being synthesised and studied and this group is invariably being expanded. To be used in organic cells, materials must exhibit certain properties. The materials must be able to absorb in the solar spectrum, thermally and photochemically stable, conductive, and form a stable excited state (so that an exciton can be formed by excitation of an electron). It is important to select HOMO and LUMO levels and electrode exit works to facilitate charge transport.
Such materials are fullerene derivatives, polymers based on carbazole and Indole $[3.2 - b]$ carbazole, fluorine and silol [88], [89].

The disadvantage of organic cells is their still low efficiency [90]. Year by year with the synthesis of new materials, it is increased, but it is possible that it will never match the efficiency of silicon cells. Unfortunately, over time the cells change their properties (efficiency decreases) due to degradation of polymers by interaction with external factors (e.g. water, oxygen). The advantage of organic cells is the low cost of materials and many simple and cheap methods of manufacturing such cells. The greatest advantage is the ability to apply organic cells to any surface. Flexible substrates are most commonly used. Clothes with built-in photovoltaic cells have appeared on the commercial market to provide quick recharging of, for example, a smartphone or portable player.

5.7 Dye cells

Dye-sensitized solar cells - also called dye-sensitized solar cells (DSSCs, DSCs or DYSCs) - are, along with organic cells, categorized as the third generation of photovoltaic cells. They were developed by Brian O'Regan and Michael Grätzel in 1991 [91]. Dye cells are also referred to as Grätzel cells due to the inventor's name.
Both electrodes in a dye cell can be transparent or semitransparent, allowing the solar cell to be illuminated from either side. A schematic of the cell design is shown in Fig. 72.
The dye is an important component in the photovoltaic process. The transparent anode is covered with a semiconducting layer (usually oxide) on which the dye is deposited. The most commonly used oxide material is titanium dioxide (TiO_2), zinc oxide (ZnO), niobium (Nb_2O_5). Among others, metal complex compounds, porphyrin derivatives, and phthalocyanines were used as dyes.

In addition to the electrode containing the dye, the cell contains a redox couple (e.g. iodide/triiodide I^{3-}) dissolved in a suitable medium (electrolyte) and a cathode (must be the material catalyzing the redox reaction). A redox reaction is a chemical reaction in which both reduction (the process by which an atom or group of atoms move from a higher oxidation state to a lower one) and oxidation (the atom moves from a lower oxidation state to a higher one, which is equivalent to donating electrons) occurs [92].

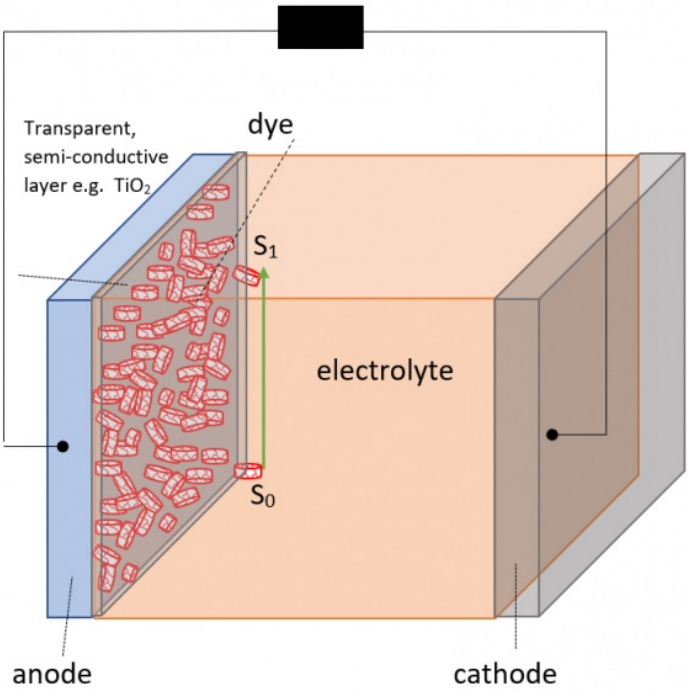

Figure 72: Schematic and operation of a dye cell. Own elaboration.

The operation of a dye cell begins with the absorption of light by the dye particles, which moves an electron from the ground state to the excited state. Now an electron is injected into the conduction band of the semiconductor (e.g. TiO_2). From there it is transported, first in the porous semiconductor layer to the conducting electrode by an external circuit to the cathode. Removal of an electron leads to a reduction of the excited state of the dye molecules (regeneration of the dye by oxidation I^- do I^{3-}). Fig. 73 shows a block diagram of how a dye cell works.

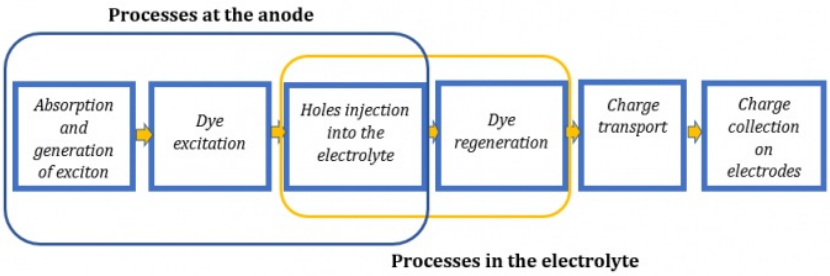

Figure 73: Block diagram of dye cell performance. Own elaboration.

The mechanism of action of dye-sensitized solar cells is used by plants to produce organic compounds, occurring in cells containing chlorophyll or bacteriochlorophyll with the help of light (photosynthesis). The principle of operation is presented in the video "C8 Dye Sensitized Solar Cells," while the method of manufacture is shown in the video "Dye-Sensitised Solar Cells: Animation".

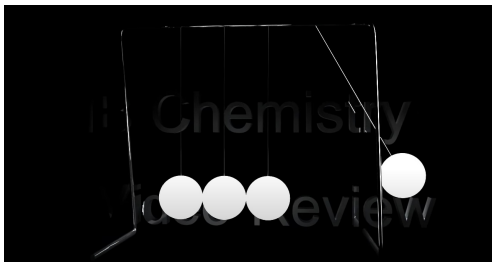

https://pre-epodreczniki.open.agh.edu.pl/openagh-video.php?id=118

Principle of operation of a dye cell
Richard Thornley, C8 Dye Sensitized Solar Cells, DSSC – HL IB Chemistry (Principle of operation of a dye cell), 26.03.2017 (accessed 10.09.2020). Available on YouTube: https://youtu.be/g1TfQ9rypHI.

TheSolarSpark, Dye-Sensitised Solar Cells: Animation (captions) (Method of fabricating a simple dye cell), 20.05.2011 (accessed). Available on Vimeo: https://vimeo.com/24015119.

The maximum efficiency that has been achieved in dye cells is 12.6%. Dye cells have many advantages. The first is the manufacturing process - requiring no complicated equipment or prerequisites. Dye cells are relatively inexpensive, despite not having an easy synthesis process. By using different dye colors, we have control over the appearance of the cell, which increases the usability. Device design can be, in addition to color change, controlled by the oxide layer used, and this increases the aesthetic value. Due to their structure, dye cells are resistant to mechanical damage and are less negatively affected by temperature than silicon cells [81], [82]. The graph in Fig. 74 shows the increasing levels of efficiency of organic, dye, quantum dot-based and tandem cells (the name of the center is on marked grey) [93].

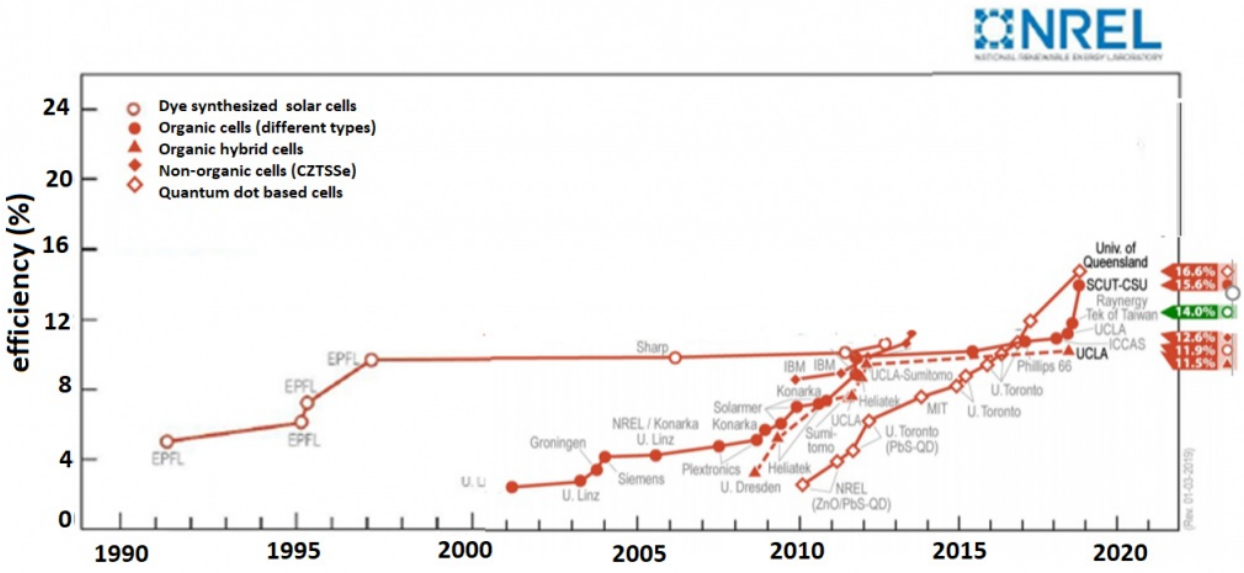

Figure 74: Performance of dye and organic cells. Source: National Renewable Energy Laboratory (NREL), CC0 license, source: Wikimedia Commons.

5.8 Perovskite cells

Perovskite is named after the Russian scientist Lev Perovsky, who studied these minerals. Perovskites have a crystal structure similar to a $CaTiO_3$. Its chemical formula is ABX_3. Atom X (oxygen) with atom B (e.g. Ca) forms a regular octahedron BX_6. The B atom is in the center of the octahedron and the X atom is in the middle. At the six vertex corners of the octahedron, neighbouring octahedrons are attached to form an extended three-dimensional lattice structure. Perovskite materials used in solar cells: A is generally an organic amine ion (such as CH_3NH^{3+}, $NH=CHNH^{3+}$), B is generally a divalent metal ion (such as Pb^{2+}, Sn^{2+} etc.), X means halogen ion (Cl^-, Br^-, JA^-). The inorganic halide metals can form a continuous octahedral structure and a more regular cube-like crystal shape - Fig. 75 (based on [94]). In photovoltaics, new materials and new methods of PV cells production are being searched for, which will allow the production of cells with higher solar energy conversion efficiency and at the same time reduce production costs. Such potential is shown by cells obtained on the basis of materials with a perovskite crystalline structure.

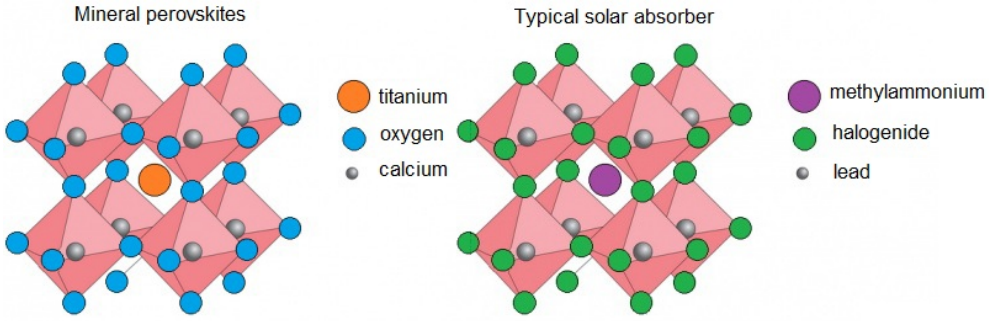

Figure 75: Structure of the mineral perovskite and perovskite used as an absorber in a photovoltaic cell. Own elaboration.

This is evidenced by the fact that after only six years of research on this type of cell, cells were obtained whose solar-to-electric conversion efficiency in the laboratory is 21.5 while silicon cells, despite 60 years of research, have achieved an efficiency of only 25. The theoretical efficiency of cells based on perovskite structures is 31.4. Considering their development rate so far, it is expected that in the near future they will reach energy conversion values comparable to those obtained by silicon cells [95]. The high efficiency of solar energy conversion to electricity is due to the optical and electrical properties of perovskite materials. First of all, perovskites have a high absorption coefficient, much higher than the absorption coefficient of silicon or GaAs (the best absorber so far). This makes it necessary to use a GaAs layer of about 1 μm thickness to achieve a conversion efficiency of 21, while in the case of perovskites, a layer of 300 nm thickness is sufficient [96].
The use of such thin absorber layers reduces the risk of recombination of current carriers. From the application point of view, it allows the reduction of material consumption, but also makes it possible to produce transparent (possibly semitransparent) photovoltaic cells, which fits into the concept of Building Integrated Photovoltaics (BIPV).
The phenomenon of perovskite cells is that they have desirable physical properties and at the same time can be manufactured from materials that are relatively easy to obtain from commonly available raw materials using uncomplicated, well-known thin film technologies. An example of a cross-section through a perovskite thin-film cell is shown in Fig. 76 [97].

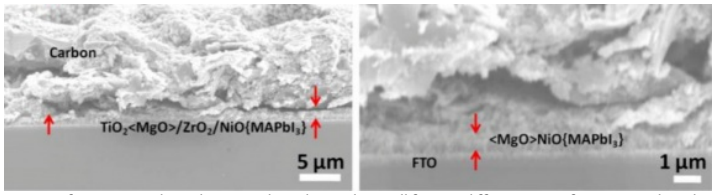

Figure 76: Scanned electron microscope image for a section through a perovskite photovoltaic cell for two different magnifications. Author photo by T. A. Nirmal Peiris et al, CC-BY 4.0 license, source: MDPI .

The high potential of perovskite cells has led to a large number of research and development centers around the world to undertake research in this area. The world's leaders at the moment are:

- Oxford University, England;
- École Polytechnique Fédérale de Lausanne EPFL, Switzerland;
- Korea Research Institute of Chemical Technology KRICT, Republic of Korea;
- The University of Valencia, Spain.

At Oxford University, Dr. H. Snaith has developed a technology for obtaining perovskite cells with an efficiency of 15.4 in which a perovskite absorber layer is obtained using a vacuum-assisted dual-source evaporation technique [98]. In 2012, a spin-off company called Oxford Photovoltaics (Oxford PV) was founded to commercialize thin film solar cell technology. In March this year, the CEO of Oxford PV declared his intention to bring perovskite solar cells to market as early as 2017. At EPFL, Prof. Michael Grätzel developed a two-step process for obtaining perovskite in a PV cell structure. Grätzel's method uses wet techniques, i.e. successive layers are deposited from a solution [99].
The perovskite cells obtained by Grätzel's team have an efficiency of nearly 16%. The technology was put into production at the Australian company Dyesol's perovskite cell factory, which was launched in Turkey in 2016. The company said it would launch pilot production of 20 000 m^2 cells per year in 2016 and mass production with a potential of up to 600 MW in 2018. In Dyesol's favour is the fact that it is a company with a tradition in dye-sensitised cell (DSC) technology, which is the forerunner of perovskite cells. Since the invention of dye-sensitized cells, Dyesol has been developing this technology in collaboration with the Swiss polytechnic EPFL. Today, they are the world leader in DSC cells, offering both the materials and the apparatus as well as the technology needed to produce them. Recent perovskite solar cell efficiency records of (20.1%) come from the Korea Research Institute of Chemical Technology (KRICT). However, it should be emphasized that the record value of efficiency was determined for a cell with an area of 0.0955 cm^2 [100]. All the mentioned centers focus on developing the technology of obtaining high-efficiency perovskite cells on glass substrates. In comparison with other research and development centers in the world, Saule Technologies laboratory is distinguished by the fact that the whole process of cell production is carried out at relatively low temperatures, not exceeding $150^o\,\mathrm{C}$. Thanks to this, materials sensitive to high temperatures, such as polymer films, can be used as substrates, which can definitely broaden the spectrum of applications for these types of devices.
Although great progress has been made in perovskite cell research since 2012, there are still several unresolved issues. A major limitation in using perovskites for the mass production of photovoltaic cells is their high sensitivity to humidity. Upon interaction with water vapor, perovskites degrade. For this reason, the process of perovskite production must be carried out in an anhydrous atmosphere, which requires the use of special chambers providing appropriate environmental conditions. The low resistance of perovskites to moisture adversely affects the stability of perovskite cells. Moreover, the structure of perovskites used in solar cells contains lead, which is a toxic and carcinogenic element. As a result of interaction with water vapor, perovskites undergo degradation and one of the degradation products is toxic lead compounds. Laboratories are working on replacing it with other elements, e.g. Sn, but the studies carried out so far show that substitution of lead in the perovskite structure with another element significantly worsens its optical and electrical properties, and thus worsens the cell efficiency. Currently, both the University of Oxford and the Technical University of Lausanne use encapsulation of cells in a polymer film to protect the cell from interaction with water vapor and improve its stability [101]. Hermetization is performed in such a way that the cell placed on a glass substrate is covered with another glass sheet and the space between them is filled with appropriate polymer solution. This solution on one hand prevents water vapor penetration and the release of lead compounds, on the other hand however, it raises the production costs of the cell. The possibility of using a flexible substrate, on the one hand, greatly

expands the range of applications of perovskite photovoltaic cells, on the other hand, strongly raises the level of difficulty in developing an appropriate deposition technology. An example of a perovskite cell on a flexible substrate is shown on fig. 5 in article D. Kim i C. Kim "A Ladder-Type Organosilicate Copolymer Gate Dielectric Materials for Organic Thin-Film Transistors" [102]. Very high repeatability must be maintained between the successive layers of the perovskite solar cell (electrodes, blocking layer, absorber layer), the layers must lie perfectly (down to the nanometer) on top of each other. Such a technological operation is difficult to realize even when the substrate is a glass sheet. When the substrate is a polymer film that is much more susceptible to deformation than glass, the execution of the process, especially in the "roll to roll" technology, is a huge technological challenge [103].

5.9 Hybrid cells

Hybrid solar cells have two meanings in the literature. A hybrid cell is defined as a multi-layer cell consisting of two or more cells of different types or generations. In the second sense, a hybrid is a combination of a photovoltaic panel and a solar collector (as described in chapter 7.6 PVT systems). Hybrid cells in the first sense will be presented below.

The aim of photovoltaic engineers and researchers is to create a cell that is highly efficient, cheap, easy to manufacture and robust. Hybrid cells are intended to combine the advantages of different cell types.

The first cell type is organic-inorganic hybrid cells. These cells can be produced by modifying the morphology of the silicon nanostructure, i.e. nanostructures were made in silicon (made by nanospheric lithography) and combined with a conductive organic polymer referred to by the acronym PEDOT:PSS. This layer was modified with silicon dioxide SiO_2 iand further processed and cleaned. A gold layer was used as the outer electrode. The cells produced achieved a short circuit current density of 39.1 $\frac{mA}{cm^2}$.
It was also possible to fabricate a cell with a metal/ organic layer/silicon modified /Au architecture. The silicon was modified by injecting multi-walled carbon nanotubes (MWNTs) and poly(3-octylthiophene), an organic donor material, into the silicon [104].
Another example of organic-inorganic hybrids are organic cells doped with silicon nanowires (SiNWs) [105]. On the indium tin oxide electrode, layers of PEDOT:PSS (as a supporting layer) and - as an active layer - a mixture of poly(-3hexylthiophene, P3HT) and methyl ester of (6,6)-phenyl-C_{61}-butyric acid were deposited successively (by the method of uncoiling). Nanotubes have been injected into this layer.
The above-mentioned hybrid organic-inorganic cells achieved efficiencies of several percent. These are not far from the efficiencies of typical organic cells. In the above cases, an increase in short-circuit current density was observed, which in combination with high open circuit voltages is a promising result.

The second cell type studied is perovskite-silicon cells. Due to the complementarity of absorption spectra (Fig. 77) [106], these are the most promising. They offer the hope of performance beyond the maximum efficiency of silicon cells while keeping production costs low. An example structure is shown in Fig. 78 (based on [106]).

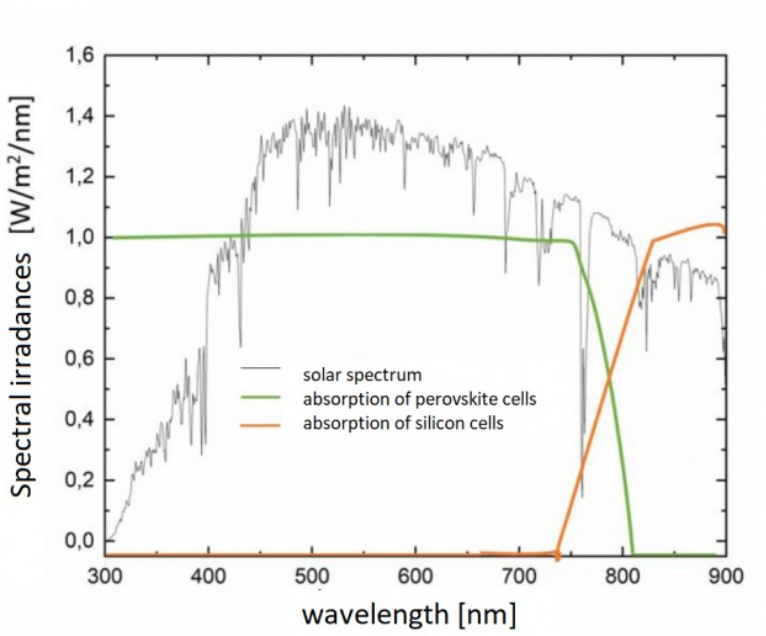

Figure 77: M1.5 solar spectrum, absorption spectrum of perovskite cells, absorption spectrum of silicon cells. Own elaboration.

The active layer of such cells consists of a silicon layer (bottom, deposited on a non-transparent electrode), an upper perovskite layer and a recombination layer between them. This type of interconnection made it possible to achieve efficiencies of up to 26% [107].

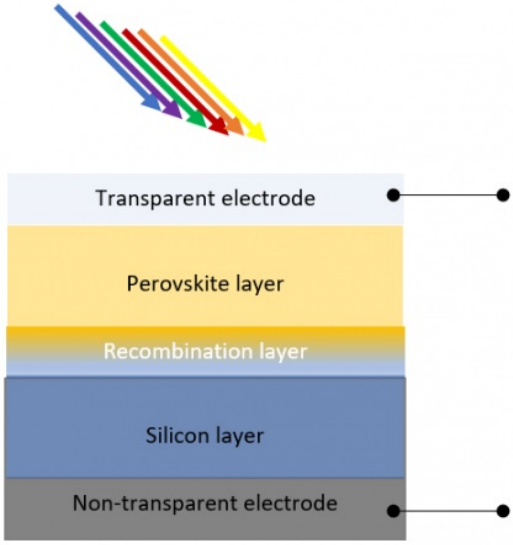

Figure 78: Example structure of a perovskite-silicon cell. Own elaboration.

The last type presented is polymer cells doped with inorganic quantum dots.
Its principle of operation is the same as that of organic cells. Quantum dots (QDs) increase the absorption of the system - the generation of charge carriers can be achieved by photons which are also absorbed in the inorganic material (dots). The addition of quantum dots is also intended to support the transport of electrons and holes across the LUMO and HOMO levels, as well as to increase charge conductivity. Additionally, acceptor inorganic materials are more stable than organic materials, which solves one of the biggest problems with organic photovoltaics - its instability. The principle of operation is similar to that of organic cells, except that the polymer acts as the donor and the quantum dots as the acceptor. A schematic representation of the cell is shown in Fig. 79 [108].

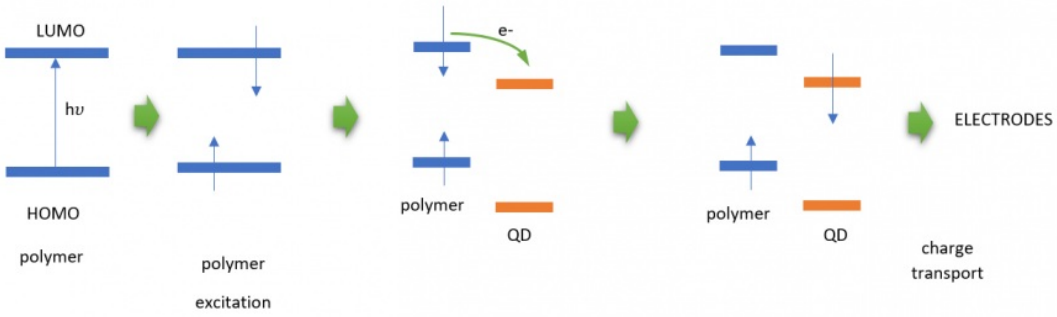

Figure 79: Operation principle of polymer cells doped with quantum dots. Own elaboration.

5.10 Concentrator photovoltaics

Concentrator systems are actually one method to increase the efficiency of photovoltaic installations. Concentrator photovoltaics (CPV) is based on the application of optical elements to focus sunlight onto a small solar cell. The development of concentrator photovoltaics began in 1976 in New Mexico (Sandia National Laboratories) with the one kilowatt Sandia I and Sandia II [109].

The introduction of an additional, expensive facility is justified when the installation is limited by free area. The use of a concentrator enables the energy flow to the cell or panel to be increased.

Concentrator photovoltaics achieve high efficiency, generate relatively low costs and therefore provide a quick payback. A major advantage of this type of installation is its scalability.
The classification of concentrator photovoltaics is based on the energy multiplicity measured by the solar concentration ratio, abbreviated as solar concentration ratio which determines the degree of concentration of the radiation. Several types of concentrator-cell systems can be distinguished according to efficiency (Fig. 80): Low Concentrator Photovoltaic (LCPV), Medium Concentrator Photovoltaic (MCPV) and High Concentrator Photovoltaic (HCPV) [110], [111]. The fastest growing and most popular technologies are HCPV [112].

LCPV	MCPV	HCPV
• modified crystalline cells • uniaxial tracking system • 1.5-10 suns	• crystalline or thin-film cells • uniaxial or biaxial tracking system • 10-300 suns	• multi-junction cells • biaxial tracking system • 300-2000 suns

Figure 80: Concentrators classification. Own elaboration.

A quantitative measure of the concentrator is the geometric concentration factor of solar radiation CR.

$$CR = \frac{A_C}{A_0} \tag{17}$$

It determines to what extent the solar radiation flux incident on the cell is increased. The geometric concentration factor is the ratio of the active area of the concentrator A_C over a surface of receiver A_0.
Another measure used to describe concentrators is the effective concentration ratio (18). It is defined as the total amount of radiation absorbed by a surface.

$$C_e = \eta \cdot C_g \tag{18}$$

In the equation C_g is the geometric concentration factor η of the solar concentrator efficiency.
As opposed to a conventional PV panel, the CPV receiver must be positioned in the direction of the direct normal irradiance. If the solar concentrator and CPV receiver are not aligned towards the sun, they will lose some of the incoming solar radiation. The maximum angle at which the incoming solar radiation can still be captured by the solar concentrator is called the angle of acceptance [113], [114]. A part of the concentrator system must therefore be a tracer. For two-dimensional concentrators, the reception angle can be different (for different directions). For a given receive angle θ, for a point-focused concentrator, the maximum possible concentration C_{max} is about

$$C_{max} = \frac{n^2}{sin^2\theta} \tag{19}$$

In the equation (19) n is the refractive index of the medium in which the receiver is located.
The world's largest operating CPV facility (138 MWp) was built by Suncore Photovoltaics and is located in the city of Golmud, China. Large facilities (19.9 MWp) of this type also include the Fort Churchill Solar Array in Yerington, Nevada.

The parabolic concentrators located in Harper Lake are presented below. The installation takes the form of an array of solar panels spread over 125 metres long. One row consists of 10 solar panels, each 12 metres long and with an aperture of 5.76 metres. The skeletal arrangement with monolithic glass reflective panels is shown on Fig. 81 [115].

Figure 81: Parabolic trough at Harper Lake in California (parabolic concentrator). Aut. photo by Z22, licensed under CC BY-SA 3.0, source: Wikipedia .

Research on concentrator techniques is conducted at Sandia National Laboratories, a US scientific research institute dedicated to scientific research and technology development in the energy field. They are featured in the film 'Parabolic Dish Stirling Engine at Sandia National Laboratories'.

https://pre-epodreczniki.open.agh.edu.pl/openagh-video.php?id=120
Concentrator Sandia National Laboratories
Sandia National Labs, Parabolic Dish Stirling Engine at Sandia National Laboratories (Concentrator Sandia National Laboratories), 29.03.2010 (accessed 12.09.2020). Available on YouTube: https://youtu.be/AdCNnSdtU7U.

6. Cell technologies

6.1 Busbar cells

More than 90% of photovoltaic cells are now mostly built from silicon. After a p-n junction is made, a forward (negative) electrode is applied to the n-type semiconductor, made as a network of thin paths horizontal to the edge of the cell (called fingers), which collect charges from the entire cell and transfer them to ribbon connection paths perpendicular to the fingers, called busbars. A positive electrode (on p-type silicon) covers the entire back surface of the cell.
Busbar technology has been used since the early introduction of photovoltaics to the market. Polycrystalline cells first used 2 junction paths, or 2 busbars, achieving efficiencies of 12%.

They had 110 to 660 contact points with horizontal paths, that is, with fingers (Fig. 82) [116].

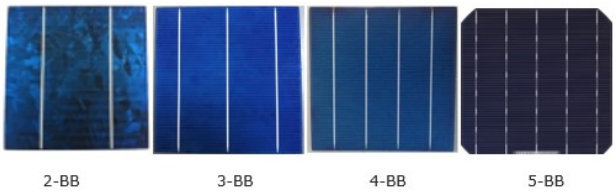

Figure 82: Photovoltaic cells from 2-BB to 5-BB. Own elaboration.

As this technology was developed, the number of busbars was increased so that in more recent developments it is 5 busbars.

When 3 busbars are used, the finger length is reduced from 39 mm to 26 mm (Fig. 83), which translates into a reduced finger cross section and at the same time the cell performance is increased.

Number of busbars	Width [mm]	Cross section [mm²]	Finger length [mm]	Optical shading [%]
2BB	4	0.6	39.0	2.6
3BB	4.5	0.68	26.0	2.9
5BB	5	0.75	15.6	3.2
6 wires	1.2	0.19	11.5	0.6
12 wires	2.4	0.38	6.5	1.2

Figure 83: Comparison of cells with different number of busbars. Own elaboration.

Increasing the number of busbars helps to avoid the large impact of microcracks on photovoltaic cell performance.

Microcracks eliminate part of the photovoltaic cell from being able to receive electricity from it. The reason for microcracks, for example, is that cells are joined by soldering at temperatures between 240 and 340 ^{o}C.

This exposes the entire structure to stresses associated with uneven heating of the cell, which can lead to degeneration of the entire panel. The lifetime of panels is shortened by microcracking, which increases the junction resistance.

The number of busbars and the number of fingers affect the performance of the cell (the so-called fill factor (FF) and series resistance) and, consequently, the total efficiency of the photovoltaic panel.

Using a larger number of busbars shortens the path that the electron and hole must travel, which decreases the internal resistance and facilitates current flow.
Increasing the number of busbars reduces the current flowing through a single busbar which results in lower operating temperature of the cell.
The resistance of the cell depends on the distance that must be overcome by the electric charge in the cell. Increasing the number of busbars decreases this distance. Increasing number of busbars [117] has an influence on the increase of cell efficiency, but also improves its work in shaded conditions or in case of mechanical damages reducing the cell surface. Increasing the number of busbars also increases the mechanical resistance of the panel to rain, snow, hail or wind.

MBB "Multi-Busbar" technology

In cells manufactured with MBB multi-path technology, wire electrodes are introduced in place of wide strip busbar electrodes, and the number of wires is 15 or more per cell. That is, each wire conducts less than 0.5 A rather than 4.5 A as with two busbars.

There are at least three different solutions in operation today: SmartWire technology from Swiss company Meyer Burger, Merlin technology, and Schmidt's Multi Busbar Connector.
Instead of the busbars described above, SmartWire technology is based on the use of a grid of wires on the plane of the photovoltaic cell. The number of electrical connections in such a single cell reaches up to 2660 (Fig. 84). This provides resistance to mechanical stress and better performance in low light conditions.

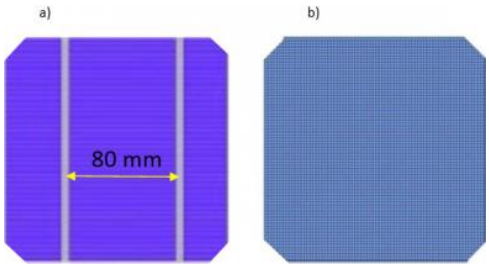

Figure 84: Appearance of a photovoltaic cell (a) with 2-BB (110 connection points) and a photovoltaic cell (b) with Smart Wire technology (2000 connection points). Own elaboration.

Merlin technology is characterized by placing a specially formed copper grid over and under the photovoltaic cell (Fig. 85) in the silicon cell. In this case, the internal connections are stronger, resulting in lighter and more durable photovoltaic panels.

Figure 85: External appearance of the cell made with Merlin technology. Own elaboration.

Here, flexible copper mesh replaces traditional busbars, which reduces material consumption and thus costs. Furthermore, Merlin's technology can be easily integrated into existing cell and panel production lines.
Multi Busbar Connector Technology (Fig. 86) is based on the use of 360 microns, coated with a thin layer of SnPbAg alloy about 15 microns thick. 12 busbars are placed on each cell. This results in an increased fill factor, which consequently increases the power produced by the photovoltaic cell.

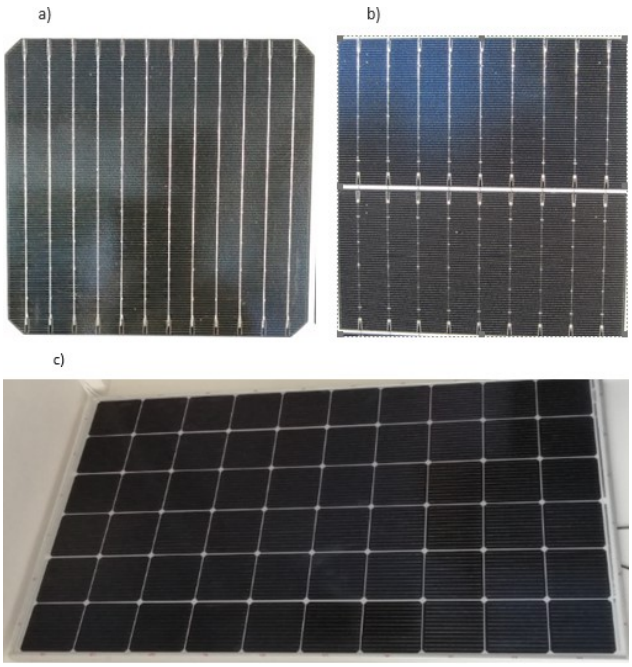

Figure 86: Cell and panel made with Multi Busbar Connector technology: a) cell (12 BB), b) half cell (9 BB), c) panel (12 BB). Own elaboration.

Passivated Emitter Rear Cell - PERC

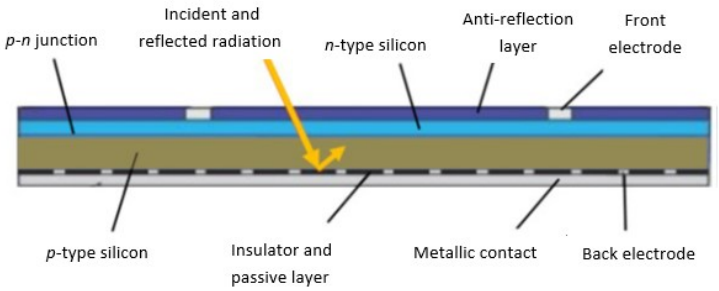

Figure 87: Construction of PERC type cell. Own elaboration.

PERC cell differs from standard photovoltaic cell in the construction of the rear electrode of the cell.
In the rear electrode, a modification is introduced, consisting of a deposition of an additional layer, which performs reflection and passivation functions.
Passivation is used to protect against oxidation of the silicon surface and reduce the recombination at the silicon metal electrode interface.
The insulator layer (Fig. 87) causes, among other things, reflection of sunlight and directing it to the cell to increase absorption, and thus the cell's power [118]. The increased reflection of electromagnetic radiation from the passivation layer increases the absorption and, therefore, also increases the obtained power of the cell.

Currently many laboratories are working on increasing the efficiency of photovoltaic cells, but many of the solutions developed have more laboratory than commercial application. In addition to the problems discussed above, there are also those related to shading, microcracks, reflection and, of course, lowering production costs. All these elements are motivation to search for solutions optimizing cell work.
Increasing the number of busbars on a cell decreases resistance, which results in an increase of power obtained from the cell. Most losses connected with microcracks are avoided. Increasing the number of busbars gives electrons more opportunities to reach the electrode.

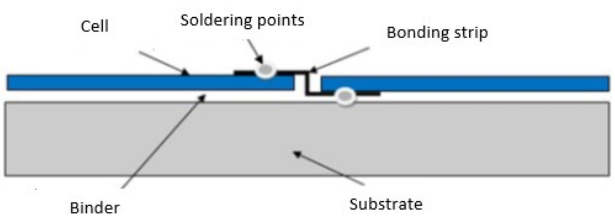

Figure 88: Combining busbar-based cells in photovoltaic panels. Own elaboration.

The way of joining photovoltaic cells in PV panels made with busbar technology are shown in Fig. 88. The soldering places are

particularly vulnerable. The soldering paces are particularly exposed to stress. This is due to the level of temperature at the time of joining the cells to each other.

6.2 PERL cells

Over the past decade, HIT-type solar cells with back electrodes have significantly improved the performance of commercially available photovoltaic panels; nevertheless, there is still scope for even higher performance cells based on crystalline silicon. A high-efficiency silicon cell made under laboratory conditions, the Passivated Emitter Rear Locally diffused cell (PERL), is shown in Fig. 89. This cell designed in the late 1980s had efficiencies as high as 23%, a huge improvement in silicon cell efficiency of 17% – the highest value just 7 years earlier. Since then, further refinement of PERL-type cells has brought their efficiency to 25%.
The PERL-type cell shares many features with the cell whose electrodes are placed at the back. Similarly, there is complete shielding in the passivating oxide layer and small surface contacts. However, the PERL type cell is a more robust design, more tolerant to environmental conditions, in view of the poor surface passivation and poor performance of classic cells.
Major improvements made in the PERL-type cell in recent years include a significant increase in the oxide passivation of the top surface, which allows the direct application of a two-layer anti-reflection coating [119]. An "annealing" sequence for this oxide and localized top contact points are used to increase the open circuit voltage and improve back surface passivation, and metallization resistance is chosen to improve the fill factor.
To maximize cell performance, as much light from useful wavelengths as possible should be absorbed by the cell. To achieve this result, modern cell designs, such as the PERL cell, incorporate several optical solutions.
In this case, the optical losses in the front of the cell are reduced by implementing a textured inverted pyramid structure (Fig. 89), coated with an anti-reflective layer, which allows the absorption of the reflected light a second time, reducing the transmission losses. The electrodes at the front were made to have the smallest possible surface area, which increases the intensity of light entering the photovoltaic cell.
The inverted pyramids along the top surface are primarily for optical purposes. Most of the radiation quanta will hit one of the side walls of the pyramids, which causes the rays to be reflected, thus increasing the optical path of the light. The reflected light ray gives the light, at least, a second chance to return to the cell and be absorbed. Some quanta near the bottom of the pyramids sometimes have more chances.

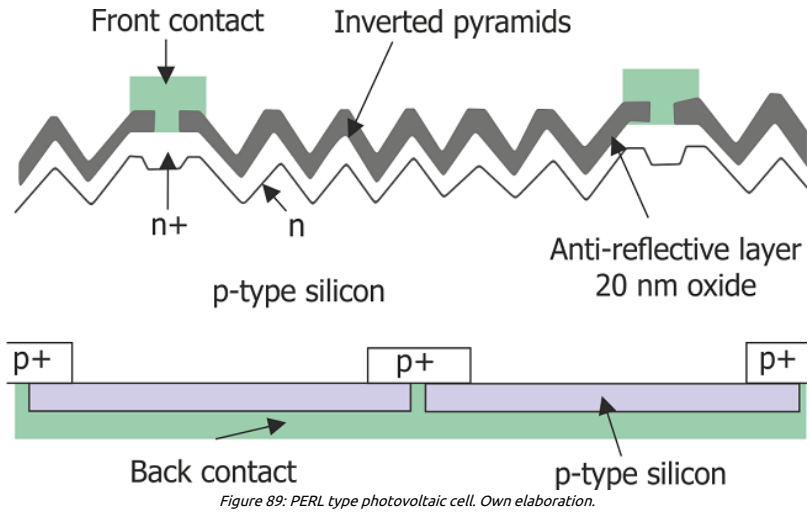

Figure 89: PERL type photovoltaic cell. Own elaboration.

Pyramids are coated with a layer of oxide thick enough to act as an anti-reflective coating. In more recent designs, the oxide layer is thin and a two-layer anti-reflection coating is used [119].
The quantum absorbed by the cell moves diagonally through the cell towards the back surface of the cell. In this way, the radiation quantum has a longer path over which it can be absorbed by the cell. The unabsorbed light reaching the back surface is reflected by a highly efficient reflector formed by combining a back oxide layer covered with a layer of aluminium [22]. The reflectance from this combination depends on the angle of incidence and the thickness of the oxide layer, but typically exceeds 95% for incidence angles near 0^o (normal). The reflection coefficient decreases below 90% when the incident angle approaches the angle of total internal reflection at the silicon/oxide interface (24.7^o) and increases again to near 100% when this angle is exceeded.
On the back surface of the photovoltaic cell, spot electrodes are used in conjunction with thermal oxide passivation layers to reduce unwanted recombination at the surface in the uncontacted region. Silicon heavily doped with boron (p+) acts as a local back surface to limit minority electron recombination.
Light reflected from the back moves toward the top surface. Some quanta of radiation reach the surface and can leave the photovoltaic cell without producing an exciton. Others undergo total internal reflection. This causes about half of the light radiation directed at the front surface from the inside to be reflected back into the cell toward the back electrode.
The number of light quanta leaving the photovoltaic cell after the first reflection depends on the geometry of the pyramids. The loss of light energy can be reduced by destroying some of the symmetries used, for example by using tilted inverted pyramids or by using the "tiler's pattern" method. The latter approach is currently used in PERL cell designs.

The combination of inverted pyramids and a back reflector creates a very efficient way to increase light absorption by increasing the path length of a light ray in a photovoltaic cell. The effective light ray path length enhancement factors are measured [22]. The increase in absorption occurs primarily in the infrared region.
The external responsivity (that is, the response of the photovoltaic panel (in amperes) to 1 watt of incident light) of PERL-type cells reaches higher values at longer wavelengths than conventional silicon cells, with values of 0.75 $\frac{A}{W}$ measured at 1.02 μm. The energy conversion efficiency for some wavelengths is even greater than 45% [120] compared to classic cells.

Current PERL-type cells lose approximately 5% of the incoming light due to absorption loss or reflection associated with the metal electrodes, combined with reflection from the non-metalized top surface of the cell. The optical losses that occur are also due to reflection and absorption by the top metal electrodes of the cell. One can minimize this reflection by sizing the electrodes, height, width, and shape. One can also try to redirect light rays into the cell by bypassing the electrodes [121]. Thus, there is some room for small to moderate increases in efficiency by further improving the optical properties of these cells.

Advanced cell designs have been used in spacecraft and terrestrial high-value applications such as solar car racing [122]. Very expensive multi-step photolithographic processes were used there. Such photovoltaic cells are too expensive for wide applications. Nevertheless, recent advances in cell construction using laser technologies make it possible to produce PERL-type cells at low cost. As mentioned, the best cell efficiency is 25%, and the best photovoltaic panel efficiency is 22.9% [123].

It appears that crystalline silicon wafer technology will be the dominant photovoltaic technology for at least the next decade. This is indicated by the investments made in photovoltaic manufacturing plants and the reduction in PV panel prices. Bifacial Cell Technology (PERL) photovoltaic panels have also recently emerged.

In summary, photovoltaic cells made with PERL technology have many advantages:

- higher cell efficiency achieved by passivation of n-type c-Si material,
- only one temperature step in the deposition technology, both phosphor and boron, that minimizes the loading on silicon wafers,
- short production time of PERL cells,
- different cell production technologies, single-sided or double-sided cells,
- higher, up to 30%, energy efficiency of double-sided cell.

6.3 Interdigitated Back Contact cells

The Interdigitated Back Contact (IBC) cell with back electrodes is an alternative approach to producing high efficiency cells. Reducing the shadowing of the photovoltaic cell by the front electrode prevents the reduction of solar energy reaching the cell (the electrodes are located at the back of the cell).
The structure of an IBC type cell is shown in Fig. 90. Light passes through the stabilizing layer SiO_2 into the interior of the cell, which is constructed from an n-type monocrystalline wafer. Both contacts are located on the back surface of the cell. The resulting exciton breaks up into charges that diffuse into the p- and n-type areas directly above the contact areas (in these areas, the oxide has been removed from the back surface). Both the n-type and p-type junctions lie on the unlit side of the cell under the contact metallization. A schematic of the IBC-type cell is presented in Fig. 90a, where the contacts are shown as combs. Fig. 90b, on the other hand, shows the contacts collecting the charges accumulated in the n-type semiconductor and p-type of the cell.

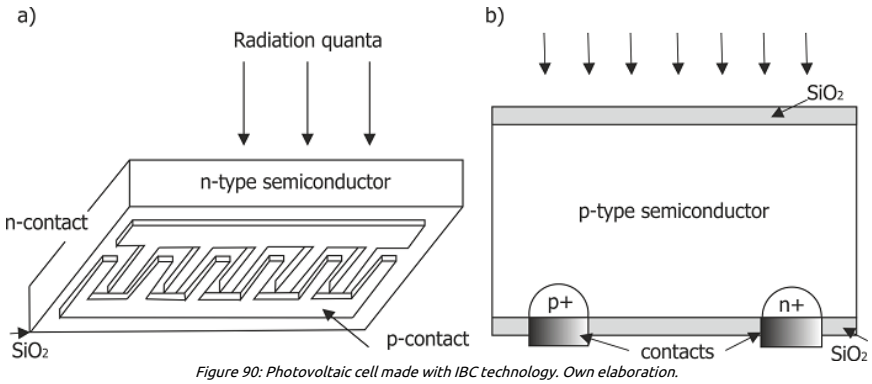

Figure 90: Photovoltaic cell made with IBC technology. Own elaboration.

The back contact cell design was perfected at Stanford University in the 1980s [124]. In the 1990s, a new company, SunPower, was formed and commercialized the technology, producing IBC photovoltaic panels with an initial 22.5% efficiency. In early 2000, production was greatly simplified and expanded. Today, SunPower manufactures IBC cells that achieve 24.2%. The efficiency performance of both cells (at 24.2%), and panels (at 22.4%) has been confirmed by independent analysis [123]. In contrast, Trina Solar reported that its Main National Laboratory has set a new efficiency record of 25.04% for an n-type monocrystalline silicon cell made with IBC technology. This result was independently confirmed by the Japan Technological Laboratory for Electrical and Environmental Safety (JET) [125].
A sketch of the current commercial cell structure is shown in Fig. 91 [126], [127]. Note that phosphor diffusion is used along the

illuminated surface to control recombination along that surface [128].

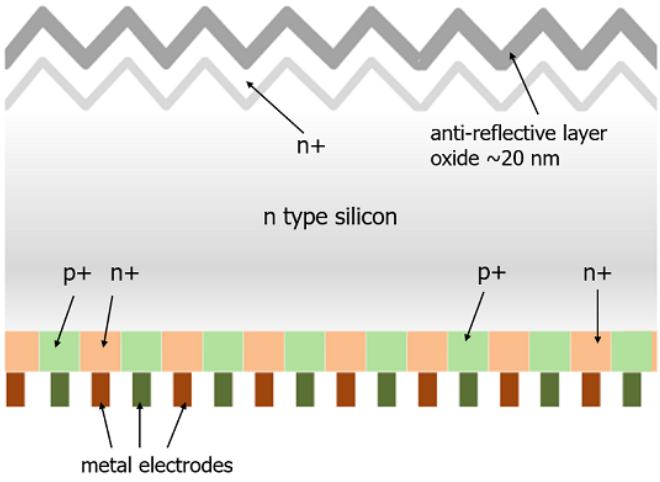

Figure 91: Photovoltaic cell made in IBC type technology. Own elaboration.

An IBC photovoltaic cell has multiple localized junctions instead of one large p-n junction. Electron-hole pairs, generated by incident light that is absorbed on the front surface, can be collected at the back of the cell. The semiconductor-metal interfaces are as small as possible to reduce unwanted recombination. As shown in Fig. 91, the back of an IBC-type photovoltaic cell has two metal combs. One collects current from the n-type contact and the other collects current from the p-type contact. The front surface area is formed by heavily doped n-type silicon in order to reduce recombination on this surface. However, the doping intensity gradually decreases toward the back to act as a p-type semiconductor region. The front surface is textured and embedded with a two-layer anti-reflective coating. It acts as a passivator (silicon dioxide) on the front side of the cell.

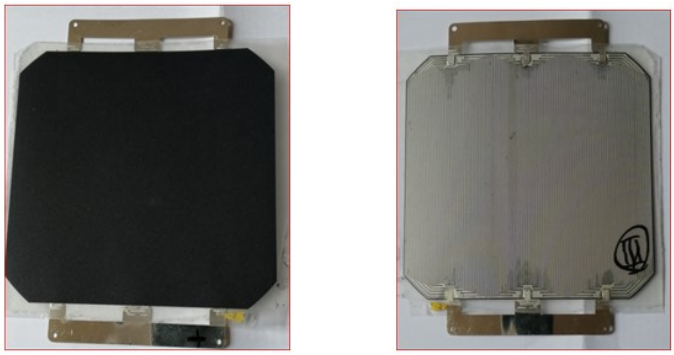

Figure 92: Photovoltaic cell of IBC type with front and back view. Own elaboration.

Fig. 92 shows a photo of the cell from the front, whose color is uniformly dark, while the photo of the cell from the back clearly shows the alignment of the electrodes, which are charge-collecting combs. The collecting electrodes do not shade the surface through which the sun's rays can reach the inside of the cell and cause exciton formation.
The IBC photovoltaic cell is the most technologically complex but has the highest efficiency among mass-produced silicon cells. In general, the structure of a cell made with this technology has several advantages over the construction of conventional photovoltaic cells. The most obvious is the elimination of shading caused by the front electrode, which in the generated current can give a gain of $5 - 7\%$. The lower series resistance during current flow in the contacts is also important, due to the fact that the back contacts occupy almost the entire back surface, so the distance between them is small. Furthermore, it is a great advantage to separate the optical optimization, performed at the front, from the electrical optimization, performed at the rear.

6.4 Smartwires cells

Photovoltaic technology is constantly evolving. Significant improvements have been made at the level of the photovoltaic cell, but there are limitations at the level of those connections into the photovoltaic panel. Swiss company Meyer Burger [129] has developed Smart Wire Connection Technology (SWCT), which does not reduce the performance of the entire photovoltaic panel compared to a single photovoltaic cell. It involves combining the lamination process and the interconnection of cells to form a photovoltaic panel in a single lamination step. During this process, material consumption and energy consumption are reduced and cell efficiency is at 25.4%.
Smartwire technology also involves the use of a grid of wires on the photovoltaic cell plane instead of the conventional solution of interconnecting busbars. Here, the number of electrical connections in a single cell reaches up to 2640, which provides resistance to mechanical stress and better performance in low-light conditions (Fig. 93).

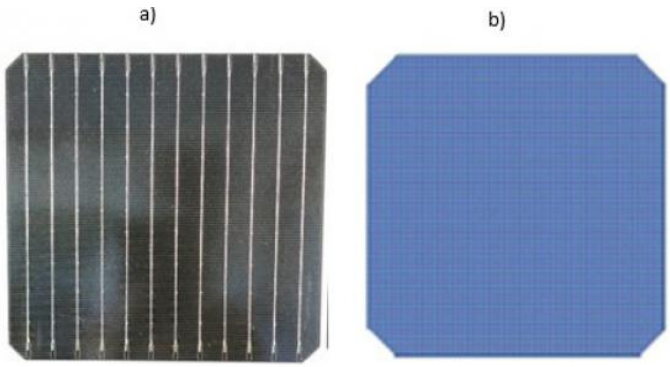

Figure 93: Appearance of photovoltaic cell with (a) 12-BB (660 connection points) and photovoltaic cell (b) with Smart Wire technology (2090 connection points). Own elaboration.

Using this process reduces electrical and optical losses in the photovoltaic panel, due to shorter charge paths to the electrodes and less shading of the cell by the electrodes than in standard busbar technologies.
SWCT technology transforms the appearance of the front surface of the photovoltaic cell and offers several additional benefits:

- connects multiple wires, reducing ohmic and optical losses by reducing the thickness of the busbars as the number of wires can be tailored to the design of a particular photovoltaic cell,
- the use of silver paste can be significantly reduced,
- the light absorption of the photovoltaic cell is improved by intelligent reflection of light through the wires,
- reducing the impact of photovoltaic cell micro-cracks by increasing the number of current collection paths,
- simplifies process steps, soldering and lamination processes are replaced by a single lamination process which are done together,
- stress in the photovoltaic cell is reduced because the temperature during the bonding process is uniform throughout the cell and is below $160^{o}\mathrm{C}$,
- the cost of making the photovoltaic panel is lower,
- the process is compatible with many types of materials such as Al, Cu, Ni, Ag and is therefore possible for new material combinations and joining new photovoltaic cell concepts such as back passivated cells, HJT, metal plating and IBC.

SWCT is an electrode-to-photovoltaic cell bonding technology based on wire bonding. It typically uses 15 to 38 wires on either side of the photovoltaic cell. The conductors are round copper-based wires coated with a low-temperature alloy, typically a layer 1-2 microns thick with 50% indium alloy. The wires are embedded in a polymer film that is applied directly to the metallized cell.

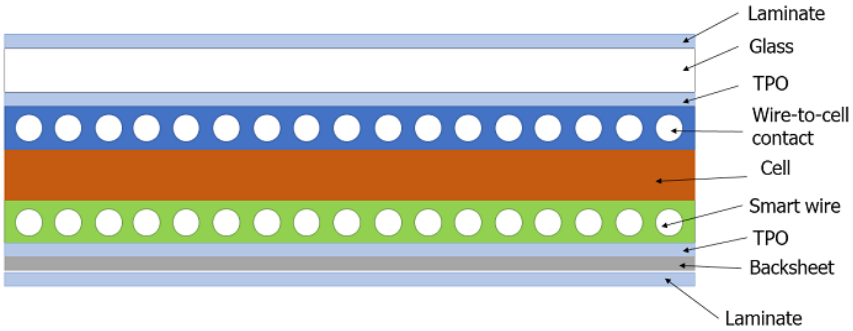

Figure 94: Cross-section through a photovoltaic cell made with SWCT technology. Own elaboration.

The components arranged in this way are laminated (Fig. 94). The busbars are associated with the photovoltaic cell metallization and provide electrical contact with most of the material (e.g., the number of busbars and their thickness can be customized for almost any cell metallization design and cell power). Busbars on the surface of the photovoltaic cell (both front and back) are not needed. This saves time and materials (the metallization process requires expensive material such as silver paste) and prevents shadowing. SWCT technology has an additional advantage, better passivation of the backside of the photovoltaic cell can be achieved with an aluminum screen printed on the backside of the surface field or with any backside passivation method (such as $SiO_2, a-Si, AlO_x$ etc.).
Photovoltaic cells are fragile and therefore need to be protected to resist external conditions such as rain, hail, moisture, wind and snow. Protection is usually achieved by embedding the photovoltaic cell in glass and an encapsulation layer. Since the generated current must be transported from one cell to another, electrical losses occur. The most reliable, proven techniques used to date are ribbon soldering.

SWCT technology offers up to 38 coated copper wires to carry the charge generated by the photovoltaic cells. The finger length can be reduced from 39 mm to 4-8 millimeters, which in turn makes the power loss at the finger negligible. This reduction in finger length is achieved without changing the cross section of the transport material. The power loss associated with resistance drops and more energy can be extracted from each individual photovoltaic cell. The comparisons in the table below show that an SWCT with 30 wires of 0.2 mm diameter has the same optical shading as one with 3 busbars. The SWCT with 18 wires of 0.3 mm

diameter has 85% higher Cu cross section compared to 3 busbars, i.e., lower resistance. In addition, optical shadowing is reduced (2.6% compared to 2.9% for 3 busbars), and there are additional benefits from the reduced finger length to 8.2 mm. In summary, the data on the Fig. 95 below [129] show that SWCT has better performance than busbar technology.

Connection method	Wire diameter [mm]	Width [mm]	Cross section [mm^2]	Finger lenght [mm]	Optical shading [%]
2 busbars		4	0.60	52.0	2.6
3 busbars		4.5	0.68	39.0	2.9
5 busbars		5	0.75	26.0	3.2
6 wires	0.2	1.2	0.19	22.3	0.6
12 wires	0.2	2.4	0.38	12.0	1.2
18 wires	0.2	3.6	0.57	8.2	1.7
22 wires	0.2	4	0.69	6.8	1.9
30 wires	0.2	6	0.94	5.0	2.9
38 wires	0.2	7.6	1.19	4.0	3.7
18 wires	0.3	5.4	1.27	8.2	2.6

Figure 95: Comparison of ribbon and wire technologies. Optical shading is calculated as the ratio of ribbon/wire width to cell length. Own elaboration.

In order to compare SWCT type technology with busbar technology, photovoltaic panels were prepared using the same type of cells. Two types of cells were used in the experiment, monocrystalline cells made by Hareon Sun (China) and cells made by HJT (Switzerland). The performance data of the c-Si monocrystalline cell were collected on Fig. 95. The panels thus fabricated were subjected to performance tests. Increasing the number of busbars to 5 raised the cell power to 102%, and in SWCT technology to 103%. If the microcracking resistance of the cells is added to this, the use of the SWCT type procedure is justified.
With SWCT technology, there is no drastic loss of power due to microcracks [130], because the generated charges can reach the collecting electrode through a different path.

The video "The Making of SmartWire Technology" shows the manufacturing technology of photovoltaic panels made with smart-wire technology.

https://pre-epodreczniki.open.agh.edu.pl/openagh-video.php?id=183
The Making of SmartWire Technology'
SolarTech Universal, The Making of SmartWire Technology, 13.10.2016 (accessed 01.08.2020). Available on YouTube: https://youtu.be/c6zbtqc7_tk.

The video "The Technology Behind SolarTech Universal" shows the manufacturing technology of photovoltaic panels made with smart-wire technology.

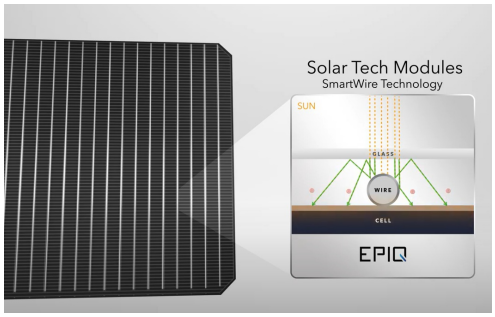

https://pre-epodreczniki.open.agh.edu.pl/openagh-video.php?id=182
The Technology Behind SolarTech Universal
SolarTech Universal, The Technology Behind SolarTech Universal, 21.09.2018 (accessed 01.08.2020). Available on YouTube: https://youtu.be/YAOed5iEnEo.

6.5 HIT technology cells

A photovoltaic cell where a thin layer of crystalline n-type silicon is sandwiched between two thin layers of amorphous silicon is called a HIT (Heterojunction with Intrinsic Thin Layer). It is one of the solutions resulting from work aimed at achieving higher efficiency commercial cells. This cell combines both crystalline and amorphous features of silicon cell design in a single structure. The structure of the HIT photovoltaic cell is shown in Fig. 96.

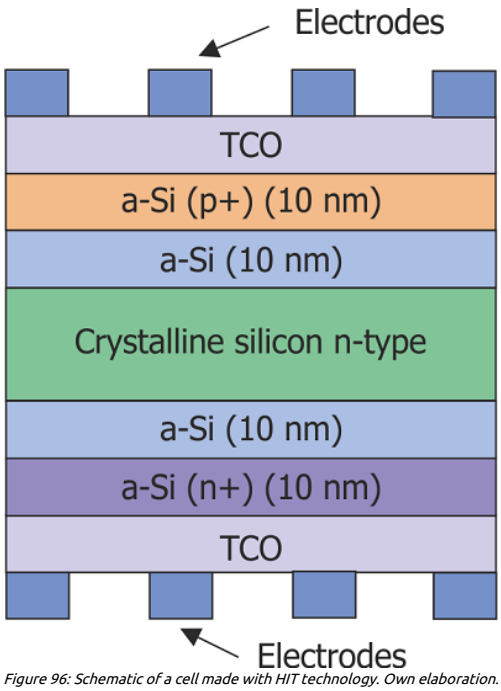

Figure 96: Schematic of a cell made with HIT technology. Own elaboration.

An inner thin layer of n-type crystalline silicon is sandwiched between two thin layers of amorphous silicon. This inner layer is first texturized (Fig. 97), and then covered with the corresponding amorphous silicon layers. The front layer of n-type crystalline silicon is covered with up to 10 nm thick amorphous a-Si followed by p-type amorphous a-Si, while the back layer is covered with up to 10 nm thick amorphous a-Si and n-type amorphous a-Si. Charge-collecting electrodes (screen contacts) are applied to the top on both sides. Very thin internal a-Si layers, occurring between the a-Si and the crystalline c-Si substrate, are designed to improve the performance of the p-n junction. Transparent conducting oxide (TCO) layers are formed on the two doped layers, and conductive paths are then printed. Backside metallization is also combed to reduce thermal and mechanical stresses, making the cell symmetrical and allowing it to be used as a double-sided cell.

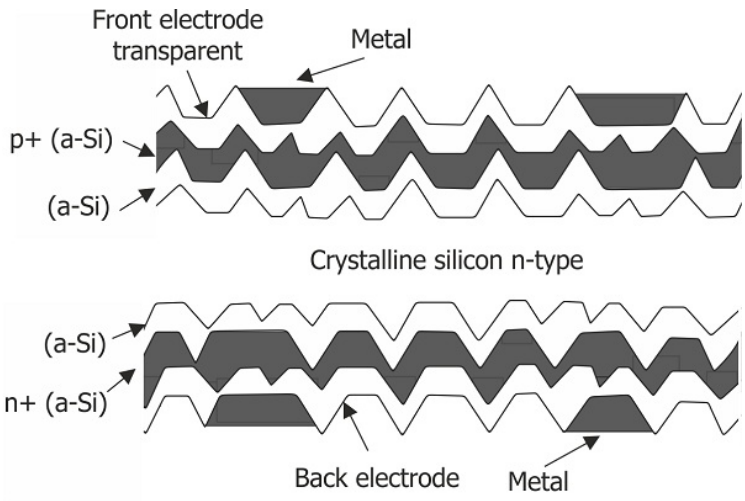

Figure 97: Photovoltaic cell made in HIT technology. Own elaboration.

The cells are designed to reduce the footprint and achieve higher efficiency compared to the standard crystal cells (Fig. 98), that are available on the market. The HIT cells were demonstrated by Sanyo Electric Solar Division, which manufactures this type of cell in classic and so-called honeycomb shapes to better utilize the relatively expensive monocrystals and the active area of the photovoltaic panel.

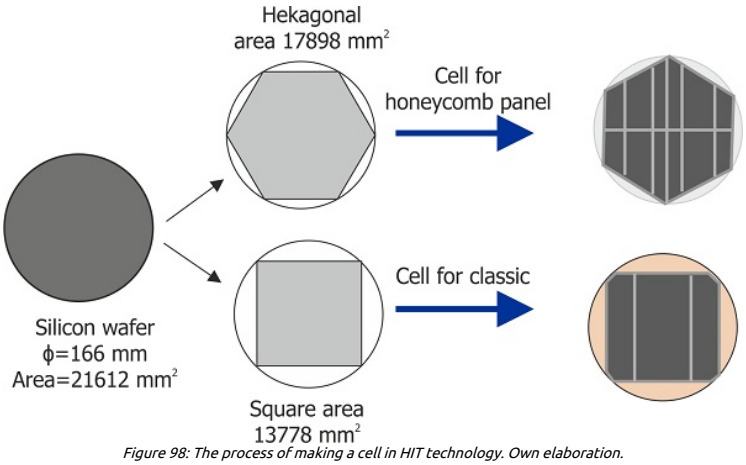

Figure 98: The process of making a cell in HIT technology. Own elaboration.

Cells of this type are not sensitive to higher temperatures, which means that their efficiency at higher temperatures does not change much [131]. This HIT technology produces cells that exhibit high efficiency at $75^{o}\mathrm{C}$. This technology provides excellent surface passivation at relatively low process temperatures (below $200^{o}\mathrm{C}$), allowing for reduced degradation over the lifetime of the photovoltaic cell.

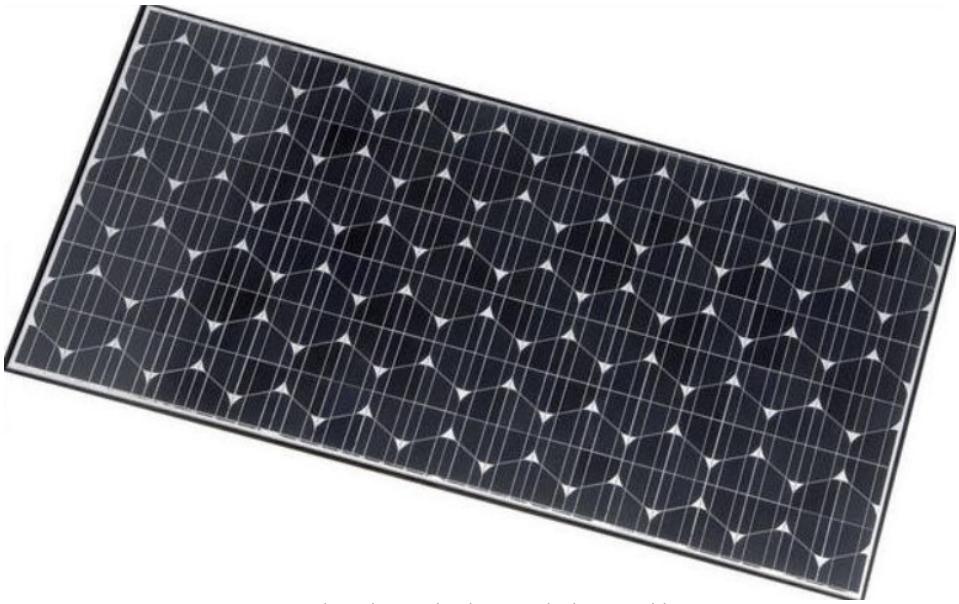

Figure 99: Photovoltaic panel made in HIT technology. Own elaboration.

Panasonic announced that it has developed a cell with an efficiency of 25.6% (Fig. 99).
Hydrogenated amorphous silicon, prepared by plasma enhanced chemical vapor deposition (PECVD), has a higher energy gap than crystalline material. Therefore, this material forms a heterojunction with a wide bandgap, providing very effective low recombination of the generated charges. The uppermost, thin, heavily-doped, p-type amorphous layer forms a junction with the n-type crystalline wafer. The intervention of the very thin internal amorphous silicon layer plays an important role in achieving high performance [132], [22].

Since the conductivity of even heavily doped amorphous silicon is quite low due to low carrier mobility, transparent conducting oxides are needed on both the front and back surfaces of the cell to allow carrier transport to the metal screen contacts on both surfaces. Since the back contact can be transparent, the cell can respond to light from both sides. This can improve the output power in installations where the back of the panel is exposed to ambient scattered light [133].
There are several other interesting features of this technology. The quality of the surface passivation obtained from the amorphous silicon layer yields record cell output voltages, which were confirmed by H. Sukatai [132], [22].

These form the basis of the cell's high energy conversion efficiency. In addition, this technology uses n-type wafers doped with phosphorus, which overcomes problems with boron and oxygen defects. Photovoltaic cell processing temperatures are typical of amorphous silicon cells and much lower than those of crystalline silicon cells.
The main technical weakness of this technology is that the transparent conductive oxide layers are neither perfectly transparent nor perfectly conductive. This forces a trade-off between light absorption in these layers and loss of lateral resistance. Light absorbed in the heavily doped amorphous layers in these cells reduces the power produced by the cell.
Individual cells achieved confirmed efficiencies up to 24.7% [123].

6.6 Thin-film photovoltaic cells

Photovoltaic cells, which are the basic component of photovoltaic panels, are made from monocrystalline, polycrystalline and amorphous silicon wafers. Technologies used in their production are constantly being modernised in order to improve their technical parameters and reduce costs, so that they become more and more attractive to buyers. Laboratories are currently working on thin-film cells made of both inorganic and organic compounds. Photovoltaic panels in the form of a thin layer, which could be placed on the roof, adjusted to its shape and roof colour, would certainly attract the attention of homeowners, architects and designers.
The thickness of the active layer in a thin film cell made of inorganic compounds usually does not exceed 20 μm. The consumption of semiconductor raw material is consequently limited [134], the potential flexibility of the cell is also ensured. It is also important that such an active layer has a high absorption coefficient value, as this affects the efficiency of light energy conversion to electricity. When organic materials are used for photovoltaic cells, the thickness of the active layer does not exceed 1 μm, because the absorption coefficient of these materials is much higher than that of semiconductor materials.
Thin film cells work efficiently even when the cell is shaded; the temperature has less effect on their power output, and they can be made in almost any shape and design. A drawback of these cells may be the lower efficiency when a material other than silicon is used and the fact that the material used may be toxic.
The active layers in thin-film photovoltaic cells are deposited on transparent or opaque substrates and different deposition methods are used. In the case of a transparent substrate, the transparent electrode is applied first, then the photovoltaic active layers and finally the second electrode. On the other hand, in the case where the substrate is opaque, an electrode which may be opaque is applied first, over it the photovoltaically active layers and finally the transparent electrode. The thickness of the individual layers ranges from 100 to 500 nm.
Materials with different properties are used to build photovoltaic cells. It is worth emphasising that substrates should ensure appropriate mechanical durability of the cell, and in the case of flexible cells, the material should be resistant to bending. Electrodes should be made of materials so selected that the resistance between the photovoltaic material and the electrode is as low as possible.

At present, the most favourable materials for thin film photovoltaic cells are polycrystalline structures containing gallium indium copper diselenide $CuIn_xGa_{1-x}Se_2$, or cadmium telluride CdTe [135]. Photovoltaic cells with a CdTe layer under laboratory conditions achieve efficiencies in the range of 16% (in production unfortunately about 10%). However, work is underway to realise the full potential of these cells, and critical issues in improving their efficiency are:

- identification and reduction of defect density at grain boundaries,
- increase in the concentration of hole carriers in the CdTe layer,
- elimination or control of parallelism,
- development of the manufacturing process,
- identifying and overcoming back contact formation problems,
- it is also necessary to develop a better hermetic enclosure as these cells interact strongly with the atmosphere (O_2, H_2O), which reduces their lifetime.

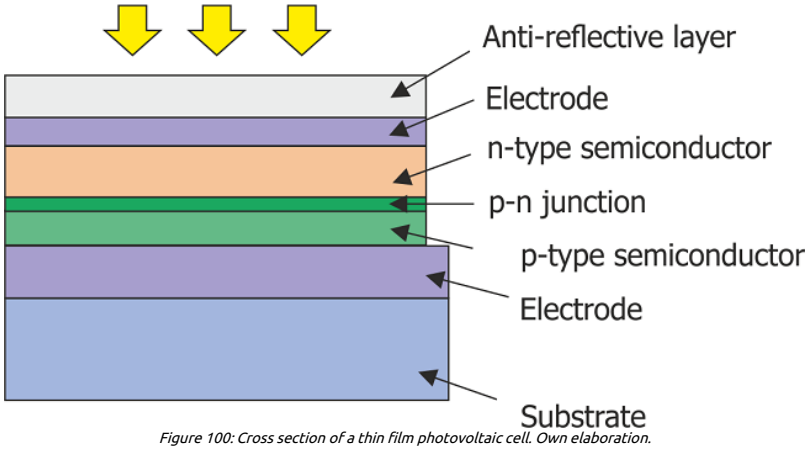

Figure 100: Cross section of a thin film photovoltaic cell. Own elaboration.

In Fig. 100 the structure of a thin-film photovoltaic cell is presented. A metal layer is placed on a glass substrate to form ohmic contact with a p-type semiconductor, i.e., the absorber layer (CIS, CIGS or CGS). The cadmium sulphide (CdS) layer forming the p-n junction with it - a semiconductor with n-type conductivity - is preceded by an Ordered Vacancy Compound, OVC). The CdS buffer layer is designed to match the edges of the conductivity bands of the CIGS layer and the which is ZnO zinc oxide.
A soda-lime glass with a thermal expansion coefficient of about $9 \cdot 10^{-6} K^{-1}$ is the most commonly used substrate for CIGS thin-film photovoltaic panels. A typical composition of this glass contains oxides such as Na_2O and CaO, which are sources of impurities in the other layers of the panel.
The absorber layer, responsible for absorbing photons and generating electric current carriers, is the most important material in a thin film cell. It usually consists of two ternary alloys: $CuInSe_2$ and $CuGaSe_2$, with the ratio y = Ga/(Ga+In) ranging from 0 to 1. The most effective layer used in photovoltaics is obtained for y = 0.11 - 0.26. The alloy $CuInSe_2$ is a semiconductor with a simple energy gap of 1.05 eV (up to ca. 1.65 eV in the case of the $CuGaSe_2$) and with a very large absorption coefficient α = 105 cm^{-1} for photons with energies > 1.4 eV.
Group II-(III)-VI materials are called chalcopyrite because they crystallize in the same arrangement as chalcopyrite $CuFeS_2$ – a common mineral in the sulfide cluster. The crystal structure is based on a regular arrangement, the so-called zinc blende structure. The semiconducting properties of chalcopyrite are related to its electrical and structural similarity to group IV semiconductors, such as silicon or germanium. One of the main features of $CuIn_xGa_{1-x}Se_2$ is the insensitivity of the structure's opto-electronic parameters to significant variations in material composition. The optical and electrical properties of $CuInSe_2$ depend strongly on the Cu/In ratio and the crystal structure of the material. The concentration of holes depends on the excess of selenium and on the Cu/In ratio. As the Cu/In ratio decreases, the concentration of holes decreases. The resistivity of the p-type layer increases by more than five orders of magnitude as the Cu/In ratio decreases from 1.1 to 0.9.
The buffer layer in CIGS thin-film photovoltaic cells is n-type conductive cadmium sulfide CdS, which together with the absorber layer forms an n-CdS/p-CIGS heterojunction structure. The cadmium sulfide has a large energy gap, E_g = 2.4 eV. The advantage of such a junction is that the material with the larger energy gap is transparent to the radiation absorbed in the material with the smaller energy gap. This causes the material with the larger energy gap to provide a window for radiation to be absorbed in the layer with the smaller energy gap width. Disadvantages include the phenomenon of radiative recombination in a semiconductor with a smaller energy gap [27], [136].
All currently manufactured CdTe cells are mainly made as heterostructures with the design shown in Fig. 100. Light falls on the heterojunction from the substrate side through a TCO (Transparent Conducting Oxide) electrode. The CdS layer acts as an optical window and helps to reduce the influence of the recombination process in the n-CdS/p-CdTe contact area.
All currently produced cells with CIGS layer are made as heterostructures, in which light falls on the heterojunction through a transparent conductive oxide layer TCO. It is usually formed by two layers of zinc oxide ZnO - one with high resistivity and the other heavily doped with n+ type conductivity. The energy gap of ZnO, E_g = 3.3 eV, allows photons of wavelength 350 nm and above to pass through the material deep into the structure.
Production costs of cells made on the basis of cadmium telluride CdTe are relatively low. However, their wider dissemination is hampered by the fact that they contain significant amounts of cadmium, which is a toxic element. Thin film photovoltaic cells with a layer of copper indium gallium diselenide CIGS are described as the most promising cells due to their manufacturing technology and low production costs. Under laboratory conditions, the efficiency of these panels is close to 20%. The size of the energy gap width close to the optimum value and the possibly wide choice of structures working with the CIGS layer, make them highly attractive from the point of view of application in the photovoltaic industry [137].

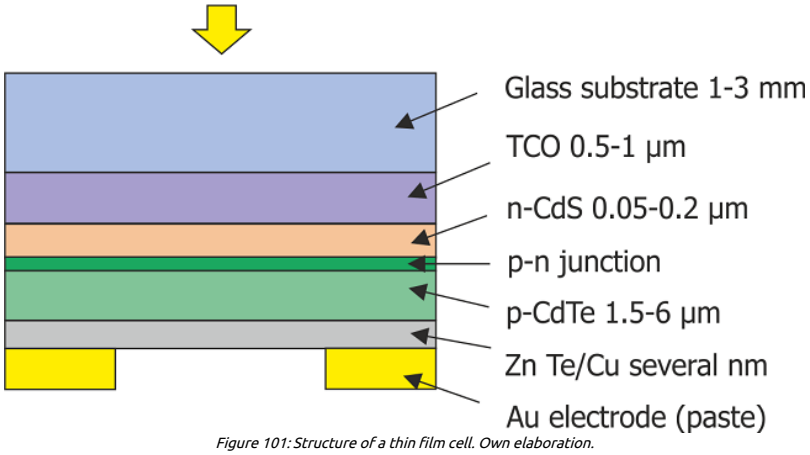

Figure 101: Structure of a thin film cell. Own elaboration.

Thin film cells (Fig. 101) are made using:

- cadmium telluride (CdTe cells) – the most widely known technology; cadmium telluride contains significant amounts of cadmium, which is toxic,
- amorphous silicon (a-Si cells) – the technology most closely resembling standard silicon panels,
- combinations of copper, indium, gallium, and selenide (CIGS cells), gallium,
- arsenide (GaAs cells) – very expensive technology, used primarily in spacecraft.

Photovoltaic thin film cells, thanks to small light absorbing layers, with efficient semiconductors, thinner and much lighter than their traditional counterparts, with very aesthetic appearance and almost any shape, are a very attractive offer to use. In summary, their undisputed advantages include:

- less effect of high temperatures on power output,
- reduced number of materials used in their production,
- efficient operation with little light,
- shading of the panel affects its power output to a lesser extent than in the case of typical panels,
- very aesthetic appearance,
- can take many different shapes, even fancy ones.

Manufacturers such as Sharp and First Solar, in addition to mono and polycrystalline silicon panels, offer thin-film panels. The name describes their construction well - the light-absorbing layers are about 350 times thinner than in standard silicon cells. They are also flexible and adapt to the shape of the roof, and are less than 20 μm. Placing them on the roof, instead of putting thick and rigid silicon panels, is a very interesting proposition.

6.7 PERC and PERT type PV cells

Conventional photovoltaic cell

One of the earliest fabricated photovoltaic cells [138] is a cell on a wafer of a p-type semiconductor. A so-called n+ emitter layer was applied to the front surface of the wafer, usually made by doping phosphorus onto the surface. Electrodes (Ag) were applied to this surface and then the cell was passivated by a dielectric (e.g., SiN_x), which also acts as an anti-reflective layer. The back surface of the p-type Si semiconductor is coated with aluminum to form a junction with Si that counteracts minority charges from reaching the back surface (Fig. 102).

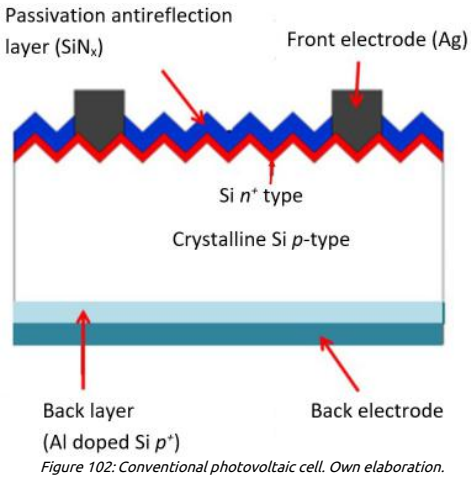

Figure 102: Conventional photovoltaic cell. Own elaboration.

Passivated Emitter and Rear Cell PERC is a passivated emitter and rear cell technology. With respect to standard cells, the PERC-type cell [139] has an additional dielectric layer that increases the efficiency of the cell by reflecting any light that reaches the back layer of the cell without generating an exciton. With this reflection, photons have a second chance to generate current.

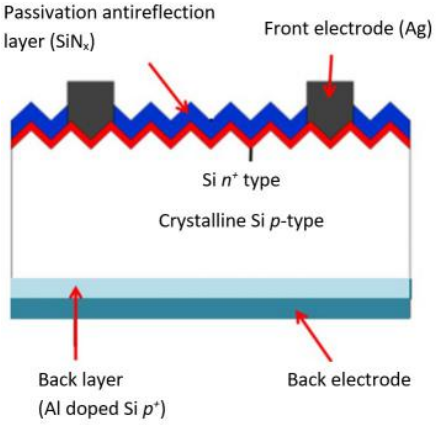

Figure 103: PERC type photovoltaic cell. Own elaboration.

A PERC-type cell can reduce electron recombination on the back surface by adding an additional dielectric layer between the silicon layers and the aluminum electrode, so that only the aluminum is in contact with a small portion of the cell area. The additional dielectric layers of SiO_2 and Al_2O_3 significantly reduce electron recombination on the surface, leading to an increase in cell efficiency.
In a PERC-type photovoltaic cell, as shown in Fig. 103, both the front and back surfaces are passivated by the dielectric. Small holes of the back dielectric layer are produced by a laser so that the electrode metal can contact the back surface of the cell. Compared to conventional Si photovoltaic cells, the PERC-type cell is able to improve the performance, mainly due to the additional passivating dielectric layer at the back. The additional back dielectric layer reflects photons back into the cell. This causes the optical path of the photon to be extended, resulting in greater light absorption and increased current generation.

PERT-type photovoltaic cells [140]
An innovative and even more electrically efficient solution, relative to PERC, is the Passivated Emitter Rear Cell Totally Diffused (PERT) photovoltaic cell. There are no holes in the back passivation layer of this cell and therefore it does not allow the electrons to escape, but forces them to bounce off the back of the cell and circulate in it again, giving the electrons a chance to get to the p-n junction. In PERT technology, the passivation layer puts up a barrier, preventing the electrons from escaping, causing them to enter the cell after bouncing off the back layer, increasing the energy yield. The following graphic illustrates this phenomenon (Fig. 104).

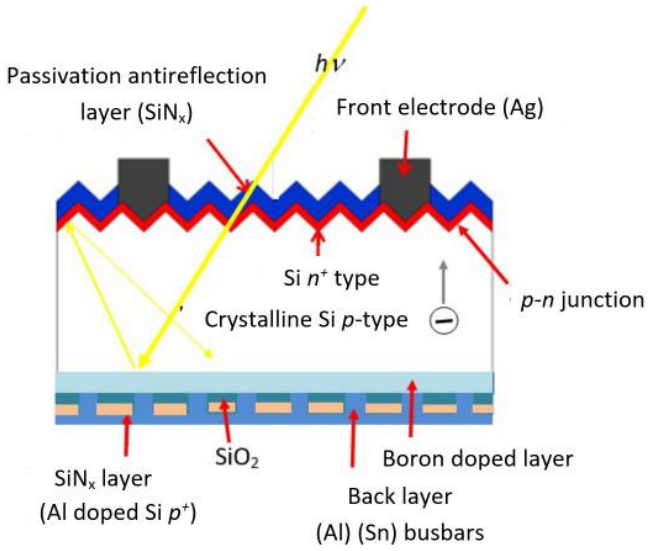

Figure 104: Solar radiation and charge behavior in a PERT type cell. Own elaboration.

PERT cells have a greater ability to absorb solar radiation and thus have a higher efficiency. Passivation of the back of the cell causes solar radiation to be reflected towards the active part of the cell, thus increasing the optical path of the ray in the cell. This is particularly important for radiation in the infrared region, since absorption in this region is characterized by a small extinction coefficient. In order to absorb radiation from the infrared spectral region (λ > 800 nm to 1100 nm for silicon), the optical path of the beam must be lengthened, which translates into increased absorption and generation of more energy.
The use of an additional layer of silicon with doped boron allows the electrode to be cut off from the interference of light rays,

since infrared radiation absorbed by the electrodes and not converted to electricity heats the cell structure lowering its efficiency. Therefore, the aim is to use this part of the solar energy. PERT cells are cells that use light also reflected from the Earth's surface and diffuse solar energy.

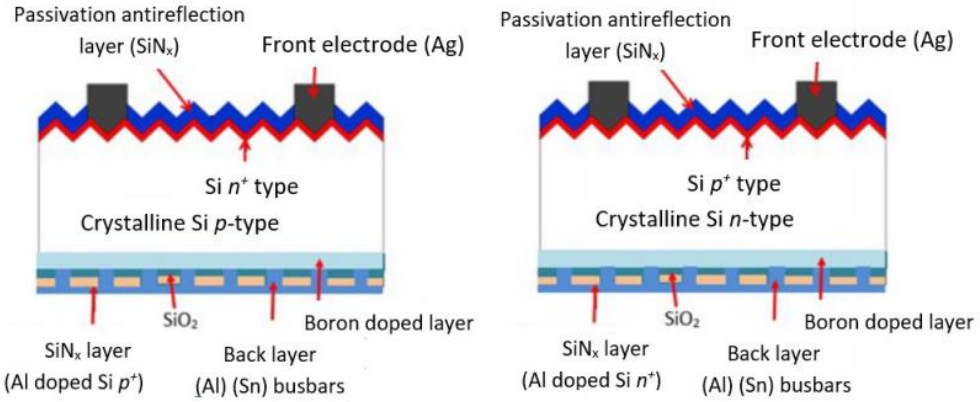

Figure 105: PERT cells constructed a) based on p-type silicon wafer, b) based on n-type silicon wafer. Own elaboration.

PERT cells are constructed using either p-type or n-type silicon wafers shown in Fig. 105. When the cell is constructed on a p-type silicon wafer, a scattering layer is formed by boron doping of the back layer of the p-type silicon wafer. The front layer, the emitter of the n-type wafer, is formed by diffusion of phosphorus. When the cell structure is based on an n-type silicon wafer, the emitter, or front layer, is obtained by diffusion of boron and the back layer is obtained by diffusion of phosphorus (Fig. 105b). PERT-type cells do not exhibit significant light-induced degradation and can be adapted to bilateral cell structures.

7. Photovoltaic modules

7.1 Photovoltaic modules

A photovoltaic cell is a basic component of a photovoltaic system. A single photovoltaic cell typically produces between 1 and 2 watts of power, which is insufficient for most applications. For higher voltages or currents, photovoltaic cells are connected in series or parallel to form a photovoltaic panel (PV panel, sometimes called a photovoltaic module). PV panels which are commercially available range in size from 0.3 to 2 m^2 depending on their power. The power output of such panels is expressed in watts of peak power (Wp - maximum power in watts), defined as the power they deliver under standard conditions (STC); this is typically between 30 Wp and 600 Wp. In practice, PV panels rarely operate under standard conditions, so it is useful to have current-voltage I(U) characteristics over a wide range of operating conditions. PV panels are encapsulated to protect them from corrosion, moisture, pollution and atmospheric influences. The enclosures must be durable as the life expectancy of PV panels is expected to be at least 20-30 years.

Each PV panel consists of photovoltaic cells. Traditional photovoltaic cells are usually 156 mm x 156 mm in size, connected in series and depending on the type, there are usually 60 or 72 cells in a PV panel. Photovoltaic cells are made in monocrystalline, polycrystalline, amorphous and thin-film technologies. The differences between them are due to the type of material used for their production. A silicon cell gives a voltage of about 0.6 V, which when the cells are connected in series gives about 36 V, and since each photovoltaic cell gives off about 9 A of current, the maximum power from a PV panel is about 300 W. The power depends on the technology used to make the photovoltaic cell. There are already emerging technologies and manufacturers announcing PV panels with 500 watts or 600 watts or more. For example, Canadian Solar announces the production of 665 W PV panels made of 132 monocrystalline PERC cells, with a side length of 210 mm, with an efficiency reaching 21.4% [141].

Photovoltaic panels produce direct current. The current intensity at the output of the panel strictly depends on the insolation. The current intensity can be increased by connecting PV panels in parallel in a photovoltaic system.

The voltage received from the PV panel depends little on the level of insolation, while it can be adjusted by series and parallel connection of photovoltaic cells in the PV panel. Photovoltaic panels can operate at 12 V or 24 V in an isolated installation and at 240 V or more when connected to the utility grid.

The construction of a photovoltaic panel can be described as a "sandwich" construction, which is one that consists of layers of materials and components applied sequentially. The manufacturing of a PV panel starts with the top layer, i.e., glass; it can be said that the PV panel is assembled from top to bottom. So, the whole process will be described from the top layer of the PV panel to its bottom layer.

From the top, i.e., from the solar side, the PV panel is protected from mechanical damage by tempered glass with a thickness of 3.2 mm or 4 mm. This glass also reduces the amount of reflected sunlight, limiting energy losses that reduce the PV panel's power output. Polishing the surface of the glass, coating it with an anti-reflective layer, or using surface texturing can help to reduce reflection.

On the other hand, silicon cells (Fig. 106) are covered with an anti-reflective layer and a very thin metal mesh and, together with the current-carrying busbars, are protected by an EVA film to form a hermetic shield. The manufacturing process is shown in the video "Solar cell manufacturing and solar panel production by Suntech".

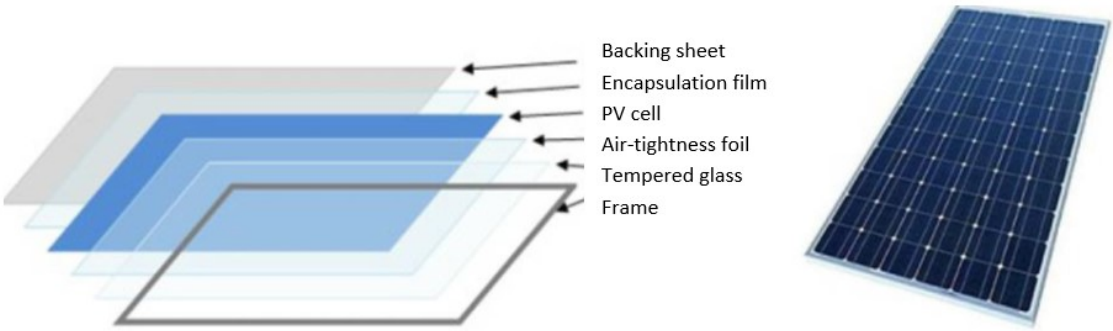

Figure 106: Sandwich construction of a photovoltaic panel and a finished PV panel. Own elaboration

https://pre-epodreczniki.open.agh.edu.pl/openagh-video.php?id=179

Solar cell manufacturing and solar panel production

BeFree Green Energy, Solar cell manufacturing and solar panel production by Suntech, 01.09.2010 (dostęp 22.12.2020).

Dostępne w YouTube: https://youtu.be/fZ1SC-vUe_I.

On the front side of conventional photovoltaic cells, a negative electrode is placed, which are thin horizontal paths (fingers). The fingers continuously collect the charges generated on the surface of the photovoltaic cell, which are then collected by wider vertical paths (busbars). The positive electrode is located at the back of the cell. From the busbars, current flows to a copper ribbon that connects the negative electrode of one cell to the positive electrode of another. The ribbons thus allow the generated photocurrent to be transported from the area of one photovoltaic cell to the next cells that make up the panel. Ten years ago, all PV panels were built with photovoltaic cells containing 2 busbars. Today, most PV panels are based on photovoltaic cell designs containing at least 5 busbars. Increasing the number of busbars improves the efficiency of the photovoltaic cells as well as their durability.

From below, the tightness of the PV panel is ensured by a special insulating film, the so-called backsheet, which also gives it a suitable color (usually white, black, or transparent). An aluminium frame is used to stiffen the whole structure. Another element is the junction box, from which two cables ending in plugs come out, connecting the panels in series.

In this junction box there are also bypass diodes [142]. Bypass diodes are an essential part of a photovoltaic panel, protecting and improving its operation. Photovoltaic cells are connected in series in the direction of conduction (Fig. 107). If one cell were to stop conducting, the entire PV panel would be out of power production, but bypass diodes connected in the negative direction allow the non-working photovoltaic cell to be bypassed. They also reduce the risk of damaging a shaded PV cell - current flows in the opposite direction through a shaded (leaves, snow) cell, causing the PV cell to overheat significantly.

When several photovoltaic panels are connected in series to increase the voltage, the current flowing in the circuit will be equal to the current of the weakest element in the system. If one of the photovoltaic panels is shaded (e.g., by a chimney or a bay window), the power of the circuit will decrease dramatically. The bypass diodes, by taking the shaded PV panel out of the chain, will reduce the losses in the entire system. Current flows as per Fig. 108. Some boxes have a special disconnect switch that will disconnect a series or individual PV panel in the event of their fault.

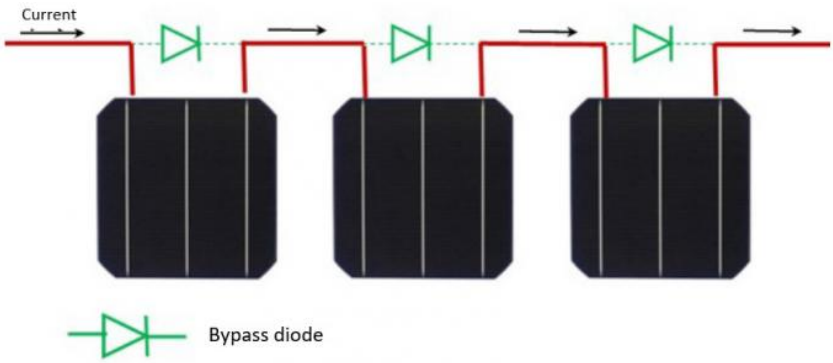

Figure 107: Current flow through cells in a photovoltaic panel under normal lighting conditions. Own elaboration.

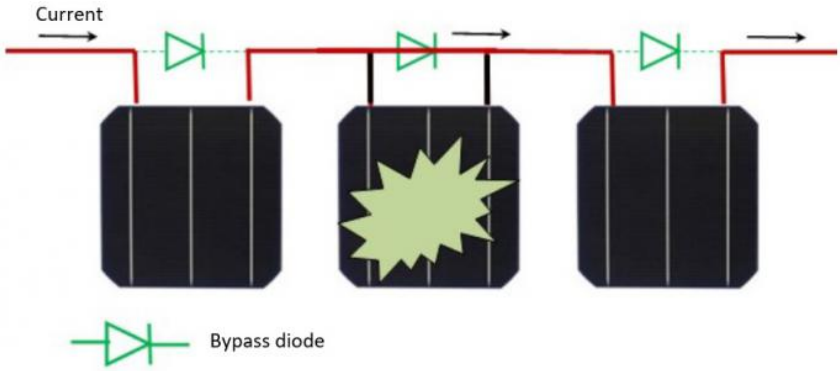

Figure 108: Current flow through the cells in the photovoltaic panel in the case of center panel shading. Elaborated. Own elaboration.

Fig. 109 shows an example connection of three and ten bypass diodes, which puts that part of the PV panel out of operation when it is shaded.

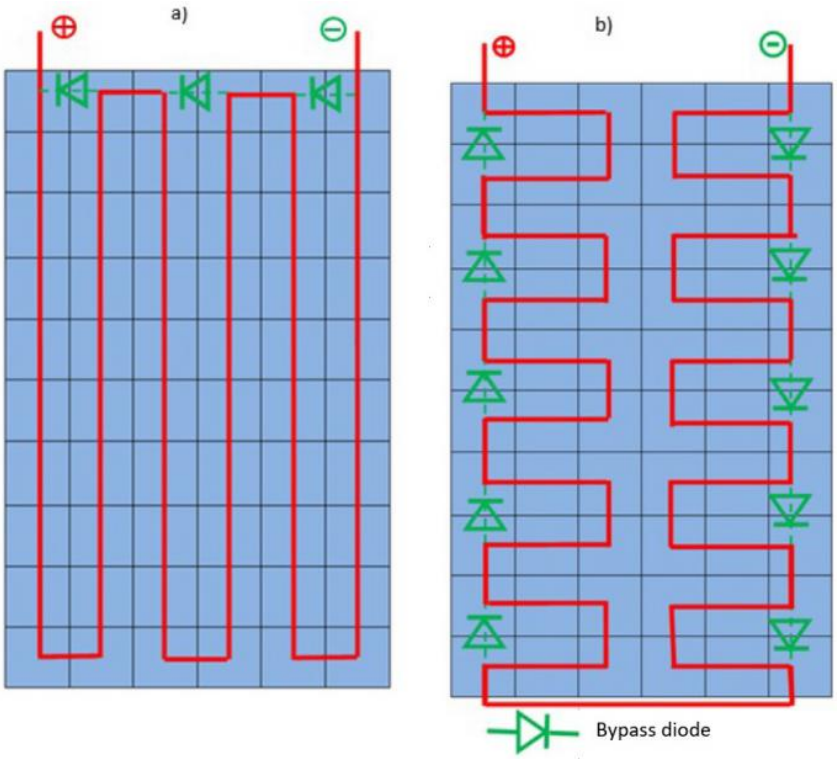

Figure 109: Activation of bypass diodes to eliminate the operation of part of the PV panel during partial shading. Own elaboration.

Including bypass diodes in a PV panel divides the panel into 3 parts if three bypass diodes are included and into 10 parts if ten bypass diodes are included. This division allows each part to be used separately to produce electricity regardless of the state of the other components of the photovoltaic cell.

Tables specifying the characteristics of photovoltaic panels typically provide:

- two power values by two standards – STC (Standard Test Conditions) rated power which means that the test was conducted

under AM1 insolation conditions 5, with a power of 1000 $\frac{W}{m^2}$ at $25^o\mathrm{C}$ and power at the so-called real-world NOCT (Normal Operating Cell Temperature) insolation intensity with AM1 spectrum. 5 800 $\frac{W}{m^2}$, wind speed $1\frac{m}{s}$ at an ambient temperature of $20^o\mathrm{C}$,

- efficiency is a quantity that describes the proportion of solar energy that can be converted into electricity; for mass-produced monocrystalline panels, it is up to 25%,
- photovoltaic module dimensions and weight – these vary and depend on the manufacturer; obviously the heavier the PV panel, the more weight it puts on the roof structure, and the larger it is, the more space it takes up,
- temperature coefficient allows you to determine how much power the module will achieve at a certain temperature; the lower the better,
- annual power loss – PV panels can lose efficiency over time; most manufacturers specify the efficiency of their PV panels at 80% after 25 years; typically, PV panels lose $2-3\%$ of efficiency in the first year, and lose between 0.3% to 0.6% of efficiency annually thereafter,
- fill factor (FF) – can be said to check the quality of the cell

$$FF = \frac{U_m \cdot I_m}{U_{oc} \cdot I_{sc}} \tag{20}$$

- dependence of PV panel efficiency on solar insolation magnitude,
- the ratio of efficiency under NOCT to STC conditions is also used, if it is 0.8 it means that the panel is usable.

These properties make it possible to evaluate the quality of the photovoltaic cells that make up the PV panel as well as the panel itself. PV panels are divided into three classes A, B and C. Class A PV panels should have an FF fill factor above 0.75. It should also be taken into account, that the insolation in Poland is usually between 200 $\frac{W}{m^2}$ and 600 $\frac{W}{m^2}$, and take this into account when planning a PV power plant.

7.2 Photovoltaic modules technologies

Photovoltaic panels are made up of cells. There are usually 60, or 72, or sometimes more, depending on the power you intend to get from a single panel. It should be clear that the efficiency of commercial photovoltaic cells is currently at 25% and for a panel to have more power it must occupy a larger area. The power output of a standard cell (with dimensions of 156 mm * 156 mm) is about 5 Wp. Therefore, in order for the panel to generate 800 Wp of power, it must consist of 200 cells, which translates into the size of its surface. A standard panel installed in popular photovoltaic installations has dimensions 165 cm * 100 cm. Sometimes these dimensions vary slightly, depending on the manufacturer. A panel made of monocrystalline silicon with such dimensions has power from 310 Wp to 340 Wp.
Depending on the type of cell used to build the panel, its name is adopted, e.g. monocrystalline panel - c-Si, polycrystalline panel - mc-Si, or amorphous panel - a-Si. In addition to typical silicon panels, thin-film panels are also produced. In this case the names are given according to the type of active layer in the cell. And so, for example, photovoltaic panel CIGS/CIS is built on one side from a mixture of copper, indium, gallium and selenium (CIGS), and on the other from copper, indium and selenium (CIS).
Among photovoltaic panels, due to the structure of the cell and the whole panel, we can distinguish groups such as: thin-film panels, panels with contacts at the back, HIT type panels, PERC type panels, double-sided panels, panels made with SmartWire technology. Of course, in each group you can specify additional types, which will be distinguished by some element, such as thin-film cells connected together in SmartWire technology.

HIT technology - photovoltaic panels with HIT cells

An inner thin layer based on n-type crystalline silicon is sandwiched between two thin amorphous layers. The technology of monocrystalline panels was developed by the Sanyo company. The advantage of this type of panels is the conversion of low energy radiation (infrared) into electricity, and low temperature power drop factor which is at $0.29\%/\,^o\mathrm{C}$. The silicon wafer processing is done at a lower temperature of about $200^o\mathrm{C}$. The panels are also produced in a hexagonal shape (bee slice, honeycomb), which results in better utilization of the crystalline silicon.

Technology based on p-type monocrystalline silicon

A typical photovoltaic cell based on p-type Si semiconductor is shown in Fig. 110. Figure (a) presents a schematic cell, while figure (b) depicts an actual cell made with 2 busbar technologies, that is, 110 common points with charge-collecting fingers. Finally in figure (c) one can see a photovoltaic panel made with 2 busbar technologies.

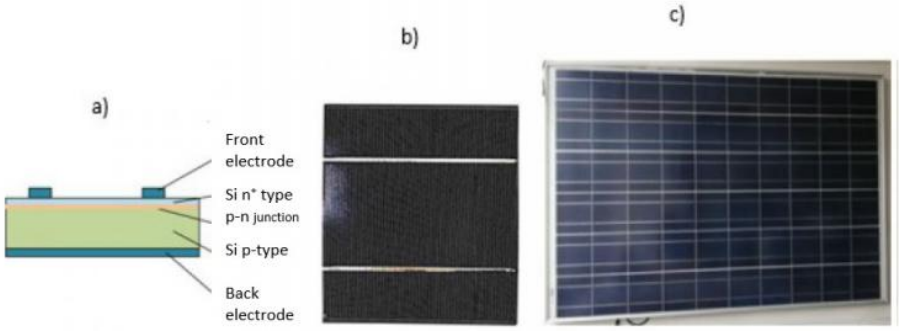

Figure 110: Shows (a) the layers present in a classical cell, (b) a cell made with 2 busbars (enlarged), (c) a photovoltaic panel made with two busbars. Own elaboration.

Nowadays you can find technology with 2, 3, 5 busbars, but also with 12 wires acting as busbars (Fig. 111).

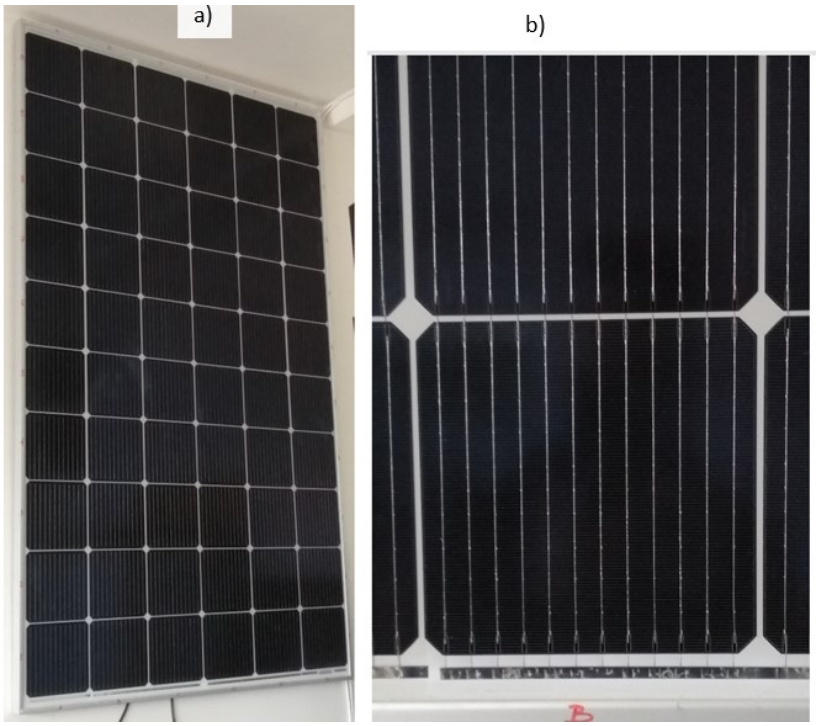

Figure 111: Monocrystalline Si p-type panel; a) photovoltaic panel, b) cell in monocrystalline panel. Own elaboration.

Panels fabricated with 12-wire busbar technology are still spot soldered at $250^{o}\,\mathrm{C}$, which stresses the cell. Polycrystalline or amorphous silicon panels are produced in a similar manner.

Panels with both electrodes at the back

'All back contact' technology with both electrodes at the back has relatively high efficiencies up to 24%. The front of the panel is homogeneous, with no electrodes visible. The location of the electrodes at the back contributes to greater corrosion resistance of the electrical connections. The disadvantage of this solution is the so-called PID degradation effect, i.e. degradation related to the occurrence of high voltages (~600V) between the panel frame and the semiconductor. This causes charges to flow to the ground and the panel power decreases. Therefore, it is necessary to ground the positive pole and appropriate selection of the inverter to adapt to the problem.

SmartWire technology - photovoltaic panels with microwires

This consists of replacing the classical soldering by lamination with a film containing 18 to 32 microwires, which from 990 to 1760 contact points with charge-collecting fingers. This reduces the temperature at which the photovoltaic panel is generated to $150^{o}\,\mathrm{C}$ across the surface, rather than point-wise, as in the case of soldering at $250^{o}\,\mathrm{C}$. The wire wrap is applied to the front and back of the panel. This allows manufacturers to save silver paste and solder material. This large number of contact points allows the cell to work even with microcracks.

Shingled technology - shingle photovoltaic panels

The photovoltaic cell in a shingled panel [143] is cut into 3 to 6 strips, which are then assembled into strings that connect the front of each strip to the back of the next strip using a suitable electrically conductive adhesive (ECA) that can be printed or dispensed onto the surface of the strip. The individual cells are assembled "overlapping", i.e., each thin strip slightly overlaps the next, and their joints are hidden under individual "busbars" (Fig. 112) [144]. To obtain the required panel layout, the cell needs to be divided into a sufficient number of parts. Typically, strip strings up to 2 m long are assembled, which corresponds to the longer side of a traditional 72-cell panel. The strips are then connected to each other by conductive ribbons, assembled according to the traditional photovoltaic panel manufacturing procedure.

This design makes optimal use of the surface area of the entire panel, which increases the active area of the panel and thus allows for higher efficiency from 1 m^2 area by up to 15%.

Figure 112: Method of assembling the cell pieces into strings. Own elaboration.

In summary, in panels made with Shingled technology, the panel area is better utilized, there are lower ohmic losses and increased reliability. Lower ohmic losses also mean lower operating temperature of the cell.

7.3 Photovoltaic modules made of PERC technology

Passivated Emitter and Rear Cell (PERC) technology is a technology of passivation of the emitter and the rear part of the cell. It defines the construction of a photovoltaic cell different from a standard cell (Fig. 113). The difference is that an additional passivation layer is added to the back of the cell. This layer reflects the sun's rays (they are not absorbed by the layer) back into the photovoltaic cell, increasing the probability of the absorption of these rays and thus electricity production. This is due to the low extinction coefficient for wavelengths in the infrared region (above 800 nm). A photovoltaic cell made with PERC technology was first demonstrated at the University of New South Wales (UNSW) in Australia in 1983 [138]. The technology has achieved an efficiency of 25%.

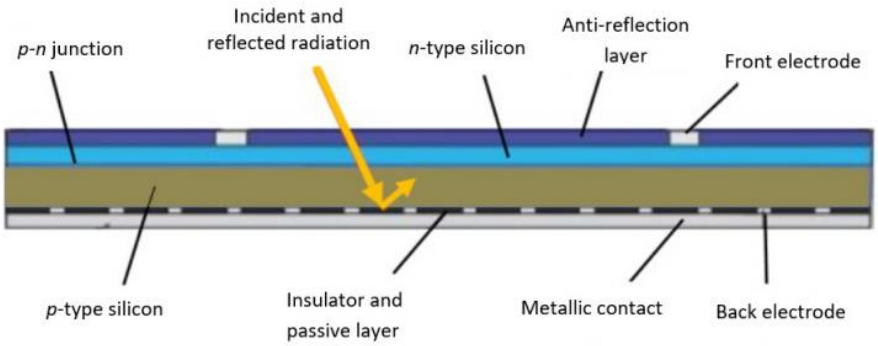

Figure 113: PERC-type cell. Own elaboration.

Such high efficiency PERC type cells are a good basis for building photovoltaic panels. PERC cells have good results on cloudy days, both in the morning and evening. Above the wavelength $\lambda = 1180nm$, the silicon-based cell does not absorb.
Since the passivation layer reflects light back to the cell, reducing the level of absorption by the back layer, this also reduces the heating of the panel. This reduction in absorption helps the panel operate at lower temperatures and positively impacts its energy efficiency.

The PERC technology increases the sensitivity of the panels for infrared wavelengths [145].
The performance of a photovoltaic panel based on PERC-type monocrystalline silicon by one of the manufacturers is shown below. The photovoltaic panels presented by the company are a cell with 12 busbars (Fig. 114) and a panel with 60 cells and a panel with half cells, where each cell is connected to the next through 12 busbars.

Figure 114: Cell with 12 busbars and panels made with this technology: classical and with half cells. Own elaboration.

See an example of a catalogue card of a photovoltaic panel made with the PERC technology with half cells used .

7.4 Half-cut modules

Photovoltaic half panels are a new technology already used in mass production. A 156x78 mm^2 half-cell is created by dividing a traditional 156x156 mm^2 cell in half. A half panel is constructed from twice the number of half links connected in chains that are connected in parallel.
Splitting a cell in half halves the current produced by a single cell, while maintaining the same voltage. It also reduces the loss of resistance inside the cell, and thus does not increase the operating temperature of the cell. This slightly increases the power generated by the panel.
There are 120 half cells in the panel, which are connected by 3 bypass diodes, dividing the panel into 6 parts of 20 cells each, working separately (Fig. 115).
Standard panels with 60 cells also have 3 bypass diodes, which also cover 20 cells each (Fig. 115), but they divide such a panel into 3 parts.
The bypass diodes are connected in the negative direction and when the cell(s) is/are not working (e.g., due to shading) they allow current to flow bypassing the non-working cell(s).
This means that when in a standard panel one cell is shaded, the bypass diode will switch off 1/3 of the panel, whereas in a panel with half cells only 1/6 of the panel will be switched off, which for obvious reasons has a positive effect on the power produced by the panel.

The panel operation with one half-cell off is shown in the image below.

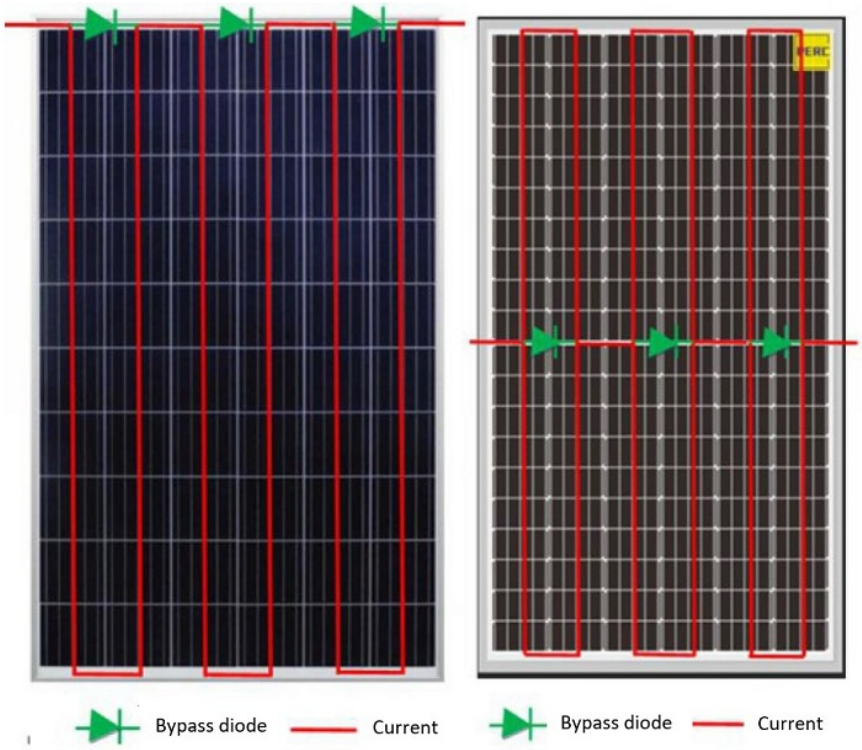

Figure 115: (a) Standard PV panel with 3 bypass diodes dividing the cell into 3 circuits inside the panel and (b) panels with half cells, 3 bypass diodes and 6 circuits inside the panel. Own elaboration.

Panel operation with one cell off in the standard and half panel is shown in Fig. 116.

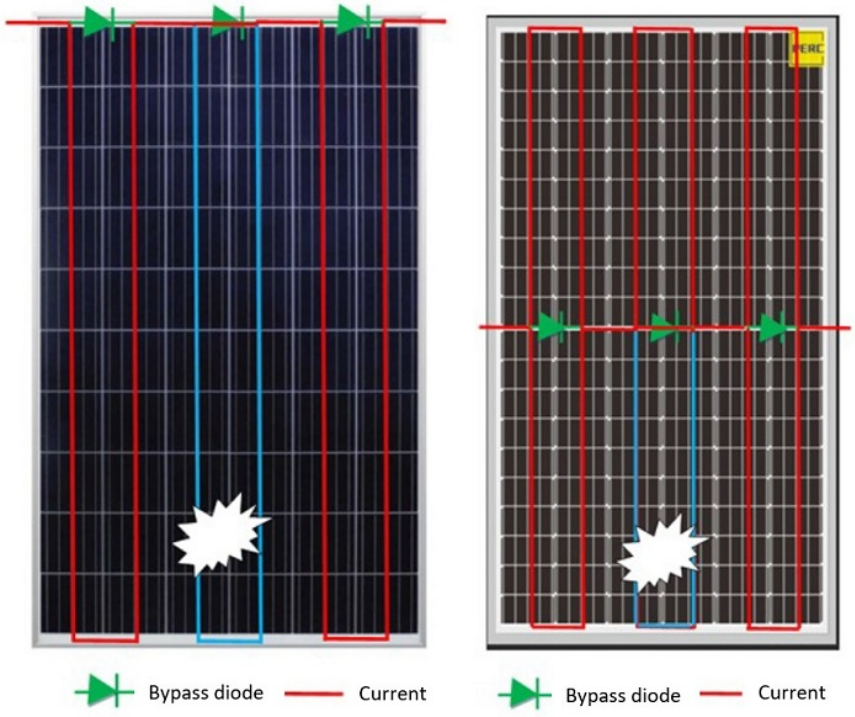

Figure 116: PV panel operation during shading of part of the cells in a) standard panel, b) panel with half cells. Own elaboration.

As can be seen from Fig. 116, the amount of energy produced by the half-cell panels under unfavorable shading conditions is higher. The losses are minimized by 50%. An even greater difference will occur when half the panel is shaded. This situation in our conditions can happen, e.g. due to snow or on roof or ground installations set at an angle. The standard panel will then be completely excluded from electricity production, while the panel with half cells (Fig. 117) will work with an efficiency of 50% of power [146].

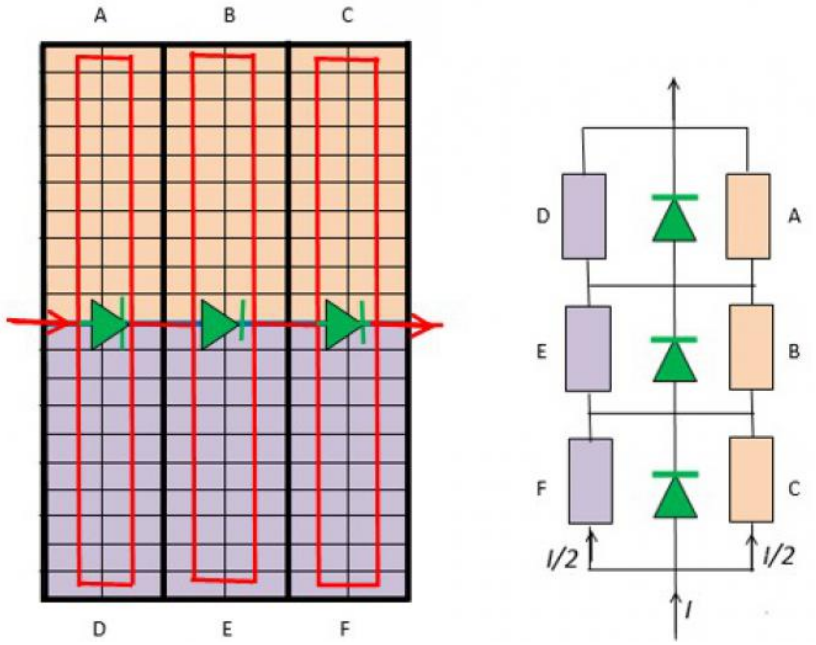

Figure 117: Photovoltaic panel with half cells and the way of connecting individual cells and bypass diodes. Own elaboration.

Each letter stands for a part of the panel consisting of 20 half-cells. They are connected to each other in series and parallel and additionally through bypass diodes. This allows the panel to work efficiently. A photovoltaic panel made of half cells has lower power losses compared to a standard panel. The power lost at the internal resistor of one cell is

$$P = R \cdot I^2 \tag{21}$$

and multiplied by 60 cells in a standard panel is

$$60 \cdot R \cdot I^2 \tag{22}$$

The cell loss in the half panel equals

$$P = \frac{R}{2} \cdot \left(\frac{I}{2}\right)^2 \tag{23}$$

which multiplied by 120 cells yields $15 \cdot R \cdot I^2$, i.e., they are 4 times smaller.

This results in a lower operating temperature of the panel and its higher efficiency [147].

7.5 Bifacial modules

Bifacial active photovoltaic panels are those whose cells absorb light from both sides, i.e., front and back (made with bifacial technology). Bifacial panels have two active sides and are covered with tempered glass or transparent film on both sides (Fig. 118). With this technology, more photons reach the panel, so the energy produced is greater than that obtained from traditional, single-sided panels, by up to 30%.

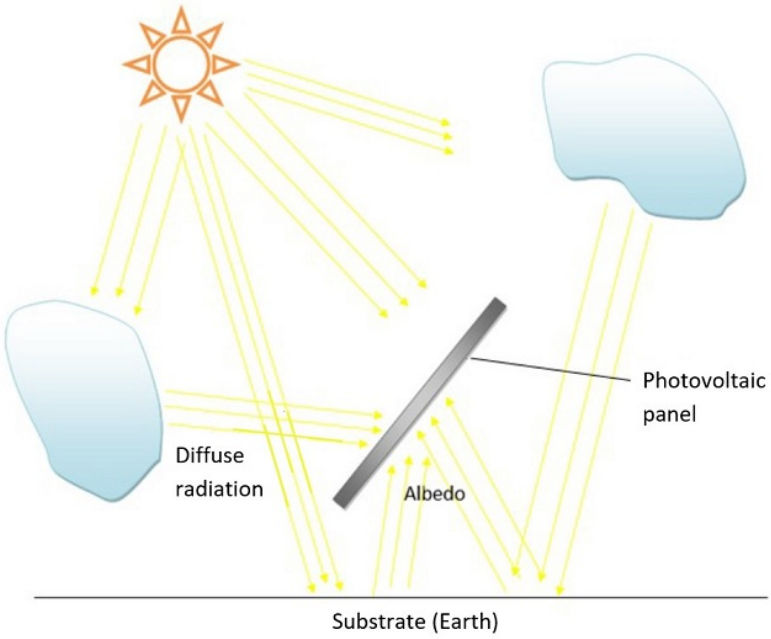

Figure 118: Rays reaching a double-sided panel. Own elaboration.

A bifacial solar cells used in double-sided panels are mostly structures:

- based on a p-type crystalline silicon wafer and with a p+-p-n+ cell structure,
- based on an n-type crystalline silicon wafer and with a p+-n-n+ cell structure,
- based on a silicon heterojunction, made with internal thin films of amorphous silicon.

Solar rays reflect off different substrates at different percentages, depending on the type of substrate (Fig. 119). For the effectiveness of double-sided panels, a key factor is the so-called albedo coefficient, which shows the ability to reflect light from a given surface. The brighter the surface, the more light it can reflect, resulting in more energy being extracted from the back surface of the panel. For very bright surfaces, the albedo coefficient can be up to 80%.

Type of surface	Albedo [%]	Type of surface	Albedo [%]
Dry concrete	17-27	River sand	43
White gravel	27	Dune sand	20-45
Sugar beet	18	Cotton field	20-22
Black road surface	5-10	Rice field	12
Black dry soil	25-30	Arable field	15-25
Moist black soil	8	Prairie	12-13
Grey dry soil	25-30	Stony desert	28-38
Moist grey soil	10-20	Sandy desert	25-30
Dry clay	23	Savannah (dry season)	25-30
Moist clay	16	Savannah (rainy season)	15-20
Granite	29-31	White roofing membrane	80
Oak woodland	18	Grey roofing membrane	62
Fir forest	10	Fresh snow	75-95
Deciduous forest	10-20	Old snow	40-70
Solid rock	12-15	Green grass	26
Sea ice	36-50	Dried grass	19
Green meadow	10-20	Tundra	15-20
Built-up area	15-25	Water	8
White sand	60	Heath	10-12
River sand	43	Potatoes	19

Figure 119: Albedo coefficients for different surfaces. Own elaboration.

White roof membrane and snow have the highest albedo coefficient.
Obtaining additional energy from the back surface of a double-sided panel, therefore, depends on the substrate, its high albedo coefficient, and in addition on the angle of the panel and the height of the location above the reflecting surface.
The load and compound resistance of double-sided glass-fire-glass panels is higher than single-sided panels. Double glazing has a higher mechanical strength, and also the resistance of the glass to chemical compounds is higher than for EVA film. The price of such a panel is also higher.
There are also panels produced that have the cells pulled apart, giving the possibility for special applications. Double glazing provides stability to the cells, which gives the possibility to use this type of construction for roofing terraces, shelters or inserting in large areas covered with glass and requiring shading. In this way, double-sided panel can be used not only as an energy producer, but also for other utility and aesthetic purposes.

Polish producer Hanplast Energy has started production of photovoltaic cells with HPERC technology. The developed cell is an intermediate solution between cells made in PERC and HIT technologies. The technology is based on n-type monocrystalline HJT cells. The cells are connected using SmartWire Connection Technology (SWCT). The manufacturer claims a panel efficiency of $23-24\%$, which is up to 10% higher efficiency than for conventional panels, maintaining 87.25% of the panel's initial power output after 25 years of operation, and a higher energy yield of up to 30%. This is all thanks to the use of bifacial cell technology (Fig. 120) [148], [149], [150].

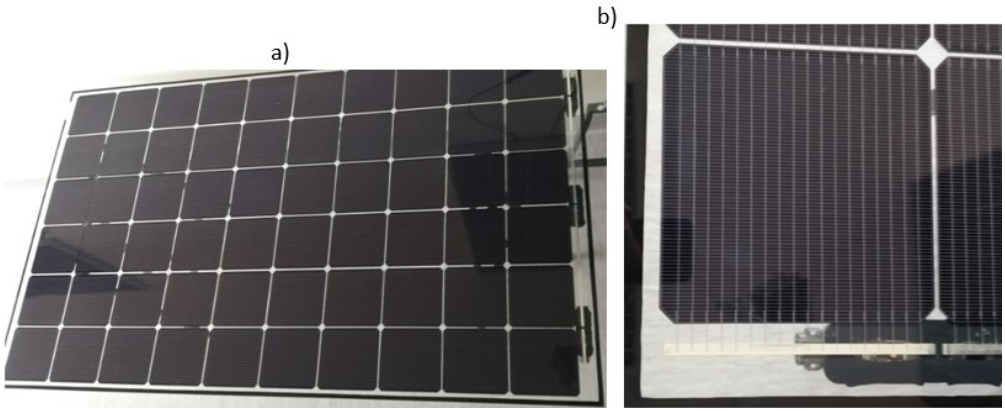

Figure 120: (a) Photograph of a bifacial photovoltaic panel made by Hanplast Energy, (b) single cell. Own elaboration.

7.6 PVT systems

Hybrid solar cells (hybrid collectors, Photovoltaic Thermal, PVT) are also systems that use a combination of a solar panel and a collector [151]. Solar collectors convert solar energy into heat, while panels convert solar energy into electricity. Therefore, the collectors can heat domestic water and support the operation of central heating. The energy generated by the panels can also be used in various ways.
As described in the previous chapters, the efficiency of silicon-based photovoltaic cells decreases with increasing temperature. The rate of that increase is described by the temperature coefficient [5]. An example system is shown in Fig. 121 [152].

Figure 121: PVT panels dedicated for solar-assisted heat pump. Experimental installation at the Department of Energy of Politecnico of Milan. Aut. photo Rich Skiz, CC BY-SA 4.0, source: Wikimedia Commons .

The great advantage is to have one installation instead of two separate ones. This solution saves space in the case of limited installation space.

An implementation example is the ISIEtherm panel [153], which, according to the manufacturers, is expected to provide an increase in electrical gain (derived from solar energy) of at least 10% annually in relation to systems without concentrators. It may be used for installations in swimming pools, hotel facilities and as heat pumps.

Przypis

1. Busbar cells are described in chapter: 6.1 Busbar cells.
2. Smartwires are described in chapter: 6.4 Smartwires cells.
3. See chapter: 6.5 HIT technology cells.
4. The cells are described in the chapters: 6.2 PERL cells i 6.7 PERC and PERT type PV cells.
5. The temperature coefficients are described in the chapter: 8.3 Temperature dependence of cell parameters.

8. Cell and modules parameters

8.1 Measurement of cell parameters

The electrical parameters of a single cell are measured using a device called a solar simulator. A solar simulator / artificial sun simulator is a laboratory device that produces lighting similar to natural sunlight. The purpose of the solar simulator is to provide a controlled test bed under laboratory conditions for testing solar cells. The solar simulator determines the current-voltage characteristics and the software integrated into it determines the cell parameters. In selected models, it is possible to change the temperature or simulate weather conditions [154].
The measurement of the current-voltage characteristics is carried out under Standard Test Conditions (STC): irradiance 1 000 $\frac{W}{m^2}$, solar spectrum AM 1.5, the cell temperature is $25^o\mathrm{C}$.

Alternative test conditions less commonly used for measurements are the so-called Normal Operating Cell Temperature (NOTC) conditions. According to NOTC, the cell is illuminated by solar radiation with an intensity of 800 $\frac{W}{m^2}$, at a temperature of $20^o\mathrm{C}$ and a wind speed of 1 m/s. The efficiencies obtained in measurements made under NOTC conditions are lower by approx. 30%, but they are close to the actual performance [155].
Solar simulators must fulfil the solar spectrum standards defined by the International Electrotechnical Commission (IEC). The spectrum of the light emitted from a source in a solar simulator is usually controlled using filters. Its temporal stability and spatial uniformity are also checked. Depending on the application, the lamp life is 1 000-5 000 hours. Depending on the degree to which the normative conditions are fulfilled, an appropriate class is assigned to each device. Solar simulator parameters are defined in three categories: spectral matching, spatial non-uniformity and temporal instability. Each category is broken down into three classes A, B, C [156].
Class AAA, according to IEC 60904-9, ASTM E927 and JIS C8912, stands for the fulfilment of three different parameters of the standard, i.e., Class A Spectral Match (the spectral match to the AM1.5 spectrum should be between 0.75 and 1.25, 1.00 being the ideal match), Class A Spatial Uniformity (the permissible non-uniformity is less than 2% for cells up to 20 cm in diameter, and 3% for larger cells) and Class A Temporal Stability (instability must be less than 2). Fulfilment of the normative conditions allows tests to be performed with the highest precision. Tests performed with such a device are the basis for the technical evaluation of the cell. Photovoltaic cells entering the market should be tested and have a certification document.

The AGH University of Science and Technology is equipped with a sunlight simulator. This is the I-V Curve Tracer For Solar Cells Qualification (Class AAA, IEC 60891 standard). It consists of a lamp, a power supply unit, a control and measurement system, a computer with software, a measurement table (holder), a temperature controller (Fig. 122).

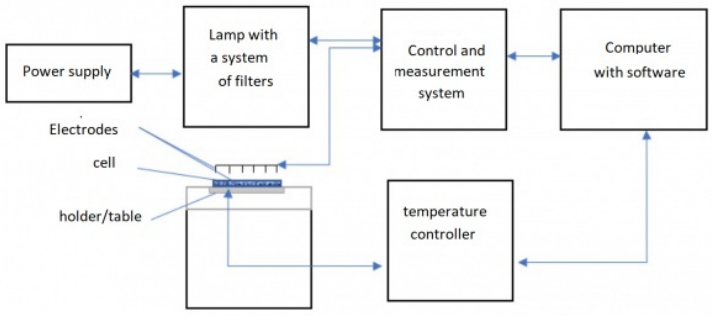

Figure 122: Scheme of the sunlight simulator. Own elaboration.

A general view of the site is shown in Fig. 123 [157]. The device performs measurements using the so-called four probes Kelvin

technique [6] – Therefore, the presence of so-called voltage and current electrodes.

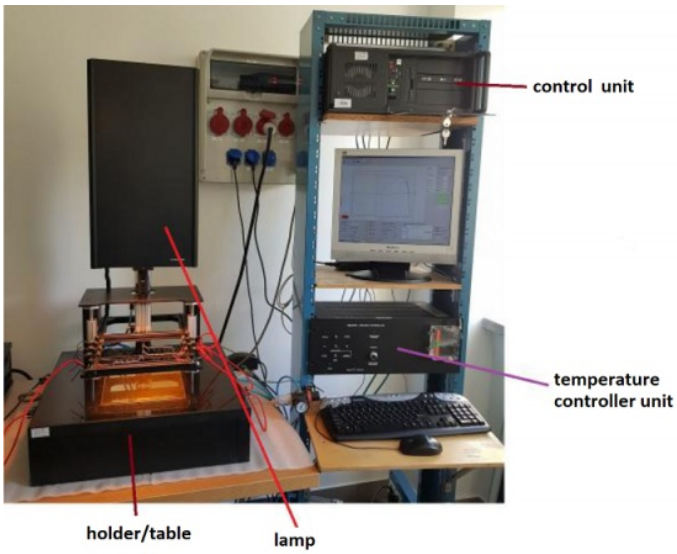

Figure 123: The PV measurement setup. Own elaboration.

The device can measure solar cells with a maximum size of 20cm x 20cm. The most important part of the measuring set is a lamp assembly with a filter giving a spectrum similar to AM1.5 which illuminates a marble measuring table with a set of electrodes (Fig. 124). The electrode assembly with the photovoltaic cell to be measured is shown on Fig. 124b. The instrument has the ability to test the temperature dependence of cell performance. Before measurements are made, the simulator should be calibrated for monosilicon and polysilicon cells respectively. The short circuit current is calibrated.

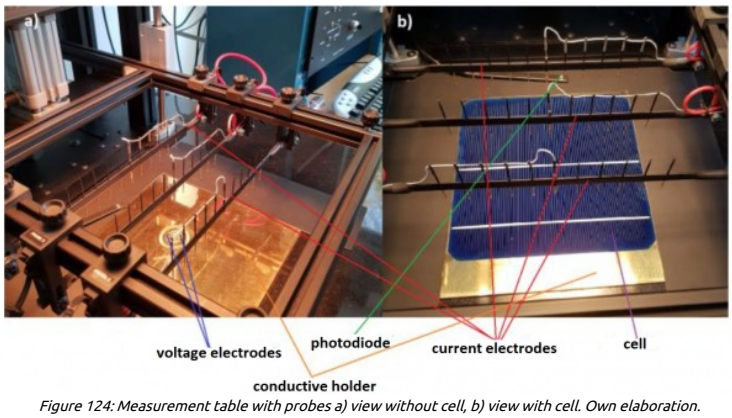

Figure 124: Measurement table with probes a) view without cell, b) view with cell. Own elaboration.

The device is controlled using the computer software Solar Cell Tester. The software is used to record and develop the current-voltage characteristics. The main screen of the program (operator panel (Fig. 125)) shows the current-voltage characteristics (red dots), the dependence of the power of a cell from the voltage measured on it (blue line). On the main screen, the measured cell parameters and measurement conditions are displayed. From the main screen information about the cell under test can be entered, calibration is carried out and results can be exported.

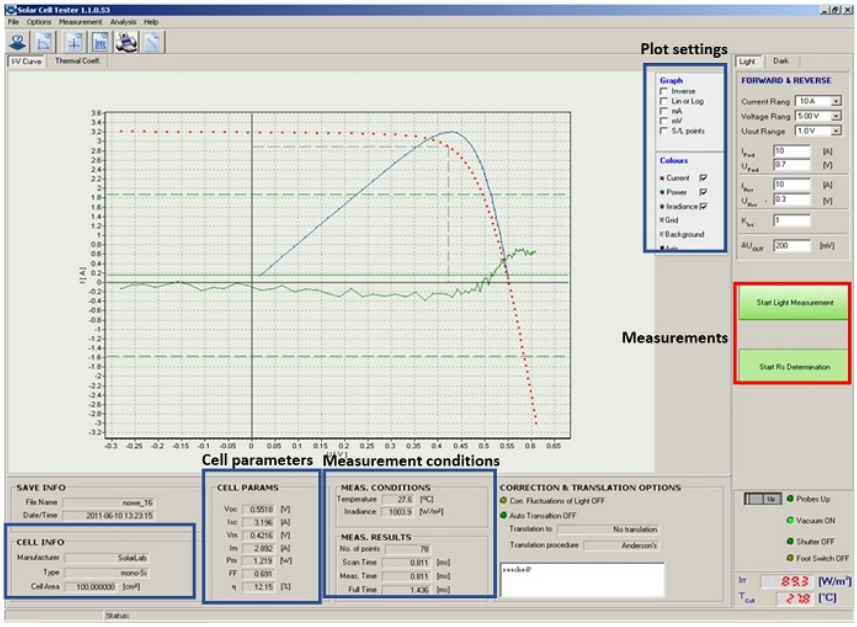

Figure 125: Screen of Solar Cell Tester software controlling the device. Own elaboration.

This video presents the compact simulator from ISOSun Solar Simulator.

https://pre-epodreczniki.open.agh.edu.pl/openagh-video.php?id=115

Light simulator presentation

InfinityPV, ISOSun Solar Simulator (Light simulator presentation), 20.11.2018 (accessed 15.09.2020). Available on YouTube: https://youtu.be/Rc_CdpqVd7c.

Przypis

1. Busbar cells are described in chapter: 6.1 Busbar cells.
2. Smartwires are described in chapter: 6.4 Smartwires cells.
3. See chapter: 6.5 HIT technology cells.
4. The cells are described in the chapters: 6.2 PERL cells i 6.7 PERC and PERT type PV cells.
5. The temperature coefficients are described in the chapter: 8.3 Temperature dependence of cell parameters.
6. Watch the film by Rafał Jackiewicz: Technical method of measuring resistance or current.

8.2 Simulation of cell parameters changes using PC1D software

The influence of factors on the characteristics and performance of photovoltaic cells can be studied experimentally. For cell design, computer simulations are a useful and inexpensive tool. An example of a program in which current-voltage characteristics can be simulated for photovoltaic cells is PC1D. PC1D is a simple program provided free of charge by the University of New South Wales (Sydney). The program solves coupled nonlinear equations for quasi-uniform electron and hole transport of semiconductor devices.

Version 5.9 of the program was used in the simulations presented below. PC1D contains library files with parameters of crystalline semiconductors used in photovoltaic technology, such as silicon, germanium, gallium arsenide, indium phosphorite, etc. (see Fig. 126, Fig. 127) [158], [159].

The simulation was performed for cells with an area of $100cm^2$ and thickness $300\mu m$. The properties (absorption spectrum, reflectance, energy gap, charge mobility, etc.) were imported from the program's material library. The simulation assumes illumination of the cell with the AM1.5 spectrum, with a light intensity of 0.1 $\frac{W}{cm^2}$, at 300 K.

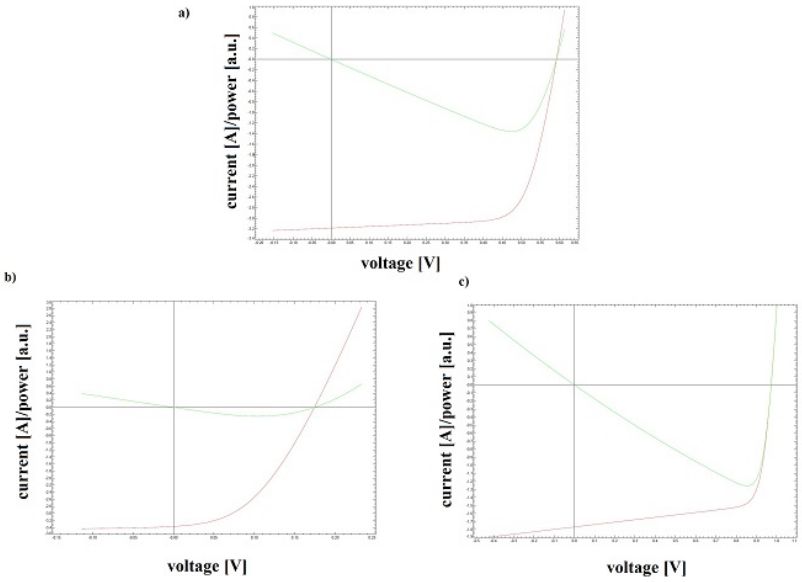

Figure 126: Current-voltage characteristics for (a) silicon Si cell, (b) germanium cell, (c) gallium arsenide AsGa-based cell. Red lines indicate current-voltage characteristics and green lines indicate power-voltage dependence. Own elaboration.

Cell type	I_{sc}	V_{oc}	P_{out} [%]	η [%]
Si	3.18	0.59	1.36	13.6
Ge	3.37	0.17	0.255	2.55
AsGa	1.77	0.972	1.26	1.21

Figure 127: Parameters of photovoltaic cells obtained by simulation. Own elaboration.

To check the influence of light intensity on the characteristics and parameters of the cell, simulations were carried out for a silicon cell at four different light intensities: 0.1 $\frac{W}{m^2}$, 0.05 $\frac{W}{m^2}$, 0.01 $\frac{W}{m^2}$, 0.001 $\frac{W}{m^2}$. The AM1.5 spectrum was used in the simulation. The current-voltage characteristics and power-voltage dependence are shown in Fig. 128. In the figure, the red lines indicate the current-voltage characteristics and the green lines indicate the power-voltage dependence for a Si silicon cell at radiant power

$$P_{in} \tag{24}$$

a) 0.1 $\frac{W}{cm^2}$ b) 0.05 $\frac{W}{cm^2}$ c) 0.01 $\frac{W}{cm^2}$ d) 0.001 $\frac{W}{m^2}$. A reduction in the intensity of the radiation incident on the cell results in a decrease in the value of I_{sc}, V_{oc} and output power P_{out} and thus the performance of the cell.

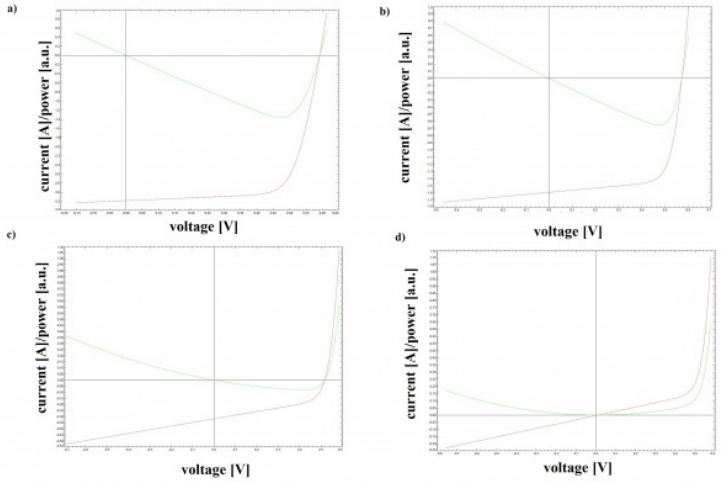

Figure 128: Current-voltage characteristics for Si silicon cell at an intensity of (a) AM1.5 0.1 W/cm2, (b) 0.05 W/cm2, (c) 0.01 W/cm2, (d) 0.001 W/cm2. Red lines represent current-voltage characteristics and green lines represent power-voltage dependence. Own elaboration.

The cell parameters are collected and shown in Fig. 129.

P_{in} [W/cm^2] AM 1.5	I_{sc}	V_{oc}	P_{out} [%]	η [%]
0.1	3.18	0.59	1.36	1.36
0.05	1.59	0.54	6.5	6.5
0.01	0.318	0.084	0.84	0.84
0.0001	$3.8 \cdot 10^{-3}$	0.017	$8 \cdot 10^{-6}$	$8 \cdot 10^{-6}$

Figure 129: Parameters of photovoltaic cells for different lighting obtained by simulation. Own elaboration.

Afterwards, to determine the effect of temperature alone on the performance of the silicon cell, a simulation was carried out in the temperature range from -30^oC to 50^oC. As shown in Fig. 130, the efficiency decreases linearly with increasing temperature. In the program, temperature can be specified in Kelvin or degrees Celsius. The programme's algorithm takes into account the effect of temperature on carrier mobility, surface and volume recombination.

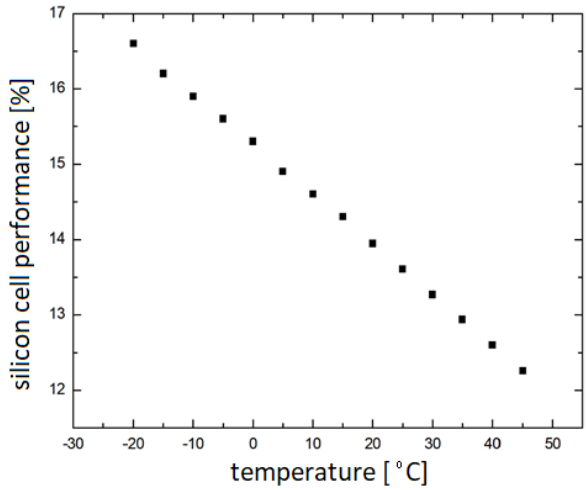

Figure 130: Silicon cell efficiency versus temperature chart. Results generated in PC1D software. Own elaboration.

The decreasing linear dependence of cell efficiency on temperature obtained from the simulation is in agreement with the results of tests carried out on real photovoltaic cells (see Chapter: 8.3 Temperature dependence of cell parameters).

8.3 Temperature dependence of cell parameters

Photovoltaic cells and panels operate under varying weather conditions. These conditions affect the cell parameters. A factor which has a significant influence on the change of cell parameters is its temperature.

Changes in incident light intensity and ambient temperature affect the temperature of the cells, as does humidity and wind speed. Wind is a natural cooling factor. Better cooling (ventilation) can be influenced by mounting the panels (placing the panels on racks increases air circulation).
In Poland, the range of considered temperatures in which photovoltaic cells work is from -20^oC to 70^oC (standard photovoltaic panels operate in a temperature range from -40^oC to $+85^oC$).

Higher light intensity means more energy is absorbed, so increasing light intensity has a positive effect on cell efficiency. In the case of commonly used silicon cells, as the temperature increases, the efficiency of the cell decreases.

The material parameters change with temperature:

- absorption coefficient,
- energy gap,
- charge mobility,
- concentration of charge carriers.

The absorption coefficient of silicon [160] and energy gap [161] decrease with decreasing temperature. Concentration of carriers increases with increasing temperature [162]. The mobility of carriers in semiconductors depends exponentially on temperature. At low temperatures, the temperature dependence of mobility is a dependency factor (25). In the formula as μ is marked as the carrier mobility and T as absolute temperature.

$$\mu \sim T^{\frac{3}{2}} \tag{25}$$

For high temperatures the mobility is described by the dependency factor (26).

$$\mu \sim T^{-\frac{3}{2}} \tag{26}$$

An increase in temperature is also associated with a decrease in the separability of holes and electrons and an increase in the dispersion of charge carriers on the vibrations of the crystal lattice. These changes cause a decrease in the voltage of the p-n junction and changes in the mobility of the charge carriers. Consequently, the short circuit current increases with increasing temperature. In the case of a temperature increase from 25^oC to 60^oC the change in the open circuit voltage value will be 1.2%, the output power intensity about 1.3%, and the coefficient about 1.0% [163].

In the case of a commercial photovoltaic panel, the susceptibility to temperature changes is indicated by parameters specified on the data sheet for each cell, the so-called temperature coefficient. The temperature coefficient is given for maximum power, open circuit voltage and short circuit current of the panel. The panel should exhibit a cell temperature during NOTC (Normal Operating Cell Temperature) conditions equal to at most 45^oC (the lower the value, the higher the quality of the panel).

In the Fig. 131 temperature parameters for four commercially available photovoltaic panels are presented:
I - monocrystalline module BEM 355W White (Extreme plus series) 66 cells (company: BrukBet),
II - double active module with PERT type cells, BEM 335W, III - Opti series Nivo Extreme (company: BrukBet),
III - polycrystalline module series SV60P 280Wp (company: Selfa),
IV- monocrystalline module series SV60M of power up to 315Wp (company: Selfa).

Panel type	Efficiency [%]	Temperature coefficient for maximum power [% /°C]	Cell temperature during operation [°C]
BEM 355W White (Extreme plus series) 66 cell monocrystalline modules (BrukBet)	19.36	-0.39	42
Double sided active module with PERT cells, BEM 335W Opti Nivo Extreme Series (BrukBet)	20.02	-0.39	42
SV60P series polycrystalline module with power 280Wp (Selfa)	17.7	-0.38	42
SV60M series monocrystalline module with power output up to 315Wp (Selfa)	19.6	-0.37	42

Figure 131: Temperature coefficients for selected panels. Own elaboration.

The performance variation as a function of temperature for the above photovoltaic panels is shown in the graph (Fig. 132).

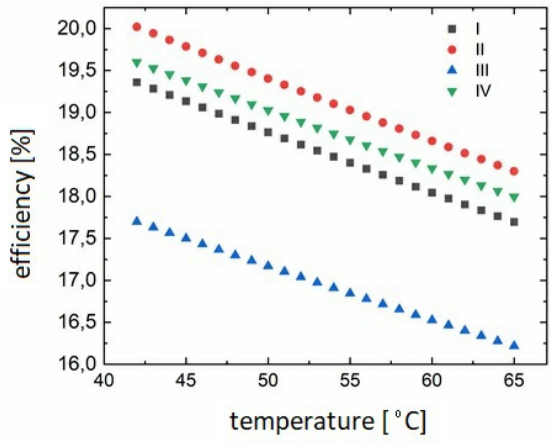

Figure 132: Temperature dependence of efficiency for four example photovoltaic panels: I - monocrystalline module BEM 355W White (Extreme plus series) 66 cells (Brukbet company), II - bilaterally active module with PERT type cells, BEM 335W, III - Opti series Nivo Extreme (BrukBet company), III - polycrystalline module SV60P series with power of 280Wp (Selfa company), IV - monocrystalline module SV60M series with power up to 315Wp (Selfa company). Own elaboration.

As can be read from the graph Fig. 132, at 60 degrees the performance drops by 1.5% relative to the value at 40 degrees Celsius. Continuous operation of photovoltaic panels at high temperatures also carries the risk of shortening their service life. Protection and longer life can be ensured by using additional protective layers (e.g. reinforced electro-insulating film or additional glass sheet) and by ensuring good ventilation.

8.4 Module parameters measurements

Power that can be obtained from the photovoltaic panel depends on the conditions in which the panel works and depends

primarily on the intensity of solar radiation and temperature. Since comparing panels working in different conditions is not reliable, two standards have been introduced to determine under which conditions measurements should be made:

- conditions for conducting tests: STC (Standard Test Conditions) specifies the type of light source with a spectrum of AM1. 5 and power of 1 000 $\frac{W}{m_2}$, and the temperature of measurement is set at $25^o\mathrm{C}$ [164],
- conditions for PV panel tests: NOCT (Normal Operating Cell Temperature) specifies the type of light source at AM1. 5 with a power of 800 $\frac{W}{m_2}$, measurement temperature at $20^o\mathrm{C}$ and wind speed at 1 m/s.

When designing a photovoltaic system, the parameters determined under STC conditions should be used, while NOCT conditions give a better idea of how the panel will behave under actual operating conditions in our climate.
Measurements of photovoltaic panels are carried out in specialized test chambers. These chambers are characterized by controlled parameters:

- radiation of the so-called artificial sun with AM1.5 spectrum,
- adjustable irradiance (from 30 $\frac{W}{m_2}$ to 1000 $\frac{W}{m_2}$,
- adjustable temperature (from $-30^o\mathrm{C}$ to $200^o\mathrm{C}$).

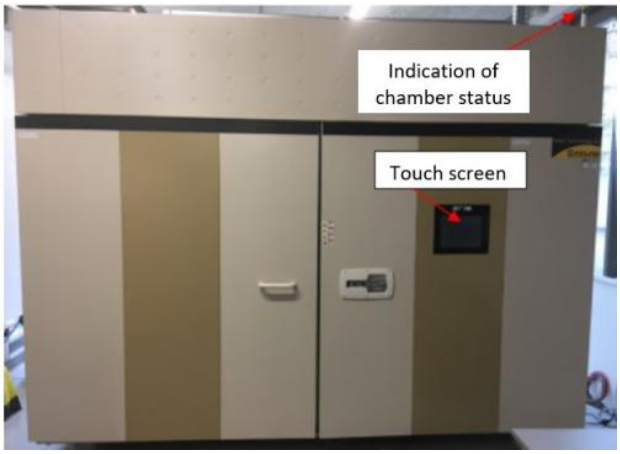

Figure 133: Environmental simulation chamber model SEC 2100/4100/6100 (manufacturer Atlas Material Testing Technology, owned by Małopolskie Laboratorium Budownictwa). Own elaboration.

Fig. 133 shows the environmental simulation chamber [165]. It meets the conditions mentioned above, both STC and NOCT tests can be performed with it. The interior size is 2m*3m and 2m height. The touch screen allows you to input the parameters of the photovoltaic panel measurement conditions: such as temperature, humidity and illumination. The status of the measuring chamber is displayed on the top of the chamber. The controls, indicators, and sensor leads are shown on Fig. 134.

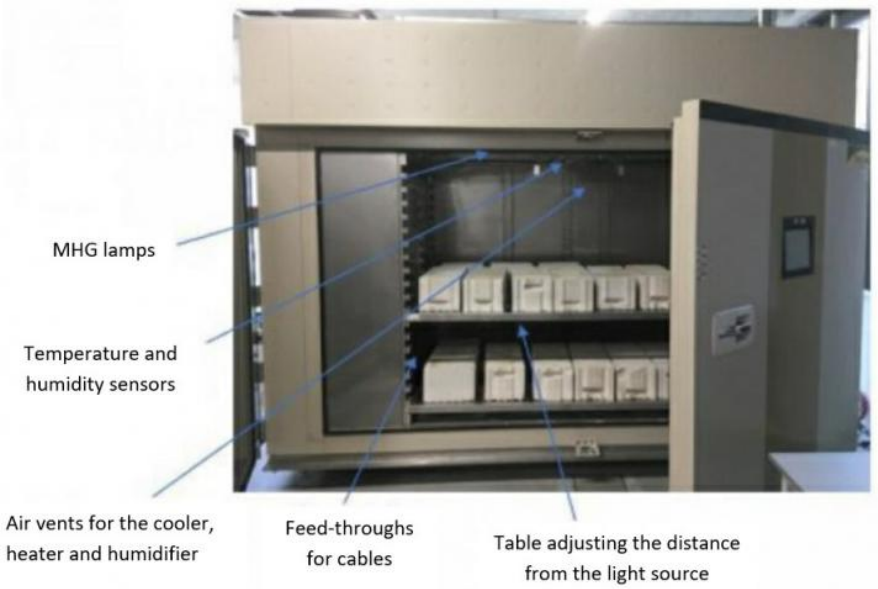

Figure 134: Description of the major components of the environmental simulation chamber. Own elaboration.

MHG lamps are protected by glass covers that are heated to protect against fogging. Temperature and humidity sensors are used to control the conditions in the measurement chamber. Fan vents introduce prepared air into the chamber to maintain set environmental conditions. At the rear of the chamber there are the humidifier, air heater and evaporator of the refrigeration system. In the picture you can also see the grommets for the measurement cables and the measurement table.

Each photovoltaic panel has a nameplate that shows the characteristic parameters of the panel Fig. 135.

Figure 135: Risen Energy's photovoltaic panel nameplate including its characteristic parameters.

In order to determine them, current-voltage characteristics tests are carried out. Measurements are carried out using specialized equipment, the schematic of which is shown in Fig. 136 [165].

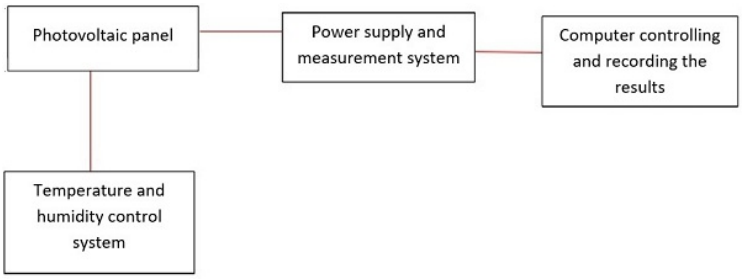

Figure 136: Schematic of the measurement system for current-voltage characteristic stripping. Own elaboration.

The photovoltaic panel is placed in a chamber to maintain a constant temperature and irradiance. It is then connected to a control voltage source and the voltage and current flowing through the PV panel are measured. The whole system is controlled by a computer used to record the measurement results and environmental conditions.
A typical current-voltage relationship for a photovoltaic panel and the characteristic electrical parameters that describe the photovoltaic panel (Fig. 137) are shown below.

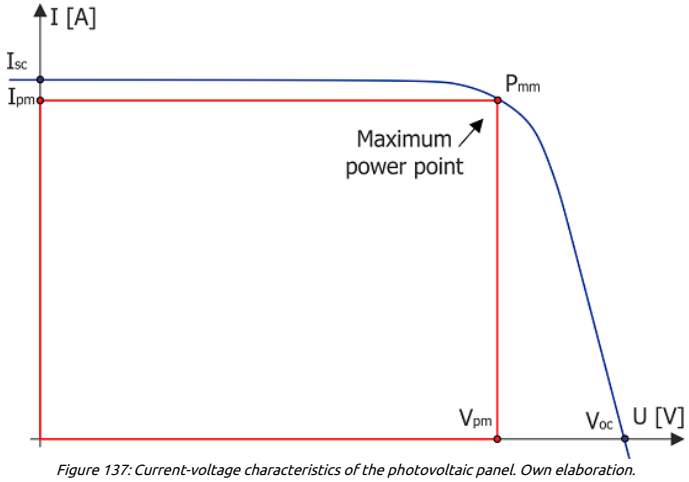

Figure 137: Current-voltage characteristics of the photovoltaic panel. Own elaboration.

The parameters of the photovoltaic cell obtained at a given operating temperature and a given solar irradiance are:
I_{sc} – short circuit current, which is the maximum current that the photovoltaic panel can generate,
I_{pm} – the current at which the maximum power can be extracted from the photovoltaic cell,
V_{oc} – the open circuit voltage, which is the maximum voltage that can be extracted from the photovoltaic panel,
V_{pm} – the voltage at which the maximum power can be extracted from the photovoltaic cell.
Based on the data for the graph and the determined quantities given above, the maximum power, efficiency, temperature power

index, temperature voltage index V_{oc}, temperature current index I_{sc} are calculated.
Here is an example of electrical parameters under standard STC conditions for BS-330=6MHB5-EL panel from Bauer Solartechnik GmbH data sheet:

- monocrystalline PV cell / PERC - double,
- PV cell arrangement 12 x 10 (120),
- nominal power at maximum power point P_{max} = 330 W,
- power production tolerance P_{max} 0 to 3%,
- operating voltage V_{pm} = 33.70 V,
- open circuit voltage V_{oc} = 40.60 V,
- short-circuit current I_{sc} = 10.35 A,
- working current I_{pm} = 9.80 V,
- panel efficiency (efficiency) 18.6%,
- operating temperature (NOCT) $45^{o}\mathrm{C}$ ± 2,
- temperature coefficient I_{sc} $+0.050\%$/K,
- temperature coefficient V_{oc} -0.290%/K,
- temperature coefficient Ppmm -0.390%/K,
- number of diodes 3x1 bypass diodes.

9. Photovoltaic systems

9.1 Off-grid photovoltaic systems

A photovoltaic system is a solar power station that allows the conversion of solar energy into electricity using photovoltaic panels.
The basic classification of photovoltaic systems is based on their power. The following types of renewable energy installations are [166]:

- micro-installations,
- small installations,
- medium installations,
- large installations.

A micro-installation is an installation of a renewable energy source with an installed total electric power (defined by the manufacturer as the nominal power of the equipment that produces electricity) of no more than 50 kW, connected to the electricity grid with a nominal voltage of less than 110 kV. The highest growth dynamics of the installed capacity is achieved by way of micro-installations.
A small installation is defined as an installation with a total installed electrical power of more than 50 kW and less than 500 kW, connected to a power grid with a nominal voltage lower than 110 kV.
The largest photovoltaic installations are photovoltaic farms with a capacity greater than 500 kW, which may even reach the order of several hundred MW. In the case of installations between 500 kW and 1 MW, we talk about a medium-sized installation, and above 1 MW - a large installation.
Photovoltaic systems are classified into two groups based on how they interact with the grid:

- island photovoltaic installations (off-grid), i.e. not connected to the electricity grid [167],
- grid-connected photovoltaic installations (on-grid) [168], which include:
- connected to the low voltage grid and are mostly micro and small installations,
- connected to the medium voltage grid, which may include medium and large installations,
- connected to the high-voltage grid, being installations of several MW or tens of MW.

Another criterion for classifying the types of photovoltaic system is the ability of the PV system to track the sun. In this respect, one can distinguish:

- stationary installations that do not follow the movement of the Sun,
- tracking installations that follow the movement of the Sun.

Based on the installation method of photovoltaic systems in a building, PV systems can be classified into two types [169]:

- Building-attached photovoltaic (BAPV) systems, in which PV modules have no direct impact on the building structure and are directly fixed to buildings with a support structure [170],
- Building-integrated photovoltaic (BIPV) systems, in which PV modules are integrated into the building structure [171].

Photovoltaic island systems type off-grid

Photovoltaic island systems type off-grid operate outside the public electricity grid. This type of system consists of photovoltaic panels, an inverter, a charge controller and energy storage. The block diagram of an island photovoltaic system is shown in Fig. 138.

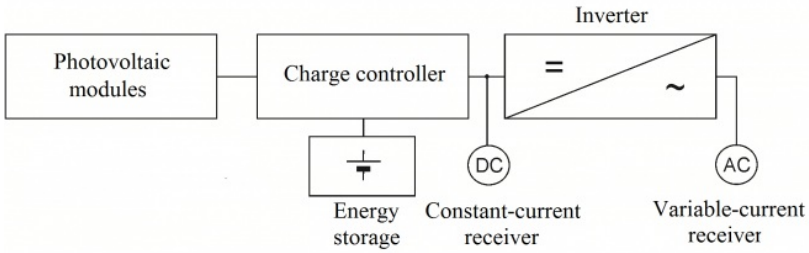

Figure 138: Block scheme of an off-grid photovoltaic system. Own elaboration.

In this type of system, the electricity generated as direct current is converted into alternating current by an inverter. If excess energy is produced, it is stored in so-called energy reservoirs for later use. In domestic installations, batteries are the most commonly used energy storage devices.
Photovoltaic island systems type off-grid are divided into:

- remote from the grid,
- with possible access to the electrical grid.

Off-grid installations are used primarily in places where the costs of connecting to the electricity grid are too high or their connection is impossible for some reason [172]. Examples of these types of sites include: vacation homes, ships, yachts, and automobiles. Off-grid photovoltaic systems are also used to power street lamps, road signs and portable devices. Examples of off-grid photovoltaic installation are presented in Fig. 139, Fig. 140 and Fig. 141.

Figure 139: Solar powered traffic signs. Photo – author archive.

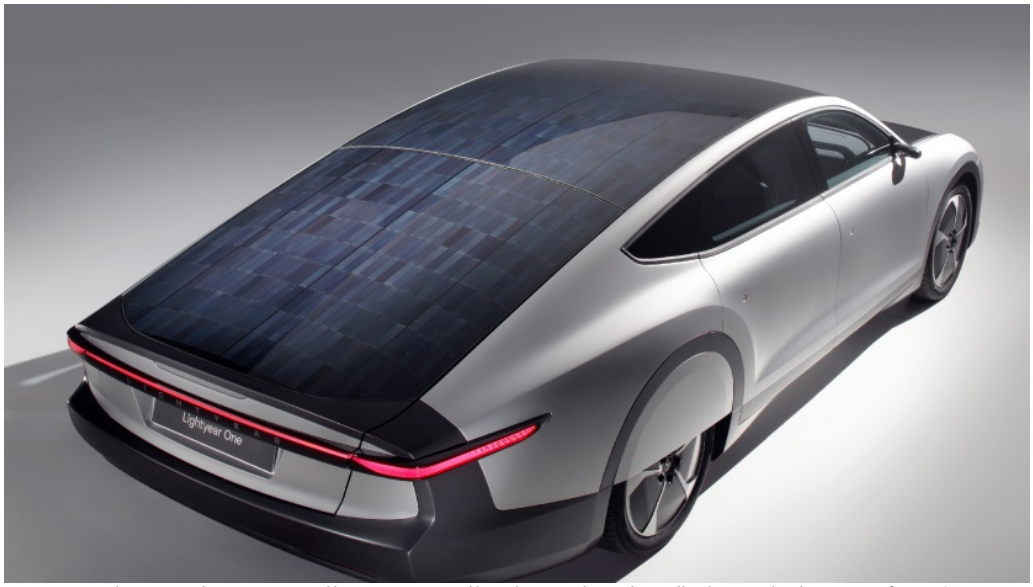

Figure 140: Lightyear One electric car powered by energy generated by Lightyear ∞ photovoltaic cells. Photo used with permission from Lightyear ∞ .

Figure 141: A yacht powered by energy generated by SolTech Service's off-grid island photovoltaic system. Photo used with permission from SolTech Service .

9.2 On-grid photovoltaic systems

The grid-connected photovoltaic system represents the largest percentage of photovoltaic installations. This type of system consists of photovoltaic panels, an inverter and a grid connection system. The block diagram of an on-grid photovoltaic system connected to the 230 V grid is presented in Fig. 142, while a photovoltaic farm in Fig. 143.

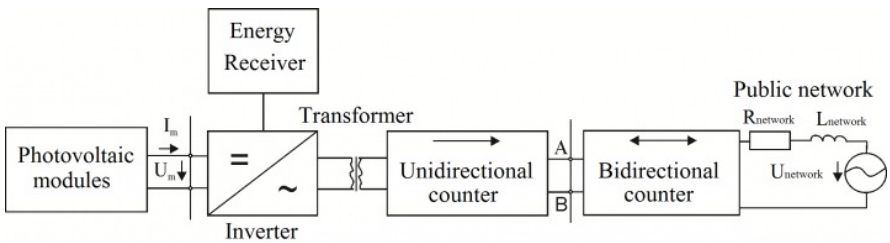

Figure 142: Block scheme of an on-grid photovoltaic system connected to the 230 V public grid. In the figure, the resistance R of the grid, the inductance L of the grid and the voltage Us are marked as parameters of the power grid, the current Im and voltage Um of the photovoltaic module assembly, and the connection points of the home installation A and B. Own elaboration.

Figure 143: Photovoltaic farm built with Sunport Power MWT 400 Wp modules from Columbus Energy. Photo used with permission from Columbus Energy .

The settlement with the power company takes place on a balance basis at the end of the settlement period, i.e. up to 365 days from the moment the energy is fed into the grid [173]. For installations up to 10 kWh, it is possible to take back 80% of the generated energy from the grid, and for installations over 10 kWh 70%. For this reason, an on-grid installation requires the installation of a bidirectional meter to measure the amount of energy taken from and returned to the grid, respectively.

9.3 Ground mount installations

The largest stationary systems are installed on the ground. In the case of photovoltaic farms with an installed capacity of several hundred MW, the area covered by the installation is in the order of several hundred hectares. One of the largest farms in Poland is a photovoltaic installation in Sokołów Małopolski with a capacity of 2 MW, covering an area of 4 hectares (it is shown in Fig. 144). The installation was built on a RS-12 steel structure by RECA SOLAR and based on bifacial module technology. The farm consists of 5970 modules. The general contractor of the farm is Great Solar sp. z o.o. Construction of the farm was completed in 2020.

Figure 144: One of the biggest photovoltaic farms in Poland with the capacity of 2 MW, located in Sokołów Małopolski by Great Solar sp. z o.o. Photo used by permission of Great Solar Sp. z o.o. .

The largest PV farm in Europe is the 500 MW Núñez de Balboa, which is located in the province of Usagre, in the Extremadura region of Spain. The farm is located over an area of nearly 1 000 hectares and consists of 1.43 million panels and 115 inverters (2020 data) [174].
The second largest PV farm in Europe is the 300 MW Cestas Solar Park in France. The installation covers 250 hectares and consists of about one million panels.This farm is presented in Fig. 145. The video "Construction of PV power plant in Cestas"

shows the construction of the Cestas Solar Par farm, while the video "Krinner Solarpark Cestas" presents a view of the completed construction.

https://pre-epodreczniki.open.agh.edu.pl/openagh-video.php?id=121
Photovoltaic farm installation
SE Solar, Construction of PV power plant in Cestas, France (Photovoltaic farm installation), 04.12.2015 (accessed). Available on YouTube: https://youtu.be/YBJHUN1og9M.

https://pre-epodreczniki.open.agh.edu.pl/openagh-video.php?id=122
Photovoltaic farm
Steffi Englram, Krinner Solarpark Cestas (Photovoltaic farm), 16.06.2015 (accessed). Available on YouTube: https://youtu.be/qw05UuGaPGM.

To find large areas of unused ground in Europe is difficult compared to Asia's desert and foothill areas. One of the largest solar PV farms installed on land in the world is the Tengger Desert Solar Park with a capacity of 1.547 GW (total installed capacity by May 2020 is 1.95 GW [175]). The farm is located in Zhongwei, China and covers the area of 4 300 hectares. Another large photovoltaic farm in the world is the Longyangxia Dam Solar Park in China. It consists of more than 4 million panels and has an installed capacity of 850 MW [176].

In addition to large photovoltaic farms, systems with capacities ranging from a few to several hundred kW are installed. The installation of this type is shown in Fig. 145.

Figure 145: SolTech Service's ground-mounted photovoltaic installation. Photo used by permission of SolTech Service .

9.4 Floating installations

The floating photovoltaics systems (FPV) are a type of system installed on the surface of water reservoirs. The use of FPV systems makes it possible to avoid the problems associated with the cost of renting land, which is becoming more expensive and less available. Installing PV systems on water also makes it possible to increase the efficiency of the installation by improving the cooling of the panels due to lower heating of the water surface in relation to the ground surface and reducing dust deposition. Installing floating systems also saves land from an agricultural and urban planning perspective. The negative aspect of installing such systems can be the exclusion of a part of the water body from the fishing industry, strong wave action in case of marine and ocean installations, as well as the problem of energy collection [177].
The floating photovoltaic systems are installed by using different mounting solutions. Photovoltaic panels are installed above water on pontoons made of plastic such as high density polyethylene (HDPE). The installation is anchored using cement weights placed at the bottom of the water body or set on its shore. A PV installation anchored to the bottom of the reservoir is shown in Fig. 146.

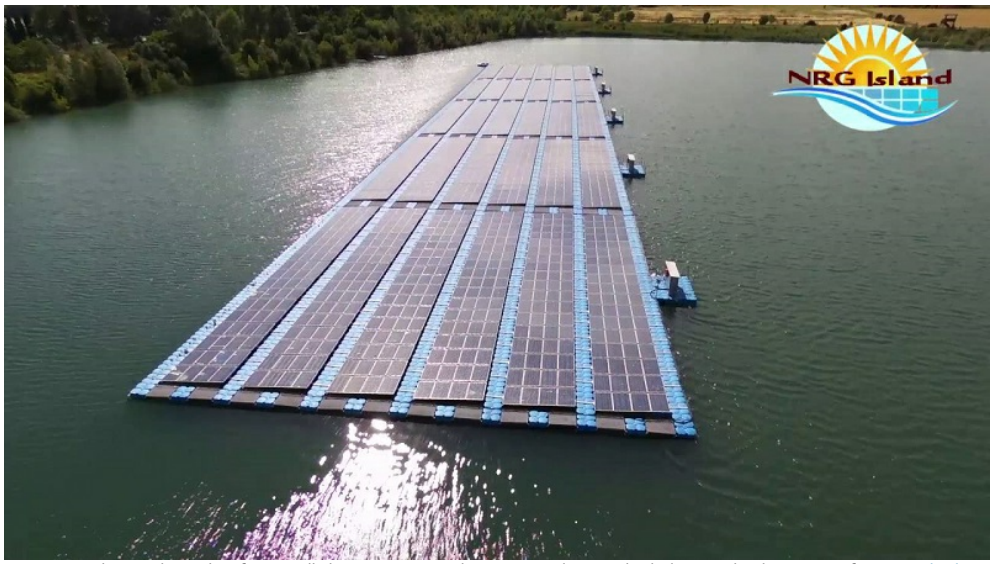

Figure 146: Floating photovoltaic farm installed over water on 500 kWp pontoons by NRG Island. Photo used with permission from NRG Island .

https://pre-epodreczniki.open.agh.edu.pl/openagh-video.php?id=123
Installation of a floating photovoltaic system
Piemme srls, Floating Photovoltaic Plant NRG ISLAND, 23.06.2020 (accessed 23.03.2020). Available on YouTube: https://youtu.be/joUC8DJwI7c.

The floating installations are also made by using a partially submerged system in which the panels are partially submerged in water, which allows the efficiency of the panels to increase due to their cooling by the water [178]. Semi-submerged systems use panels on flexible substrates that float directly on the water. The panels float by using floats placed at the edge of the panels and anchored with ropes. Such a concept of installation of PV systems was first presented by MIRACO, which installed a system with a total area of 75 m^2 and 8 kW in Comino, Malta.
The first floating photovoltaic system was fabricated for research purposes in 2007 in Aichi, Japan with a capacity of 20 kW. The panels were placed on foam polystyrene panels and raised at an angle of 1.3^o toward the south [177]. The first commercial PV system floating on surface water was a 175 kW installation. The installation was made by SPG Solar in 2008 at Far Niente Winery. The first floating PV power plant at sea was a farm made by Ocean of Energy. This farm was installed in the Dutch North Sea in late November 2019 (Fig. 147). The power of the system was initially 8.5 kW and consisted of 28 panels, and on January 20, 2020 it was increased to 17.5 kW by installing 28 more panels. The farm has so far survived several storms, including Orkan "Sabina", during which it remained intact despite wind speeds exceeding 30 $\frac{m}{s}$, as well as 5-meter waves.

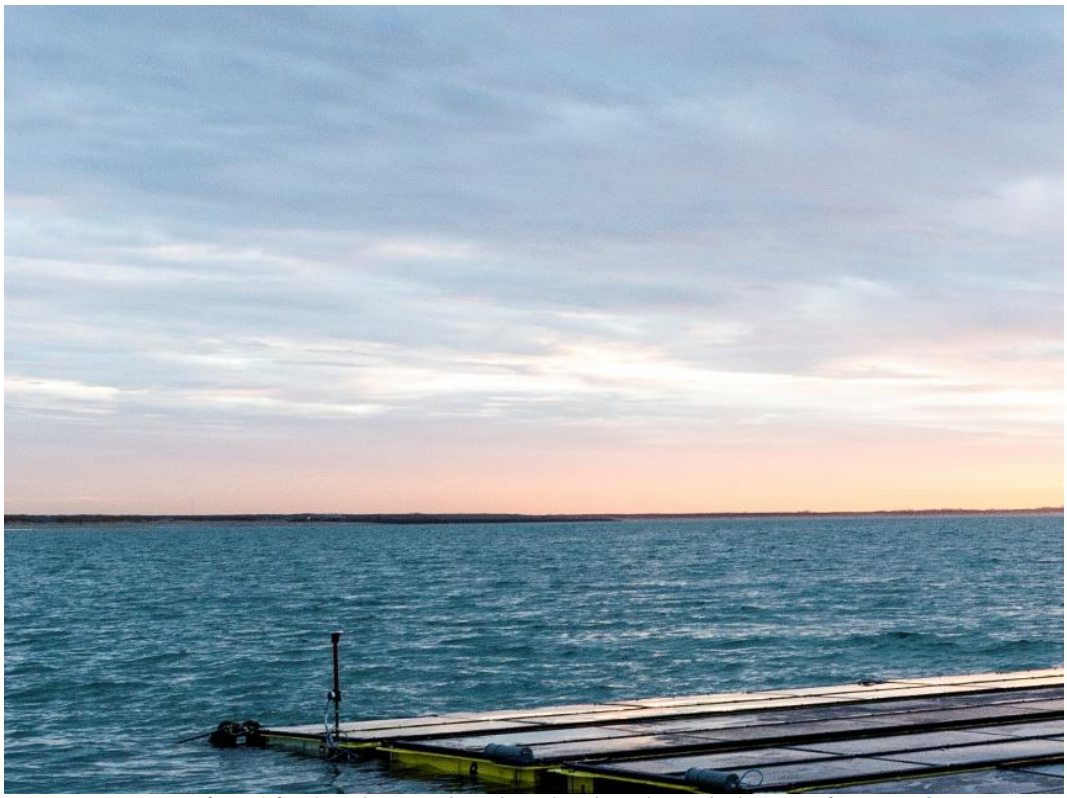

Figure 147: Oceans of Energy's first photovoltaic power plant in the Dutch North Sea. Photo used with permission from Oceans of Energy .

One of the largest floating photovoltaic installations was built on a lake in Anhui, China. It has more than 165 000 photovoltaic panels and produces 40 MWp of electricity per year [179]. A floating installation in Anhui is shown in this video "World's largest floating solar farm in E China".

https://pre-epodreczniki.open.agh.edu.pl/openagh-video.php?id=124
World's largest floating solar farm in Anhui (China)
New China TV, World's largest floating solar farm in E China, 21.06.2017 (accessed 14.12.2020). Available on YouTube: https://youtu.be/qKpYH5SYUeo .

9.5 Tracking systems

Moving photovoltaic systems are installations whose orientation relative to the direction of the sun's rays changes as the sun's movement changes, or whose position changes as the objects on which they are installed change. Mobile PV systems are classified into two main groups:

- tracking systems [180], [181],
- mobile systems [182], [183].

Tracking systems

Photovoltaic tracking systems are those systems in which the plane of the panels rotates so that the sun's rays fall perpendicular to the plane of the panel to increase the amount of energy absorbed. Trailing systems produce up to 40% more electricity compared to stationary systems [184], [185].
There are two types of tracking installations. The first group includes ground-based installations, in which the panels are placed on rotating poles called trackers. The second is floating installations, in which the planes of the panels rotate in the direction of the sun's current position.
Due to the number of planes in which the movement of photovoltaic panels takes place, the systems are divided into uniaxial and biaxial. Single-axis systems are installations with the ability to move panels from east to west only relative to one axis of rotation. Biaxial trackers allow simultaneous movement of panels in relation to two axes of rotation [186]. The dual-axis tracking systems move from east to west along with the ability to change the angle of the panels relative to the ground surface. The types of single-axis and dual-axis trackers are shown in the Fig. 148.

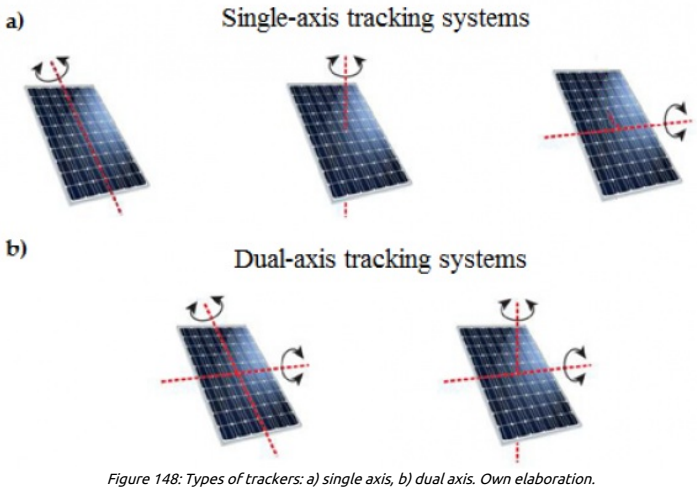

Figure 148: Types of trackers: a) single axis, b) dual axis. Own elaboration.

The working principle of both types of trackers is shown in the videos "Single Axial Solar Tracker" and "ASUN 2 Axis Solar Tracker".

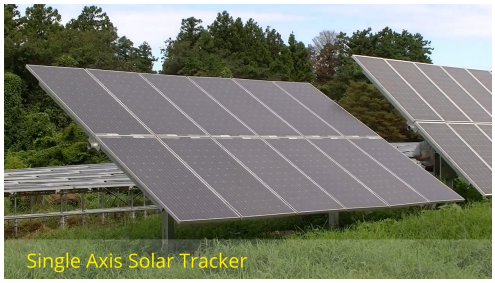

https://pre-epodreczniki.open.agh.edu.pl/openagh-video.php?id=126
Single Axial Solar Tracker
Solar Trackers, Single Axial Solar Tracker, 22.01.2019 (accessed 02.12.2020). Available on YouTube: https://youtu.be/eJv39HPSLus.

https://pre-epodreczniki.open.agh.edu.pl/openagh-video.php?id=125
Two-axis photovoltaic system that follows the movement of the sun
Asun Trackers Pvt. Ltd, ASUN 2 Axis Solar Tracker (Two-axis photovoltaic system that follows the movement of the sun), 10.08.2019 (accessed 02.12.2020). Available on YouTube: https://youtu.be/NGvcINzsweQ.

The tracking systems are also classified according to the control system used, namely as follows [187]:

- open system (passive), open loop controlled,
- a closed system (active) in which the control is closed loop.

In an open system, control of the position of the tracker relative to the Sun is based on mathematical models. The models are based on data determining the position of the Sun at a given day and time for a given latitude, i.e. on the astronomical calendar. In closed loop trackers, the position of the system is controlled by sensors e.g. photoresistors, i.e. resistors with a resistance depending on the light dependent resistor (LDR) illumination [188], [189]. Another way to control the position of the tracker is to find the maximum power point (MPP) [190]. It changes according to the irradiance and temperature. The control system with MPP works by changing the position of the installation in small intervals and comparing the resulting power values. Based on the result obtained, the installation moves to the position for which it receives the highest power.
In order to increase the efficiency of the tracking PV systems, concentrated photovoltaics (CPV) are also used [191]. The CPV technology is a new emerging technology for photovoltaic systems that allows solar radiation to be focused onto PV cells through the use of lenses or curved mirrors.

Ground tracking systems

A ground tracking installation consists of a set of photovoltaic modules placed on a frame located on a rotating pole. An example of a single-axis tracking installation is the 172 MW system located in Telangana, India (Fig. 149) [192]. The entire installation consists of more than 520 000 panels made from Hareon Solar's multicrystalline silicon and covers more than 450 hectares. An example of a dual-axis tracking installation is shown in the figure Fig. 150.

Figure 149: Photovoltaic farm built with single-axis tracking systems in India. Aut. photo Vinaykumar8687, licensed under CC BY-SA 4.0, source: Wikimedia Commons .

Figure 150: Photovoltaic installation built with dual-axis tracking systems from Solar Tracker Polska. Photo used by permission of Solar Tracker Polska .

Photovoltaic tracking systems are also made with one of the latest Concentrating Photovoltaics (CPV) technologies using solar concentrators. The world's largest tracking biaxial photovoltaic farm made with CPV technology is the 138 MWp Golmud CPV Solar Park, which is located near the city of Golmud, China (Fig. 151) [193].

Figure 151: Largest photovoltaic farm made of CPV bi-axial trackers with ray concentrators in Golmud, China with a capacity of 138 MWp. Aut. photo Vinaykumar8687, licensed under CC BY-SA 4.0, source: Wikimedia Commons .

Tracking systems located on the water

Photovoltaic installations installed on the water surface are the least common of all types of photovoltaic installations. In this type of installation, the panels are placed on a floating platform and follow the movement of the sun by rotating it around its axis. One way of making the platform with PV panels move is by twisting it thanks to a rolling wheel. Another way to put a floating installation into rotation is by using a fixed mooring and steering a cable. Another example of a floating tracking installation is the floating tracking cooling concentrator (FTCC) photovoltaic system. An FTCC installation consists of floating platforms on which photovoltaic panels are mounted horizontally and concentrators are mounted at an angle to the surface of the panels, as shown schematically in Fig. 152.

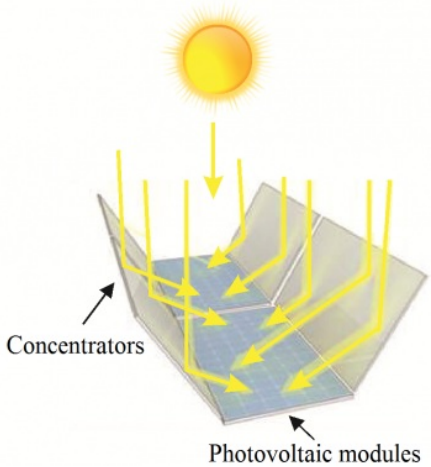

Figure 152: Schematic of a photovoltaic system with solar concentrators. Own elaboration.

The FTCC system moves in a disorderly motion with the ripples of the water. The first installation of this type was performed in Colignola, Tuscany, in 2011; it is shown in the video "Italian engineers pioneer floating solar panels".

https://pre-epodreczniki.open.agh.edu.pl/openagh-video.php?id=129
Italian engineers pioneer floating solar modules in Colignola, Tuscany
AFP News Agency, Italian engineers pioneer floating solar modules in Colignola, Tuscany, 22.02.2012 (accessed 02.12.2020).
Available on YouTube: https://youtu.be/foGaExl84gw .

9.6 Portable installations - everyday objects

Photovoltaic portable systems enable power supply to devices and objects in places where traditional power supply would be impossible or difficult due to technical reasons. This group includes, among others: calculators, watches, backpacks, clothes, as well as toys. Examples of everyday objects are shown in Fig. 153, Fig. 154, Fig. 155.

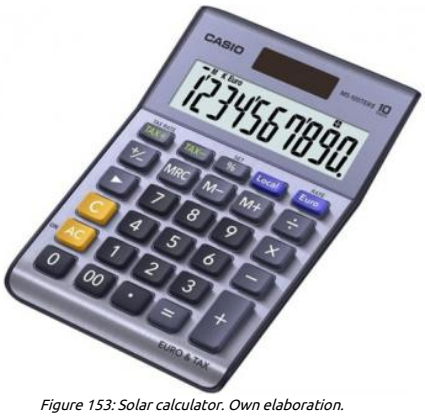

Figure 153: Solar calculator. Own elaboration.

Figure 154: Garmin Fenix 6X Pro Solar powered watch. Aut. photo by Crishazzard, licensed under CC BY-SA 4.0, source: Wikimedia Commons .

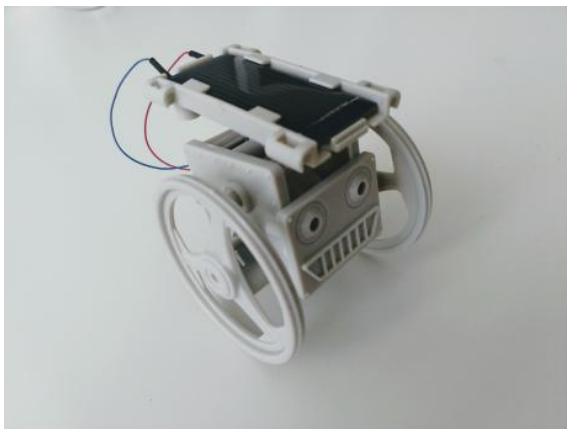

Figure 155: A toy solar robot powered by solar radiation energy. Own elaboration.

9.7 Portable installations - vehicles

Photovoltaic modules are used in transportation equipment such as satellites, airplanes, automobiles, yachts, boats, water streetcars etc. The inventor of the first solar-powered aircraft, shown in Fig. 156 and called Solar Impulse, was Bertrand Piccard. The plane made its first flight in 2010 and completed its round-the-world journey in 2016.

Figure 156: The first Solar Impulse aircraft powered by solar radiation energy. Aut. photo Rama, licensed under CC BY-SA 2.0 FR, source: Wikimedia Commons .

The first unmanned aircraft in Poland was created by the AGH Solar Plane Scientific Association in Krakow (Fig. 157). The aircraft has a wingspan of almost 4 m and weighs only 5 kg and can reach speeds of about 50 $\frac{km}{h}$. The aircraft is powered by energy from 48 photovoltaic modules with a total output of 167 W.

Figure 157: Solar powered unmanned aircraft made by AGH Solar Plane. Photo: Maciej Talar, KSAF Krakow Student Photographic Agency AGH .

The photovoltaic cells have also found their way into the wings of the International Space Station, which is shown in the Fig. 158.

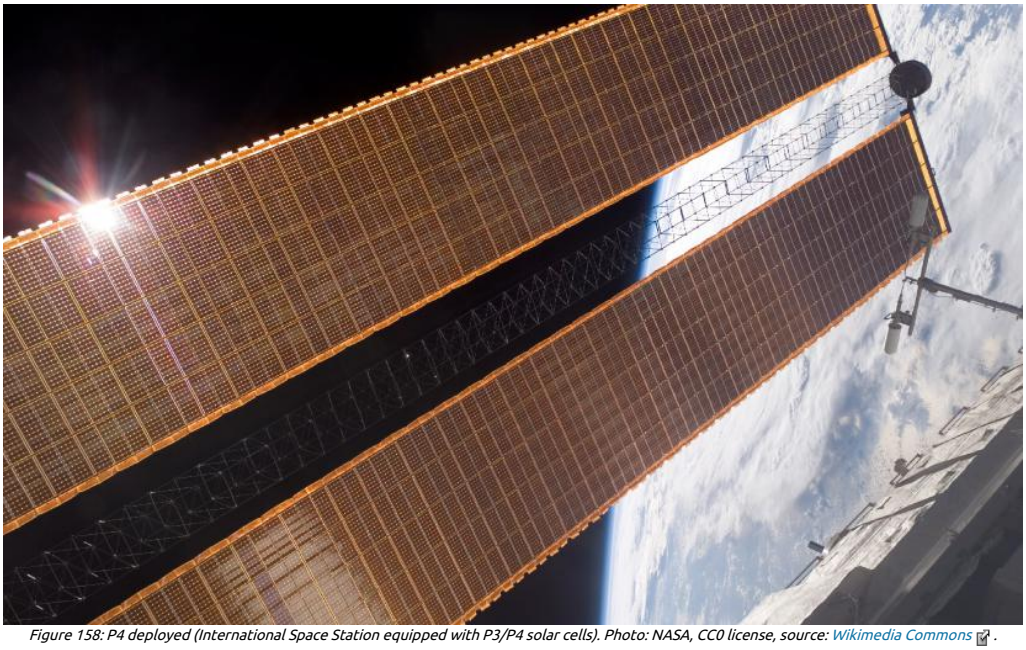

Figure 158: P4 deployed (International Space Station equipped with P3/P4 solar cells). Photo: NASA, CC0 license, source: Wikimedia Commons .

The automotive market is also a recipient of photovoltaic installations. Electric cars can be charged using electric charging stations as well as electricity generated by photovoltaic cells that are directly installed on the vehicle. An example of the use of photovoltaic cells to power vehicles is the Lightyear One electric car, whose hood, roof and trunk are covered with PV cells totaling 5 m^2. This car is presented in Fig. 159.

Figure 159: Lightyear One electric car covered with Lightyear ∞ photovoltaic cells. Photo used with permission from Lightyear ∞ .

Modules made of 156 mm by 156 mm monocrystalline silicon cells were used in the Volkswagen T5 California car, shown in Fig. 160. Flexible photovoltaic modules from Solbian's Solbian Flex CP series are used in the car.

Figure 160: Solbian Flex CP Series modules used in a Volkswagen T5 California by Solbian Energie Alternative SRL. Photo used with permission from Solbian Energie Alternative SRL

.

An example of the application of photovoltaic systems on vessels is the ship "Harta", shown in Fig. 161. The ship was designed and built by Januszkowice Shipyard. The engines used in the ship are of Polish production made by the Institute of Propulsion and Electrical Machines Komel, while Soltech Service is the photovoltaic and battery supplier. Photovoltaic modules used in the ship project have a maximum power of about 8 kW.

Figure 161: The ship "Harta" equipped with a solar installation by SolTech Service. Photo used by permission of SolTech Service .

Solar cells are also used in boats. Case in point: Maya and Aladino's Vindo 32 from the YouTube channel Sailing Magic Carpet, who have set their sights on circumnavigating the world. The boat, Vindo 32, was equipped with Solbian's SP-Series 130W flexible photovoltaic module made of monocrystalline silicon cells. Solbian's SP-Series flexible photovoltaic panels were also used on the Alibi 54 catamaran, shown in Fig. 162.

Figure 162: Alibi 54 catamaran equipped with 12 Solbian SP series flexible modules from Solbian Energie Alternative SRL. Photo used with permission from Solbian Energie Alternative SRL .

Students from the AGH University of Science and Technology in Krakow have decided to build a zero-emission racing boat powered by 100% renewable solar energy. The AGH Solar Boat Team is powered by 384 SunPower c60 series monocrystalline photovoltaic cells, providing up to 1 kW of power (Fig. 163). This energy is accumulated in 1.5 kWh lithium-ion batteries. The team participates in many international solar boat races and in 2018 took 3rd place in the Monaco Solar & Energy Boat Challenge [194].

Figure 163: AGH Solar Boat Team boat powered by solar radiation energy. Photo used by permission of AGH Solar Boat Team .

Photovoltaic cells are also used in tents and sunshades, for example, at the U.S. Army military base in Africa shown in Fig. 164.

Figure 164: Sunshade equipped with photovoltaic cells. Photo US Army Africa, licensed under CC BY 2.0, source: Wikimedia Commons .

Another interesting application of photovoltaic cells is their installation in smart clothing equipped with sensors monitoring vital signs. Researchers from the University of Salento in Italy have worked on this type of solution, developing clothing powered by PV cells with a power of 265 mW [195].
One of the problems of using photovoltaic cells on clothing is the lack of water resistance. A water-resistant garment with a photovoltaic system was made by researchers in Tokyo. They created an ultra-thin photovoltaic cell covered on both sides with a stretchable and waterproof layer. When subjected to stretching and water exposure, this type of cell does not lose its photovoltaic properties [196].

10. Inverters

10.1 Inverters functions

Inverters, also called DC/AC converters, are devices used to change direct current (DC) voltage and current into alternating current (AC) sinusoidal voltage and current with parameters consistent with their values in the public low voltage network (230/400V, 50Hz). These devices are used in the photovoltaic systems because photovoltaic modules generate electricity in the form of DC current and voltage, which must be converted into AC current and voltage. In order to obtain the appropriate parameters of current and voltage, inverters are built of the following components [197]:

- DC/DC converter with Maximum Power Point Tracker (MPPT),
- DC/AC converter (main inverter),
- LC smoothing filter.

The DC/DC converter matches the input voltage to the output voltage. After the DC current passes through the DC/DC converter, the current is sent to the DC/AC converter. This converter converts the DC voltage of a specific value into an AC voltage of an amplitude and frequency matched to the parameters of the power network (230V, 50 Hz). The last element of a standard inverter is an LC smoothing filter which limits the content of higher harmonics to the level specified by the standards. Fig. 165 (compiled based on [197]) shows the scheme of DC/DC converter for voltage reduction (Fig. 165a) and voltage enhanced (Fig. 165b) (compiled based on [197]).
The scheme of the DC/AC converter is shown in Fig. 166 (compiled based on [197]), while the smoothing filter scheme is presented in Fig. 167 (compiled based on [197]). The schemes use the following symbols: L - coil, D - diode, C - capacitor, R - resistor, F - fuse, Ł - switch, T - transistor and Tr - transformer, and a detailed description of the principle of operation of individual electronic circuits can be found, for example, in the book by A. Filipowicz [198].

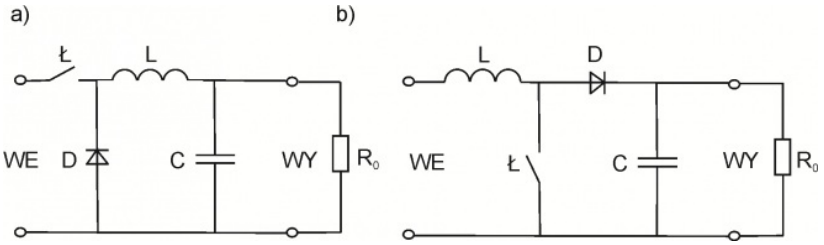

Figure 165: The scheme of DC/DC converter (a) increasing voltage, (b) decreasing voltage. Own elaboration.

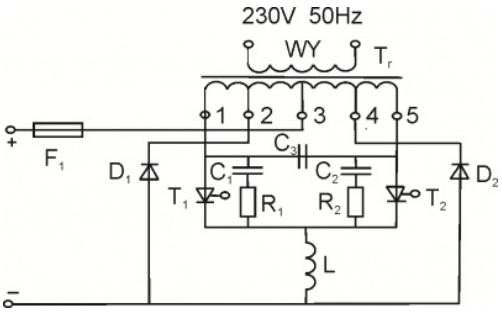

Figure 166: The scheme of an example DC/AC converter with a transformer at the output. Own elaboration.

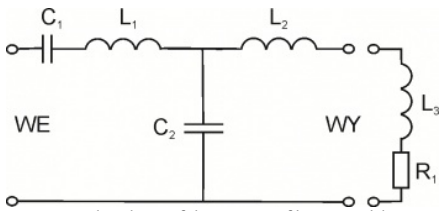

Figure 167: The scheme of the AC output filter. Own elaboration.

10.2 Inverters classification

The PV installations can be connected to the power grid or can be a stand-alone installation. Due to this division of installations, inverters are divided into:

- island,
- grid,
- hybrid.

The island inverters provide battery charging and they are not connected to the power grid. Grid inverters have the ability to transmit power to the grid without charging the batteries. With grid-tied inverters, if the grid voltage disappears, the inverter automatically shuts down. This is crucial for safety reasons, e.g. if maintenance work is being carried out, the power distributor stops supplying the grid and it is undesirable to return the current generated by the PV installations. Hybrid inverters can be switched to both modes of operation.
Inverters used in photovoltaic installations are also classified according to their size, i.e. the power of the photovoltaic installation with which they work [155]:

- microinverters, working with only one module of about 0.35 kW,
- string inverters (series), used in small installations built with a number of photovoltaic modules with a power from 1 to 50 kW,
- central inverters, used in large photovoltaic installations such as PV farms, generating power of around several dozen MW.

Depending on the presence of a transformer in the inverter, which is to galvanically separate the DC side from the AC side, inverters are divided into [199]:

- transformer inverter,
  - low frequency LF, where the transformer is at the output and operates at 50Hz,
  - high-frequency HF, where the transformer is at the input of the device and works with a frequency of 20-24 kHz (at the output to the network, the frequency is 50Hz),
- inverter without transformers.

Another classification of inverters is based on the number of phases to which they can be connected. Among them, inverters are distinguished by:

- single-phase, used for small installations of a few kW,
- three phase inverters, dedicated for installations with more than a few kW [155].

10.3 Inverters selection methods

The choice of inverter for the photovoltaic installation is a very important step in the design of PV systems. A poorly chosen inverter, even with good quality photovoltaic modules, can significantly reduce the efficiency of the entire installation. The key parameter in the selection of the inverter is its power on the DC side. According to the generally accepted principle, the power of the photovoltaic installation should be between 85 and 118 $\%$ of the inverter power. This is because the actual operating conditions of photovoltaic modules are different from the laboratory conditions under which they are tested (STC conditions: 1 000 $\frac{W}{m^2}$, 25^oC, AM1.5). A photovoltaic system rarely operates at its nominal power.
The selection of an inverter for a photovoltaic installation can be done in terms of the number of MPPT (maximum power point controllers). In the case where the photovoltaic installation is built with an inverter with one MPPT, then the MPPT maximum power point will be sought for all modules simultaneously. This is also the case when the modules form several chains and are connected separately to the inverter. Therefore, it is important that each PV module has similar operating conditions and parameters. On the other hand, a photovoltaic installation built with several chains with different numbers of panels or uneven lighting requires an inverter with a higher number of MPPTs. In this case, each chain of PV modules connected to a given MPPT will be received by the inverter as one separate energy generator [200].
Inverter matching is also carried out based on the technology in which the modules used in the photovoltaic system were manufactured. In the case of monocrystalline, polycrystalline, thin-film CIS/CIGS panels, as well as micromorphic modules in which a layer of transparent conductive oxides (TCO) is separated from the glass by a laminate, it is possible to use both transformerless and transformer inverters. Galvanically isolated transformer inverters are used for installations made of panels in which the TCO layer is not isolated from the glass. This applies to CdTe thin-film and amorphous modules, which require the negative pole to be grounded [201]. The lack of grounding can cause current to flow into the module frame, which in turn can cause sodium ions to precipitate from the glass and tarnish it. By using a transformer inverter, galvanic separation is provided between the DC and AC sides of the PV system. If a short circuit occurs on the DC side, the short circuit current does not flow through the inverter, which protects it from damage.

11. Electricity storage

11.1 Energy storage methods

Energy storage is one of the fundamental elements in renewable energy production systems. This is especially important when energy is produced unsystematically, as is the case in photovoltaic systems, where the availability of solar energy varies throughout the year - from season to season, day to night, and day to day (different weather conditions). The energy consumption according to time of day and time of year is illustrated in Fig. 168. To balance the different time patterns of solar loads and production, energy storage must be included in almost all stand-alone power systems.

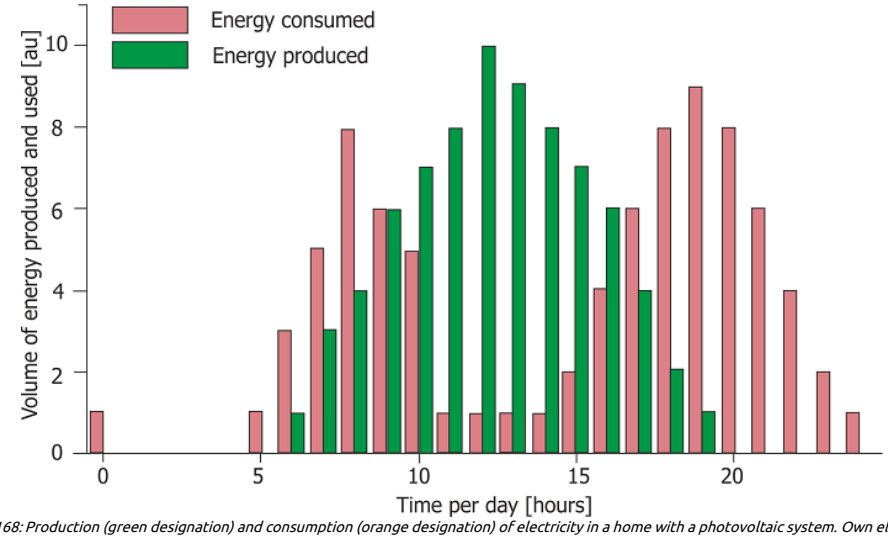

Figure 168: Production (green designation) and consumption (orange designation) of electricity in a home with a photovoltaic system. Own elaboration.

Requirements for electrical energy storage systems [149]:

- high energy efficiency,
- long service life,
- good charging performance even at very low currents,
- low self-discharge rate,
- high power availability,
- easy to estimate the state of charge and the state of wear,
- safe overcharge or deep discharge behavior,
- voltage and capacity easy to increase through series and parallel connection,
- small voltage difference between charging and discharging,
- fast charging capability,
- no capacity loss effect,
- low explosive potential,
- high operational reliability,
- easy to recycle,
- low toxicity of materials,
- low cost.

Energy storage is definated here as any method that allows you to store electricity produced.
Currently, professional energy storage in the world is based on special power plants [202]. According to the RES Act, an energy storage is a separate device or a set of devices for storing energy in any form, not causing emissions that are a burden to the environment, in a way that allows at least partial recovery of energy.

Storage of solar electricity

Storage of electricity in the electricity grid
It is possible to consider the electricity grid as a way to store solar energy. During periods of excessive power production, the excess is fed into the grid from where it can be withdrawn at any time, but only at 80%, the remaining 20% is counted as a "charge" due to the power company for this form of energy storage. The free flow of energy between the grid and the consumer is made possible by a two-way meter. This form of photovoltaic installation is on-grid. Of course, it does not allow you to achieve energy autonomy, but it allows you to use electricity generated in your own home without having a battery bank.

Electricity storage - other ways
Other ways to store electricity are available in electric and magnetic fields, and by converting it into electrochemical energy, mechanical energy, chemical energy, and thermal energy. Some of this stored energy can be used by households and others in industrial applications.

Conversion to Electrochemical Energy
The most intuitive and simple method of energy storage is battery charging. The batteries currently used are lead-acid, nickel-cadmium (NiCd), nickel-metal-hydride (NiMH), and lithium-ion [203]. Batteries store direct current at a voltage, such as 12 volts. In order to use the energy stored in batteries, it is necessary to connect them to electrial devices that convert direct current to alternating current, that is, the use of inverters.
Issues regarding battery energy storage require discussion of several more topics, such as the maximum and minimum voltages for receiving and delivering current to the battery.

Conversion into mechanical energy

Large power plants with gas turbines use compressed air as a way to store energy. During the day, when electricity production is the highest, the air is compressed. When there is demand on the grid, this compressed air is used to produce electricity. Due to low efficiency, such energy storage is not cost effective for small plants.
Electricity can be stored using pumped storage plants, equipped with pump-turbines, which pump water into a higher reservoir during lower electricity demand. And the energy thus stored is recovered by a reversible pump-turbine during periods of increased energy demand. Pumped storage plants are ideal for storing huge amounts of energy over long periods of time, taking power out of the system during times of oversupply and supplying it during times of increased demand. The efficiency of pumped storage ranges from 65 to 85%, which is very good compared to other energy storage technologies.

Conversion to kinetic energy
In the short term, energy can be stored in the form of the kinetic energy of a spinning flywheel (Fig. 169) [202]. These are often used in internal combustion engines (with less than 6 cylinders) to equalize their operation, so the technology is fairly well mastered. But apart from a few applications (e.g. in hybrid cars) on a larger scale they do not appear.

Figure 169: G2 front2 (G2 flywheel). Photo NASA, CC0 license, source: Wikimedia Commons .

Chemical storage of electricity - hydrogen production
One way to produce hydrogen is through electrolysis. The advantage of energy storage in the form of hydrogen is that it can be stored for long periods of time and has a high energy density (three times that of gasoline and more than 100 times that of batteries). This gives it the potential to be used as a vehicle fuel. The use of hydrogen in fuel cells offers the possibility, like flywheels, of responding to rapid changes in energy demand on the grid.
An alternative to storing energy as hydrogen is to store it as methane. It is easier to store for long periods of time, and can be used directly in existing gas-fired power plants. The disadvantage is further energy losses in the methane generation process, which make the total amount of energy recovered less than 38% [204]. Methane generation is attractive for storing excess energy produced by photovoltaic power plants as well as wind [205]. Installations converting excess energy into methane have been built in Denmark and Germany.

Storage of electricity in supercapacitors
A supercapacitor is a type of high-capacity electrolytic capacitor. It works by accumulating charge on a double electrical layer that forms at the boundary between the electrolyte and the electrode. The carbon nanotubes used allow for a large surface area, and this increases the capacitance of the capacitors. The advantage of supercapacitors [206] over batteries is higher energy density. This means that they can give off energy with high power. Moreover, their huge advantage is the small decrease in performance characteristics and long service life (up to 20 years of operation).

Magnetic Field Utilization
The use of a magnetic field as an energy store for direct current requires a superconductor. The magnetic field created by the current in a superconductor persists indefinitely, and thus energy can be stored in it for any length of time. Unfortunately, superconductors require low temperatures, or cooling, which is very expensive. The efficiency of such a system is on the order of 95%, unfortunately storing large amounts of energy is not possible [207].

Storage of electrical energy - thermal processes
Excess energy can be stored by cooling air to $-195^{o}\mathrm{C}$ which causes it to condense. The volume of air decreases a thousand times, and storing it becomes much simpler than storing compressed hydrogen. When needed, the liquefied air can be heated, turning it into a high-pressure gas that can be used to drive a turbine that generates electricity. Using waste heat from a power plant can increase its efficiency to 70% [208], [209].
There are a number of methods to store energy in the form of temperature differences. In most applications, however, this energy is not later converted to electricity, but rather it is used in its stored form (e.g., for heating).
Methods that allow the storage of electrical energy include the heat pump. A heat pump can be used to store energy in the following way: two tanks with a large thermal capacity are connected by a pump. When there is little demand for electricity, heat is pumped into the hot tank. At times of higher demand, the pump is turned off and instead turbines are run to generate electricity through the temperature difference. British company Isentropic is developing this method, predicting that it could become a competitor to pumped storage power plants, with the costs of $35/MWh and energy recovery efficiencies of $72-80\%$ [210].

11.2 Accumulators

90% of the energy produced by the photovoltaic panels during the day that was not consumed by the consumers is stored in batteries 90%. The stored energy may be consumed at night or on days with bad weather conditions. The cost of off-grid energy storage comes to about 30% of the cost of the entire PV system. An electrical schematic of an off-grid photovoltaic system with energy storage, i.e., a set of batteries, is shown in Fig. 170. When charging, electrical energy is converted to chemical energy, and in the process of discharging (energy extraction), chemical energy is converted to electrical energy. The advantages of batteries are:

1. the ability to carry electrical energy storage,
2. the ability to deliver a large amount of energy in a short time,
3. reliability,
4. delivery of energy in the form of direct current.

The energy generated in photovoltaic panels during the day that was not consumed by the receiver is stored in batteries. The stored energy can be used at night or on days with bad weather conditions. Batteries in photovoltaic systems are often charged/discharged, so they must meet more requirements than batteries used in cars, for example. The most commonly used batteries are classic lead-acid (PbA) batteries manufactured specifically for photovoltaic systems, which however, have the disadvantage that they break down when regularly discharged below 50%. Other types of batteries used include nickel-cadmium (NiCd) or nickel-metal-hydride (NiMH) batteries, where deep discharge is required, as well as lithium-ion batteries.
Hermetic batteries often contain a gel electrolyte and thus do not require maintenance. The life of typical batteries connected to photovoltaic systems is three to five years, depending on charge/discharge cycles, temperature, and other parameters. The more often a battery is charged/discharged, the shorter its life.

Depending on the type, batteries can be charged in different ways, such as at a constant current, at a constant voltage, etc. The charging method is determined by the manufacturer.
Batteries developed specifically for photovoltaic systems are designed to have the following properties [149]:

1. cyclic resilience,
2. reliability under cyclic discharge conditions,
3. increased performance at slow discharge rates,
4. low self-discharge,
5. high energy (kWh - kilowatt-hours) and capacity (Ah-amp-hours),
6. ability to operate over a wide temperature range,
7. profitability,
8. long life,
9. low maintenance.

Technical requirements for off-grid, or on-grid, photovoltaic system performance and energy are presented by Rydh and Sandén [150]. To get enough energy in winter for storage, more photovoltaic panels are required than the average energy consumption. They are needed to capture enough energy during the few sunny hours in winter and store it in batteries. To harness the energy from the batteries and from the photovoltaic panels, a suitable electronic circuit is needed, a schematic of which is shown in Fig. 170.

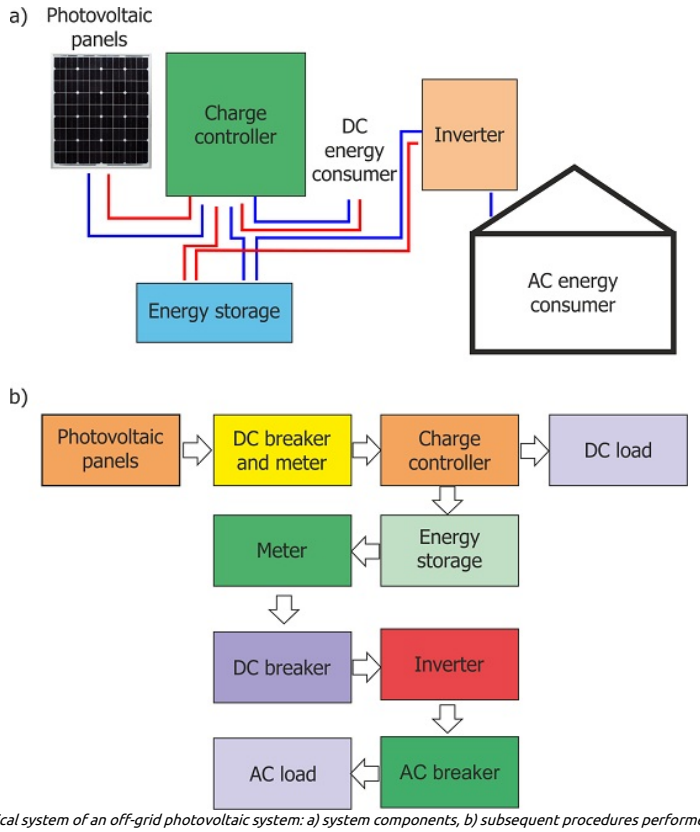

Figure 170: Schematic of the electrical system of an off-grid photovoltaic system: a) system components, b) subsequent procedures performed by the devices. Own elaboration.

A schematic of how the electrical system of an off-grid photovoltaic system works is shown in Fig. 170. The photovoltaic panel converts solar energy into electrical energy, which is directed through a switch and a meter to a charge controller, then to energy storage and subsequently to direct current (DC) consumers. From the energy storage, energy flows through the meter and the switch to the inverter, which converts the direct current (DC) into alternating current (AC). The AC current is then passed on to the consumers (AC).
Energy stores in the form of lead batteries consist of a chamber that contains a liquid electrolyte, H_2SO_4 in which the electrodes, the positive electrode PbO_2 and the negative electrode Pb, are immersed. The following charge and discharge processes occur here - see Fig. 171.

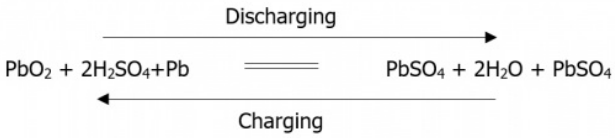

Figure 171: Battery charging and discharging process. Own elaboration.

A fully charged battery is one in which the positive electrode is coated with lead peroxide and the negative electrode is pure lead. At this point, all of the acid is in the electrolyte, meaning the specific gravity of the electrolyte is at its highest. During discharge, some of the acid combines with the electrode plate to form the compound lead sulfate, which is formed on both electrodes. During this process, the specific gravity of the electrolyte can be measured and will decrease, giving an indication of the battery's state of discharge. As the battery is charged, the sulfuric acid is forced out of the battery plates into the electrolyte. At this point, the specific gravity of the electrolyte will increase until the battery is fully charged.
Once the battery is fully charged, the energy delivered to the battery causes electrolysis of water, during which hydrogen and oxygen are released. This is the main reason for adding water to battery cells.

Popular battery manufacturers include Tesla, Mercedes Benz, MA, LG Chem, and Enphase [203]. Tesla batteries have a high efficiency of 90% with a 10-year warranty. Mercedes Benz makes 2.5 kWh batteries that can be combined in an assembly of up to 8 batteries.
Tesla's PowerWall 2 product includes a battery (made by Panasonic) along with an inverter. It features an efficiency of 90% and the possibility of discharging up to 100%. SMA manufactures inverters that can be used in off-grid and on-grid systems as well as integrated with batteries from Mercedes-Benz, LG Chem, Sony and others. LG Chem has developed a series of batteries with efficiencies as high as 95%. The Enphase brand produces small batteries with efficiencies up to 96% and discharge capabilities up to 95%. The table (on Fig. 172) shows a comparison of battery parameters from different manufacturers. The most important of these are capacity and guaranteed life.
The table compares the parameters of batteries from different manufacturers.

Company	Tesla Powerwall 2.0	Fronius solar Battery	LG Chem Resu	Samsung Sdi-ESS	Pylontech US2000	Pylontech Force H2	MET	Varta Pulse 6
Capacity [kWh]	13.5	4.5-12	3.3-13.1	3.6	4.8	7.1-14.21	3.5-7.0	6.5
Technology	Li-ion NMC	$LiFePO_4$	Li-ion NMC	Li-ion NMC	$LiFePO_4$	$LiFePO_4$	Li-ion	Li-ion NMC
Warranty/ Life	10 years – 70% EOL	10 years – 80% EOL	10 years – 60% EOL	10 years – 65% EOL, 6 000 cycles	10 years – 80% EOL, 6 000 cycles	10 years – 90% DOD	5 years, 3 000 cycles	10 years, 4 000 cycles
Weight [kg]	125	91-176	31-98.5	95	24	38	60	65
Dimensions [mm]	1150x 755x 155	955x 570x 611	425x 403x 120	1000x 267x 680	440x 410x 89	450x 300x 300	1500x 650x 280	190x 600x 690
Backup functions UPS	yes	yes	no	yes	yes	yes	yes	no
Expendable	no	yes	yes	yes	yes	yes	yes	yes

Figure 172: Comparison of battery parameters of different manufacturers. Own elaboration.

The capacity of the battery determines how much energy can be stored, obviously the higher the value the better. The next parameter is the technology in which the battery is manufactured. The service life of the battery determines after how long (how many years) the ability to store energy will decrease to what initial value. The next lines give the weight, dimensions, possibility of expansion and use as a UPS.

11.3 Compressed air tanks

One way to store energy is to compress air. At times when energy is cheap or while using renewable sources, we compress air and store it in tanks. The scheme of such a system of compression and production of electric energy with the use of energy accumulated in gas tanks is shown in the film "CAES - Compressed Air Energy Storage - IMAGES Project – animation".

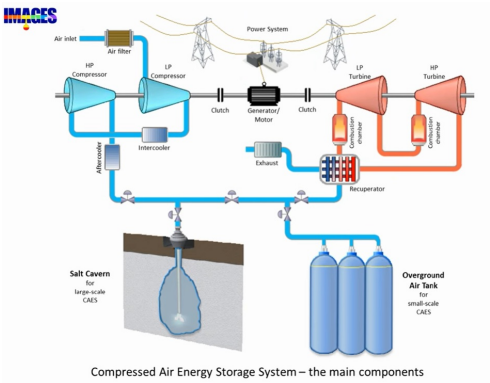

Compressed Air Energy Storage System – the main components

https://pre-epodreczniki.open.agh.edu.pl/openagh-video.php?id=178

Compressed Air Energy Storage

IMAGES Project, CAES - Compressed Air Energy Storage - IMAGES Project – animation, 18.12.2015 (accessed 12.12.2020). Available on YouTube: https://youtu.be/MNVG7x9ZKBc.

The system introduces gas through a filter, low-pressure and high-pressure compressors into large volume natural tanks such as an underground salt chamber or smaller volume artificial tanks. A cooler lowers the gas temperature to reduce thermal stresses

in the system. The processes of filling both the natural tank and the artificial one are shown in the following frames of the video. The energy stored in this way can be used at any time, e.g., during energy peaks when electricity prices are highest or in emergency situations to produce electricity. The compressed gas is released through a recuperator and preheating chambers, which drive high-pressure turbines and then low-pressure turbines. Coaxially with the turbines, a generator is placed to generate electricity, which is transmitted to the grid. A schematic of the electricity production process is shown in the final frames of the film, where compressed air is drawn from an underground salt chamber.

The production is analogous if we draw compressed gas from artificial reservoirs. Just filling the tanks in times of cheap energy and then switching to produce it when energy prices are high makes economic sense. The process becomes even more profitable if the system is fed by a photovoltaic power plant whose peaks in production do not coincide with the peaks in grid consumption. A second even more relevant aspect is energy security. Similar to pumped-storage power plants, compressed-air systems are an important means of securing the continuity of the electricity supply in case of failure of other sources.
An example of a compressed air system is shown in the film "RWE Power: ADELE - Adiabatic compressed-air energy storage (CAES) for electricity supply".

https://pre-epodreczniki.open.agh.edu.pl/openagh-video.php?id=176
Operation of compressed air systems
RWE, RWE Power: ADELE - Adiabatic compressed-air energy storage (CAES) for electricity supply (Operation of compressed air systems), 12.05.2010 (accessed). Available on YouTube: https://youtu.be/K4yJx5yTzO4 .

11.4 Liquid gas tanks

Compressed air energy storage has a strong competitor - liquid air tanks. The main difference - apart from the gas compression system being turned into a liquefaction system - is that in the same tank volume we can store much larger amounts of gas if it is in liquid form. An additional sentiment is connected with this technology, because similarly to the production of monocrystals, where the creator of the method was a Pole, Jan Czochralski, the first scientists who were able to liquefy air were professors of the Jagiellonian University, Karol Olszewski and Zygmunt Wróblewski, in 1883. The process of liquefying and then producing electricity is shown in a video animation (see "Liquid Air Energy Storage Animation 2018"). It depicts the idea of using liquid air production as a storage tank for electricity production. The Liquid Air Energy Storage (LAES) system, conceptually developed in the UK as a modular system for replication to high-capacity manufacturing plants, was launched as a pilot in a plant in Slough.

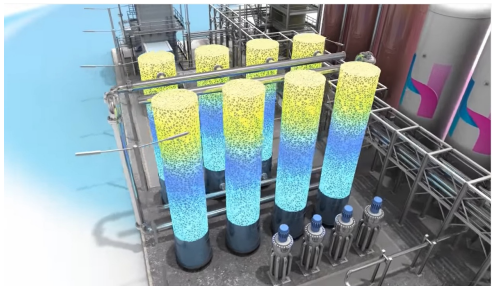

https://pre-epodreczniki.open.agh.edu.pl/openagh-video.php?id=177
Liquid Air Energy Storage Animation
Highview Power, Liquid Air Energy Storage Animation 2018, 17.04.2018 (accessed 12.12.2020). Available on YouTube: https://youtu.be/kDvlh_aG7iA.

12. Computer-aided design of PV installations

12.1 PV simulation programs

The design of a photovoltaic installation is possible through the use of specialized software. Simulation programs allow the optimization of the PV installation, as well as the evaluation of the expected effects and the designer's assumptions. Examples of programs used for PV plant design are:

- PV*SOL,
- Polysun,
- Easy Solar,
- PV Designer,
- PV Manager,
- Blue Sol,
- Fronius Solar Configuration.

These programs are dedicated to designers of photovoltaic installations, as well as architects or installers. The programs can also be used as a teaching or learning aid for university students. The Photovoltaic Laboratory at the Department of Computer Science, Electronics and Telecommunications at AGH University of Science and Technology is equipped with two specialized programs for designing photovoltaic installations. These programs are PV*SOL and Polysun - used by designers all over the world.

12.2 PV*SOL software for system planning

The PV*SOL program is a software from Valentin Software GmbH used to design, dynamically simulate and calculate the energy yield of rooftop and ground-mounted photovoltaic systems. Before starting the design of photovoltaic systems, an interview with the customer should be carried out in order to obtain information about the building and the area to be installed. It is important to determine the orientation of the facility relative to the sun, the type of roof sheathing, and the roof pitch, as well as gain knowledge of the terrain if designing a ground-mounted installation. The design should also take into account the presence of objects near the future installation site that can affect its shading. It is necessary to determine the demand for energy on the basis of electricity bills, the number of household members and the anticipated possible additional consumers in the future. Once all the necessary information has been collected, the design of the photovoltaic installation is made using the software.
The PV*SOL program allows you to enter project data such as bid number and designer, customer contact information, project description, installation address and planned commissioning date. The PV*SOL program working screen for entering the most important design data is shown in Fig. 173.

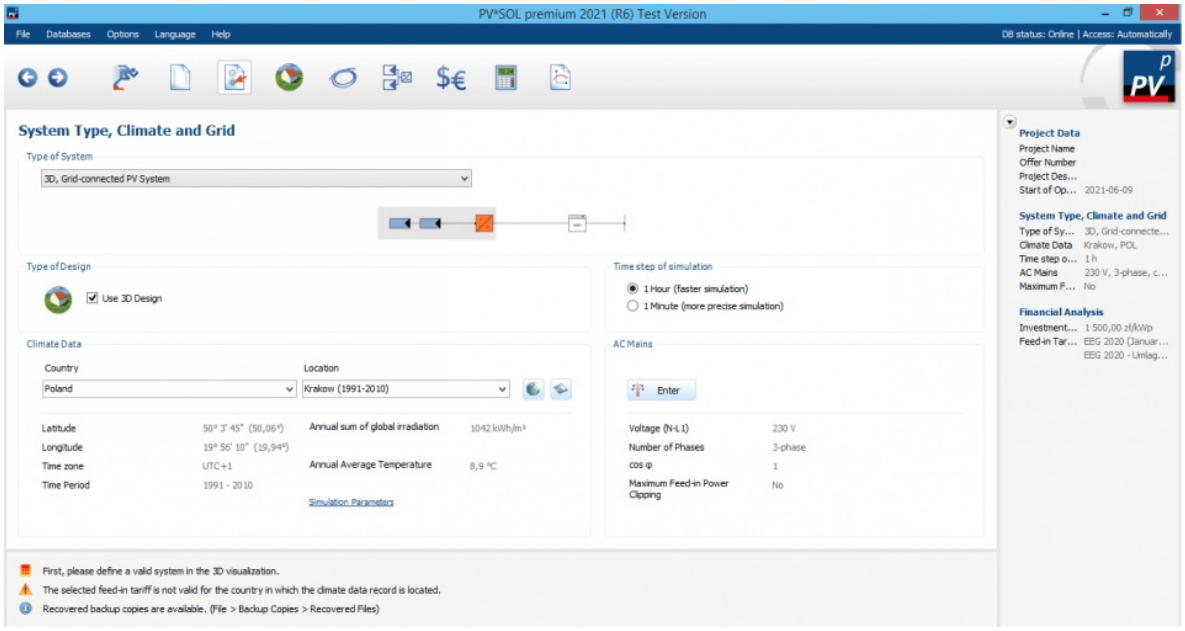

*Figure 173: PV*SOL program work screen – entering design data. Own elaboration on the basis of the PV*SOL premium 2021 software from Valentin Software GmbH .*

12.2.1 3D objects design

The design of a photovoltaic system in the PV*SOL program begins by entering preliminary information on the type of PV system to be designed.
Depending on the version of the PV*SOL program, the list of types of photovoltaic systems to be designed varies and is extended from year to year. The PV*SOL Premium 2021 version allows you to design one of the photovoltaic systems listed below, i.e:

- connected to the grid,
- connected to the grid with electrical equipment,
- connected to the grid with electrical equipment and battery systems,
- connected to the grid with electrical loads and electric vehicles,
- connected to the grid with electrical loads, electric vehicles and battery systems,
- self-sufficient,
- self-sufficient with auxiliary generator.

After selecting the type of installation, the designer visualizes the photovoltaic system and, for a given location, enters its geographical data and, from the database, enters the climatic condition (Fig. 174).

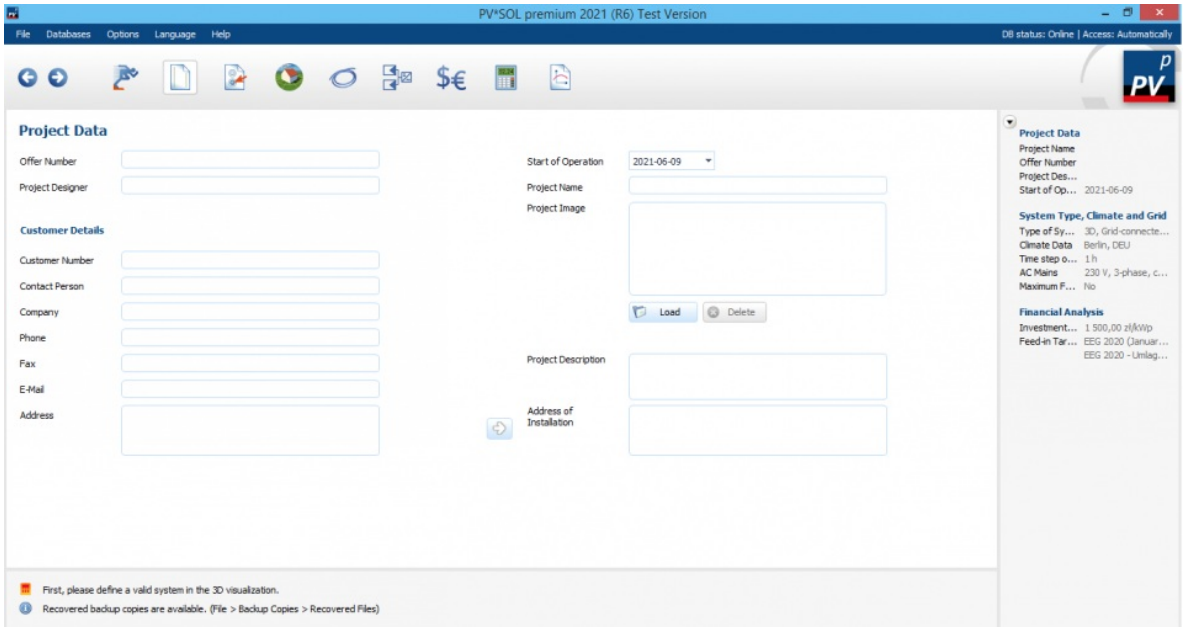

*Figure 174: PV*SOL program work screen – selecting installation type and climate data. Own elaboration on the basis of the PV*SOL premium 2021 software from Valentin Software Gmb .*

Searching for a given location from around the world with its assigned climate data in PV*SOL is easy thanks to the interactive map built into the MeteoSyn database, the main working window of which is shown in Fig. 175.

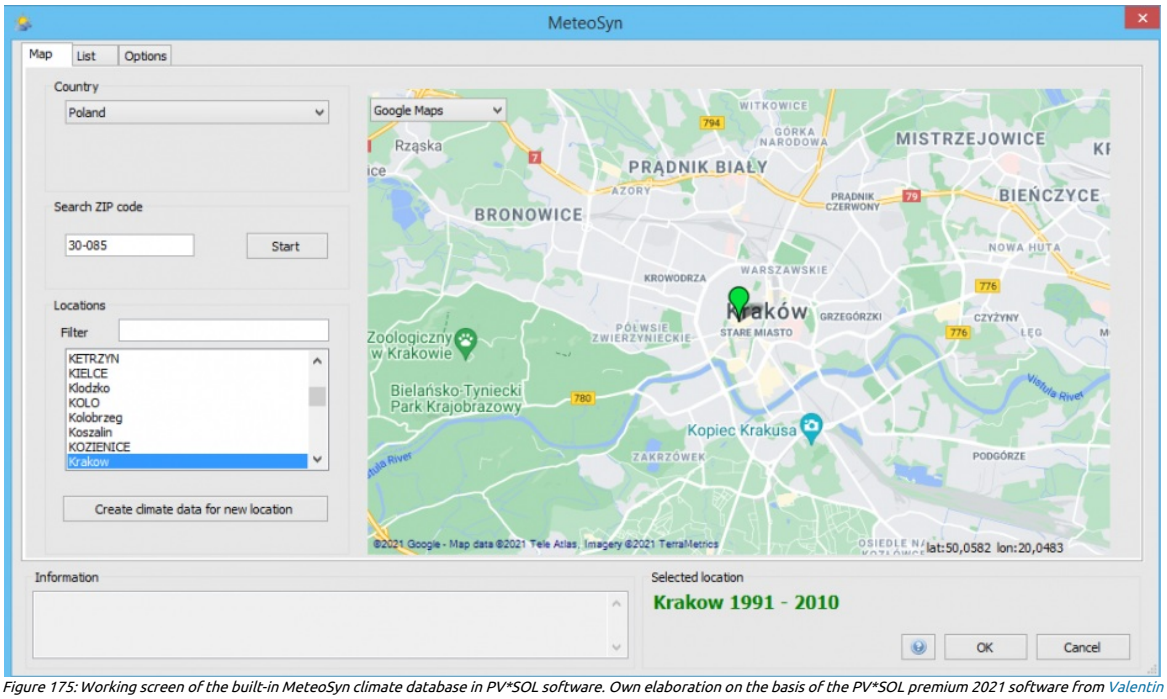

*Figure 175: Working screen of the built-in MeteoSyn climate database in PV*SOL software. Own elaboration on the basis of the PV*SOL premium 2021 software from Valentin Software GmbH.*

Climatic conditions such as annual sum of insolation and annual average temperature are assigned to each location. The program also enables the creation of new climate data either by the interpolation method from existing measurement data or based on one's own monthly data.
The program enables three-dimensional design of objects to be covered with PV modules, thanks to a built-in module for selecting the type of 3D object, whose functions are shown in Fig. 176. The program also allows you to introduce ready-made building elements into the project. Examples of these include windows, doors, roofs (e.g. chimneys, dormers) and objects (e.g. fences, trees) that may be located near the installation.

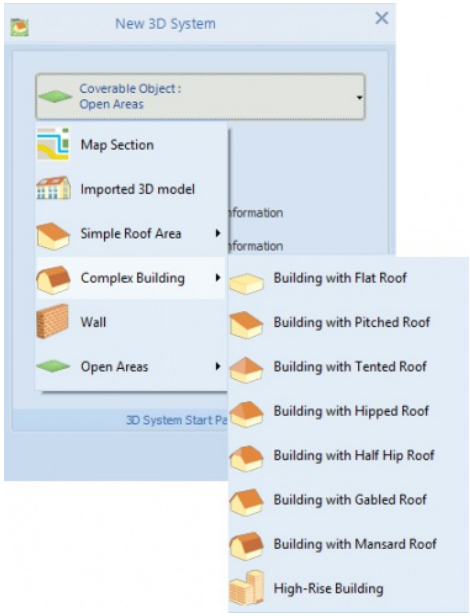

*Figure 176: The working screen of the built-in 3D object type selection module in PV*SOL software. Own elaboration on the basis of the PV*SOL premium 2021 software from Valentin Software GmbH.*

The dimensions and orientation of the chosen object to be clad with photovoltaic modules as well as the other objects in the project can be freely changed using the editing window shown in Fig. 177.

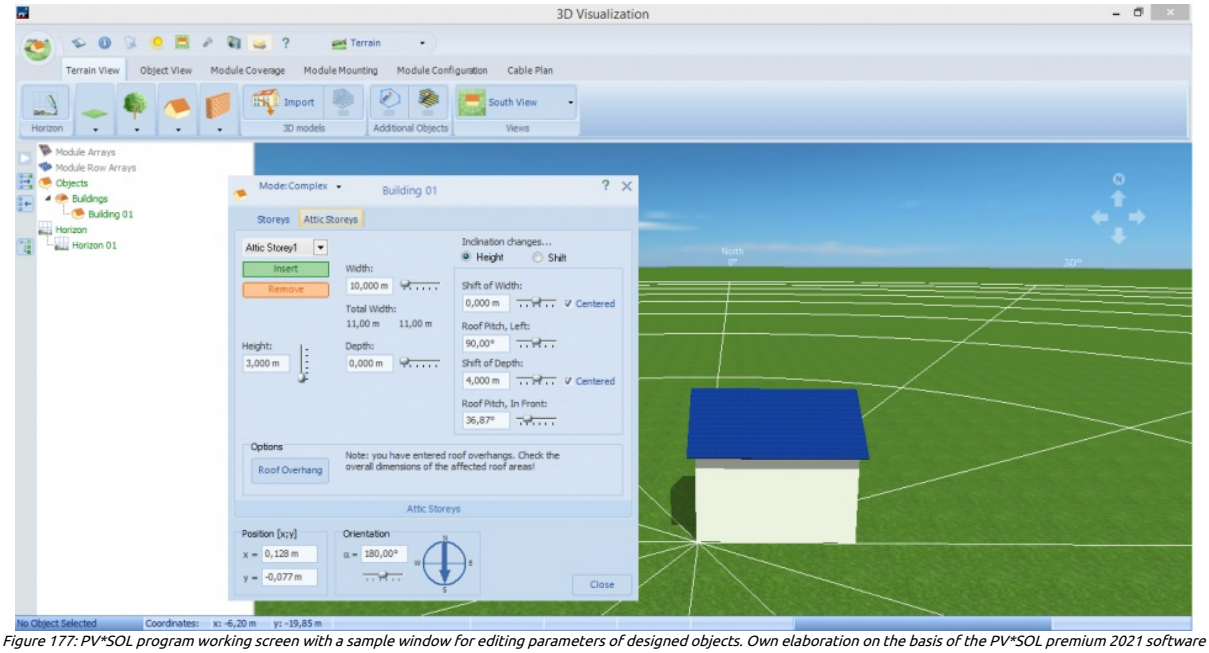

*Figure 177: PV*SOL program working screen with a sample window for editing parameters of designed objects. Own elaboration on the basis of the PV*SOL premium 2021 software from Valentin Software GmbH .*

12.2.2 PV plant design

The distribution of photovoltaic modules in the PV*SOL program is realized with the tab named Module Coverage (Fig. 178). This option allows coverage of the installation area in two ways. The first is to manually fill individual modules, and the second is to automatically fill the entire available area.

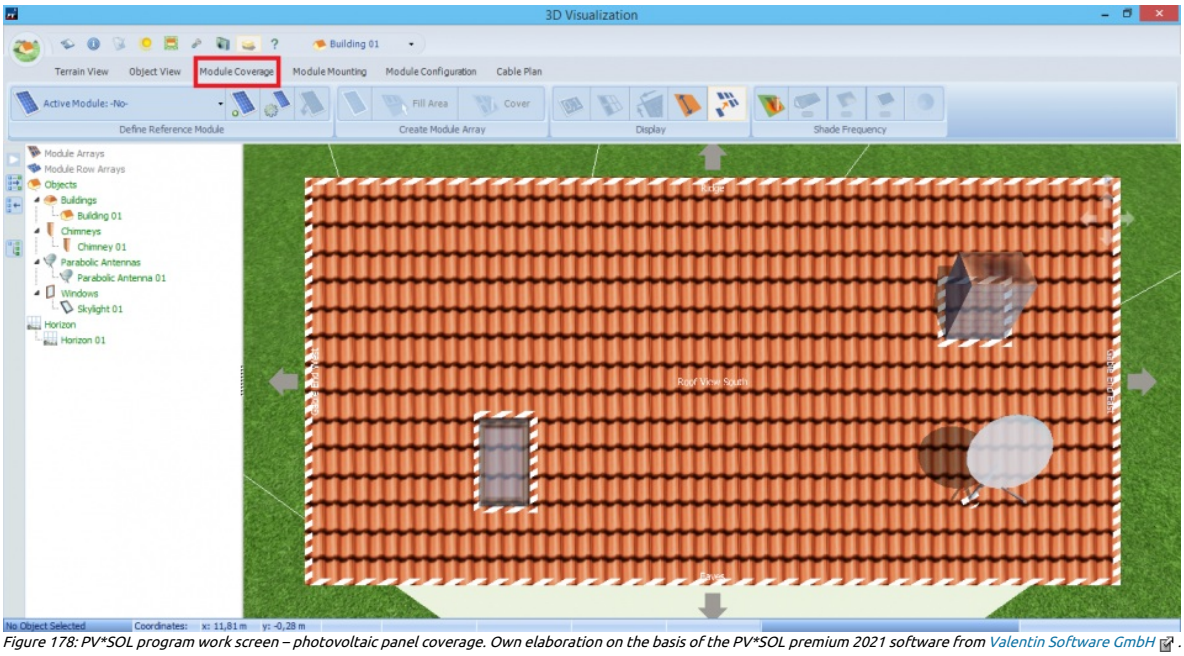

*Figure 178: PV*SOL program work screen – photovoltaic panel coverage. Own elaboration on the basis of the PV*SOL premium 2021 software from Valentin Software GmbH .*

The photovoltaic modules, like inverters, are chosen from a database built into the program, which is constantly updated by the producer. Thanks to it, it is possible to quickly select photovoltaic modules for which the most important parameters are given, such as: rated power, voltage, current and dimensions, as well as the type of PV cell used. An example of the component database is shown in Fig. 179.

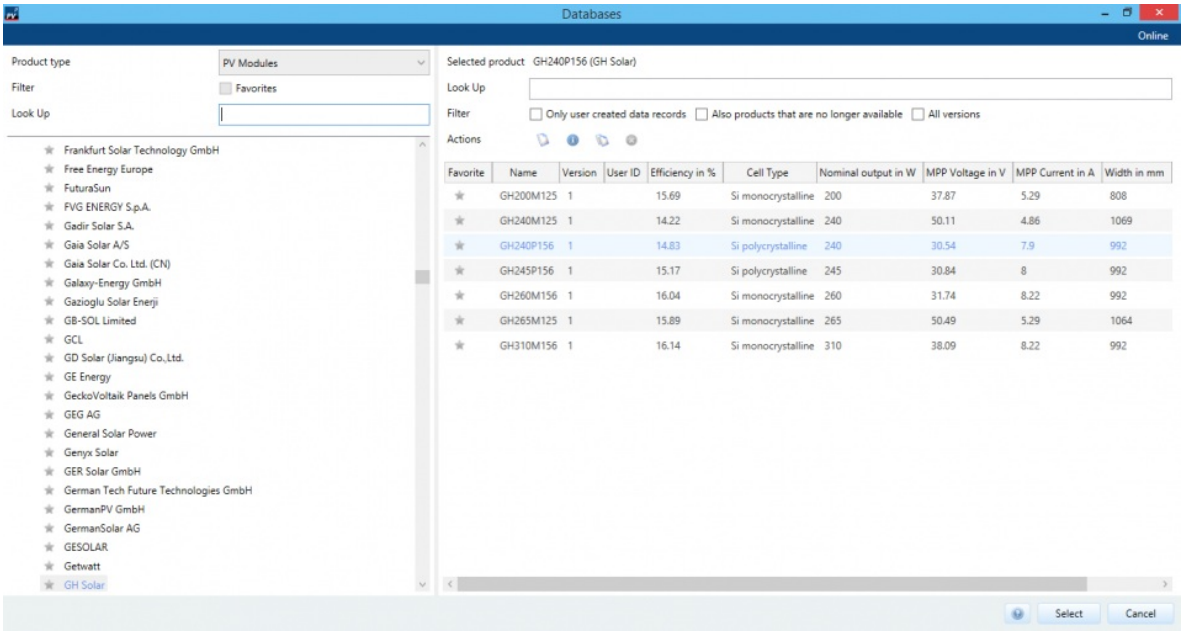

*Figure 179: The database of photovoltaic module producers in the PV*SOL program. Own elaboration on the basis of the PV*SOL premium 2021 software from Valentin Software GmbH .*

An example of the design of a photovoltaic system installed on a south-facing pitched roof is shown in Fig. 180. The program allows you to edit the parameters of the modules such as the distance between the modules and the position relative to the roof. The example installation consists of 19 GH240P156 series photovoltaic panels from GH Solar with a total capacity of 4.56 kWp. In addition, the program allows you to automatically design the cabling for the photovoltaic installation Fig. 181. The program calculates the cross-sections of all the cables used, their lengths, as well as the cable losses of the entire installation.

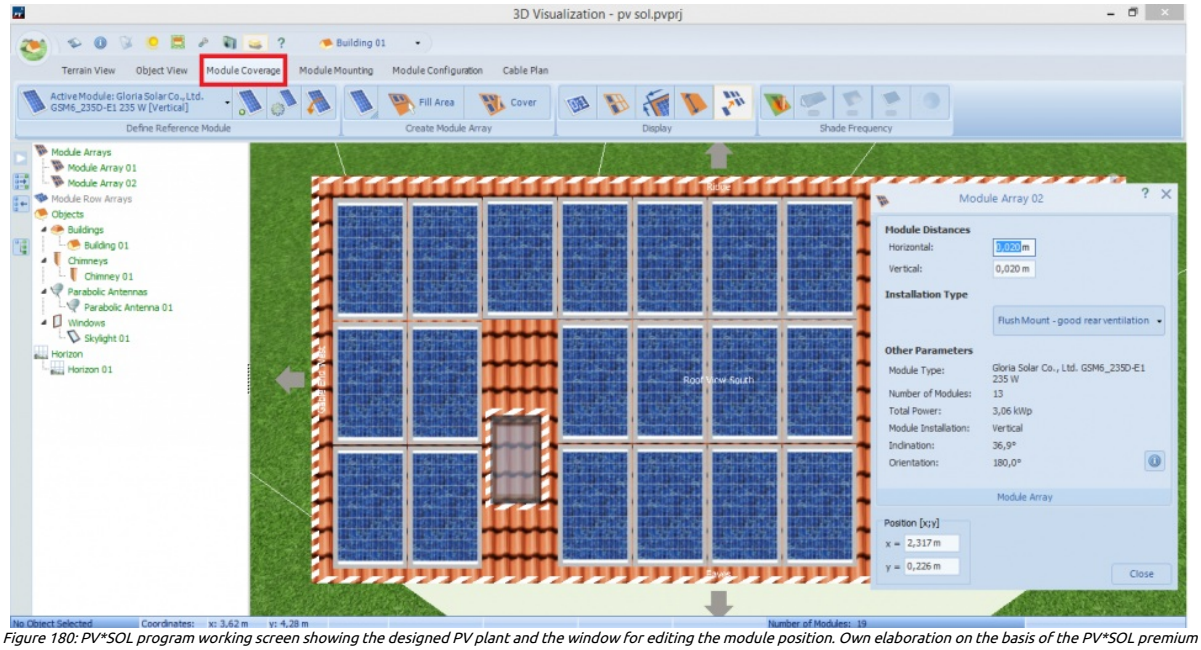

*Figure 180: PV*SOL program working screen showing the designed PV plant and the window for editing the module position. Own elaboration on the basis of the PV*SOL premium 2021 software from Valentin Software GmbH .*

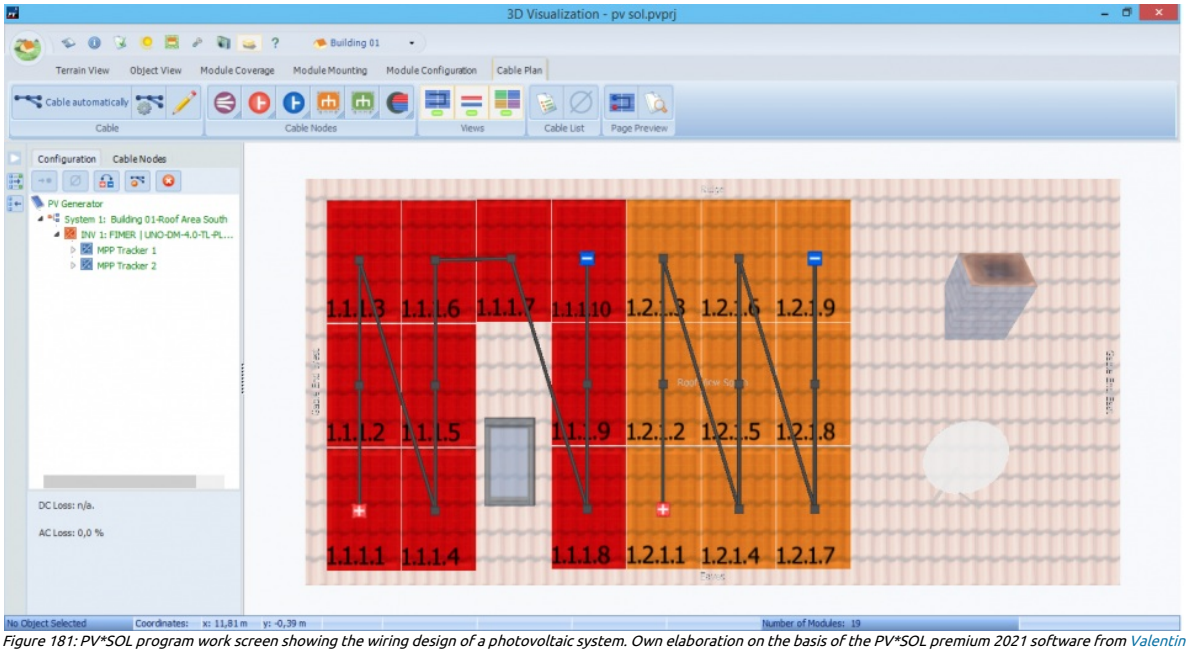

*Figure 181: PV*SOL program work screen showing the wiring design of a photovoltaic system. Own elaboration on the basis of the PV*SOL premium 2021 software from Valentin Software GmbH .*

12.2.3 PV plant efficiency

Thanks to built-in databases on climate data, electrical parameters of photovoltaic modules and inverters, the PV*SOL program allows you to simulate the efficiency of the designed photovoltaic installation. The program enables simulation of module shading throughout the year, whose exemplary result is shown in Fig. 182. The simulation results allow the designer to select the optimal arrangement of photovoltaic modules.

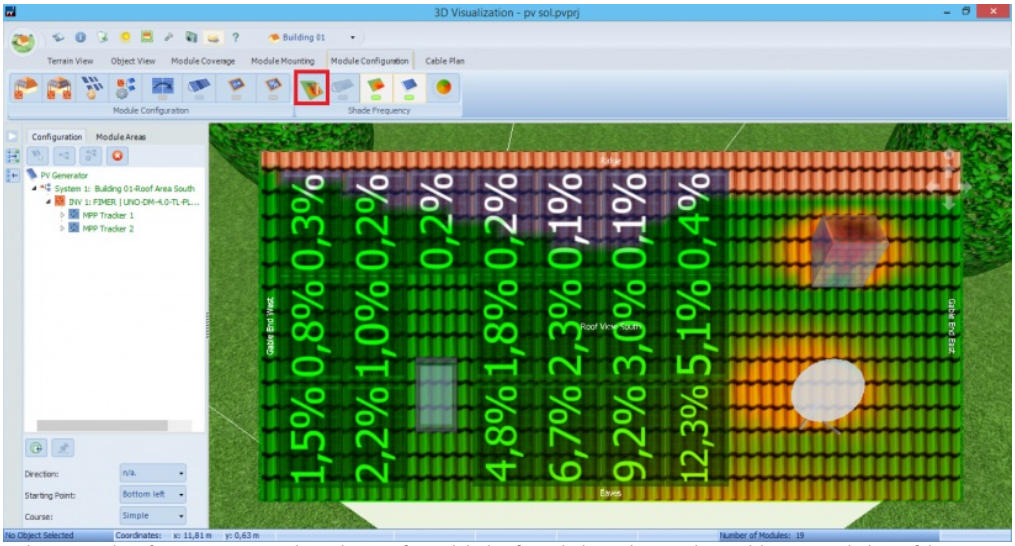

*Figure 182: Working screen shot of PV*SOL program with visualization of annual shading for each photovoltaic panel. Own elaboration on the basis of the PV*SOL premium 2021 software from Valentin Software GmbH .*

Once the design is completed, it is possible to produce a report for the designed installation. The design generated in the PV*SOL program also includes:

- visualization of the photovoltaic installation,
- type of devices selected with their connection diagrams (an example is shown in Fig. 183).
- amount of reduced CO_2 emissions,
- technical data of the modules, inverters, structures and cabling used,
- time and financial analysis of the energy produced,
- data about the average intensity of solar radiation on the surface of the module and its temperature.

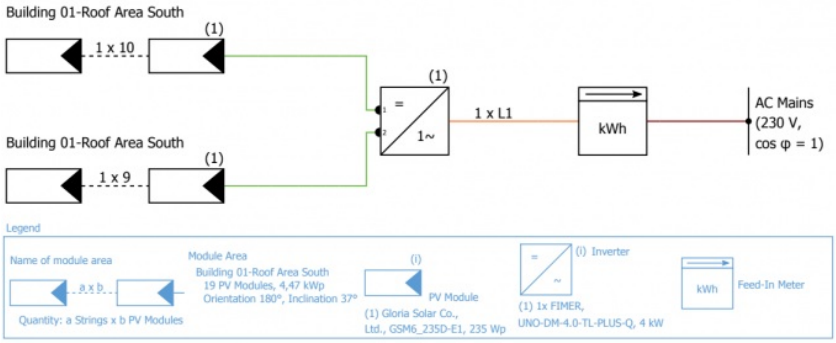

*Figure 183: The scheme of an example photovoltaic installation plotted in PV*SOL software. Own elaboration on the basis of the PV*SOL premium 2021 software from Valentin Software GmbH.*

The program makes it possible to present data in graphs on the generated energy in particular months. An example of the obtained results is presented below Fig. 184.

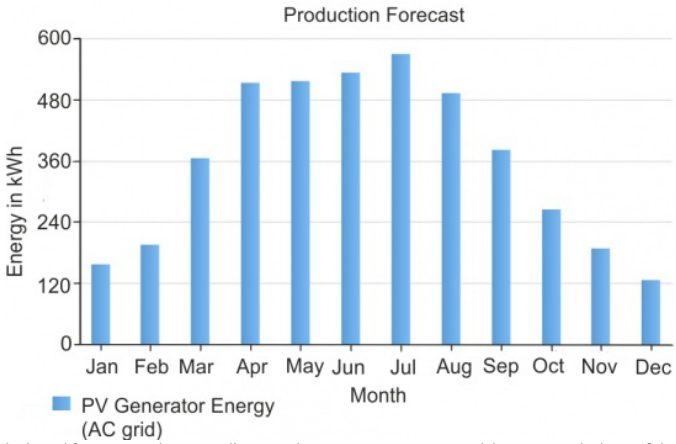

*Figure 184: Energy yield forecast graph plotted for an example PV installation in the PV*SOL program. Own elaboration on the basis of the PV*SOL premium 2021 software from Valentin Software GmbH.*

The report includes the expected payback time of the planned investment and its economic viability analysis, an example of which is shown in Fig. 185.

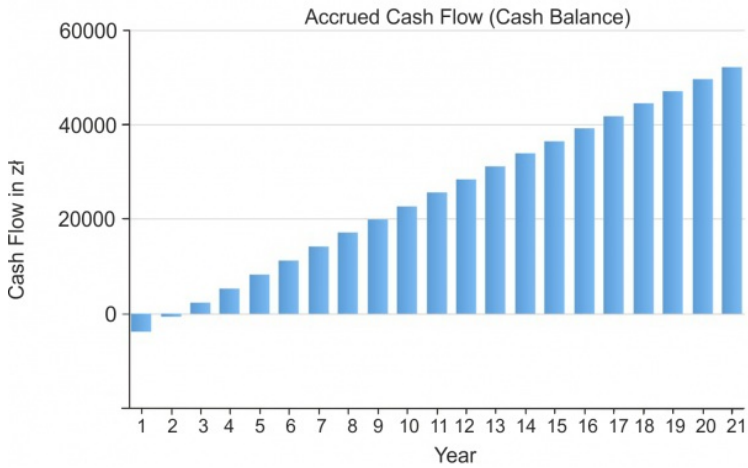

*Figure 185: The graph of cumulative cashflow by year plotted in the PV*SOL program. Own elaboration on the basis of the PV*SOL premium 2021 software from Valentin Software GmbH.*

Thanks to the climatic data entered into the program, it is possible to obtain the dependence of the insolation intensity on the surface of the module in particular months of the year (Fig. 186).

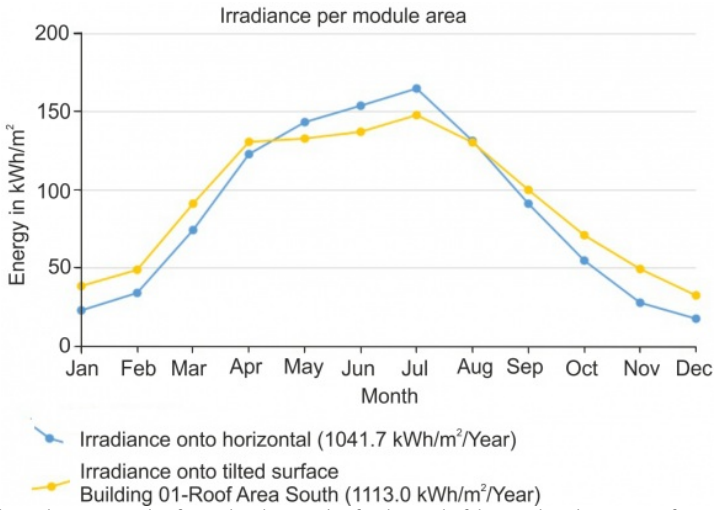

*Figure 186: The graph of average solar irradiance per panel surface and per horizontal surface by month of the year plotted in PV*SOL software. Own elaboration on the basis of the PV*SOL premium 2021 software from Valentin Software GmbH .*

It is also possible, among other things, to determine the average temperature during each month for module surfaces and horizontal surfaces Fig. 187.

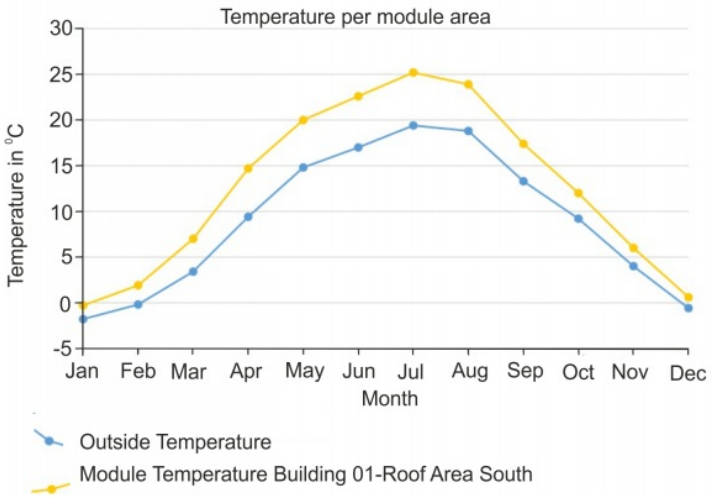

Figure 187: Example system supplying heating, swimming pool and a two-storey detached house. Energy is generated using eight high-quality photovoltaic-thermal panels. Own elaboration on the basis of the Polysun software by Vela Solaris .

12.3 Polysun designing of PV installation

Vera Solaris' Polysun software is used to design, calculate performance and optimise photovoltaic installations. In addition to typical PV systems, it offers the possibility to simulate PVT (photovoltaic-thermal) hybrid collectors and to combine photovoltaic systems with heat pumps, coolers and boilers. The programme has a library with ready-made designs, which can be modified. It is possible to select the right system for the customer. The applied demand can be optimised for customers who are interested in generating energy for heating, domestic hot water (DHW) or swimming pool Fig. 188.

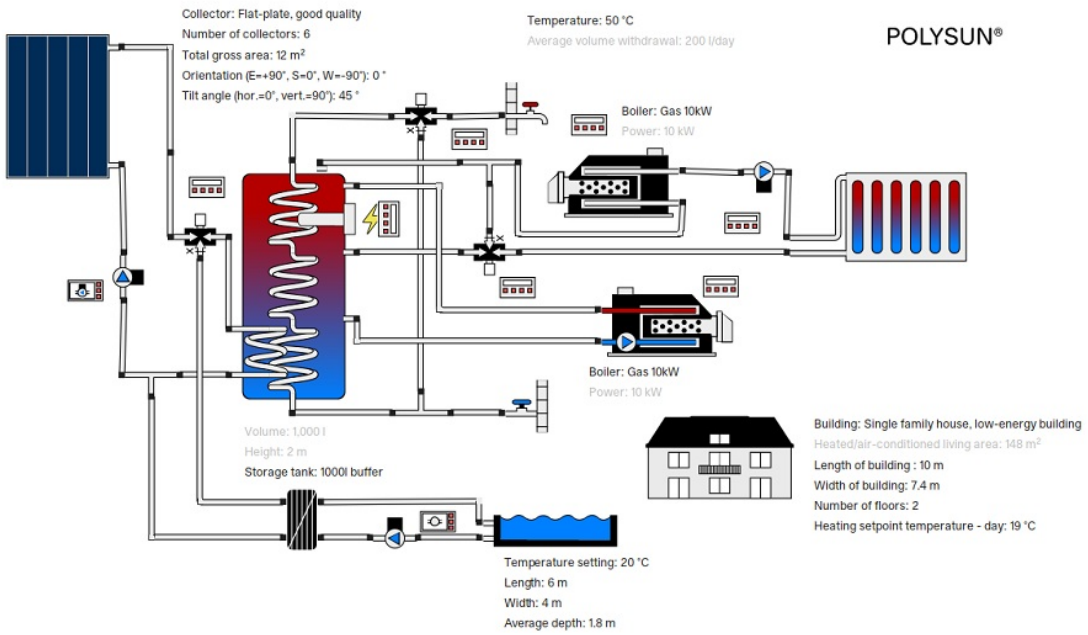

Figure 188: Example system supplying heating, swimming pool and a two-storey detached house. Energy is generated using eight high-quality photovoltaic-thermal panels. Own elaboration on the basis of the Polysun software by Vela Solaris .

13. Connection of a power plant to the grid

13.1 Legal rules concerning the connection of power plants

Due to the variety of aspects that concern photovoltaics, regulations and legal acts come from the fields of construction law, energy law, renewable energy sources law, anti-fire and anti-electric shock protection law (Fig. 189). The chapter will discuss these issues.

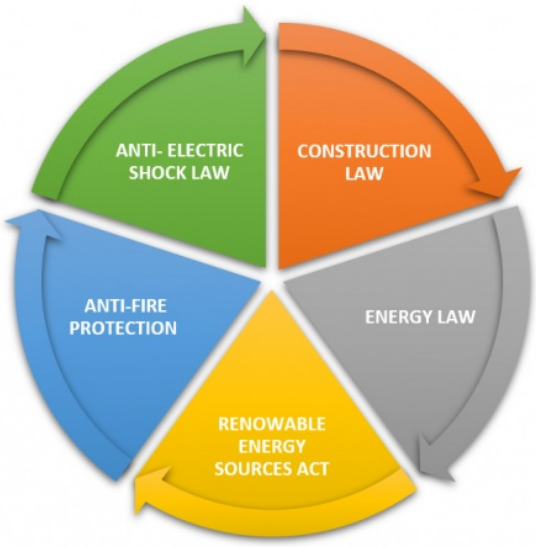

Figure 189: Legal aspects of photovoltaic installations. Own elaboration.

On 19 September 2020, an amendment to the Construction Law came into force. The Act of 13 February 2020 on amending the Act - Construction Law and certain other acts [211].

According to art. 29. sec. 4 item. 3, a decision on a building permit is not required, nor is a notification of the execution of construction works involving the installation of heat pumps, free-standing solar collectors, photovoltaic devices with an installed electrical power of no more than 50 kW. A permit is required if additional circumstances occur, e.g. the installation is performed on an object entered in the register of historic monuments, belongs to a Natura 2000 area, or requires an environmental impact assessment [212], [213]. If, in connection with a photovoltaic installation, an extension to the building on which the installation is to be made is planned, a building permit is also required. This obligation rests with the investor and must be fulfilled before the

construction work starts. Every investment (not only the photovoltaic one) must be in line with the zoning plan or the decision on outline planning and spatial development.

However, the legislation provides that in the case of installations with an installed electrical capacity exceeding 6,5 kW, there is an obligation to agree on the design of the photovoltaic installation with a fire protection expert with respect to its compliance with fire protection requirements and, at the same time, the obligation to notify the authorities of the State Fire Service (Article 56, paragraph 1 of the Act). It is not specified what scope of the project should be agreed with the expert. Nevertheless, the Photovoltaic Industry Association has prepared and outlined suggested good fire practices for installations in buildings, making connections with quick connectors, thermal imaging studies, protecting cables and wires from damage, appropriate tools, marking PV installations, servicing inspections and additional safeguards in terms of fire protection [214]. Fire protection is regulated by the Fire Protection Act of 24 August 1991 as amended [215].

The grid connection itself is regulated by Commission Regulation (EU) 2016/631 of 14 April 2016, laying down a network code on requirements for the connection of generating units to the grid [216], [217].

13.2 Connection of a power plant to the grid

The **connection to the grid** is regulated by legislation [216], [217], of which the most relevant is the Commission Regulation (EU) 2016/631 of 14 April 2016. Notification of connection of an installation to the grid can be made by several types of entities: individuals, sole traders, companies (most often micro, small and medium-sized companies) and other legal entities. The conditions for connection derive from Commission Regulation (EU) 2016/631 of 14 April 2016 establishing the Code NC RfG (Network Code Requirements for Generators). It is an Act whose application in the legal orders of the EU Member Nations is direct (i.e. it does not require direct acts).
The Code has defined types of generating units due to the different voltage level at which the generating units are connected and the maximum generating capacity.
These are summarised in a table on Fig. 190.

Type	Details
Type A	A connection point with a voltage lower than 110 kV and a maximum power of 0.8 kW or more
Type B	A connection point with a voltage lower than 110 kV and a maximum power at or above the 1 MW threshold
Type C	Connection point with a voltage lower than 110 kV and a maximum power at or above the 50 MW threshold
Type D	A connection point with a voltage of 110 kV or more; an energy generation module is also classified as type D if the connection point has a voltage below 110 kV and a maximum capacity of 75 MW or more

Figure 190: Generator types according to the voltage level at which they are connected and their maximum generating capacity. Own elaboration.

If the facility equipped with photovoltaics is already connected to the grid of the distributor, and the capacity of the installation does not exceed the connection capacity, the connection can be made on the basis of an application. If, however, the building is not connected, or the photovoltaic power is greater than the connection capacity, the connection shall be made on the basis of an application. In that case, it is necessary to apply for an increase in the connection capacity or to adapt the energy connection to the planned increase in the connection capacity. The subsequent connection stages are presented in Fig. 191.

Figure 191: Stages of connection of a generating unit to the power grid. Own elaboration.

The **connection procedure** is free of charge. The most common and simplest are the so-called micro-installation connections. A micro-installation is defined as an installation where the peak power does not exceed 50 kWp, at the same time the installed power cannot exceed the connection power (defined in the service agreement). The Act on Renewable Energy Sources (RES) contains a number of simplifications for the so-called **prosumers** [218]. Prosumer is a combination of the words 'producer' and 'consumer'. A prosumer is a consumer involved in the production of the goods consumed, in this case energy.

A renewable energy prosumer is a final consumer, who produces electricity exclusively from renewable energy sources for their own use in a micro-installation, provided that, in the case of a final consumer who is not a household consumer of electricity, this

does not constitute the object of a predominant economic activity defined in accordance with the provisions issued pursuant to Article 40(2) of the Act of 29 June 1995 on public statistics (Dz. U. z 2019 r. poz. 649 i 730).

In such a case, the connection shall be made on the basis of the application submitted. The application contains the applicant's data, data of the building connected to the grid where the micro-installation was built, data of the micro-installation to be connected (number of modules, power, inverter data) and additional information. Detailed lists of documents and applications are presented by specific distribution network owners.
The act defines the response time to the application, e.g. the application of the applicant not equipped with a source, who wants to be connected to the grid above 1 kV, will be examined within 60 days. The application of an applicant equipped with a source should be processed within 120 days. After verification and approval of the installation application, the network owner installs the bidirectional meter. The relevant contract governing the cooperation (sales or distribution contract) is then signed. In the case of prosumers, i.e. people who also produce electricity for their own use, a comprehensive contract is signed.
In the case of changes concerning the system (change of capacity, suspension of production lasting from 30 days to 24 months, termination of electricity generation), the consumer is obliged to inform the energy company.

Sample applications:
TAURON – Mikroinstalation
Energa – Installation notification

13.3 Lightning protection systems

Grounding is an important part of the safety and performance of photovoltaic systems. Grounding means connecting to earth at a point with zero reference potential. Two methods are used for equipment grounding and system grounding. Equipment grounding means the bonding together of metal frames, enclosures, or conductive materials that normally do not transmit electricity and connecting them to earth. This keeps these materials at a potential of 0 volts to earth.
System grounding is the connection of one of the current-carrying conductors in the system (DC or AC) to ground at a single point, which means that the conductor will be referenced to ground and thus will remain at a potential of 0 V to ground. Since potentials on exposed surfaces must be prevented, therefore equipment grounding is required on all systems, while system grounding is not necessary [219]. All power grids in houses or apartments are grounded, which means that both the equipment and the system are grounded. System grounding is the connections made for DC to the negative wire and for AC to the neutral wire, these wires become the ground wires.
A ground fault is an unintentional, electrically conductive connection between the current conductor of an electrical circuit and normally non-current conductors, such as metal enclosures, metal raceways, metal equipment, or grounding (Fig. 192).

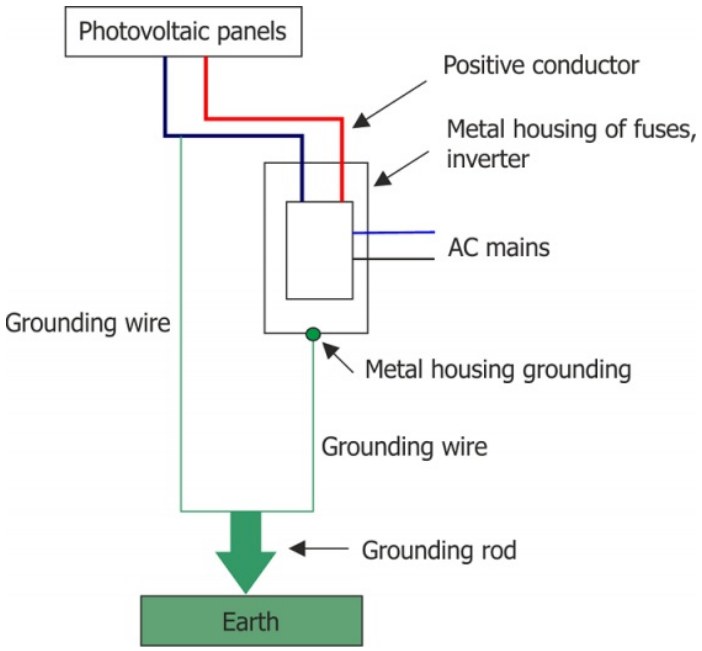

Figure 192: Proper equipment grounding provides a low resistance path to ground for any current spikes that may occur. Own elaboration.

A properly grounded PV panel is shown in Fig. 193. The metal enclosure is connected to the ground rod via the equipment grounding conductor. This grounding connection provides a zero potential to earth, making it safe for a person to touch the box and the electronics used in the PV system.

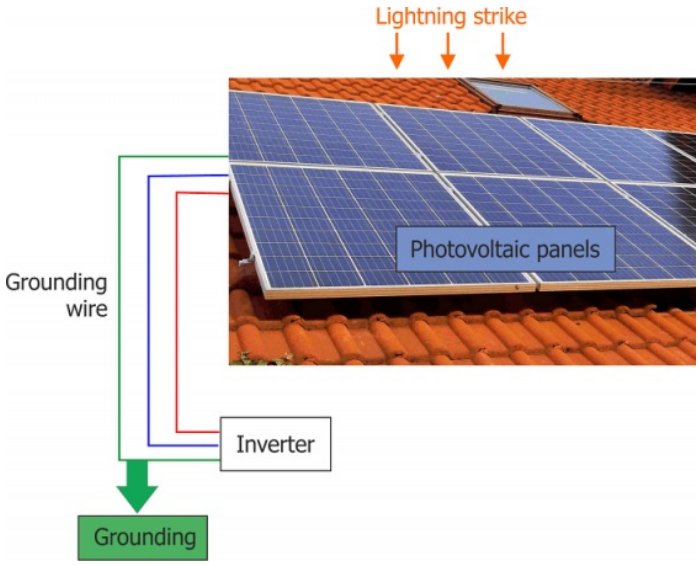

Figure 193: Grounding photovoltaic panels directly to ground. Own elaboration.

The Fig. 193 shows lightning protection with an additional grounding conductor directly connecting the photovoltaic panel to the ground rod. This connection provides a direct, low-ohm path. The electronics have their own connection to ground. With this grounding, the risk of lightning effects is greatly reduced. All electrical systems are subject to transient surges. Voltage spikes can be caused by direct lightning strikes, nearby lightning that induces current and voltage on system conductors, or power line surges that are often caused by large industrial motors or other large inductive loads that are turned off and on. While lightning is always a problem, the most common probability of a surge comes from the utility grid, so entire houses and their appliances need surge protection. Long wire runs between the board and the inverter also increase this risk. Typical surge protection locations are at the entrance to the AC grid and the system monitoring equipment that is part of the photovoltaic system. The best surge protection is a well-grounded system.
Equipment grounding is absolutely necessary in all photovoltaic systems [220]. A grounding conductor is used to connect all supporting components and exposed metal parts that may come in contact with current-carrying conductors, such as PV panel frames, system mounting components, metal bases of equipment such as inverters, disconnects, and meters, metal junction boxes, metal brackets that support conductors, and any exposed metal part that may come in contact with conductors. Under normal conditions, current does not flow in the grounding conductor. The only time it conducts current is during a fault, when current flows through a low resistance path to ground. The grounding element is a galvanized steel tape (called cooper) buried in the ground or a rod driven into the ground (Fig. 194). There may also be other methods that give direct contact between the grounding conductor and the ground in a hole, trench, or foundation.

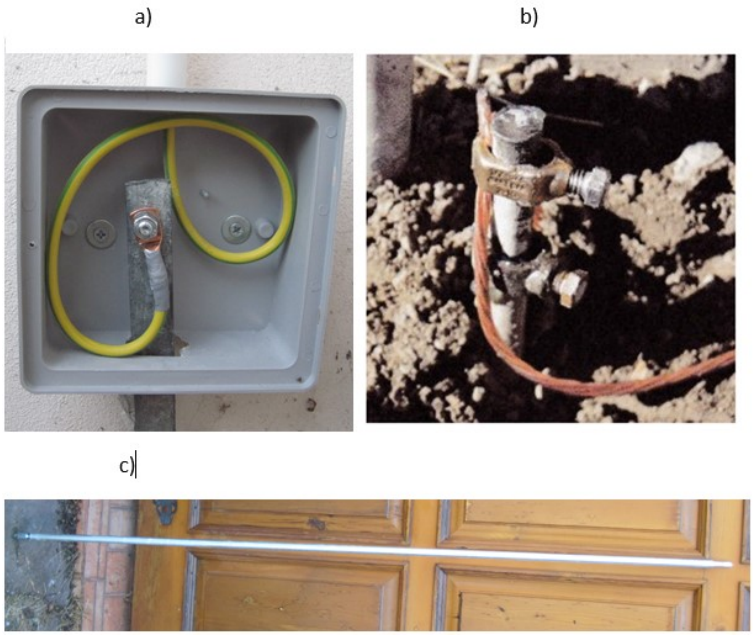

Figure 194: Two grounding methods a) connecting the grounding of the photovoltaic system to the so-called cooper (galvanized steel tape around the building) and b) a rod (galvanized steel pin) driven into the ground used as a grounding electrode, in addition c) a grounding rod ending in a spike. Own elaboration.

A ground wire is usually a bare copper wire used to connect to a grounding element. The differences between the materials that make up the connector must be considered here. The wrong ones will cause corrosion, followed by increased resistance and loss of connection to earth.

An example grounding scheme for a complete photovoltaic system mounted on the roof or façade of a building is shown on Fig. 195. Structural components and boxes with electronic and switching equipment are grounded. The negative wire of the photovoltaic panels (DC) is grounded to earth before the inverter. This protects the inverter from malfunction. This creates a system ground on the DC side. The AC side equipment ground wire runs from the inverter to the main service system, connecting all wires and grounding them.
An ungrounded PV system must meet all equipment grounding requirements, that is, all boxes and structural components must be grounded. No negative or positive conductor is grounded on the DC side, that is, there is no grounding on the DC side. None of the current-carrying conductors on the DC side are connected to ground. The lack of system grounding does not affect the functionality of the system, but it does provide an opportunity to more easily detect faults, either between the current-carrying conductors or the ground. In this case, special inverters for use in ungrounded systems must be used. PV panel circuits must be protected, and insulated multi-conductor cables should be installed in special raceways. The cables for PV panels must have insulation that is more durable than other single-wire cables. Both must be protected by overcurrent protective devices and must be disconnectable.

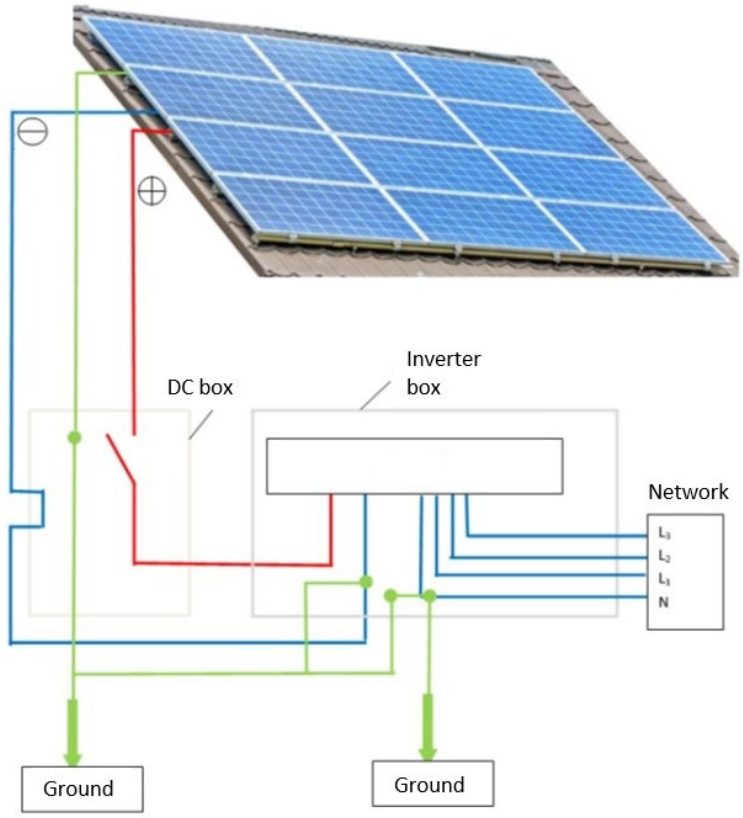

Figure 195: Schematic shows grounding conductors in a roof mounted system negatively grounded. Own elaboration.

Grounding on the AC side is accomplished by connecting the AC neutral wire to ground at one point. The AC grounding is made in the main service box, which is connected to the boxes and components. The neutral wire, which becomes the grounded conductor, is connected to the wire that connects the rails and metal housing bodies.

14. Assembly of a photovoltaic system

14.1 Assembly requirements

The installation of a photovoltaic system is preceded by the preparation of project documentation. The design of the installation should include the following information:

- investor data,
- installation capacity,
- amount of energy produced per month,
- number and method of combining the PV modules,
- way of arranging the PV modules,
- technical data of used equipment and instrumentation of the installation.

Depending on the location of the PV installation, we select appropriate mounting systems. The individual steps of the installation are similar regardless of its type. In each case, it is important to remember that all panel frames must be grounded.

Grounding is done by connecting all modules through grounding bridges, which should then be grounded to the grounding rod. The resistance of the grounding rod should be less than 10 Ω.

When installing a photovoltaic system on a flat or sloping roof, it is important to keep a certain margin from the edge of the roof. In the edge areas of the roof, the photovoltaic system is exposed to the wind; therefore, a margin in which the modules should not be installed is calculated based on the dimensions of the buildings.
For the longer roof edge this margin is:

$$a = \frac{x}{10} = \frac{y}{5} \tag{27}$$

where:
a – the width of the area from the edge of the roof excluded from the installation of photovoltaic modules,
x – width of the building measured along the building wall parallel to the edge a,
y – height of the building measured from the ground to the highest point of the roof.

In designing the distribution of modules, the spacing between panels on the clamps and the separation distances between rows, which are at least 2 cm, should be taken into account for all types of installations.
The following subsections will present the stages of making photovoltaic installations depending on where they are located.

14.2 Ground mount and flat roof installation assembly

The installation of a photovoltaic system on a flat roof is not limited by the slant imposed by the house design. The angle of inclination of the modules should be $15 - 20^o$ in order to maximize the surface coverage and prevent wind effects. The system of mounting PV modules on a flat roof requires the use of a frame made mostly of aluminium profiles that allow adjusting the angle of inclination of the photovoltaic modules. Three types of flat roof mounts are possible:

- unballasted installation system,
- ballasted installation system,
- self-supporting installation system.

Systems of up to 10 kW can be installed on the roof, while larger systems should be installed on the ground. The steps for installing on the ground are similar to those for a flat roof without ballast. The exception is how to attach the support structure to the ground.

14.2.1 Ground mount and flat roof installation assembly without ballast

The use of a ballast-free mounting system makes it possible to build a support structure for PV modules without any additional load. In the case of roofs, this system requires the fixing points to be sealed. The connection of the substructure to the roof is carried out with screws, bolts or pins. A PV installation on a ballasted substructure is shown in the following Fig. 196.

Figure 196: PV installation installed on a flat roof using SolTech Service's ballast-free mounting system. Photo used with permission of SolTech Service .

Mounting a photovoltaic system without ballast can be divided into several stages.

- The first stage of installation consists of planning the placement of the angular substructure at the right angle with

appropriate distances between its rows to avoid shading. Fixing the substructure to the roof is done with screws, for example. In the case of a sheet metal roof, identify the locations of the rafters where the screws must be screwed in. An example of how to fix a substructure to a concrete roof with screws is shown in Fig. 197.

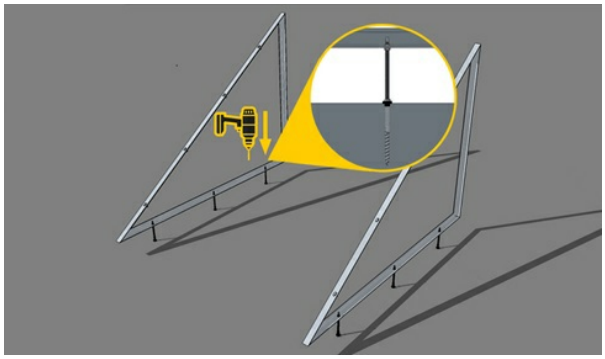

Figure 197: Aluminium support structure without ballast bolted on a flat roof – installation systems by KENO Sp. z o.o. Photo used with permission of KENO Sp. z o.o. .

When the structure is installed on the ground, care must be taken to ensure that there is a suitable foundation, which should form the basis for the entire length of the support structure. It is also permissible to use three-point support by using, for example, prefabricated concrete blocks filled with concrete to a depth of about 70 cm. An example of such a solution is presented on Fig. 198. In this case, the structure is attached to the foundation with concrete screws. There are also used structures screwed into the ground without the need for a concrete foundation.

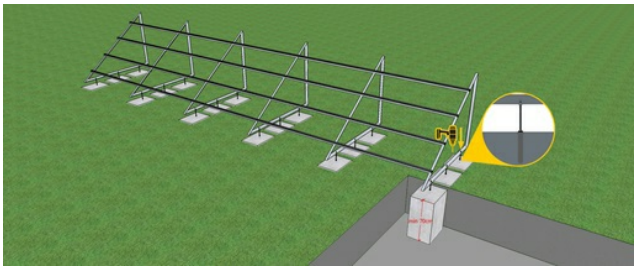

Figure 198: Assembly of a support structure to concrete precast elements for a photovoltaic system installed on the ground – KENO Sp. z o.o. assembly systems. Photo used with permission of KENO Sp. z o.o. .

- In the second step of the assembly, aluminium profiles are attached to the angular substructure, to which the photovoltaic modules are screwed using clamps. The positioning of the clamps is carried out by inserting the appropriate number of sliding grooves into the profiles at intervals equal to the width or length of the panels in the case of vertical or horizontal arrangement of the modules respectively. The installation of the profiles into the angular substructure and the positioning of the clamps is shown in Fig. 199.

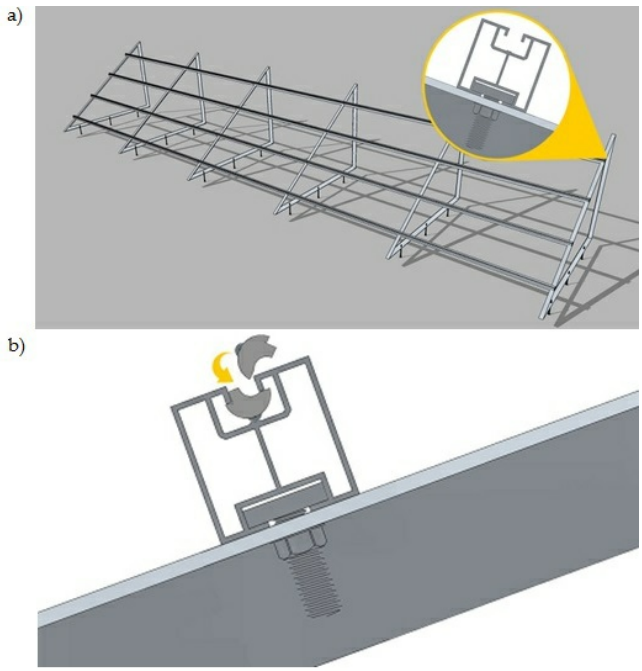

Figure 199: Arrangement of a) aluminium profiles on the supporting structure together with b) location of the sliding sockets – KENO Sp. z o.o. assembly systems. Photo used with permission of KENO Sp. z o.o. .

- In the third step, the photovoltaic modules are screwed on using clamps. An example photovoltaic installation with a horizontal arrangement of PV modules is shown in Fig. 200.

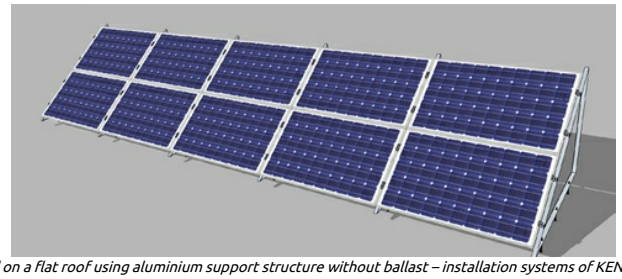

Figure 200: Photovoltaic panels mounted on a flat roof using aluminium support structure without ballast – installation systems of KENO Sp. z o.o. Photo used with permission of KENO Sp. z o.o. .

14.2.2 Ground mount and flat roof installation assembly with ballast

The ballast structures, in which the load is applied, are a solution for the installation of photovoltaic systems on roofs, such as membrane roofs, for which the preservation of warranty and tightness is an important aspect. In this case, the support structure for the photovoltaic panels is not screwed permanently to the roof. For this reason, the structure requires additional loading with concrete blocks, as shown in Fig. 201 and Fig. 202.

Figure 201: PV installation installed on a flat roof using SolTech Service's ballasted mounting system. Photo used by permission of SolTech Service .

Figure 202: Scheme of installation structure for flat roofs with ballast – installation systems of KENO Sp. z o.o. Photo used by permission of KENO Sp. z o.o. .

When a ballasted structure is used, the steps for mounting the PV modules to the support structure are similar to those for an unballasted installation. The weight of the load per PV module depends on the wind zone, the angle of inclination of the panel, as well as the height of the building. For one panel with standard dimensions (about 100 cm x 164 cm), this load is about 60 kg. For this reason, an important limitation for the use of this type of fixing system is the roof load capacity.

14.2.3 Self-supporting PV systems

The self-supporting mounting systems are used for photovoltaic systems with small areas. Self-supporting systems use ballast weight to prevent the structure from being lifted by e.g. wind force. This type of construction is shown in Fig. 203.

Figure 203: Photovoltaic installation on a flat roof in SolTech Service's self-supporting mounting system (east-west orientation). Photo used with permission from SolTech Service .

The advantage of this type of system is that its design means that it is not permanently attached to the roof and does not require a large load to be placed around the perimeter. Consequently, it is easy to move. The angle of inclination with respect to the roof level is small in this case and is up to 15^o.

14.3 Assembly of a PV on a pitched roof

Photovoltaic systems are most often installed on pitched roofs. Depending on the roofing, the appropriate type of fasteners is chosen for the installation. The most commonly used connecting elements include: adjustable mounting brackets (trapezoidal metal sheet), hooks (ceramic tile), double-threaded screws (metal tile), L-type mounting brackets (roofing felt), and mounting brackets without regulation (plain tile), which are presented on Fig. 204.

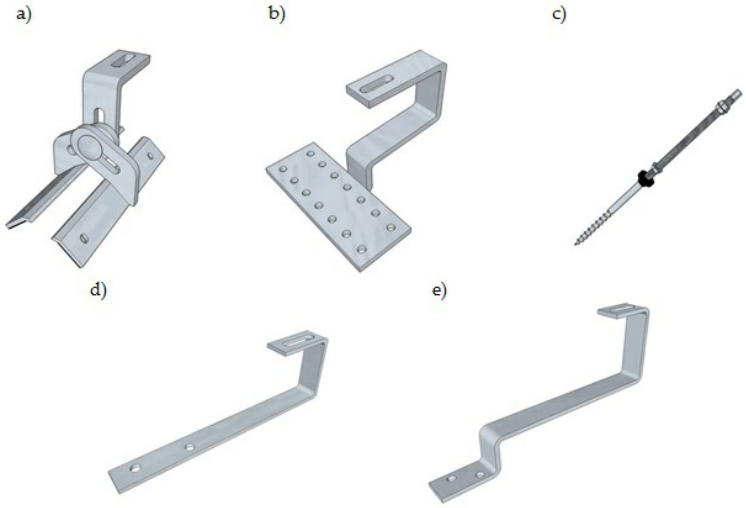

Figure 204: Examples of elements for connecting the roof with the support structure for the PV system: a) adjustable mounting brackets (trapezoidal metal sheet), b) hook (ceramic tile), c) double-threaded bolt (tile sheet), d) L-type mounting bracket (roofing felt), and e) non-adjustable mounting bracket (plain tile) – KENO Sp. z o.o. mounting elements. Photo used by permission of KENO Sp. z o.o. .

Installation of photovoltaic modules on a pitched roof is presented in the subsection using the example of a roof covered with ceramic tiles. The installation consists of the following steps.

- In the first step, the tile is lifted and slid under the higher row to expose the rafters, as shown in Fig. 205.

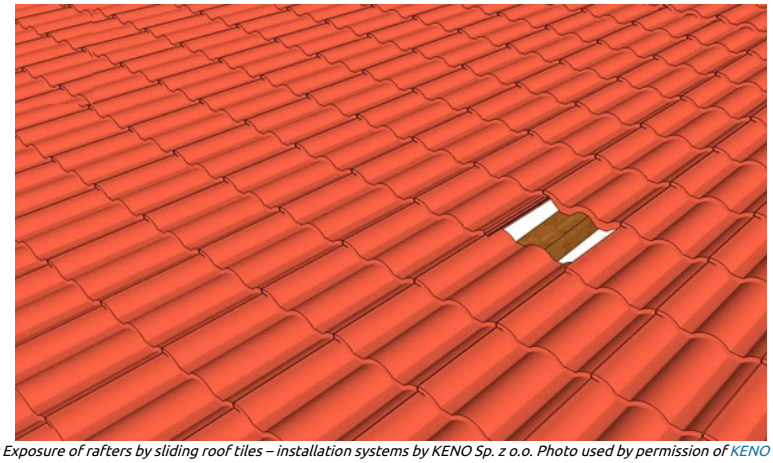

Figure 205: Exposure of rafters by sliding roof tiles – installation systems by KENO Sp. z o.o. Photo used by permission of KENO Sp. z o.o. .

- The second step is to screw the mounting hook to the rafters. The spacing of the brackets depends on the dimensions of the modules. In the case of corrugated roof tiles, the mounting hooks should be hung on the roof tile, so that the support part lies in its hollow. In the case of installation of photovoltaic modules on the roof where the rafter spacing is larger than the width of the module, the roof truss has to be extended by means of reinforcement between two rafters, to which the mounting hooks can be screwed. The reinforcement is made of battens screwed to two fixing angles, which are in turn screwed to the rafters. The method of screwing the mounting hook to the rafters is shown in Fig. 206.

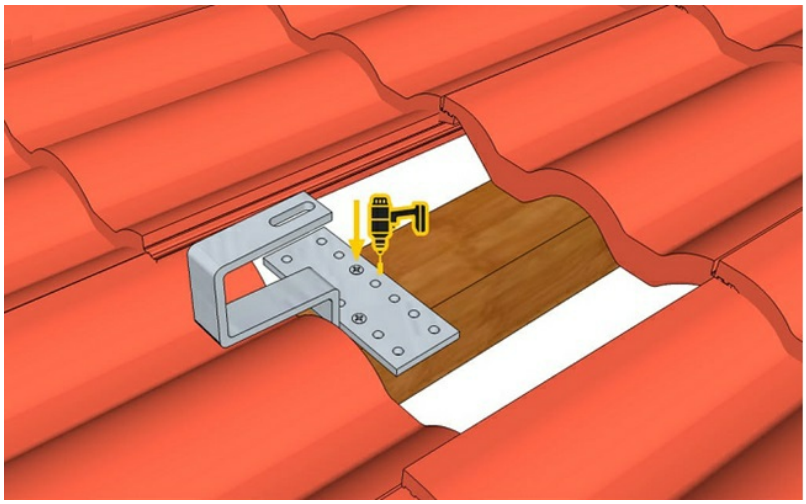

Figure 206: Screwing the mounting hook to the rafter – KENO Sp. z o.o. mounting systems. Photo used by permission of KENO Sp. z o.o. .

- The third step is to cut the tiles in such a way that the protruding hook does not catch on the tiles and to fix the tiles in their original place (Fig. 207).

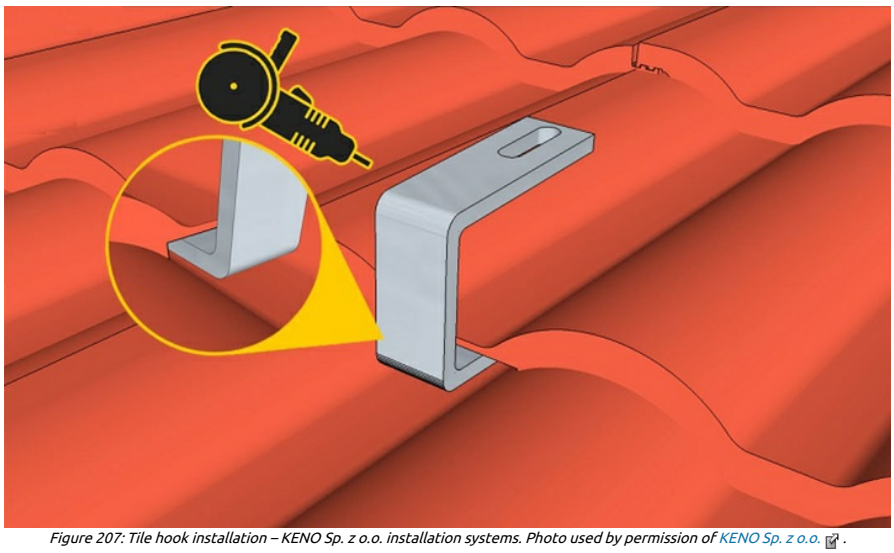

Figure 207: Tile hook installation – KENO Sp. z o.o. installation systems. Photo used by permission of KENO Sp. z o.o. .

- In the fourth step, the rail profiles are screwed to the hooks. The profiles should be placed between $\frac{1}{8}$ and $\frac{1}{4}$ of the module height in order to evenly distribute the forces acting on the module when they are loaded, e.g. during rain, snow and wind.

- In the fifth step, the positioning of the clamps on the profiles is performed and they are screwed to the sliding grooves with Allen screws, as shown in Fig. 208. Place the appropriate number of sliding grooves in the profile at intervals equal to the width of the photovoltaic panels or their length depending on the orientation of the module installation.

Figure 208: Mounted ties for profile grooves – installation systems of KENO Sp. z o.o. Photo used with permission of KENO Sp. z o.o. .

- The final step is to mount the photovoltaic modules to the profiles using clamps (Fig. 209). During installation it is important to keep a space between the modules and the roof sheathing to allow air circulation.

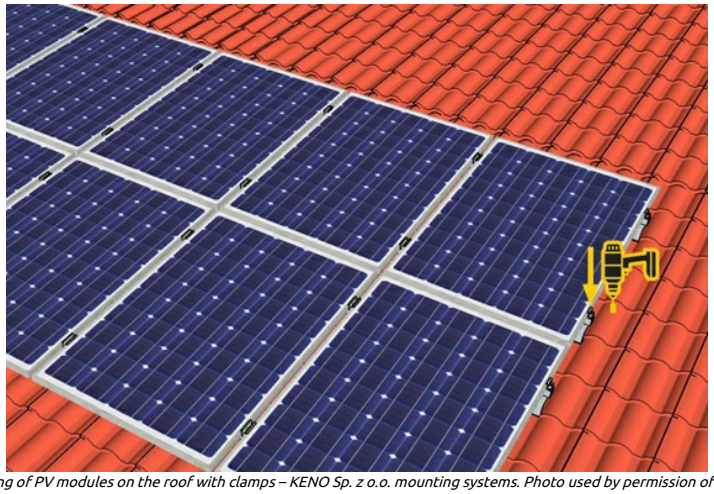

Figure 209: Mounting of PV modules on the roof with clamps – KENO Sp. z o.o. mounting systems. Photo used by permission of KENO Sp. z o.o. .

14.4 Assembly of PV tracking system

Photovoltaic tracking systems are mounted on mobile structures called trackers. The installation of photovoltaic modules in a tracking system can be divided into the following steps:

1. **Making the foundation for the tracker column and installing it**. The foundation seating depth depends on the specific site conditions. The foundation embedment depth must also be greater than the ground frost depth, which depends mainly on the climatic zone. Dimensions of the foundation are determined by the designers and Polish standards and are calculated in the case of photovoltaic panels for the third climate zone and made of concrete class 25. It is also possible to mount a photovoltaic installation on a supporting pole. This type of structure is offered by the company Solar Tracker Polska, of which the PV installation is presented in Fig. 210.

Figure 210: Tracker support structure located on a concrete support pole by Solar Tracker Polska. Photo used with permission of Solar Tracker Polska .

One construction solution is to install a so-called basket in the foundation, which is shown in Fig. 211 and Fig. 212, to which the tracker column is screwed. The column is made, for example, of ST3 S steel pipe 230 mm in diameter with a wall thickness of 6 mm and a height of 2 000 mm.

Figure 211: Construction basket for mounting the tracker support pole by Solar Tracker Polska. Photo used by permission of Solar Tracker Polska .

Figure 212: Foundation with placed basket for mounting the tracker support pole by Solar Tracker Polska. Photo used with permission of Solar Tracker Polska .

2. **Installation of the support construction** for photovoltaic modules is shown in Fig. 213.

Figure 213: Installed tracker support structure for photovoltaic modules by Solar Tracker Polska. Photo used by permission of Solar Tracker Polska .

3. **Installation of PV modules to the support construction** using sliding clamps and electrical installation (Fig. 214).

Figure 214: Installation of photovoltaic modules – Solar Tracker Polska company. Photo used by permission of Solar Tracker Polska .

15. Panels and PV installation tests

15.1 Photovoltaic installation control

Photovoltaic systems are very popular, which in turn leads to an increase in their production. This situation very often results in a decrease in the quality of the components and the quality of the PV installation service. For this reason, testing of the photovoltaic installation after its completion is important. Testing of photovoltaic installation should begin with a visual inspection to verify the correct selection and installation of components, as well as its compliance with the project documentation. This stage of testing photovoltaic installation is very important, because thanks to it you can prevent the operation of a defective installation, as well as protect the person performing the inspection from danger.
After the visual inspection of the installation, the corresponding measurements of the photovoltaic installation are carried out. The conduct of tests of the installation after its execution is defined by the PN-EN 62446-1:2016 standard [221]. The measurements of installations are carried out with specialized instruments that must meet the requirements of PN-EN 61557 standard [222] and PN-EN 61010 [223].

15.2 Testing a new installation

Each newly installed photovoltaic array shall pass **post-construction inspection**. It is intended to check that the panel chains are connected correctly and that the panels themselves are not damaged, and to eliminate potential manufacturing errors [224].
The installation documentation should include its schematic diagram, dates of commissioning and inspection, technical data of the panels and inverters, power rating (the maximum power at which the equipment can operate for a long time without suffering damage with minimum distortion), and details of the installing company. The diagram should give the number of panels and their types, as well as:

- the number of strings together with the number of panels that make up the string,
- inverters with assignments to the strings,
- type and cross section of wires,
- connection locations,
- protection information,
- DC switch (parameters, location, protection elements),
- grounding system,
- charging regulator (if any),
- energy storage tank,
- MPT tracker (if not integrated in the inverter).

In addition, data sheets of the equipment should be attached to the documentation. An important part of the documentation are the instructions on how to behave in case of a breakdown or a random event (e.g. fire).
The first step is to perform a visual inspection of the installation (procedures included in the provisions of the PN-EN 62446-1 standard), while the basis for the visual inspection of the installation are the guidelines of the PN-HD 60364-6 standard.
Based on the documentation of the photovoltaic installation, it should be checked whether the assumed operating parameters of the panels are actually achieved. The test should be conducted in accordance with the PN-EN 62446 standard.

The tests (according to PN-HD 60364-6) are divided into two categories. They are presented in Fig. 215 [225].

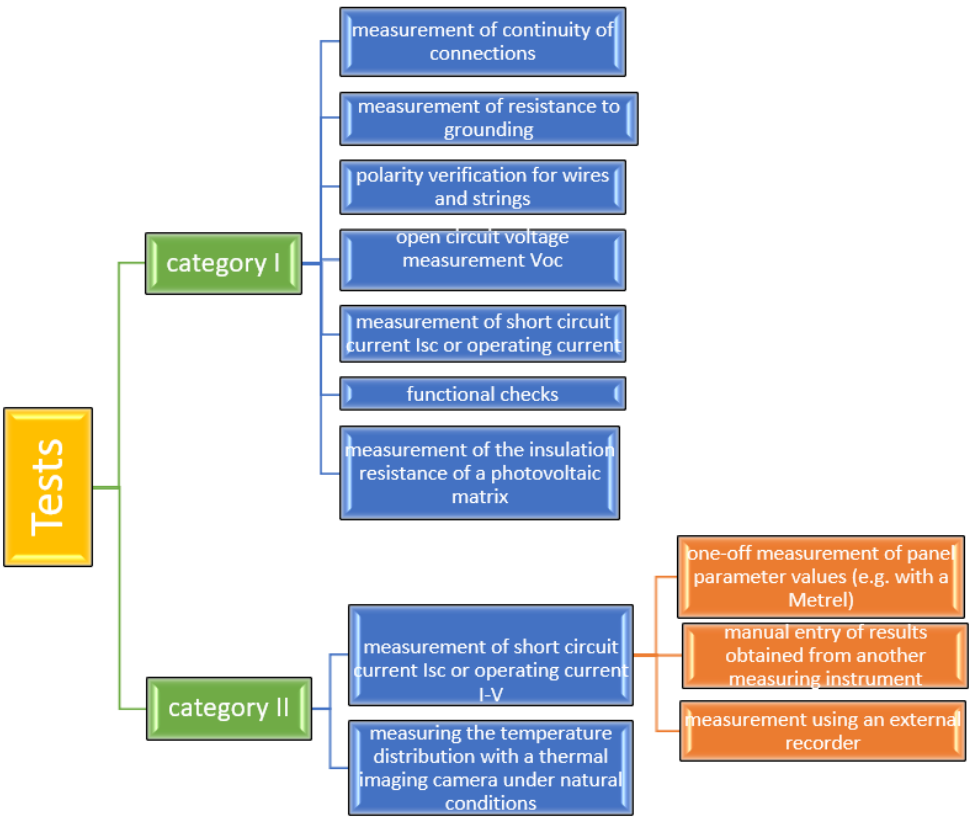

Figure 215: Test classification. Own elaboration.

Category I includes tests which should be performed for all installations. The AC side of the installation should be tested first (in accordance with PN-HD 60364-6), followed by the DC side. If category I tests are passed, category II tests may be performed. The basic test methods in this category are testing the temperature distribution of individual panels using a thermal imaging camera and analysis of current-voltage characteristics.
If category I or II tests reveal any irregularities, additional tests are performed, e.g. voltage-to-ground test, barrier diode test, wet insulation resistance measurement and shading assessment.
Upon completion of the tests, a report shall be prepared and submitted to the investor, containing the results of all tests carried out, the characteristics and the date of the next inspection. This report is the basis for warranty and compensation claims [226].

15.3 Selection and verification of modules for testing

Photovoltaic modules to be tested shall be properly labeled. The rear surface of the photovoltaic module shall have a nameplate as shown in Fig. 216. Each nameplate should contain information about:

- module producer,
- module type and series number,
- module dimensions,
- production date,
- voltage value at MPP and V_{oc} given in volts,
- maximum system voltage that the module insulation is rated for,
- current rating of the fuse,
- maximum power in watts,
- power tolerance in percent,
- the measurement conditions for which the electrical parameters of the module are specified,
- information about certificates and standards that the module meets.

Figure 216: Nameplate of a photovoltaic module made with CIGS technology from DCH Energy GmbH.

The technical documentation shall include information on the power rating of the installation, information on the manufacturer, model and number of modules and inverters, dates of installation and commissioning, as well as information on the installer and the address of the installed system. The documentation should also include information about the company that designed the installation and its diagram. An important part of the documentation is to specify safety systems and how to behave during a failure of the photovoltaic installation. Requirements for labeling, preparation of technical documentation, as well as how to select modules for testing are specified in UL 4730 Ed. 1 (2017) "Labeling, Technical Data, and Sampling Requirements for Photovoltaic Modules", while not addressing systems with light concentrators, CPV. The standard specifies requirements for the manufacturer regarding:

- method of determining the number of modules to determine their rated power,
- information to be included in the technical documentation and on the nameplate,
- information to be placed on the technical documentation and on the nameplate, regarding the tolerances of the nominal parameters placed on the nameplate,
- conditions for which the electrical parameters of the modules are determined.

The standard EN 50380:2017 "Requirements for marking and documentation of photovoltaic panels" specifies what information should be included in the technical documentation of the panel. The standard obliges to label the panel permanently, specify the rated parameters and indicate how to use it safely and correctly. On the other hand, the standard EN 50461:2015 "Solar cells - Product information sheet and parameter specification for crystalline solar silicon cells" determines what information should be provided regarding the technical data and parameters of monocrystalline and multicrystalline silicon cells, which determine the optimal and safe production of photovoltaic modules.

15.4 Module strings functioning accuracy tests

To verify the correct operation of the module chains, **current-voltage characteristics** are determined. For measuring the current-voltage characteristics, specialized instruments are used, such as the Metrel MI 3108 Eurotest PV multifunction meter, which is shown in Fig. 217.
The meter allows for testing photovoltaic installations according to the PN-EN 62446 standard, which at the same time meet the requirements of the PN-EN 61557 and PN-EN 61010 standards. The instrument combines the functions of an electrical installation parameter meter and photovoltaic installation tester. It allows, among others, to create current-voltage characteristics, to convert the parameters to STC values (standard test conditions) and to measure the power on AC and DC sides of the inverter. An important aspect in the measurement of PV installations is the simultaneous measurement of environmental parameters such as panel temperature and solar radiation intensity.

Figure 217: Metrel MI 3108 installation meter. Own elaboration.

Measurement of continuity of protective and equipotential

connections

In accordance with PN-EN 62446-1 standard, the continuity measurement of protective (earthing) and equipotential bonding is recommended first. In Fig. 218 a scheme for measuring the continuity of protective connections using the MI 3108 Eurotest PV instrument, which was connected to the PV panel frame and to the inverter housing, is shown.

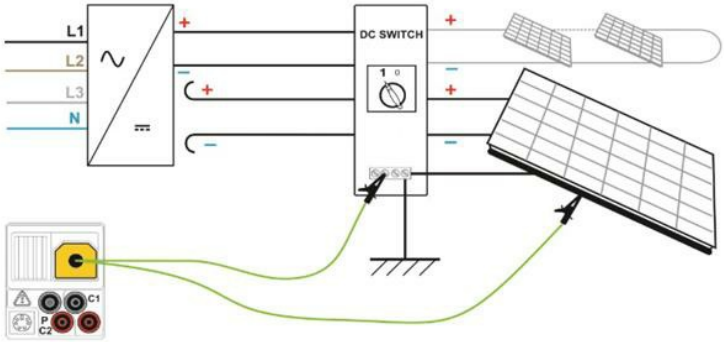

Figure 218: The scheme showing a PV installation during a continuity measurement of the protective connections with the MI 3109 Eurotest PV instrument. Source: part of the Metrel MI 3108 Eurotest PV instrument manual.

Testing the polarity of the wires and strings

An important step in verifying the correct operation of the PV installation is to test the polarity of the wires and to check the correct connection of the module strings. The procedure for the polarity test is described in detail in the standard PN-EN 62446-1, while the wiring diagram of the MI 3109 Eurotest PV meter is presented in Fig. 219. The polarity measurement consists of connecting all wires of negative polarity and checking the voltages between all wires of positive polarity to the first reference wire in turn. The resulting voltage value of approximately 0 V indicates correct connections, and twice the voltage rating will indicate a reverse connection.

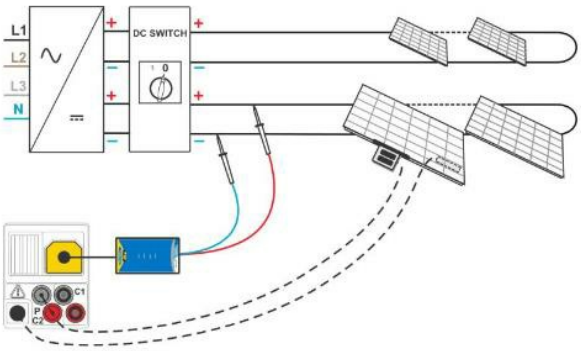

Figure 219: Schematic of a PV installation when measuring Voc/Isc values with the MI 3108 Eurotest PV instrument. Source: part of the user manual of the Metrel MI 3108 Eurotest PV instrument.

Open circuit voltage measurement V_{oc}

Measurement of the open circuit voltage V_{oc} is one of the most important tests that allows to quickly verify the correctness of the connections of the modules in the chain. The measurement is carried out using the MI 3109 Eurotest PV meter with the following connection diagram (Fig. 220). When measuring V_{oc}, the PV system must not be connected to the load and the meter is connected to the wires coming out of the PV modules.
The voltage value of a given string allows you to verify that the right number of modules are connected in the right way. The ability to enter environmental parameter values into the meter allows the open circuit voltage value to be converted to STC conditions. In the test, either the data from the module data sheet or the measured values V_{oc} for a single module are taken as reference values. Obtained results that deviate from expected results may suggest:

- incorrect connection of system components such as missing connection or reversed polarity of modules,
- short-circuit of some bypass diodes,
- damage to the insulation or the insulation of the connecting components.

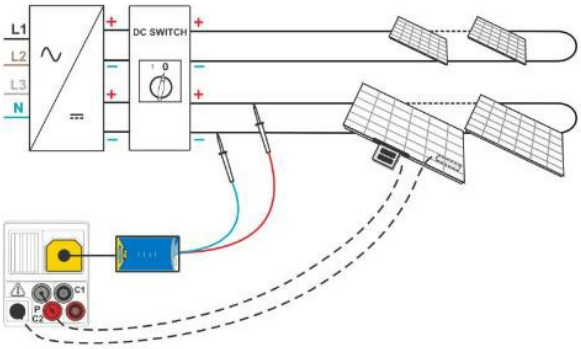

Figure 220: The scheme of PV installation during measurement of Voc/Isc values with the MI 3108 Eurotest PV instrument. Source: part of the user manual of the Metrel MI 3108 Eurotest PV instrument.

Measurement of short circuit current Isc or operating current

The test recommended by the PN-EN 62446-1 standard is the measurement of the short-circuit current I_{sc}, which can be performed with the MI 3108 meter. It is also possible to measure the operating current using the Metrel A 1391 clamps. On Fig. 221 there is a diagram of how to connect the meter to the PV installation in order to measure the DC current. The short-circuit current is measured by connecting the wires coming out of the PV module to each other and putting the clamps on the wire. On the other hand, the operating current is measured while the installation is running.

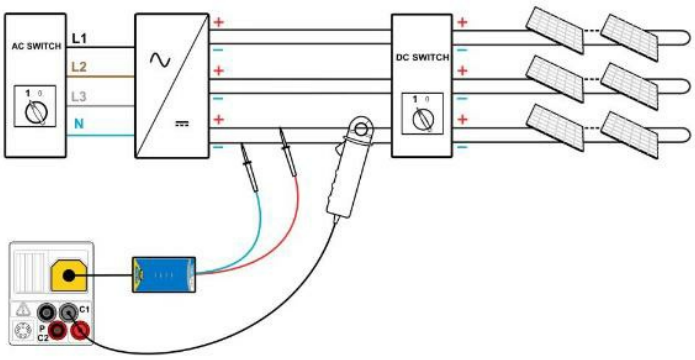

Figure 221: The scheme of PV installation during measurement of Voc/Isc values with the MI 3108 Eurotest PV instrument. Source: part of the user manual of the Metrel MI 3108 Eurotest PV instrument.

Current-voltage I(U) characteristics test

An important step in verifying the correct operation of a photovoltaic installation is to check the current-voltage characteristics of the module chains. This is an extended version of measurements V_{oc} and I_{sc}, whereby plotting the entire I(U) characteristic makes it possible to provide information about the voltage of the maximum power point V_{sc}, the current of the maximum power point I_{mpp} and the maximum power obtained just at that point. By using the solar irradiance meter in the measurement, the current-voltage characteristic curve can be recalculated to STC conditions, as a result of which it is possible to make a real comparison of the efficiency of the installation with the manufacturer's catalog data. The shape of the characteristics also allows to diagnose errors in the operation of the installation. The changes of the I(U) characteristic and the factors causing the anomalies are shown in Fig. 222 and Fig. 223.

I	II	III	IV	V
Reduced current	**Increased slope of the I-U curve**	**Possible loss of matching**	**Reduced slope of the I-U curve**	**Reduced V_{oc} voltage**
Module contamination	Presence of shunt paths in the cell	Overstated resistance and/or mismatched wiring cross section	Increase in series resistance	Defective bypass diodes
Incorrect solar radiation intensity reading	Presence of shunt paths in the cell connection	Emergence of resistive connections on the chain	Wrong connection in chains	PV module degradation (potential induced degradation, PID)
Destruction of modules	No I_{sc} current matching	Increase in module resistance		High shading of the module chain

Figure 222: Change in current-voltage characteristics. Own elaboration.

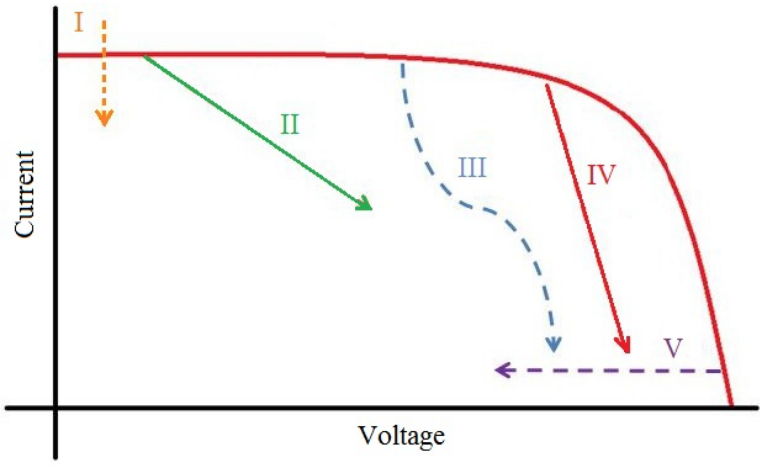

Figure 223: Causes and effects of change in current-voltage characteristic curve. Own elaboration.

In the test it is important to determine the current value of solar irradiance in the plane of the modules. This is important because the PN-EN 62446-1 standard defines the minimum irradiance at which the current-voltage characteristics test is reliable and can be converted to STC conditions. In case of using Metrel devices, radiation intensity should be above 500 $\frac{W}{m^2}$. PN-EN 61829 standard defines the way of performing an effectiveness test of photovoltaic modules and an exact conversion of measurements to STC conditions defining the minimum value of solar radiation intensity as 700 $\frac{W}{m^2}$. Solar irradiance testing is possible in several ways, namely using Metrel's A 1378 PV Remote Unit external temperature and solar irradiance recorder, or using the pyranometer shown in Fig. 224.

Figure 224: Pyranometer working in real conditions installed to the photovoltaic module in the Photovoltaic Center in Miękinia. Photo – author's archive.

In measuring environmental parameters, it is important that the solar intensity sensor be placed in the plane of the module so that it is not shaded or exposed to reflected light. The temperature sensor should be placed on the back of the module and closest to the center of either cell and module.

15.5 Hail test

Extreme weather conditions like severe hailstorms can lead to visible damage of the modules, as well as to micro-damage that is difficult to identify visually. For this reason, solar modules are compulsorily tested for hail resistance according to international standards (IEC 61215). The test is performed at a temperature of about 4 $^{o}\mathrm{C}$, using special hail ball launchers with a diameter of 1 inch (25.4 mm) and a weight of about 7.53 g. The hail balls hit the panel in 11 cycles at a velocity of 23 $\frac{m}{s}$. At the end of the test, there should be no visible damage such as cell and glass cracks, microcracks and structural deformations (Fig. 225).

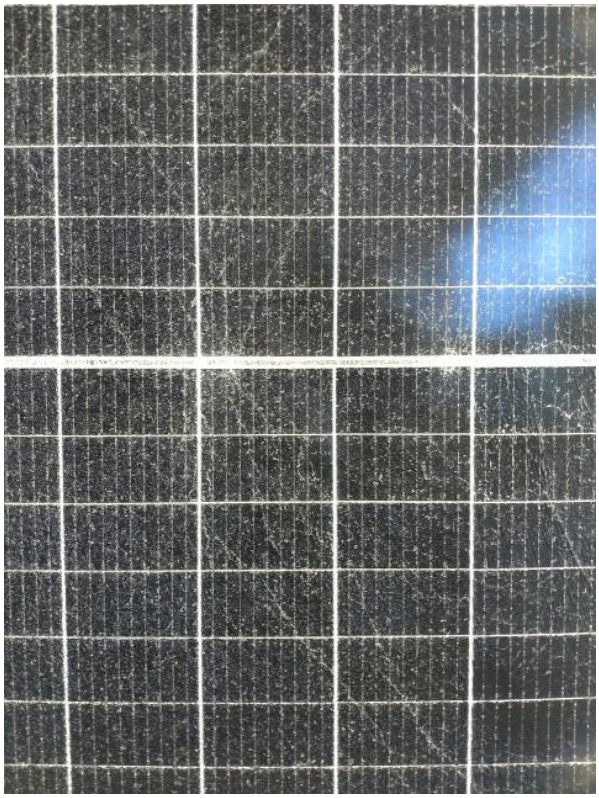

Figure 225: Photovoltaic module destroyed by hailstorm. Photo – author's archive.

15.6 Mechanical static load on module test

The resistance of photovoltaic modules to static load test is verified on the basis of tests in which the modules are loaded with a pressure of 2 400 Pa, thus inducing stress for a period of 1 h. The test is continued as long as the module does not break.

15.7 Electroluminescence tests

Electroluminescence tests are used to identify micro-damage that is not visible to the naked eye. This type of damage can occur e.g. during heavy hailstorms, when weather conditions are much more unfavorable than those during hail tests and as a consequence the strength limit of the panels may be exceeded. Micro-damage may also occur during transport or installation. Electroluminescence tests can also be used to detect micro-damage from induced PID voltage. They are performed when current flows through the module. At this time, two independent electroluminescent cameras take images of the photovoltaic cells so that the modules are overexposed. A detailed description of how the electroluminescence tests are performed is given in [227].

16. Photovoltaic systems damage

16.1 Types of damage in PV installations

Damage to photovoltaic installation

Damage can occur to cells, modules, as well as to connecting elements, e.g.: cables, connectors, junction boxes.
Damage can appear during production, transport, assembly, as well as during operation, when many factors are present. During production, the modules are subjected to e.g. chemical agents, high temperature and mechanical stress. During transport and installation, damage to the modules may occur due to inadequate protection against falling or improper behaviour of the installer during installation, e.g. walking on the modules, overtightening to the supporting structure. During operation, the modules may be exposed to e.g. strong wind, hail. In a marine environment, the modules and elements of the supporting structure can be permanently damaged by the humid and corrosive atmosphere e.g. as a result of salt accumulation on the elements of the installation.
The most common defects and damage include:

CELLS

- hot-spots,
- microcracks and cracks,
- transparent electrode corrosion (TCO),
- Potential Induced Degradation (PID),
- Light Induced Degradation (LID),
- Light and elevated Temperature Induced Degradation (TeLID).

MODULES

- delamination,
- glass cracks.

INSTALLATION COMPONENTS

- connector defects,
- burned-out junction boxes.

16.2 Hot spots

Hot spots are areas where an uncontrolled change in resistance has occurred causing a significant amount of Joule-Lenz heat to be released and the cell temperature to rise in these areas. The presence of hot spots can be due to the presence of current path defects such as the presence of undersoldings and changes in cross-section, as well as cell microdamage. In the defective area, the cell dissipates energy as heat instead of generating it. The problem of hot spots becomes very serious when part of the cell is shaded. In such a situation, the shaded cell does not produce electricity, but the reverse current, generated by unshaded cells, flows through it, causing an increase in temperature [228]. In order to prevent the occurrence of hot spots in modules, by-pass diodes are used. The purpose of the bypass diodes is to redirect the generated current in such a way that no current flows through the damaged and shaded cell [155].
The temperature of the hot spot depends on the location and conductivity of the material used to produce the photovoltaic cells [229]. The hot spot near the edge of the silicon module achieves much higher temperatures than the hot spot occurring in the center of the module. This is because the thermal conductivity in the silicon cell is higher than in the laminate. For this reason, heat is distributed over a larger area if the hot spot occurs in the center of the panel. Hot spots can be detected by a thermal imaging survey of the photovoltaic system. An image taken with a thermographic camera is shown in Fig. 226. It shows the temperature distribution on the surface of the photovoltaic module. The surface temperature of a properly working module should be identical over its entire area. The image shows an area with an increased temperature in comparison with the rest of the module, which indicates the presence of hot spots.

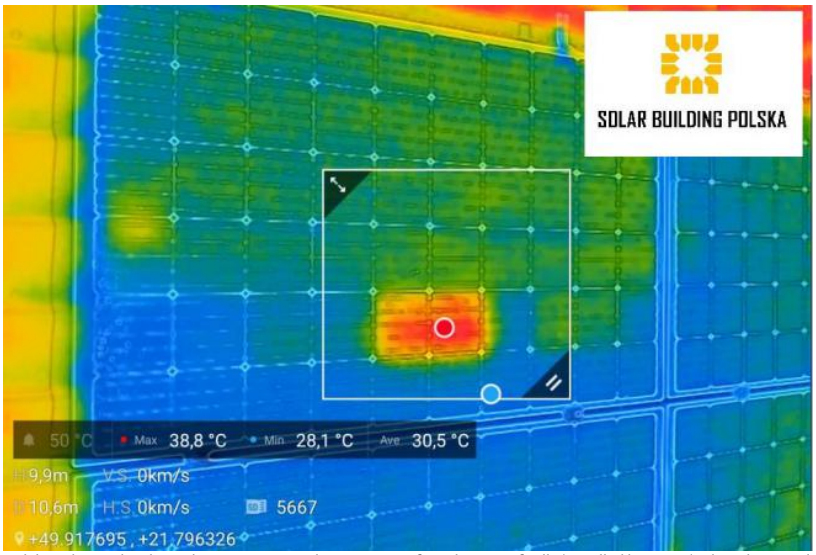

Figure 226: Photographs of modules taken with a thermal imaging camera showing areas of overheating of cells (so-called hot spots). Photo by Stanisław Bajorski – PV thermovision

measurements – used with permission of Solar Building Polska .

Photovoltaic cells in hot-spot areas can heat up to over 250 $^{o}\mathrm{C}$ [228]. Heating the cell to temperatures exceeding the strength of the EVA film can lead to permanent damage, resulting in a dark discolouration on the cell surface. The occurrence of "hot-spots" accelerates the ageing of the cell, which can result in shortened lifetime of the module and decrease in energy efficiency by over 15% [230], and in extreme situations can lead to a system fire.

16.3 Delamination

Delamination is damage to the panels by degrading the EVA (ethylene vinyl acetate) film, which is used to cover the photovoltaic modules. The process of covering the panels with EVA film, i.e. laminating, takes place under specific technological parameters such as temperature and pressure. A consequence of the wrong choice of technological parameters of this process is delamination, which occurs during operation. It most often occurs in hot and humid climate and is observed near current paths. Delamination causes opacity of the EVA film, which can be seen on the Fig. 227.

Figure 227: Delamination of EVA film along the module Photo by Stanisław Bajorski used with permission of Solar Building Polska .

The consequence of delamination is a worsening of the protective properties against moisture penetration into the cells, as well as a worsening of the light transmission to the cell, which results in a worsening of the modules' working efficiency [231], [232], [233].

16.4 Cracks and micro-cracks in PV cells

Cell **microcracks and cracks** are damage that can occur during manufacturing, transport and installation of photovoltaic modules. Cracks can also occur during the operation of the modules due to impact or atmospheric factors such as snow loads, strong winds and hail [234].
Several types of cell cracks can be distinguished depending on their direction of occurrence:

- diagonal cracks,
- cracks parallel to the busbars,
- cracks perpendicular to the busbars,
- cracks in many directions.

Diagonal cracks and cracks in multiple directions have the greatest impact on reducing the efficiency of photovoltaic modules, as they can lead to the disconnection of parts of the cells from the busbars, and thus the loss of the total power generated by the module [235], [236].
In the places of micro-cracks as well as on the edges of cells, so called "snail tracks" can appear [237], which are the consequence of ongoing chemical reactions between elements from panel components and oxygen and moisture from the environment. Because different reactions can produce "snail trails," the term refers to a class of defects rather than describing one particular reaction event. One mechanism describing the formation of "snail trails" is based on the assumption that moisture and oxygen diffuse through the EVA film and reach the cell surface through microcracks. Reactions between oxygen molecules from the EVA film and the environment and silver molecules from the so-called cell fingers (the thin mesh visible on the front of the cell) produce compounds such as silver oxide, silver chloride, silver carbonate and silver acetate, for example [238]. An example of the reaction of creating so-called "snail trails" (silver acetate, $AgC_2H_3O_2$), due to solar radiation and temperature can be described as:

$$4Ag_{(S)} + O_2 + 4CH_3COOH_{(g)} \overset{UV,T}{\rightarrow} 4AgC_2H_3O_2H_{(s)} + H_2O_{(g)} \tag{28}$$

The cause of "snail trails" may also be the introduction of silver particles in the manufacturing process as contaminants, which may not be related to the presence of microcracks in the cell.

16.5 Connector and junction box defects

Defects in photovoltaic installations can include **defects in connectors and junction boxes**. The consequence of poor quality connectors is poor electrical contact, damage during installation or after exposure to the elements. Eventually, parts of the installation may burn out. Another cause of burnout is poor quality junction boxes with incorrectly installed bypass diodes. Junction boxes contain 'by-pass' diodes in their design, whose role is to cause current to flow outside the shaded cell. If they are not working properly they can overheat and then burn out.

16.6 Glass cracks

Cracks in the glass of photovoltaic modules are usually caused by external factors such as hail, stone, etc. An example of broken photovoltaic panel glass is shown in Fig. 228. It is also possible to damage the glass layer due to improper behavior of the installer during the photovoltaic installation, e.g. over-tightening of clamps or by walking on the module.

Figure 228: Damaged PV photovoltaic panel glass by stone impact. Photo – author's archive.

16.7 Corrosion of TCO layer in amorphous silicon cells

Corrosion of the transparent TCO (Transparent Conductive Oxide) layer is its opacity and applies to thin-film cells [239], as well as those produced from amorphous silicon [240]. The TCO corrosion occurs in the presence of leakage currents that generate a voltage between the cell and the ground, which causes sodium atoms, a component of glass, to enter the TCO layer. The corrosion progression starts at the edges of the photovoltaic module, then the process progresses to further areas of the cell. As a consequence, the layer becomes cloudy and the cell efficiency decreases.
Depending on the position of the TCO layer in the cell, we distinguish between substrate technologies, when the layer is directly adjacent to the glass layer of the cell, and superstrate technologies, when the TCO layer is separated from the glass by a luminate layer. For this reason, cells manufactured using substrate technology are most vulnerable. In order to prevent corrosion of the TCO layer, it is recommended to use transformer inverters (galvanic isolation) and to ground the pole „-" of the module table.

16.8 Potential Induced Degradation (PID)

The **power loss of PV modules** can occur due to the occurrence of Potential Induced Degradation (PID), consisting of a small current leakage [241]. This phenomenon occurs when there is a high potential difference between the grounded frame of photovoltaic panels with a potential of 0 V and the extreme panels (extreme cells) in the string with different polarity. If the PID phenomenon occurs systematically, irreversible damage to the cell junctions can occur. On the other hand, when the phenomenon occurs irregularly, reversible cell polarity may occur and cause no permanent damage [242].

16.9 Technology markers on cell edges

Technology markers are often mistakenly thought of as defects. Cell technology markers are formed during the production process at the anti-reflective layer manufacturing stage. During production, the wafers are usually held at two points on the edge of the cell, resulting in darker areas on the surface of the cell called technology markers. Defects of this type do not affect the performance of photovoltaic modules.

17. Economic aspects of photovoltaics

17.1 Photovoltaic installation costs

Due to high energy needs, the use of photovoltaics is becoming increasingly profitable. In general, the profitability of investing in a photovoltaic power plant depends on the price of the installation and the energy prices. The costs of photovoltaics largely consist of the costs of the installation itself, which are incurred on a one-off basis. The price of the installation kit also depends on where the panels will be installed. The cost of the installation is influenced by:

- photovoltaic panels,
- inverters,
- wiring,
- energy meters,
- electrical equipment with lightning protection,
- labor costs,
- additional components costs (especially relevant for tracker systems),
- maintenance costs for the period of operation,
- disposal costs after plant closure.

An example of the percentage distribution of costs for an installation company is shown in Fig. 229 – compiled on the basis of [243], [244].

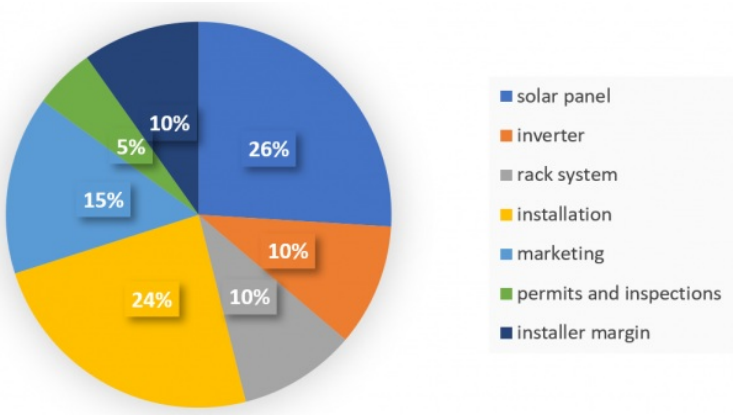

Figure 229: Percentage distribution of photovoltaic installation costs. Own elaboration.

The current average installation price in the United States by size is shown in Fig. 230. For 1kW we get a cost of $5/kW, and for i 74 kW the cost per 1kW is $3.
The average cost of installing solar photovoltaics worldwide from 2010 to 2019 has been falling for many years and is now $995/kW (Fig. 230 – based on data from [245]).

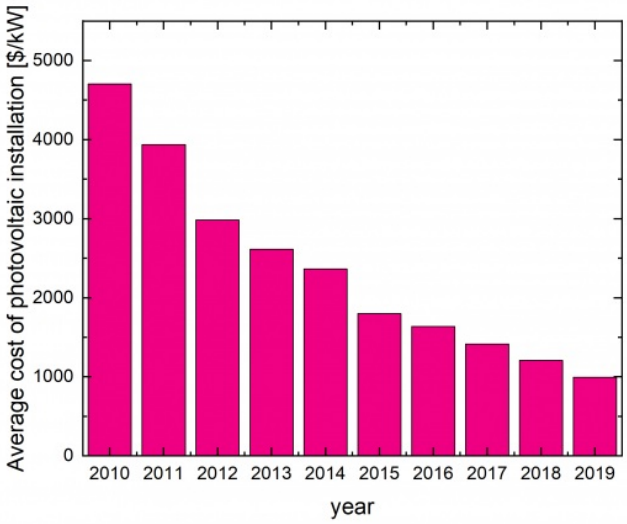

Figure 230: Average cost of solar photovoltaic installation worldwide from 2010 to 2019. (In US dollars per kW). Own elaboration.

17.2 Module prices

The most popular cell types are **silicon cells** and **thin film, multi-junction cells** (due to cost) and **dye synthesised solar cells** (for reasons of efficiency, however, they represent a marginal part of sales). Among those commonly available, **monocrystalline panels** are the most expensive, but due to their being the highest efficiency they are the preferred choice. Cheaper cells are polycrystalline cells, while the cheapest option is amorphous silicon cells (table on Fig. 231 – based on [243]).

Cell type	Price $/W
Monocrystalline silicon cells	1.0-1.4
Polycrystalline silicon cells	0.80-0.90
Amorphous silicon cells	0.45-0.53
CIGS thin film cells	0.55-0.66
CdTe thin film cells	0.50-0.60
Dye cells	0.25-4.0
Multi-junction cells	15-23

Figure 231: Cost comparison for different types of photovoltaic panels. Own elaboration.

As technology advances, manufacturing techniques improve, and the price of the panels themselves falls. Richard Swanson - founder of SunPower Corporation, a solar panel manufacturer - has proposed the equivalent of Moore's Law for solar panels. **Swanson's law** [246] postulates that the price of solar photovoltaic panels tends to fall by 20% for each doubling of the cumulative quantity shipped. This is an empirical law. Prices for crystalline solar cells fell from $76.67/W in 1977 to a projected $0.74/W in 2013, were $0.63/W in 2017 to reach a price of $0.21/W in 2020 [247] (Fig. 232 – based on [248]).

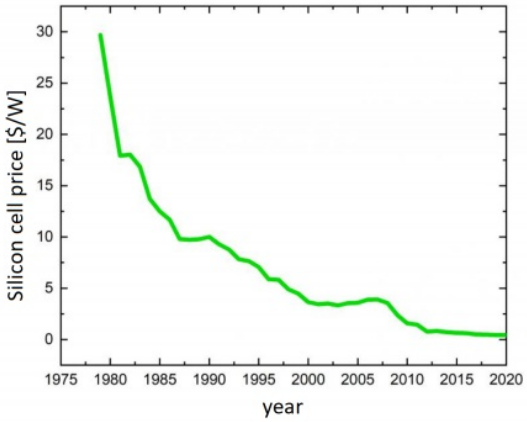

Figure 232: History of silicon cell prices in US dollars per 1W from 1977-2020. Own elaboration.

17.3 Installations development in Poland

The total amount of energy produced from photovoltaics in 2019 in Poland was about 924 GWh, while the forecast for 2020 is about 2190 GWh. The amount of energy produced in Poland by source is shown in Fig. 233, while the percentage distribution of energy sources in energy production is shown in Fig. 234. The energy produced by photovoltaics represents 1.9% of total energy produced in 2020 in Poland [249].

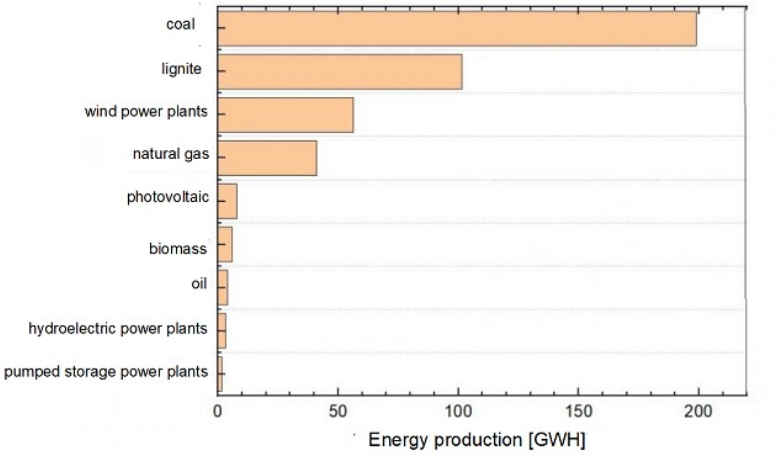

Figure 233: Energy production by source in GWh in 2019 in Poland. Own elaboration.

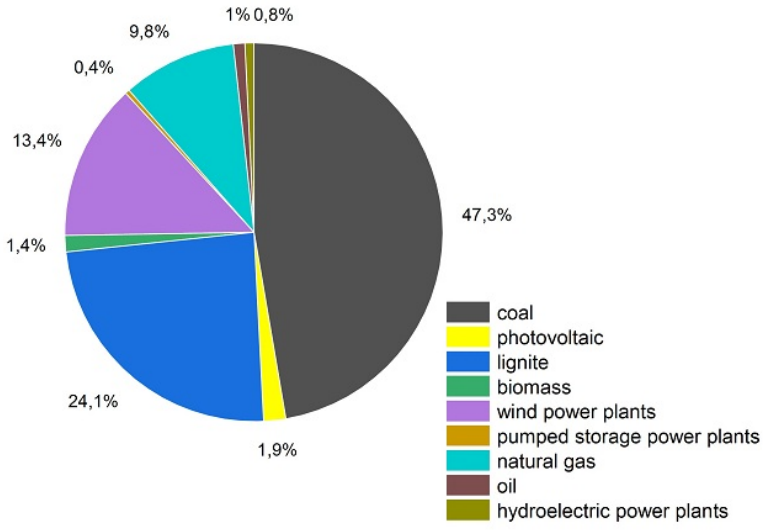

Figure 234: Participation of energy types in Poland in 2019. Own elaboration.

The PV sector in Poland employs 5-6 thousand people, with about 1000 people employed in companies producing panels and

installation components. The rate of growth of new capacities of photovoltaic installations is approx. 150% per year (Fig. 235). In 2020, Poland was ranked fifth in Europe in terms of growth of new photovoltaic power capacity [250]. 71% of installed photovoltaic sources are microinstallations.

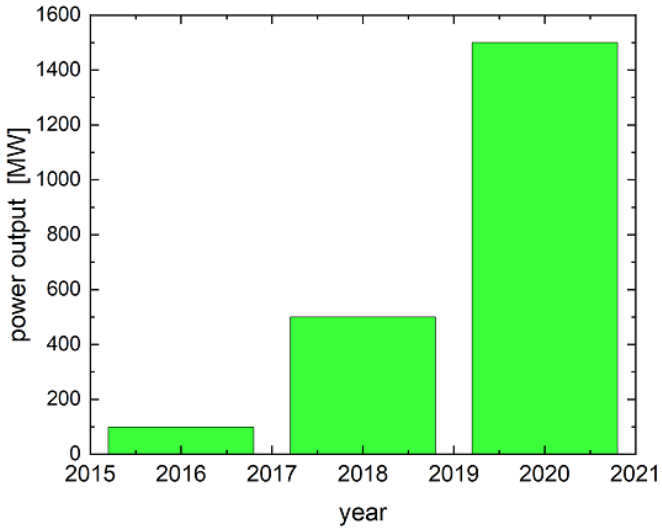

Figure 235: Power generated in Poland in 2016, 2018 and projected in 2020. Own elaboration.

The average price of electricity in Poland is 0.62 PLN/kWh and is constantly increasing, which, combined with decreasing installation costs, makes photovoltaics the most promising field of RES.
In recent years, conditions have emerged to stimulate investments in the production of electricity and heat. The rules for grid connection have been tidied up - paper-based documentation has been abandoned, which has shortened the installation procedure. The obligation for owners of renewable energy sources with a power of up to 50 kWp to obtain a license was also removed [249].
In recent years, government programmes to support photovoltaic installations have emerged in Poland. Since 2014, there have been subsidies under the **Prosument programme**. The programme offered preferential credit up to 100% installation costs and subsidies at the amount of 20% or 40% subsidies (15% or 30% after 2016). The programme was established as a continuation of the earlier **programme "Wspieranie rozproszonych, odnawialnych źródeł energii" (Support for distributed, renewable energy sources)**. From the historical programmes, it is worth mentioning **the programme "BOCIAN-rozproszone, odnawialne źródła energii" (Distributed Renewable Energy Sources)** implemented by the National Fund for Environmental Protection and Water Management since 2015. As of 30.08.2019, it has started a subsidiary programme called **"Mój Prąd" (My Current)**, where the owner of each new photovoltaic installation can expect to receive funding in the form of a subsidy to 50% the eligible costs of the micro-installation included in the project (no more than PLN 5 000 per project). The budget for non-refundable forms of co-financing amounted to PLN 1 billion. Under the programme, by 21 May 2020, installations with a total capacity of 200.77 MW were connected, granting almost 26 thousand subsidies [251], [252].

From 2019, PLN 53 000 can be deducted from income tax in respect to all thermal modernisation projects carried out in individual single-family buildings of which the taxpayer is the owner or co-owner. The installation of photovoltaics within the meaning of the Act is treated as a thermomodernization project [253].

The development of the photovoltaic industry is very strongly influenced by changes in legal regulations. The development of photovoltaics is related to the obligation imposed on countries belonging to the European Union to provide 20% the share of energy from renewable sources in total energy consumption by 2020. This obligation came into force with the signing of the Directive in 2009. According to the Directive, the target share of RES in gross final energy consumption by the end of 2020 for Poland is to be at least 15% [254].
A report on the photovoltaic market in Poland 2019 [255] indicates the dynamic growth of micro-installations in the last two years. A comparison of installed photovoltaic capacity from 2014 to June 2019 by type of photovoltaic installation is shown in Fig. 236 – based on [249].

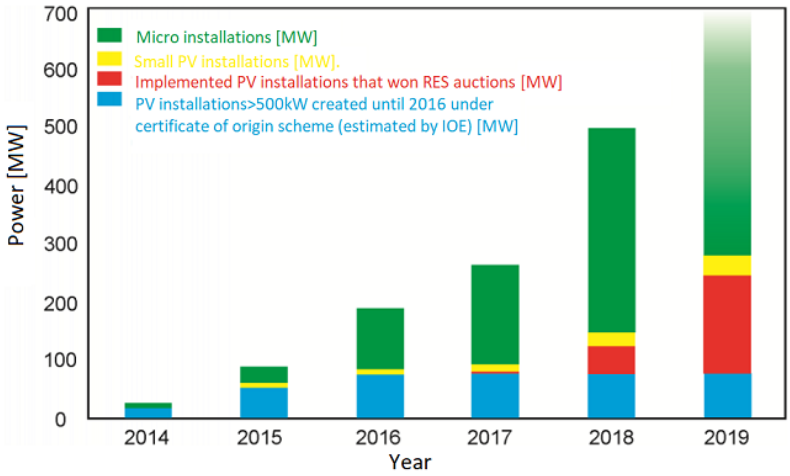

Figure 236: Photovoltaic power installed and connected to the grid in Poland 2014-2019. Own elaboration.

The increase in power from micro-installations has been observed since 2015, when the Renewable Energy Sources Act came into law [256]. The increase in electricity production from micro-installations was also a consequence of the Regional Operational Programmes 2014-2020. The total installed capacity of photovoltaic sources at the end of 2018 was about 500 MW; in May 2019 it exceeded 700 MW, and just six months later about 1.5 GW; while in May 2020, it exceeded 1.95 GW.
The increase in sales of energy from renewable sources was also due to the introduction of the auction system. In the auction system, generators declare the amount of energy supplied over 15 years and the price at which they will sell the energy. The winners of the auctions are the energy producers that offered the lowest price. Energy auctions were introduced under the Renewable Energy Act 2015 [254], which did not come into force immediately, but after its amendment in 2016 [255]. In 2018, the installed capacity from installations that won RES auctions was about 50 MW, while in 2019 it will be about 170 MW, which is almost a 3.5-fold increase in capacity. The auctions are controlled by the Energy Regulatory Office, and their course is described in the Auction Regulations [256].

17.4 Installations development in Europe

The installed capacity of photovoltaic cells has increased by around 100 GW in recent years. In 2019, it was 130 GW. The average growth is 10 GW/year, its rate, as in the rest of the world, is increasing - in 2019 capacity increased by 13%. In Europe, 16.7 GW were installed, an increase of more than 100% compared to 8.2 GW at the end of 2018. The largest increases were recorded by Spain (4.7 GW), Germany (4 GW), the Netherlands (2.5 GW) and France (1.1 GW). This was influenced by the implementation and enforcement of the RES Directive (28/2009/EC) in 2009. Between 2007 and 2014, installations were concentrated in Spain. The second largest European photovoltaic market is Italy, where the total capacity of photovoltaic plants already exceeds 21 GW. Photovoltaics accounted for 92% growth of new capacities in small-scale RES installations – Fig. 237 [257].

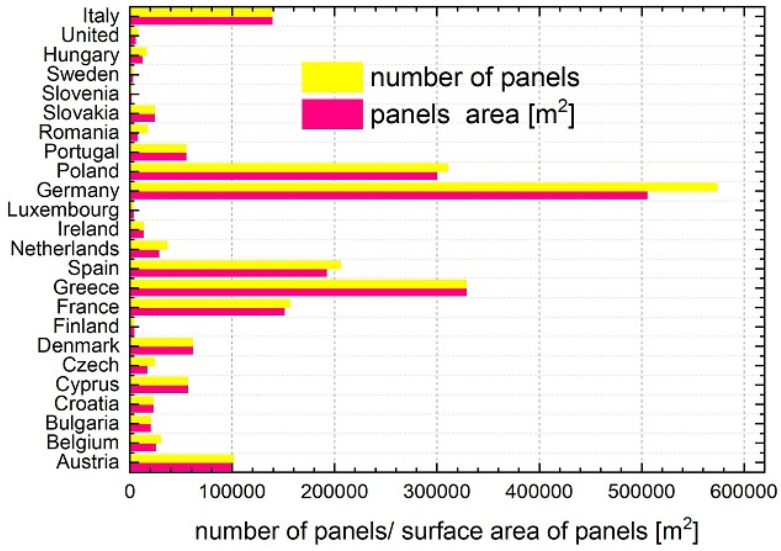

Figure 237: PV panel deployment growth in 2019. Own elaboration.

17.5 Installations development in the World

Worldwide energy consumption is increasing regularly - according to British Petrol Statistical Review of World Energy 2020

total energy consumption increased by 1.3% in relation to the previous year (Fig. 238). Renewable energy sources (including biofuels) have seen record growth in energy consumption ($3.2EJ = 3.2 \cdot 10^{18} J$). Wind was the largest contributor to the development of renewable energy sources (1.4 EJ), followed by solar energy (1.2 EJ). The photovoltaic market in China has been the fastest growing for several years. 16 GW of new installations have been installed in the European Union, with 13 GW in the United States.
Research and development spending on renewable energy has increased by 10%, reaching $13 billion. Approximately half of this amount was spent on solar energy [258], [259].

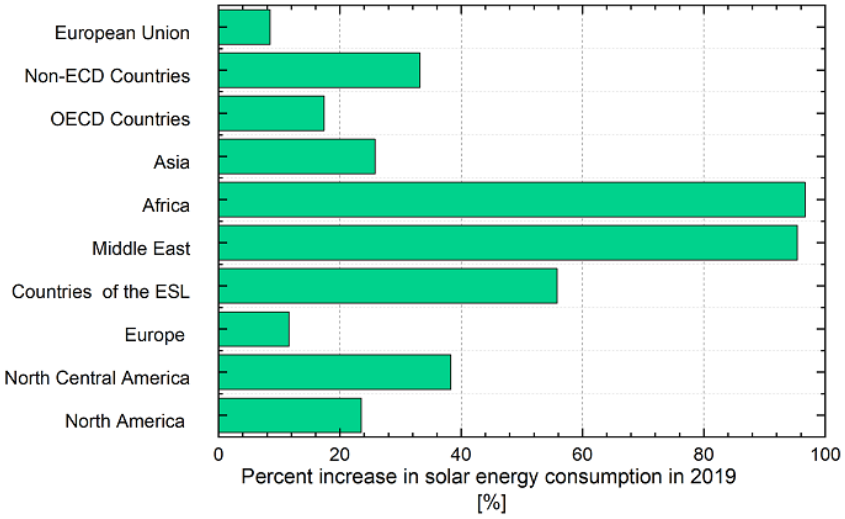

Figure 238: Percentage increase in solar energy use in 2019. Own elaboration.

China (responsible for 28.5% global emissions CO_2) have declared that they want to achieve climate neutrality by 2060, i.e. to stop emitting excess carbon dioxide into the atmosphere. IHS Markit points out that the capacity of photovoltaic panels will have to increase more than tenfold from the current 213 GW to 2200 GW, and the capacity of windmills from 231 GW to 1700 GW. The development of renewable energy technologies, including photovoltaics, will become one of the key areas of the economy in the coming years [260].

Bibliography

1. A. Jaeger-Waldau: Snapshot of photovoltaics – February 2019, Energies 2019, Vol. 12, Iss. 5, 769, dostęp:14.12.2020
2. N. Scafetta, R. C. Willson: ACRIM total solar irradiance satellite composite validation versus TSI proxy models, Astrophysics and Space Science 2014, Vol. 350, Iss. 2, pp. 421-442, dostęp:28.09.2020
3. OpenStreetMap: Copyright and License, OpenStreetMap contributors, dostęp:12.10.2020
4. Solargis: Global Solar Atlas, GHI map © 2020, dostęp:12.10.2020
5. E. Popko: Efekt fotowoltaiczny – ogniwo słoneczne, dostęp:14.12.2020
6. A. Masłowski: Energia słoneczna w Polsce – nasłonecznienie, dostęp:18.12.2020
7. M. Sibiński, K. Znajdek: Przyrządy i instalacje fotowoltaiczne, Wydawnictwo Naukowe PWN, Warszawa 2016.
8. K. T. Wojciechowski, K. Marszałek: A hybrid solar energy converter, EP2827383A1 2017, dostęp:14.12.2020
9. T. Markvart (Ed.): Solar Electricity, 2nd Edition, Wiley, Chichester 2000.
10. F. Kasten: A new table and approximate formula for the relative optical air mass, Archiv für Meteorologie, Geophysik und Bioklimatologie, Serie B 1965, Vol. 14, pp. 206-223, dostęp:14.12.2020
11. Friko.net: Wschód i zachód Słońca w Krakowie, dostęp:12.12.2020
12. B. Szymański: Pochylenie i kierunek instalacji fotowoltaicznej, GLOBEnergia : Odnawialne Źródła i Poszanowanie Energii 2013/1, s. 34.
13. : Willoughby Smith, Wikipedia, the free encyclopedia, dostęp:10.10.2020
14. : Philipp Lenard, Wikipedia, the free encyclopedia, dostęp:05.06.2020
15. : Wilhelm Hallwachs, Wikipedia, the free encyclopedia, dostęp:05.06.2020
16. : Jan Czochralski, Wikipedia, wolna encyklopedia, dostęp:05.06.2020
17. : Explorer 6 (NASA), Wikipedia, wolna encyklopedia, dostęp:05.06.2020
18. : Telstar (NASA), Wikimedia Commons, dostęp:5.11.2020
19. : Solar Challenger (NASA), Wikimedia Commons, dostęp:5.11.2020
20. C. Kittel: Wstęp do fizyki ciała stałego, PWN, Warszawa 1974.
21. N. W. Ashcroft, N. D. Mermin: Fizyka ciała stałego, PWN, Warszawa 1986.
22. M. A. Green: Silicon Solar Cells : Advanced Principles & Practice, Centre for Photovoltaic Devices and Systems – University of New South Wales, Sydney 1995.
23. M. S. Tyagi: Introduction to semiconductor materials and devices, Wiley, New York 1991.
24. T. Soga: Nanostructured materials for solar energy conversion, Elsevier, Amsterdam, Boston 2006.
25. A. Luque, S. Hegedus: Handbook of photovoltaic science and engineering, Wiley, Chichester, West Sussex 2014.

26. B. Szymański: STC, NOCT. Warunki w jakich badane są baterie PV, GLOBEnergia : Odnawialne Źródła i Poszanowanie Energii 2013/3.
27. A. Luque, S. Hegedus: Handbook of photovoltaic science and engineering, Wiley, Hoboken, New Jork 2003.
28. JA Solar: 330W PERC Module JAM60S09 310-330/PR, [karta katalogowa], dostęp:10.09.2020
29. W. Shockley: The theory of p-n junctions in semiconductors and p-n junction transistors, The Bell System Technical Journal 1949, Vol. 28, Iss. 3, pp. 435-489.
30. K. Drabczyk, P. Panek: Silicon-based solar cells : characteristics and production processes, Institute of Metallurgy and Materials Science of Polish Academy of Sciences, Kraków 2012.
31. P. Menna, G. Di Francia, V. La Ferrara: Porous silicon in solar Cells: a review and a description of its application as an AR coating, Solar Energy Materials and Solar Cells 1995, Vol. 37, Iss. 1, pp. 13-24, dostęp:14.12.2020
32. M. Wolf, G. T. Noel, R. J. Stirn: Investigation of the double exponential in the Current-Voltage Characteristics of Silicon Solar Cells, IEEE Transactions on Electron Devices 1977, Vol. 24, Iss. 4, pp. 419-428.
33. L.-M. Huang, H.-Y. Hsu, R.-Ch. Lai, F.-M. Lin, Ch.-Y. Peng, F.-Y. Yeh: Physical Properties of EVA and PVB Encapsulant Materials for Thin Film Photovoltaic Module Applications, 23rd EUPVSEC (Conference), Valencia, Spain, 2008, dostęp:14.12.2020
34. K. Drabczyk: Modyfikacje elektrod na bazie srebra w aspekcie zastosowań w krzemowych krystalicznych ogniwach fotowoltaicznych, Instytut Metalurgii i Inżynierii Materiałowej Polskiej Akademii Nauk, Kraków, Kozy 2018.
35. K. Drabczyk: Kontakty elektryczne krystalicznych krzemowych ogniw fotowoltaicznych, Prace Instytutu Elektrotechniki 2014, Z. 264, s. 41-49, dostęp:14.12.2020
36. G. Beaucarne, G. Schubert, J. Hoornstra, J. Horzel, S. W. Glunz: Summary of the third workshop on metallization for crystalline silicon solar cells, Energy Procedia 2012, Vol. 21, pp. 2-13, dostęp:14.12.2020
37. T. Minami: Transparent conducting oxide semiconductors for transparent electrodes, Semiconductor Science and Technology 2005 Vol. 20, Nr 4, pp. 35-44.
38. S. H. Mohamed, F. M. El-Hossary, G. A. Gamal, M. M. Kahlid: Properties of Indium Tin Oxide Thin Films Deposited on Polymer Substrates, Acta Physica Polonica A 2009, Vol. 115, No. 3, pp. 704-708, dostęp:14.12.2020
39. A. Way, J. Luke, A. D. Evans, Z. Li, J.-S. Kim, J. R. Durrant, H. Ka Hin Lee, W. C. Tsoi: Fluorine doped tin oxide as an alternative of indium tin oxide for bottom electrode of semi-transparent organic photovoltaic devices, AIP Advances 2019, 9, 085220, dostęp:14.12.2020
40. : Fluorine doped Tin Oxide (FTO) Glass, dostęp:08.09.2020
41. Z. Y. Banyamin, P. J. Kelly, G. West, J. Boardman: Electrical and Optical Properties of Fluorine Doped Tin Oxide Thin Films Prepared by Magnetron Sputtering, Coatings 2014, Vol. 4, Iss. 4, pp.732-746, dostęp:14.12.2020
42. M. A. Aouaj, R. Diaz, A. Belayachi, F. Rueda, M. Abd-Lefdil: Comparative study of ITO and FTO thin films grown by spray pyrolysis, Materials Research Bulletin 2009, Vol. 44, Iss. 7, pp. 1458-1461, dostęp:14.12.2020
43. J. W. Cleary, E. M. Smith, K. D. Leedy, G. Grzybowski, J. Guo: Optical and electrical properties of ultra-thin indium tin oxide nanofilms on silicon for infrared photonics, Optical Materials Express 2018, Vol. 8, Iss. 5, pp. 1231-1245, dostęp:14.12.2020
44. R. Pietruszka, G. Luka, B. S. Witkowski, L. Wachnicki, S. Gieraltowska, K. Marszałek, T. Stapiński, M. Godlewski: Opracowanie efektywnych metod domieszkowania warstw ZnO glinem w procesie ALD i optymalizacja tych warstw, Przegląd Elektrotechniczny 2014, R. 90, Nr 10, s. 203-205, dostęp:14.12.2020
45. L. Schmidt-Mende, J. L. MacManus-Driscoll: ZnO – nanostructures, defects, and devices, Materials Today 2007, Vol. 10, Iss. 5, pp. 40-48, dostęp:14.12.2020
46. G. C. Yi, C. Wang, W. I. Park: ZnO nanorods: Synthesis, characterization and applications, Semiconductor Science and Technology 2005, Vol. 20, Nr 4, pp. 22-34, dostęp:14.12.2020
47. D. C. Look: Electrical and optical properties of p-type ZnO, Semiconductor Science and Technology 2005, Vol. 20, Nr 4, pp. 55, dostęp:14.12.2020
48. K. Znajdek, M. Sibiński, K. Przymęcki, Z. Lisik: Transparentne warstwy drukowane PEDOT jako kontakty emiterowe do aplikacji w elastycznych ogniwach fotowoltaicznych, Przegląd Elektrotechniczny 2014, R. 90, nr 9, s. 101-104, dostęp:8.09.2020
49. I. Khrapach, F. Withers, T. H. Bointon, D. K. Polyushkin, W. L. Barnes, S. Russo, M. F. Craciun: Novel Highly Conductive and Transparent Graphene-Based Conductors, Advanced Materials 2012, Vol. 24, Iss. 21, pp. 2844-2849, dostęp:14.12.2020
50. D. Janczak, M. Słoma, G. Wróblewski, M. Jakubowska, A. Młożniak: Grafenowe elektrody transparentne dla drukowanych ogniw fotowoltaicznych, Elektronika : konstrukcje, technologie, zastosowania 2013, Vol. 54, nr 5, s. 35-37.
51. F. I. Chowdhury, T. Blaine, A. B. Gougam: Optical transmission enhancement of fluorine doped tin oxide (FTO) on glass for thin film photovoltaic applications, Energy Procedia 2013, Vol. 42, pp. 660-669, dostęp:14.12.2020
52. PVEducation: Anti-Reflection Coatings, dostęp:10.10.2020
53. T. Stapiński, K. Marszałek, J. Jaglarz: Właściwości optyczne pokryć antyrefleksyjnych dla zastosowań fotowoltaicznych, Przegląd Elektrotechniczny 2014, R. 90, Nr 9, s. 91-93, dostęp:14.12.2020
54. A. G. Aberle: Surface passivation of crystalline silicon solar cells: a review, Progress in Photovoltaics 2000, Vol. 8, Iss. 5, pp. 473-487.
55. J. Zhao, A. Wang, M. A. Green: High-efficiency PERL and PERT silicon solar cells on FZ and MCZ substrates, Solar Energy Materials and Solar Cells 2001, Vol. 65, Iss. 1-4, pp. 429-435, dostęp:14.12.2020
56. B. Szymański: Moduły fotowoltaiczne PERC – Co je wyróżnia i dlaczego zdobywają rynek?, GLOBEnergia : : Odnawialne Źródła i Poszanowanie Energii 2017/6.
57. M. Fisher: ITRPV 11th edition, October 2020, key findings - maturity report update, International Technology Roadmap for Photovoltaic (ITRPV).
58. P. Kumar: Organic solar cells : device physics, processing, degradation, and prevention, CRC Press, Taylor et Francis Group, Boca Raton 2017.
59. D. Angmo, N. Espinosa, F. C. Krebs: Indium Tin Oxide-Free Polymer Solar Cells: Toward Commercial Reality. In: Z. Lin, J. Wang

(Eds.), Low-cost Nanomaterials, Springer, London 2014.
60. NREL: Best Research-Cell Efficiency Chart, dostęp:08.05.2020
61. Solar Power Europe: Global Market Outlook for Photovoltaics, dostęp:14.12.2020
62. G. Masson, I. Kaizuka, J. Lindahl, A. Jaeger-Waldau, G. Neubourg, P. Ahm, J. Donoso, F. Tilli: A Snapshot of Global PV Markets - The Latest Survey Results on PV Markets and Policies from the IEA PVPS Programme in 2017. In: 2018 IEEE 7th World Conference on Photovoltaic Energy Conversion (WCPEC) (A Joint Conference of 45th IEEE PVSC, 28th PVSEC & 34th EU PVSEC), dostęp:14.12.2020
63. R. Doering, Y. Nishi (Eds.): Handbook of Semiconductor Manufacturing Technology, CRC Press, Boca Raton, London, New York 2000, pp. 67-71.
64. Omron Semiconductor: Wafer preparation, slicing the ingot. In Industrial Automation, An Introduction to Application Expertise-Semiconductor, Photovoltaic & Electronics Industry, 2010.
65. Wafel krzemowy: WikiZero, dostęp:08.10.2020
66. D-H. Neuhaus, A. Münzer: Industrial Silicon Wafer Solar Cells, Advances in OptoElectronics 2007, Vol. 2007, Article ID 24521, doi:10.1155/2007/24521, dostęp:14.12.2020
67. J. E. Cotter, B. S. Richards, F. Ferraza, C. B. Honsberg, T. W. Leong, H. R. Mehrvarz, G. A. Naik, S. R. Wenham: Design of a Simplified Emiter Structure for Buried Contact Solar Cells, Proc. of the 2nd World Conf. and Exibition on Photovoltaic Solar Energy Conversion, 6-10 Juli, 1998, Vienna, p. 1511-1514.
68. V. Meemongkolkiat, K. Nakayashiki, D. S. Kim, R. Kopecek, A. Rohatgi: Factors limiting the formation of uniform and thick aluminum back surface field and its potential, Journal of The Electrochemical Society 2006, Vol. 153, Nr 1, p. 53, dostęp:14.12.2020
69. W. C. O'Mara, R. B. Herring, L. P. Hunt: Handbook of semiconductor silicon technology, Elveiser 1990.
70. : Silicon single crystal (aut. M. Lincetto), Wikimedia Commons, dostęp:10.12.2020
71. : Wafer 2 Zoll bis 8 Zoll 2, Wikimedia Commons, dostęp:08.12.2020
72. : Thin Film Flexible Solar PV Ken Fields 1 (aut. Ken Fields), Wikimedia Commons, dostęp:20.09.2020
73. J. Ramanujam, D. M. Bishop, T. K. Todorov, O. Gunawan, J. Rath, R. Nekovei, E. Artegiani, A. Romeo: Flexible CIGS, CdTe and a-Si:H based thin film solar cells: A review, Progress in Materials Science 2020, Vol. 110, (Article Nr) 100619, dostęp:14.12.2020
74. R. Figura, W. Zientarski: Analiza parametrów pracy modułu fotowoltaicznego, Autobusy : technika, eksploatacja, systemy transportowe 2016, R. 17, nr 12, s. 602-611, dostęp:14.12.2020
75. T. Markvat, L. Castañer: Solar cells : materials, manufacture and operation, Elsevier, Oxford 2005.
76. R. W. Birkmire, B. E. McCandless: CdTe thin film technology: Leading thin film PV into the future, Current Opinion in Solid State and Materials Science 2010, Vol. 14, Iss. 6, pp. 139-142, dostęp:14.12.2020
77. Max-Planck-Institut für Eisenforschung GmbH: CdTe solar cell material, dostęp:07.10.2020
78. D. Lan, M. A. Green: Up-conversion of sunlight by GaInP/GaAs/Ge cell stacks: Limiting efficiency, practical limitation and comparison with tandem cells, Energy Procedia 2017, Vol. 130, pp. 60-65, dostęp:14.12.2020
79. J. M. Romá: State-of-the-art of III-V Solar Cell Fabrication Technologies, Device Designs and Applicatione, Materials Science 2004, dostęp:14.12.2020
80. J. W. Garland, T. Biegala, M. Carmody, C. Gilmore, S. Sivananthan: Next-generation multijunction solar cells: The promise of II-VI materials, Journal of Applied Physics 2011, Vol. 109, Iss. 10, (Article nr 102423), dostęp:14.12.2020
81. E. Dumiszewska, P. Knyps, M. Wesołowski, W. Strupiński: Wielozłączowe ogniwa słoneczne, Przegląd Elektrotechniczny 2014, R. 90, Nr 5, s. 215-221, dostęp:14.12.2020
82. W. Shockley, H. J. Queisser: Detailed Balance Limit of Efficiency of p-n Junction Solar Cells, Journal of Applied Physics 1961, Vol. 32, Iss. 3, pp. 510-519.
83. C. B. Honsberg, A. M. Barnett: Paths to Ultra-High Efficiency (>50% Efficient) Photovoltaic Devices (pp. 453-456). In: 20th EUPVSEC (Conference), Barcelona, Spain, 2005, dostęp:14.12.2020
84. A. Belghachi: Theoretical Calculation of the Efficiency Limit for Solar Cells (chapter 2, pp. 47-76). In: L. A. Kosyachenko (Ed.), Solar Cells : New Approaches and Reviews, dostęp:5.12.2020
85. NREL: Best Research-Cell Efficiency Chart, dostęp:10.09.2020
86. B. R. Weinberger, M. Akhtar, S. C. Gau: Polyacetylene photovoltaic devices, Synthetic Metals 1982, Vol. 4, Iss. 3, pp. 187-197, dostęp:14.12.2020
87. S. Glenis, G. Tourillon, F. Garnier: Influence of the doping on the photovoltaic properties of thin films of poly-3-methylthiophene, Thin Solid Films 1986, Vol. 139, Iss. 3, pp. 221-231, dostęp:14.12.2020
88. N. Kaur, M. Singh, D. Pathak, T. Wagner, J. M. Nunzi: Organic materials for photovoltaic applications: Review and mechanism, Synthetic Metals 2014, Vol. 190, pp. 20-26, dostęp:14.12.2020
89. A. Sharma, D. Pathak, T. Wagner: Organic photovoltaic materials: A review on synthesis, structure and properties, Journal of Optoelectronics and Advanced Materials 2014, Vol. 16, No. 11-12, pp. 1257-1268, dostęp:14.12.2020
90. NREL: Best Reserch-Cell Efficiences, dostęp:21.09.2020
91. B. O'Regan, M. Grätzel: A low-cost, high-efficiency solar cell based on dye-sensitized colloidal TiO2 films, Nature 1991, Vol. 353, pp. 737-740.
92. K. Siuzdak, M. Klein, K. Łapiński, A. Cenian: Barwnikowe ogniwa słoneczne, Rynek Energii 2015, Nr 5, s. 75-83.
93. NREL: Best Reserch-Cell Efficiences, dostęp:17.10.2020
94. M. Dusza, M. Woźniak, O. Malinkiewicz: Perowskity – przyszłość fotowoltaiki, dostęp:10.12.2020
95. NREL: Perovskite Solar Cells, dostęp:20.10.2020
96. W.-J. Yin, T. Shi, Y. Yan: Unique Properties of Halide Perovskites as Possible Origins of the Superior Solar Cell Performance, Advanced Materials 2014, Vol. 26, Iss. 27, pp. 4653-4658, dostęp:14.12.2020
97. T. A. N. Peiris, A. K. Baranwal, H. Kanda, S. Fukumoto, S. Kanaya, T. Bessho, L. Cojocaru, T. Miyasaka, H. Segawa, S. Ito: Effect of

Electrochemically Deposited MgO Coating on Printable Perovskite Solar Cell Performance, Coatings 2017, Vol. 7, Iss. 3, (Article nr 36), dostęp:14.12.2020
98. M. Liu, M. B. Johnston, H. J. Snaith: Efficient planar heterojunction perovskite solar cells by vapour deposition, Nature 2013, Vol. 501, pp. 395-398.
99. J. Burschka, N. Pellet, S.-J. Moon, R. Humphry-Baker, P. Gao, M. K. Nazeeruddin, M. Grätzel: Sequential deposition as a route to high-performance perovskite-sensitized solar cells, Nature 2013, Vol. 499, pp. 316-319.
100. : First certified efficiency of 15% in perovskite solar cells with area of over 1 square cm, Science Daily 2015, dostęp:14.12.2020
101. : Dyesol to commercialize perovskite cells in Turkey, PV Magazine 2015, dostęp:01.09.2020
102. D. Kim, C. Kim: A Ladder-Type Organosilicate Copolymer Gate Dielectric Materials for Organic Thin-Film Transistors, Coatings 2018, Vol. 8, Iss. 7, (Article Nr 236), dostęp:14.12.2020
103. S. Ryu, J. Seo, S. S. Shin, Y. C. Kim, N. J. Jeon, J. H. Noh, S. I. Seok: Fabrication of metal-oxide-free CH3NH3PbI3 perovskite solar cells processed at low temperature, Journal of Materials Chemistry A 2015, Vol. 3, Iss. 7, pp. 3271-3275, dostęp:14.12.2020
104. J.-S. Huang, C.-Y. Hsiao, S.-J. Syu, J.-J. Chao, C.-F. Lin: Well-aligned single-crystalline silicon nanowire hybrid solar cells on glass, Solar Energy Materials and Solar Cells 2009, Vol. 93, Iss. 5, pp. 621-624, dostęp:14.12.2020
105. X. Wang, A. Bolag, W. Yun, Y. Du, C. Eerdun, X. Zhang, T. Bao, J. Ning, H. Alata, T. Ojiyed: Enhanced performance of dye-sensitized solar cells based on a dual anchored diphenylpyranylidene dye and N719 co-sensitization, Journal of Molecular Structure 2020, Vol. 1206, (Article Nr) 127694, dostęp:14.12.2020
106. L. L. Yan, C. Han, B. Shi, Y. Zhao, X. D. Zhang: A review on the crystalline silicon bottom cell for monolithic perovskite/silicon tandem solar cells, Materials Today Nano 2019, Vol. 7, (Atricle Nr) 100045, dostęp:14.12.2020
107. Q. Jeangros, M. Bräuninger, T. C. J. Yang, J. Werner, F. Sahli, P. Fiala: Perovskite Cells for Tandem Applications, dostęp:12.07.2020
108. H. Wei, H. Zhang, H. Sun, B. Yang: Preparation of polymer–nanocrystals hybrid solar cells through aqueous approaches, Nano Today 2012, Vol. 7, Iss. 4, pp. 316-326, dostęp:14.12.2020
109. A. Luque, V. M. Andreev: Concentrator Photovoltaics, Springer, Berlin 2007.
110. A. Mroziński (Red.), J. Flizikowski: Inżynieria instalacji fotowoltaicznych : monografia, Grafpol Agnieszka Blicharz-Krupińska, Bydgoszcz 2016.
111. X. Ning, R. Winston, J. O'Gallagher: Dielectric totally internally reflecting concentrators, Applied Optics 1987, Vol. 26, Iss. 2, pp. 300-305.
112. R. A. Sherif, R. R. King, N. H. Karam, D. R. Lillington: The path to 1 GW of concentrator photovoltaics using multijunction solar cells, Conference Record of the Thirty-first IEEE Photovoltaic Specialists Conference, 3-7 January 2005, pp. 17-22.
113. A. Hasan, J. Sarwar, A. H. Shah: Concentrated photovoltaic: A review of thermal aspects, challenges and opportunities, Renewable and Sustainable Energy Reviews 2018, Vol. 94, pp. 835-852, dostęp:14.12.2020
114. S. S. Indira, C. A. Vaithilingam, K.-K. Chong, R. Saidur, M. Faizal, S. Abubakar, S. Paiman: A review on various configurations of hybrid concentrator photovoltaic and thermoelectric generator system, Solar Energy 2020, Vol. 201, pp. 122-148, dostęp:14.12.2020
115. : Parabolic trough at Harper Lake in California (Mojave Solar Project), Wikipedia, the free encyclopedia, dostęp:10.10.2020
116. : Front (left) and back side (right) of a standard solar cell with a three busbar metallization layout, dostęp:15.09.2020
117. SOLsum blog: Moduł fotowoltaiczny mono PERC 315-325Wp z innowacjami, dostęp:19.10.2020
118. Redakcja GLOBEnergia: GLOBEnergia, GLOBEnergia, 2/2017.
119. J. Zhao, M. A. Green: Optimized antireflection coatings for high-efficiency silicon solar cells, IEEE Transactions on Electron Devices 1991, Vol. 38, Iss. 8, pp. 1925-1934.
120. M. A. Green, J. Zhao, A. Wang, S. R. Wenham: 45% Efficient Silicon Photovoltaic Cell Under Monochromatic Light, IEEE Electron Device Letters 1992, Vol. 13, Iss. 6, pp. 317-318.
121. M. A. Green, Z. Jianhua, A. W. Blakers, M. Taouk, S. Narayanan: 25-Percent Efficient Low-Resistivity Silicon Concentrator Solar Cells, IEEE Electron Device Letters 1986, Vol. 7, Iss. 10, pp. 583-585.
122. A. Wang, F. Yun, G. Zhang, D. M. Roche, S. R. Wenham, M. A. Green: 20 000 PERL silicon cells for the '1996 World Solar Challenge' solar car race, Progress in Photovoltaics 1997, Vol. 5, Iss. 4, pp. 269-276, dostęp:14.12.2020
123. M. A. Green, K. Emery, Y. Hishikawa, W. Warta, E. D. Dunlop: Solar Cell Efficiency Tables (Version 42), Progress in Photovoltaics 2013, Vol. 21, Iss. 5, pp. 827-837, dostęp:14.12.2020
124. R. J. Schwartz: Review of Silicon Solar Cells for High Concentrations, Solar Cells 1982, Vol. 6, Iss. 1, pp. 17-38, dostęp:14.12.2020
125. Rekord sprawności ogniwa: Magazyn Fotowoltaika, dostęp:13.10.2020
126. M. A. Green, J. Hansen: Catalogue of Photovoltaic Drawings, Photovoltaics Special Research Centre – University of New South Wales, Sydney 2002.
127. R. R. King, R. A. Sinton, R. M. Swanson: Front and Back Surface Fields for Point-Contact Solar Cells, Conference Record of the Twentieth IEEE Photovoltaic Specialists Conference, Las Vegas, NV, USA, 26-30 Sept. 1988, pp. 538-544.
128. R. Swanson: Photovoltaics: The Path from Niche to Mainstream Supplier of Clean Energy, Solar Power, San Jose 2006.
129. Meyer Burger: Mehr Solarstrom für alle durch hocheffiziente Technologie, dostęp:09.07.2020
130. : Nowe rozwiązania w ogniwach PV krzemowych, dostęp:10.07.2020
131. Panasonic: HIT Photovoltaic module, dostęp:06.07.2020
132. H. Sakata, T. Nakai, T. Baba, M. Taguchi, S. Tsuge, K. Uchihashi, S. Kiyama: 20.7% highest efficiency large area (100.5 cm2) HIT/sup TM/ cell, Conference Record of the Twenty-Eighth IEEE Photovoltaic Specialists Conference – 2000 (Cat. No.00CH37036), Anchorage, AK, USA, 15-22 Sept. 2000.
133. Y. K. Chieng, M. A.Green: Computer simulation of enhanced output from bifacial photovoltaic modules, Progress in

Photovoltaics 1993, Vol. 1, Iss. 4, pp. 293-299, dostęp:14.12.2020
134. M. Pagliaro, R. Ciriminna, G. Palmisano: Flexible Solar Cells, Wiley-Vch, Weineheim 2009.
135. Z. M. Jarzębski: Energia słoneczna : konwersja fotowoltaiczna, PWN, Warszawa 1990.
136. S. Schuler, S. Siebentritt, S. Nishiwaki, N. Rega, J. Beckmann, S. Brehme, M. Ch. Lux-Steiner: Self-compensation of intrinsic defects in the ternary semiconductor CuGaSe2, Physical Review B 2004, Vol. 69, Iss. 4, pp. 045210-1 – 045210-9, dostęp:14.12.2020
137. E. Dunlop, T. Huld, M. Suri, H. Ossenbrink: Is solar electricity in Europe expensive?, Proceedings of the 20th European Photovoltaic Solar Energy Conference and Exhibition, Barcelona, 2005, p. 2865-2868.
138. M. D. Archer, M. A. Green: Clean electricity from photovoltaics, Imperial College Press, London 2015.
139. : Moduł fotowoltaiczny mono PERC 315-325Wp z innowacjami, dostęp:19.06.2019
140. : Npeak-Cells, dostęp:dostęp 15.09.2020
141. Gramwzielone.pl: Kolejny producent wprowadza moduł fotowoltaiczny o mocy +600 W, dostęp:10.10.2020
142. B. Szymański: Dioda bypass w panelach fotowoltaicznych, dostęp:08.10.2020
143. Gramwzielone.pl: Panele w technologii Shingled od Hyundai Energy Solution, dostęp:12.10.2020
144. D. Tonini, G. Cellere, M. Bertazzo, A. Fecchio, L. Cerasti, M. Galiazzo: Shingling Technology For Cell Interconnection: Technological Aspects And Process Integration, Energy Procedia 2018, Vol. 150, pp. 36-43, dostęp:14.12.2020
145. LG: Neon 2 Black Flat, dostęp:12.09.2020
146. Emiternet: Fotowoltaiczne moduły połówkowe – Nowa technologia w seryjnej produkcji, dostęp:13.09.2020
147. S. Lewkowicz: Ogniwa fotowoltaiczne HALF CUT – czyli dlaczego 0,5 + 0,5 > 1?, dostęp:12.09.2020
148. Hanplast Energy: PV – SmartWire Bi-facial, dostęp:17.08.2020
149. A. Chaurey, S. Deambi: Battery storage for PV power systems: An overview, Renewable Energy 1992, Vol. 2, Iss. 3, pp. 227-235, dostęp:14.12.2020
150. C. J. Rydh, B. A. Sandén: Energy analysis of batteries in photovoltaic systems. Part I: Performance and energy requirements, Energy Conversion and Management 2005, Vol. 46, Iss. 11-12, pp. 1957-1979, dostęp:14.12.2020
151. E-instalacje: Kolektory hybrydowe – zasada działania, ich zalety i wady, dostęp:13.08.2020
152. R. Skiz: SAHP - PVT Panels, Wikipedia, dostęp:13.08.2020
153. PRE Edward Biel: Panele hybrydowe, ISIEtherm, dostęp:13.08.2020
154. : Solar Electric Handbook: Photovoltaic Fundamentals and Applications, Pearson Learning Solutions, Boston 2013.
155. B. Szymański: Instalacje fotowoltaiczne : teoria i praktyka od pomysłu do realizacji, GlobEnergia, Kraków 2020.
156. F. C. Krebs (Ed.): Polymer Photovoltaic: A Practical Approach, Society of Photo-Optical Instrumentation Engineers (SPIE) Press, Bellingham 2008, dostęp:14.12.2020
157. "PV Test Solutions": "PV Test Solutions", dostęp:22.10.2020
158. PVEducation: PC1D, dostęp:08.08.2020
159. M. Belarbi, A. Benyoucef, B. Benyoucef: Simulation of the solar cells with PC1D, application to cells based on silicon, Advanced Energy: An International Journal (AEIJ) 2014, Vol. 1, No. 3, dostęp:14.12.2020
160. R. Braunstein, A. R. Moore, F. Herman: Intrinsic Optical Absorption in Germanium-Silicon Alloys, Physical Review 1958, Vol. 109, Iss. 3, dostęp:14.12.2020
161. L. Nascimento, L. C. L. A. Jamshidi, C. M. B. de Menezes Barbosa, R. J. Rodbari: Semiconductors of crystalline alloys in superlattices, Revista Tecnológica 2015, Vol. 24, Iss. 1, pp. 81-93, dostęp:14.12.2020
162. W. Spitzer, H. Y. Fan: Infrared Absorption in n-Type Silicon, Physical Review 1957, Vol. 108, Iss. 2, pp. 268-271
163. E. Radziemska: The effect of temperature on the power drop in crystalline silicon solar cells, Renewable Energy 2003, Vol. 28, Iss. 1, pp. 1-12, dostęp:14.12.2020
164. : PN-EN 61853-1:2011 : Badanie własności modułów fotowoltaicznych (PV) i wyznaczanie ich energii znamionowej -- Część 1: Pomiary wpływu natężenia promieniowania i temperatury na parametry i moc znamionową.
165. : SEC komory do symulacji środowiska z lampami MHG. Instrukcja obsługi.
166. Dziennik Ustaw: Ustawa z dnia 7 czerwca 2018 r. o zmianie ustawy o odnawialnych źródłach energii oraz niektórych innych ustaw, dostęp:14.12.2020
167. Z. Hanzelka, A. Firlit: Elektrownie ze źródłami odnawialnymi : zagadnienia wybrane, Wydawnictwa AGH, Kraków 2015.
168. A. De Almeida, P. Moura, N. Quaresma: Energy-efficient off-grid systems – review, Energy Efficiency 2020, Vol. 13, pp. 349-376, dostęp:14.12.2020
169. N. M. Kumar, K. Sudhakar, M. Samykano: Performance comparison of BAPV and BIPV systems with c-Si, CIS and CdTe photovoltaic technologies under tropical weather conditions, Case Studies in Thermal Engineering 2019, Vol. 13, (Article nr) 100374, dostęp:14.12.2020
170. N. M. Kumar, K. Sudhakar, M. Samykano: Performance of thin-film BIPV as double sloped pitched roof in buildings of Malaysia, Energy Sources, Part A: Recovery, Utilization, and Environmental Effects 2018, Vol. 40, Iss. 20, pp. 2476-2484, dostęp:14.12.2020
171. E. Biyik, M. Araz, A. Hepbasli, M. Shahrestani, R. Yao, L. Shao, E. Essah, A. C. Oliveira, T. del Caño, E. Rico, J. L. Lechón, L. Andrade, A. Mendes, Y. B. Atli: A key review of building integrated photovoltaic (BIPV) systems, Engineering Science and Technology : an International Journal 2017, Vol. 20, Iss. 3, pp. 833-858, dostęp:14.12.2020
172. K. Ukoba, O. Fadare, T.-C. Jen: Powering Africa Using An Off-Grid, Stand-Alone, Solar Photovoltaic Model, Journal of Physics: Conference Series 2019, Vol. 1378, Iss. 2, (Article Nr) 022031, dostęp:14.12.2020
173. Dziennik Ustaw: Ustawa z dnia 19 lipca 2019 r. o zmianie ustawy o odnawialnych źródłach energii oraz niektórych innych ustaw, dostęp:14.12.2020
174. Gramwzielone.pl: Powstała największa elektrownia fotowoltaiczna w Europie, dostęp:01.05.2020
175. EC BREC Instytut Energetyki Odnawialnej: Raport Rynek Fotowoltaiki w Polsce 2020, dostęp:08.09.2020

176. SolarInsure: Top 5 largest solar power plant of the world, dostęp:03.04.2020
177. K. Trapani, M. R. Santafé: A review of floating photovoltaic installations: 2007-2013, Progress in Photovoltaics 2015, Vol. 23, Iss. 4, pp. 524-532, dostęp:14.12.2020
178. M. Rosa-Clot, P. Rosa-Clot, G. M. Tina, P. F. Scandura: Submerged photovoltaic solar panel: SP2, Renewable Energy 2010, Vol. 35, Iss. 8, pp. 1862-1865, dostęp:14.12.2020
179. Planete Energies: Huainan: Largest Floating Solar Farm in the World, dostęp:12.04.2020
180. A. Awasthi, A. K. Shukla, S. R. Murali Manohar, C. Dondariya, N. K. Shukla, D. Porwal, G. Richhariya: Review on sun tracking technology in solar PV system, Energy Reports 2020, Vol. 6, pp. 392-405, dostęp:14.12.2020
181. M. Kurantowicz: Trackery – instalacje fotowoltaiczne nadążne za słońcem, cz.1, dostęp:01.07.2020
182. M. B. Schubert, J. H. Werner: Flexible solar cells for clothing, Materials Today 2006, Vol. 9, Iss. 6, pp. 42-50, dostęp:14.12.2020
183. A. H. M. E. Reinders: Options for Photovoltaic Solar Energy Systems in Portable Products. In: Horvath, I. Li, P. and Vergeest, J. (Eds.), Proceedings of TMCE 2002, Forth International Symposium, April 22-26, 2002, Wuhan, P.R. China, dostęp:14.12.2020
184. W. Trzasko: Analiza wydajności dwuosiowego solarnego układu nadążnego, Pomiary Automatyka Robotyka 2018, R. 22, nr 1, s. 11-17, dostęp:14.12.2020
185. H. Moradi, A. Abtahi, R. Messenger: Annual performance comparison between tracking and fixed photovoltaic arrays, 2016 IEEE 43rd Photovoltaic Specialists Conference (PVSC), 5-10 June 2016, Portland, OR, USA, dostęp:14.12.2020
186. T. Hong, K. Jeong, C. Ban, J. Oh, C. Koo, J. Kim, M. Lee: A preliminary study on the 2-axis hybrid solar tracking method for the smart photovoltaic blind, Energy Procedia 2016, Vol. 88, pp. 484-490, dostęp:14.12.2020
187. C.-Y. Lee, P.-C. Chou, C.-M. Chiang, C.-F. Lin: Sun tracking systems: A review, Sensors 2009, Vol. 9, Iss. 5, pp. 3875-3890, dostęp:14.12.2020
188. A. G. Melo, D. O Filho, M. M. Oliveira Júnior, S. Zolnier, A. Ribeiro: Development of a closed and open loop solar tracker technology, Acta Scientiarum. Technology 2017, Vol. 39, Iss. 2, pp. 177-183, dostęp:14.12.2020
189. J. M. Wang, C. L. Lu: Design and implementation of a sun tracker with a dual-axis single motor for an optical sensor-based photovoltaic system, Sensors 2013, Vol. 13, Iss. 3, pp. 3157-3168, dostęp:14.12.2020
190. R. Aparnathi, V. V. Dwivedi: Maximum Power Point Tracking in PV System with Industry Applications, International Journal of Power Electronics and Drive Systems 2013, Vol. 3, Nr 4, pp. 417-423, dostęp:14.12.2020
191. M. Wiesenfarth, I. Anton, A. W. Bett: Challenges in the design of concentrator photovoltaic (CPV) modules to achieve highest efficiencies, Applied Physics Reviews 2018, Vol. 5, Iss. 4, (Article Nr) 041601, pp. 1-27, dostęp:14.12.2020
192. 172MW Single Axis Tracker Project in India from Arctech Solar: Wikipedia, dostęp:20.10.2020
193. 3 MW CPV project in Golmud, China (Dual axis tracker with CPV modules in Golmud): Wikipedia, dostęp:20.10.2020
194. "AGH Solar Boat Team": "AGH Solar Boat Team", dostęp:20.10.2020
195. R. De Fazio, D. Cafagna, G. Marcuccio, A. Minerba, P. Visconti: A multi-source harvesting system applied to sensor-based smart garments for monitoring workers' bio-physical parameters in harsh environments, Energies 2020, Vol. 13, Iss. 9, (Article Nr) 2161, dostęp:14.12.2020
196. H. Jinno, K. Fukuda, X. Xu, S. Park, Y. Suzuki, M. Koizumi, T. Yokota, I. Osaka, K. Takimiya, T. Someya: Stretchable and waterproof elastomer-coated organic photovoltaics for washable electronic textile applications, Nature Energy 2017, Iss. 2, pp. 780-785, dostęp:14.12.2020
197. J. Bakalczyk: Przekształtniki energoelektroniczne w instalacjach fotowoltaicznych, Czasopismo Inżynierii Lądowej, Środowiska i Architektury (JCEEA) 2014, z. 61, nr 3/II, s. 19-32, dostęp:14.12.2020
198. A. Filipkowski: Układy elektroniczne analogowe i cyfrowe, Wydawnictwa Naukowo-Techniczne, Warszawa 2006.
199. GLOBEnergia: Dopasowanie mocy falownika do generatora PV, dostęp:18.07.2020
200. B. Szymański: Instalacje fotowoltaiczne: teoria i praktyka od pomysłu do realizacji, GlobEnergia, Kraków 2020.
201. GLOBEnergia: Dopasowanie mocy falownika do generatora PV, dostęp:16.07.2020
202. Wikipedia: Magazynowanie energii elektrycznej, dostęp:14.12.2020
203. D. Kaczmarczyk: Akumulatory do fotowoltaiki, dostęp:02.01.2020
204. M. Sterner, M. Jentsch, U. Holzhammer: Energiewirtschaftliche und ökologische Bewertung eines Windgas-Angebotes - Energy-economic and ecological evaluation of a windgas offer (Power-to-Gas), dostęp:14.12.2020
205. T. Smedley: Power-to-gas energy storage could help displace use of fossil fuels, dostęp:14.12.2020
206. M. Harasimczuk: Hybrydowy system amagazynowania energii fotowoltaicznej, Poznan University of Technology Academic Journals. Electrical Engineering 2016, No. 87, pp. 109-118, dostęp:14.12.2020
207. P. Kundur: Power system stability and control, McGraw-Hill, New York 1994.
208. J. Hruska: British company offers efficient energy storage using liquid air, dostęp:14.12.2020
209. K. Bullis: The Resurgence of Liquid Air for Energy Storage, MIT Technology Review 2013.
210. Interesting Engineering: Rio Madeira, World's Longest Transmission Link, dostęp:14.12.2020
211. Ustawa z dnia 13 lutego 2020 r. o zmianie ustawy: Prawo budowlane oraz niektórych innych ustaw, dostęp:20.09.2020
212. Urząd Nadzoru Budowlanego: Opinia Głównego Urzędu Nadzoru Budowlanego (2014), dostęp:07.08.2020
213. Wojewódzki Sąd Administracyjny: Orzeczenie Wojewódzkiego Sądu Administracyjnego w Łodzi z dnia 30 listopada 2017 r. o sygnaturze III SA/Łd 974/17 2017, dostęp:07.07.2020
214. Stowarzyszenie Branży Fotowoltaicznej: Fotowoltaiczny dekalog dobrych praktyk : 10 zasad bezpiecznej instalacji PV ppoż., dostęp:10.10.2020
215. Ustawa z dnia 24 sierpnia 1991 r.: o ochronie przeciwpożarowej, dostęp:10.10.2020
216. Rozporządzenie Komisji (UE) 2016/631 z dnia 14 kwietnia 2016 r.: ustanawiające kodeks sieci dotyczący wymogów w zakresie przyłączenia jednostek wytwórczych do sieci, dostęp:14.12.2020
217. Polskie Towarzystwo Przemysłu i Rozdziału Energii Elektrycznej: Warunki i procedury wykorzystania certyfikatów w procesie

przyłączenia modułów wytwarzania energii do sieci elektroenergetycznych, dostęp:17.09.2020
218. J. Popczyk: Energetyka rozproszona : od dominacji energetyki w gospodarce do zrównoważonego rozwoju, od paliw kopalnych do energii odnawialnej i efektywności energetycznej, Polski Klub Ekologiczny Okręg Mazowiecki, Warszawa 2011.
219. Solar Electric Handbook: Photovoltaic Fundamentals and Applications, Pearson Learning Solutions, Boston 2013.
220. W. Jaskółowski, J. Wiatr: Instalacje fotowoltaiczne. Podstawy fizyczne działania. Ochrona odgromowa. Zasady neutralizacji zagrożeń porażenia prądem elektrycznym w czasie pożaru, Zeszyty Naukowe SGSP / Szkoła Główna Służby Pożarniczej 2016, Nr 59 (3), s. 71-99, dostęp:14.12.2020
221. PN-EN 62446-1:2016-08: Systemy fotowoltaiczne (PV) – Wymagania dotyczące badań, dokumentacji i utrzymania – Część 1: Systemy podłączone do sieci – Dokumentacja, odbiory i nadzór.
222. PN-EN 61557-1:2009: Bezpieczeństwo elektryczne w niskonapięciowych sieciach elektroenergetycznych o napięciach przemiennych do 1000 V i stałych do 1500 V – Urządzenia przeznaczone do sprawdzania, pomiarów lub monitorowania środków ochronnych – Część 1: Wymagania ogólne.
223. PN-EN 61010-1:2011: Wymagania bezpieczeństwa dotyczące elektrycznych przyrządów pomiarowych, automatyki i urządzeń laboratoryjnych – Część 1: Wymagania ogólne.
224. T. Lipiński: Badanie bezpieczeństwa i efektywności instalacji fotowoltaicznych zgodnie z normą PN-EN 62446 cz. 1, dostęp:04.08.2020
225. T. Lipiński: Badanie bezpieczeństwa i efektywności instalacji fotowoltaicznych zgodnie z normą PN-EN 62446 cz. 2 - Testy kat. 1, dostęp:04.08.2020
226. T. Lipiński: Badanie bezpieczeństwa i efektywności instalacji fotowoltaicznych zgodnie z normą PN-EN 62446 cz. 3 - Testy kat. 2, dostęp:04.08.2020
227. K. Mik, M. Juźwik: Zobaczyć niewidoczne: elektroluminescencja modułów fotowoltaicznych, Magazyn Fotowoltaika 2020/2.
228. B. Szymański: Gorące punkty – tzw. hot spoty mogą stanowić istotny problem dla instalacji fotowoltaicznej, GLOBEnergia 2013/4, dostęp:10.06.2020
229. H. J. Solheim, H. G. Fjær, E. A. Sørheim, S. E. Foss: Measurement and simulation of hot spots in solar cells, Energy Procedia 2013, Vol. 38, pp. 183-189, dostęp:10.06.2020
230. C. Olalla, M. N. Hasan, C. Deline, D. Maksimović: Mitigation of hot-spots in photovoltaic systems using distributed power electronics, Energies 2018, Vol. 11, Iss. 4, (Article Nr) 726, dostęp:11.06.2020
231. A. R. Gxasheka, E. E. van Dyk, E. L. Meyer: Evaluation of performance parameters of PV modules deployed outdoors, Renewable Energy 2005, Vol. 30, Iss. 4 , pp. 611-620, dostęp:14.12.2020
232. N. C. Park, J. S. Jeong, B. J. Kang, D. H. Kim: The effect of encapsulant discoloration and delamination on the electrical characteristics of photovoltaic module, Microelectronics Reliability 2013, Vol. 53, Iss. 9-11, pp. 1818-1822, dostęp:14.12.2020
233. E. E. van Dyk, J. B. Chamel, A. R. Gxasheka: Investigation of delamination in an edge-defined film-fed growth photovoltaic module, Solar Energy Materials and Solar Cells 2005, Vol. 88, Iss. 4, pp. 403-411, dostęp:14.12.2020
234. M. Dhimish, V. Holmes, B. Mehrdadi, M. Dales: The impact of cracks on photovoltaic power performance, Journal of Science: Advanced Materials and Devices 2017, Vol. 2, Iss. 2, pp. 199-209, dostęp:14.12.2020
235. M. Köntges, I. Kunze, S. Kajari-Schröder, X. Breitenmoser, B. Bjørneklett: Quantifying the risk of power loss in PV modules due to micro cracks, 25th European Photovoltaic Solar Energy Conference and Exhibition / 5th World Conference on Photovoltaic Energy Conversion, 6-10 September 2010, Valencia, Spain (pp. 3745-3752).
236. S. Kajari-Schröder, I. Kunze, U. Eitner, M. Köntges: Spatial and orientational distribution of cracks in crystalline photovoltaic modules generated by mechanical load tests, Solar Energy Materials and Solar Cells 2011, Vol. 95, Iss. 11, pp. 3054-3059, dostęp:14.12.2020
237. I. Rutschmann: Unlocking the Secret of Snail Trails, Photon International 2012, pp. 114-125.
238. J. Fan, D. Ju, X. Yao, Z. Pan, M. Terry, W. Gambogi, K. Stika, J. Liu, W. Tao, Z. Liu, Y. Liu, M. Wang, Q. Wu, T. J. Trout: Study on snail trail formation in PV module through modeling and accelerated aging tests, Solar Energy Materials and Solar Cells 2017, Vol. 164, pp. 80-86, dostęp:14.12.2020
239. S. J. Ikhmayies: Transparent Conducting Oxides for Solar Cell Applications (pp. 899-907). In: Ali Sayigh (Ed.), Mediterranean Green Buildings & Renewable Energy : Selected Papers from the World Renewable Energy Network's Med Green Forum, Springer Nature, Cham 2017, dostęp:14.12.2020
240. C. Ballif, S. De Wolf, A. Descoeudres, Z. C. Holman: Chapter Two – Amorphous Silicon/Crystalline Silicon Heterojunction Solar Cells. In: G. P. Willeke, E. R. Weber (Eds.), Advances in Photovoltaics: Part 3, Semiconductors and Semimetals, Vol. 90 (Series), Elsevier 2014, dostęp:14.12.2020
241. S. Pingel, O. Frank, M. Winkler, S. Daryan, T. Geipel, H. Hoehne, J. Berghold: Potential induced degradation of solar cells and panels (pp. 2817-2822), 35th IEEE Photovoltaic Specialists Conference, 20-25 June 2010, Honolulu, HI, USA, dostęp:14.12.2020
242. W. Luo, Y. S. Khoo, P. Hacke, V. Naumann, D. Lausch, S. P. Harvey, J. P. Singh, J. Chai, Y. Wang, A. G. Aberle, S. Ramakrishna: Potential-induced degradation in photovoltaic modules: A critical review, Energy & Environmental Science 2017, Vol. 10, Iss. 1, pp. 43-68, dostęp:14.12.2020
243. EnergySage: The cost of solar panels in 2021: are they worth it?, dostęp:18.09.2020
244. SunWaySolar: Solar System, dostęp:12.09.2020
245. Statista: Average installed cost for solar photovoltaics worldwide from 2010 to 2019 (in U.S. dollars per kilowatt), dostęp:10.09.2020
246. L. Partain, R. Hansen, S. Hansen, D. Bennett, A. Newlands, L. Fraas: 'Swanson's Law' plan to mitigate global climate change, IEEE 43rd Photovoltaic Specialists Conference (PVSC), 5-10 June 2016, Portland, OR, USA, dostęp:14.12.2020
247. L. Shih, R. Tsao, S. Chen, Y. Lee: EnergyTrend Market Intelligence, 2018 Global Photovoltaic Market Overview.
248. Rfassbind: Price history of silicon PV cells since 1977, Wikipedia, dostęp:10.09.2020
249. Instytut Energetyki Odnawialnej: Rynek fotowoltaiki w Polsce 2020. Streszczenie i wnioski raportu, dostęp:14.12.2020

250. Europejska firma: Polska na piątym miejscu w UE pod względem rozwoju fotowoltaiki, dostęp:12.09.2020
251. Narodowy Fundusz Ochrony Środowiska i Gospodarki Wodnej: Lista programów priorytetowych, dostęp:12.09.2020
252. Program priorytetowy Mój Prąd: Program dofinansowania mikroinstalacji fotowoltaicznych, dostęp:12.09.2020
253. Ustawa z dnia 20 listopada 1998 r.: o zryczałtowanym podatku dochodowym od niektórych przychodów osiąganych przez osoby fizyczne, dostęp:18.09.2020
254. Ustawa z dnia 20 lutego 2015 r.: o odnawialnych źródłach energii, dostęp:14.12.2020
255. Ustawa z dnia 22 czerwca 2016 r.: o zmianie ustawy o odnawialnych źródłach energii oraz niektórych innych ustaw, dostęp:14.12.2020
256. Urząd Regulacji Energetyki: Regulamin Aukcji – według stanu prawnego na październik 2019 r., dostęp:10.10.2020
257. EUobserv'ER: Solar thermal and concentrated solar power barometer 2019, dostęp:18.09.2020
258. A. Jäger-Waldau: PV Status Report 2019, dostęp:18.09.2020
259. British Petrol: Statistical Review of World Energy 2020 : 69th edition, dostęp:18.09.2020
260. D. Szymański: Chiny mówią światu sprawdzam. Ta deklaracja dotknie każdego z nas, dostęp:18.09.2020

The publication is available under the Creative Commons Attribution-ShareAlike 4.0 (CC BY-SA 4.0).
Some rights reserved for the authors and the AGH University of Science and Technology.
This license allows reusers to distribute, remix, adapt, and build upon the material in any medium or format, so long as attribution is given to the authors and the AGH University of Science and Technology.
The full text of the license is available at https://creativecommons.org/licenses/by-sa/4.0/deed.en.

Document generation date: 2022-10-24 09:11:10

The original document is available at: http://pre-epodreczniki.open.agh.edu.pl/openagh-podreczniki_view.php?categId=143&handbookId=129